According to the result, the effect of furnace temperature and total flow rate of carrier gas had an impact on diameter and crystallinity of the obtained CNTs. By varying the furnace temperature, the formation of SWCNTs could be observed when the temperature was higher than 850°C. Increasing temperature resulted in both large diameter and high crystallinity of SWCNTs. The CNTs synthesized at 1050°C exhibited the highest I_G/I_D value of about 9.2. For the flow rate in the range of 600 – 2500 sccm, there was no significant relation between the flow rate of carrier gas and the crystallinity of CNTs. However, it was fond that the diameter of CNTs tended to decrease with increasing the flow rete. Using the optimal temperature and flow rate of carrier gas, SWCNTs with a narrow diameter (0.9 ~1.4 nm) and high crystallinity (I_G/I_D: 6~9) could be obtained. This method does not require vacuum and hazardous gases and is economical and easily scalable for synthesis of SWCNTs.

Acknowledgements

References

[1] Iijima and T. Ichihashi, *Nature.* **363** (1988), pp.603

[2] M.S. Dresselhaus, G. Dresselhaus and P.C. Eklund, *Academic Press, San Diego*. (1995)

[3] J S. Reich, C. Thomsen and J. Maultzsch, *Encyclopedia of Nuclear Magnetic Resonance,* Wiley-VCH Verlag GmbH&Co., Weinheim, Germany (2004)

[4] S. Chaisitsak, J. Nukeaw and A. Tuantranont, *Diamond & Related Materials*. **16** (2007) 1958 – 1966.

[5] M.S. Dresselhaus, G. Dresselhaus and P. Avouris, *Springer*. (2001).

[6] S. Ijima, *Nature*. **354** (1991)

[7] S Thess A, R. Lee, P. Nikolaev, H. Dai, P. Petit, RE. Smalley, et al., *Science.* **273** (1996) 483–7.

[8] H. Dai, AG. Rinzler, P. Nikolaev, A. Thess, DT. Colbert and RE. Smalley, *Chem Phys Lett*. **260** (1996) 471-5.

[9] R. Bhowmick , Bruce M. Clemens , Brett A. Cruden, *Carbon*. **46** (2008) 907-922.

[10] S. Maruyama, R. Kojima, R. Miyauchi, S. Chiashi and M. Kohno, *Chem Phys Lett*. **360** (2002) 229-334.

[11] M. Krhno and S. Maruyama, *Applied Physics A*. **79** (2004) 787-790.

[12] Zhu HW, Xu CL, Wu DH, Wei BQ, Vajtai R, Ajayan PM, *Science*. **296** (2002) 884–6.

[13] M.S. Dresselhaus, G. Dresselhaus, R. Saito and A. Jorio, *Phys. Rep*. **409** (2005) 47-99.

[14] K. Kuwana and K. Saito, *Carbon*. **43** (2005) 2088.

[15] D. Kim, E.S. Vasilieva, A.G. Nasibulin, D.W. Lee and O.V. Tolochko , B.K. Kim, *Materials Science*. Forum Vols. (2007) 534-536 pp. 9-12

[16] P. Chiwsitthiprapai, J. Nukeaw, A. Tuantranont and S. Chaisitsak, *Ladkrabang Engineering Journal*. Vol23, No.2 , (2006)

[17] Y. Tian, Albert G. Nasibulin, B. Aitchison, T Nikitin, Jan v. Pfaler, H. Jiang, Z. Zhu, L. Khriachtchev, David P. Brown, and Esko I. Kauppinen*, J. Phys. Chem*. **115** (2011), 7309 –7318.

[18] A. Moisala, Albert G. Nasibulin, David P. Brown, H. Jiang, L. Khriachtchev, and Esko I. Kauppinen*, Chemical Engineering Science.* **61** (2006) 4393 – 4402.

SYNTHESIS AND CHARACTERIZATION OF DyBa$_2$Cu$_3$O$_y$ POWDER PREPARED BY SOLID-STATE REACTION METHOD

Poom Prayoonphokkharat[1,2], Sukanda Jiansirisomboon[1,3], Anucha Watcharapasorn[1,3*]

[1] Department of Physics and Materials Science, Faculty of Science, Chiang Mai University, Chiang Mai 50200 Thailand
[2] Departments of Science, Takpittayakhom School, Tak 63000 Thailand
[3] Materials Science Research Center, Faculty of Science, Chiang Mai University, Chiang Mai 50200 Thailand

[*] Author for correspondence; E-Mail: anucha@stanfordalumni.org, Tel. +66 53 943369, Fax. +66 53 943445

Abstract: DyBa$_2$Cu$_3$O$_y$ (or DyBCO, Dy-123) is one of the promising candidates for high-field applications such as magnetic bearing, flywheels, permanent magnets and generators. In previous research, the typical preparation of DyBCO employed by solid-state reaction method, but with wide range and inconsistent experimental conditions. In addition, second phases and impurities such as Dy-211, BaCO$_3$ and CuO, were observed which affected microstructure and properties such that they could decrease the densification rate and thermal conductivity as well as influence the change in critical current density value. Moreover, the microstructural characteristics were not adequately discussed. The synthesis and characterization of DyBCO powder were therefore investigated in this study. DyBCO powder was prepared by mixing Dy$_2$O$_3$, BaCO$_3$ and CuO powders in the stoichiometric ratio of Dy : Ba : Cu = 1 : 2 : 3 and calcining at 800 – 930 °C for 4 h. Phase identification was performed using X-Ray diffraction (XRD) analysis, and microstructures were studied using scanning electron microscopy (SEM) and energy dispersive X-Ray spectroscopy analysis (EDS). It was found that, starting from 900 °C, virtually pure phase of DyBCO was produced. In contrast, the DyBCO powders calcined at 800 and 850 °C consisted of certain amount of unreacted raw materials and Dy-211 second phase. The SEM-EDS image showed that the powder contained large agglomerates of about 6 - 14 μm size and some scattered small particles had Ba- and Cu-rich composition.

Keywords: DyBCO; powder; calcination; phase; microstructure

1. Introduction

RE-Ba$_2$-Cu$_3$-O$_y$ (RE = rare earth element such as Y, Dy, Gd) material is known as a high-T$_c$ superconductor whose properties are suitable for high-field electronic applications such as power cable, magnetic bearing, fault current limiter and permanent magnet [1-3]. The crystal structure of RE-Ba$_2$-Cu$_3$-O$_y$ is orthorhombic perovskite structure. Oxygen content is one of the most significant factors that cause its electrical properties to change from superconducting (y ≥ 6.5) to semiconducting (y < 6.5) behavior. This oxygen stoichiometry depends on the temperature and oxygen pressure [2,4-5]. Since the discovery of YBa$_2$Cu$_3$O$_{7-x}$ (YBCO or Y-123), the investigation of relationship between processing and microstructure has been widely studied and discussed. A number of literatures have reported various fabrication methods such as melt process, nitrate compound route, multi-step solid solution method with a wide range of processing conditions and typically under oxygen flow atmosphere [6-8]. However, most of these methods are complex and not safe for production, e.g., nitrate compounds are explosive. In addition, small quantities of second phases and unreacted raw materials of Y-211, Y$_2$Cu$_2$O$_5$, CuO or BaCO$_3$ were often obtained [4,9]. In contrary, the investigation of other rare earth compounds is not so extensive and rarely focused on ceramic processing [1,3,10]. Nevertheless, in order to obtain properties of bulk ceramics, high quality powder is essential. Although, the superconducting materials based on Bi and Tl such as HgBa$_2$Ca$_{n-1}$Cu$_n$O$_{2n+2+x}$ (**HBCCO**), Bi$_2$Sr$_2$Ca$_{n-1}$Cu$_n$O$_{2n+4+x}$ (**BiSCCO**) and Tl$_2$Ba$_2$Ca$_{n-1}$Cu$_n$O$_{2n+4+x}$ (**TlBCCO**) have been shown to have higher T$_c$, the difficulties of consolidation due to micaceous structure of Bi, and the volatility and high toxicity of Hg and Tl are of major concerns for use in large-scale applications [2,11-12].

The aim of this work is to investigate the influence of calcination temperature on synthesis of DyBCO powder by simple solid-state reaction method without oxygen flow in the system. The optimum processing conditions are concluded based on the results of phase, chemical, and microstructural analysis.

2. Materials and Methods

DyBCO powders were prepared by solid-state reaction method using Dy$_2$O$_3$ (99.99%, Aldrich), BaCO$_3$ (≥99%, Sigma-Aldrich) and CuO (98%, Sigma-Aldrich) starting powders. These powders were mixed in a stoichiometric ratio of Dy : Ba : Cu = 1 : 2 : 3 and ball milled for 24 h in polyethylene jar with zirconia balls as milling media. The mixed powders were dried and calcined in an open alumina crucible at 800, 850, 900 and 930 °C for 4 h under normal atmosphere.

The powders were characterized for phase identification by X-ray diffraction technique (XRD: Rikagu, Miniflex II) with Cu K$_\alpha$ (λ = 1.5405 Å) over angle 2θ = 20 - 80°. The microstructure of powders was observed with scanning electron microscopy (SEM: JEOL, JSM5910LV) and chemical composition

identification was carried out using energy-dispersive X-Ray spectroscopy analysis (SEM-EDS).

3. Results and Discussion

Figure 1 shows XRD patterns of DyBCO powders calcined at 800 – 930 °C. In all cases, the powders consisted of $DyBa_2Cu_3O_y$ (Dy-123) main peaks at 2θ (°) = 32.44, 32.77, 46.62, 58.02 and 58.12. The XRD patterns corresponded well with JCPDS standard file No. 79-0047 indicating oxygen deficient orthorhombic perovskite structure [5,12-13]. However, at 800 °C, some unreacted raw materials of Dy_2O_3, $BaCO_3$ and CuO were present. It could be because the temperature was not high enough to reach complete reaction due to the rate-limiting step of $BaCO_3$ decomposition [14]. At temperature of 850 °C, the amount of raw materials decreased but small amount of the second phase Dy_2BaCuO_5 (Dy-211) was found. Similar phase was found in the peritectic reaction between $\langle 123 \rangle$ phase (e.g., $YBa_2Cu_3O_y$) and CuO [1,4,10] as shown in (1).

$$CuO + YBa_2Cu_3O_y \leftrightarrow Y_2BaCuO_5 + Liquid \quad (1)$$
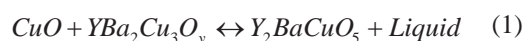
After increasing the calcination temperature to 900 and 930 °C, the DyBCO powders were quite pure. The difference of these XRD patterns was the separation magnitude of peaks such as (013)/(103), (200)/(020) and (213)/(123) due to chemical fluctuation and ionic distribution in the materials. The relative peak intensities of certain reflections were also slightly different. This implied that the calcination temperature had some influences on preferred orientation of powders [15].
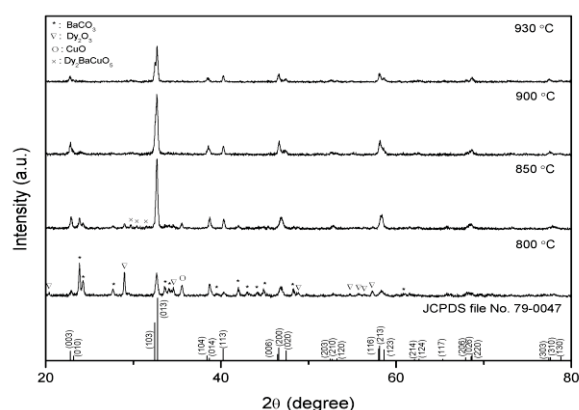

Figure 1. X-Ray diffraction patterns of $DyBa_2Cu_3O_y$ powder calcined at different temperatures.

The microstructures of DyBCO powders with different calcination temperatures are shown in Figure 2 and chemical analysis using SEM-EDS were tabulated in Table 1. It was observed that the DyBCO powders had irregular shape with size range of 6-14 μm similar to as-synthesized powders obtained by multi-step solid-state reaction process [1,12].

However, at 800 °C, the powder consisted of two particle size ranges, i.e., ~5-7 μm and <1 μm. When the temperature was increased to 850 °C, DyBCO was observed with particle size ~1-3 μm and atomic percentage ratio of Dy : Ba : Cu : O was about 13.34 : 18.18 : 21.30 : 47.18. Nevertheless, it was also found that the relatively large particle (~5 μm) had Ba-rich composition. For 900 and 930 °C, dense agglomerates of particles were observed. Their size increased from ~6-8 μm for calcining at 900 °C to 10-14 μm at 930 °C. In addition, EDS analysis showed the atomic ratio of element was about 7.26 : 15.43 : 23.49 : 53.83 and 7.83 : 15.27 : 21.43 : 55.47, respectively. It has to be noted that the measured stoichiometry deviation about 2 – 13% from nominal composition was partly due to the measurement error of EDS technique (typically about 5%). However, for temperature of 930 °C, SEM-EDS analysis also showed that the small size particles (≤1 μm) were Ba- and Cu-rich. This might be because the temperature was so high such that material loss and Ba- and Cu-rich liquid phase formed during calcination [4,11,16].
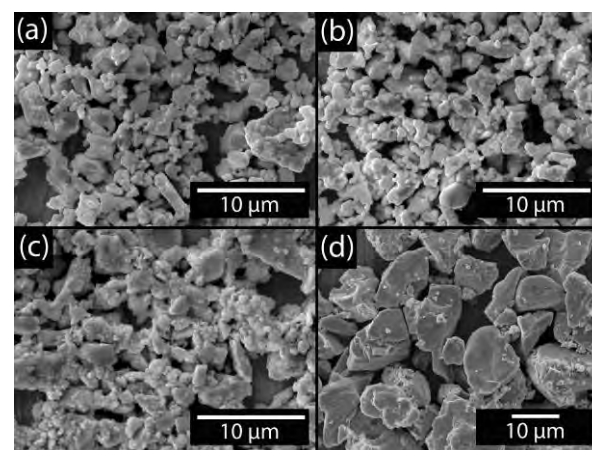

Figure 2. Scanning electron microscopy (SEM) micrograph of $DyBa_2Cu_3O_y$ powder with calcination at (a) 800 °C (b) 850 °C (c) 900 °C and (d) 930 °C.

Table 1. Atomic ratio of elements for $DyBa_2Cu_3O_y$ powder at different calcination temperatures.

Calcination Temp. (°C)	Evaluated elemental composition (at. %)				Composition error (%)			
	Dy	Ba	Cu	O	Dy	Ba	Cu	O
$DyBa_2Cu_3O_{6.5}$	8	16	24	52	n/a	n/a	n/a	n/a
850	13.34	18.18	21.30	47.18	66.75	13.63	11.25	9.27
900	7.26	15.43	23.49	53.83	9.25	3.57	2.13	3.52
930	7.83	15.27	21.43	55.47	2.13	4.56	10.71	6.67

4. Conclusions

In this study, DyBCO powder produced by solid-state reaction method under normal atmosphere was reported. At calcination temperature of 800 and 850 °C, XRD analysis indicated that raw materials and second phase remained. Quite pure DyBCO powder

was successfully synthesized starting at calcination temperature of 900 °C. SEM-EDS analysis showed fine particles with nearly ideal stoichiometry. By increasing temperature to 930 °C, the large agglomeration of particles was found, and Ba- and Cu-rich liquid phase was observed. In summary, the calcination temperature at 900 °C and 4 h dwell time was found to be the optimum synthesis condition of DyBCO in this study.

Acknowledgements

References

[1] C. Andreouli and A. Tsetsekou, *J. Eur. Ceram. Soc.* **20** (2000) 2101-2114.

[2] J.M.S Skakle, *Mater. Sci. Eng.* **R23** (1998) 1-40.

[3] S. Nariki and M. Murakami, *Supercond. Sci. Technol.* **15** (2002) 786-790.

[4] T.L. Aselage, *Physica C.* **233** (1994) 292-300.

[5] A. Chroneos, R.V. Vovk, I.L. Goulatis and L.I. Goulatis, *J. Alloy. Compd.* **494** (2010) 190-195.

[6] U. Topal and M. Akdogan, *J. Alloy. Compd.* **503** (2010) 1-5.

[7] E.Hasegawa, H. Aono, T. Igoshi, M. Sakamoto, E. Traversa and Y. Sadaoka, *J. Alloy. Compd.* **287** (1999) 150-158.

[8] S.H. Lee, *Physica C.* **469** (2009) 944-974.

[9] R. Jones, R. Janes, R. Armstrong, N. C. Pyper and P. P. Edwards, *J. Chem. Soc. Faraday. Trans.* **86(4)** (1990) 675-682.

[10] H. Ishizuka, Y. Idemoto and K. Fueki, *Physica C.* **195** (1992) 145-156.

[11] K.C. Goretta, I. Bloom, N. Chen, G.T. Goudey, M.C. Hash, G. Klassen, M.T. Lanagan, R.B. Poeppel, J.P. Singh, D. Shi, U. Balachandran, J.T. Dusek and D.W. Capone, Mater. Lett. **7** (1988) 161-164.

[12] S. Mohan and T. R. Koumar, Mat. Res. Bull. **26** (1991) 317-322.

[13] J.-M. Triscone, M.G. Karkut, L. Antognazza, O. Brunner and O. Fischer, Phys. Rev. Lett. **63** (1989) 1016-1019.

[14] C. Legros, C. Haut, L. Ponsonnet-Mora and J. Ayache, J. Eur. Ceram. Soc. **19** (1999) 165-173.

[15] A. Ates and E. Yanmaz, J. Alloy. Compd. **279** (1998) 220-228.

[16] T. Wolf, I. Apfelstedt, W. Goldacker, H. Kupfer and R. Flukiger, Physica C. **153-155** (1988) 351-352.

CHITOSAN PRETREATMENT AND ALUM MORDANTING ON NATURAL DYEING OF COTTON

Nootsara Narumol[1], Buppha Somboon[1], Usa Sangwatanaroj[2], Monthon Nakpathom[1]*

[1] National Science and Technology Development Agency, National Metal and Materials Technology Center, Textile Laboratory, Pathumthani, 12120 Thailand
[2] Chulalongkorn University, Department of Materials Science, Faculty of Science, Bangkok, 10330 Thailand

*Author for correspondence; E-Mail: monthonn@mtec.or.th, Tel. +66 2 5646500, Fax. +66 2 5646446

Abstract: Since there is growing interest in developing of eco-friendly products worldwide, natural dyes have been employed more frequently in textile industry. However, textile goods dyed with natural dyes have some limitations compared to synthetic dyes, especially in aspects of color yield and color fastness properties. In this study, the use of chitosan pretreatment and alum mordanting for improving the dyeability of cotton fabrics with two natural dyes, lac (*Laccifer lacca Kerr.*) and Siamese neem tree bark (*Azadirachta indica var. siamensis* Valeton) was explored. A low molecular weight (approximately 20,000-30,000 daltons) of chitosan in acidic medium was applied to cotton fabrics using pad-dry-cure technique. Three mordanting methods, pre-mordanting, meta-mordanting and post-mordanting by exhaustion were performed. Color strength and color fastness to washing, light and crocking properties of the dyed fabrics were also determined. The results revealed that dyeing of cotton fabrics after pretreated with chitosan and mordanted with alum clearly enhanced the color yield, especially in the case of lac dye. However, the color fastness to washing and light of the dyed fabrics could be improved by the use of crosslinking treatment.

1. Introduction

Recently, natural dyeing has gained more significant attention owing to environmental concern on the use of certain toxic synthetic dyes. Despite of their lower toxicity, natural dyes have the following disadvantages; limited availability, low color yield, poor reproducibility and inferior fastness properties [1,2]. In order to obtain high color yield, different color shades and good fastness properties, metallic salt mordants such as alum (aluminum potassium sulfate), iron sulfate and copper sulfate are normally employed. Such enhanced characteristics are due to their ability to form coordination complexes with the dye molecules. However, some of these metallic mordants such as copper sulfate and potassium dichromate are considered to be hazardous and the excess usage can later lead to consumers harm and environmental risk.

Biodegradability, non-toxicity, antimicrobial property and polycationic nature make chitosan suitable for textile dyeing and finishing applications [3]. In view of textile coloration, a major role of chitosan is to increase the dye uptake on substrates. Shin and Yoo found that chitosan pretreatment had improved direct, acid and reactive dye uptake on cotton and durable press-finished cotton [4]. Yen used chitosan and nonionic surfactant mixtures to improve the dyeability of wool fabrics with reactive dyes [5]. Abou-Okeil and Hakeim used chitosan to improve copper sulfate binding of wool fabrics before printing with a natural lawsone dye [6]. Hakeim *et al.* studied the effect of molecular weight of chitosan on natural color printing of curcumin on cotton [7]. Suitcharit *et. al*. prepared and used various low molecular weight chitosan to enhance the dyeability of mangosteen dye on cotton fabrics [8]. Kampeerapappun *et. al* explored the effects of chitosan, mordant types and dyeing methods on dyeing of popping pod or meadow weed on cotton fabrics [9].

The goal of this present study was to investigate the effect of chitosan pretreatment together with alum mordanting of cotton fabrics on natural dyeing of lac (*Laccifer lacca Kerr.*) and Siamese neem tree bark (*Azadirachta indica var. siamensis* Valeton) in terms of color yield and fastness properties. Alum was selected as a metallic mordant because of its ability to maintain the original color of natural dyes and for being relatively environmentally friendly.

2. Materials and Methods
2.1 Materials

A commercially scoured and bleached plain woven cotton fabric (weight 137.50 g/m^2) was used. Natural lac and Siamese neem tree bark dyes were obtained from the northern and northeastern parts of Thailand. A low molecular weight (approximately 20,000-30,000 daltons, >90% degree of acetylation) of 1%w/v of chitosan in 1%v/v acetic acid was supplied by Department of Biochemistry, Faculty of Science, Chulalongkorn university, Thailand. Knittex CHN crosslinking agent, Knittex Catalyst MO and Ultratex FMW softener were obtained from Huntsman Co., Ltd. Alum (aluminium potassium sulfate, $AlK(SO_4)_2.12H_2O$) was supplied by Asia Pacific Specialty Chemicals Ltd., Thailand. Soaping agent, Lavenol PA, was supplied by Boonthawee Chemephan Co., Ltd. Other chemical reagents were of analytical grade and purchased from either Aldrich Chemical Company or Merck Ltd.

2.2 Natural Dye Extraction

The color components of each natural dye were extracted by boiling material in water for 1 hour and then filtered.

2.3 Chitosan treatment

Cotton fabrics were padded at 80%wpu (wet pick up) with a 1%w/v chitosan in 1%v/v acetic acid solution on a laboratory padding mangle, and then dried at 100°C for 3 min and cured at 150°C for 3 min in a laboratory mini dryer.

2.4 Dyeing without a mordant

The untreated and chitosan treated fabrics were dyed with natural dye solutions at 95°C for 45 min with a heating rate of 1°C/min and then cooled to 60°C. The dyeings were carried out in a DaeLim Starlet II infrared lab dyeing machine at a liquor ratio of 1:30. The dyed fabrics were successively rinsed with water, soaped with 2 g/L Lavenol PA at 50°C for 20 min, washed with water, squeezed and air-dried.

2.5 Dyeing with mordants

The three mordanting methods used were pre-mordanting, meta-mordanting and post-mordanting. Alum mordant concentration of 5%owf (on the weight of fabric) were used and mordantings were performed using DaeLim Starlet II infrared lab dyeing machine at a liquor ratio of 1:30.

For the pre-mordanting method, the fabrics were first immersed in an aqueous solution of alum at 60°C for 45 min. The pre-mordanted fabrics were then dyed by the above dyeing method.

In the meta-mordanting method, the fabrics were immersed in a dyebath containing alum and the dye extract and then dyed as the same procedure.

For the post-mordanting method, the fabrics were first dyed in the absence of alum mordant, followed by mordanting in a separate bath containing alum solution at 60°C for 45 min. The dyed fabrics were later rinsed, soaped, washed with water, squeezed and air-dried.

2.6 Crosslinking treatment

Some of the dyed fabrics was padded at 80%wpu with a mixture of 50 g/L Knittex CHN, 14 g/L Knittex catalyst MO and 25 g/L Ultratex FMW. After padding, the samples were dried at 110°C for 3 min and cured at 150°C for 4 min.

2.7 Testing and Measurements.

The color strength (K/S value) and CIE whiteness index of the fabrics were evaluated using Datacolor 650 spectrophotometer with illuminant D65 at 10 degree observer. The K/S value is a function of color depth and is calculated by the Kubelka-Munk equation, $K/S = (1-R)^2/2R$, where R is the reflectance of the dyed fabrics. The color fastness to washing, light and crocking of the dyed samples was determined according to ISO 105-C01:1989, ISO 105-B02:1994 and AATCC Test Method 8-2005, respectively. The stiffness values of the dyed fabrics were assessed for the warp and weft directions using ASTM D 1388-96.

3. Results and Discussion

The K/S values, color fastness to washing, light and crocking and stiffness results of cotton fabrics dyed with lac and neem tree bark are presented in Tables 1

and 2, respectively. It is clear that the K/S values of the lac dyed fabric pre-mordanted with alum was higher than the corresponding unmordanted sample, while alum mordanting increased K/S values of fabrics dyed with neem tree bark, irrespective of mordanting method. This was due to the ability of mordant to form an insoluble complex with the dye on the substrate, resulting in greater dye absorption [1]. Furthermore, additional chitosan treatment along with alum mordanting gave considerably higher K/S values. The highest K/S values of 6.44 and 3.78 was observed for lac dyed fabric with alum meta-mordanting and neem tree bark dyed fabric with alum post-mordanting, respectively. It is known that chitosan not only provides more dye sites on cellulosic fibers via its cationic characteristic, but it also binds metal ions, which in turn act as a bridge between chitosan and fiber [10].

However, both the untreated and chitosan treated fabrics dyed with lac in the presence or absence of alum mordant exhibited very poor to poor color fastness to washing with the grey scale ratings for color change from 1 to 1-2. In case of neem tree bark dye, the washing fastness was generally fair to good (3, 3-4). The different behavior in color yield and color fastness properties between lac dye and neem tree bark dye may be attributed to their distinct chemical dye structures. The major component of lac dye is based on hydroxy anthraquinone carboxylic acids, while neem tree bark dye is mainly composed of tannin and flavonoids [11,12].

A noticeable improvement in color fastness to washing occurred when a crosslinking treatment with Knittex CHN, a commercial alkyl modified melamine resin, was given to the dyed fabrics. Fair to very good (3, 3-4, 4-5) was obtained for lac dye, and good to very good (4, 4-5) for neem tree bark dye. There was almost no color staining on adjacent cotton and wool fabrics during washing test.

All lac and neem bark tree dyed fabrics showed mostly fair to good (3, 3-4, 4) light fastness property. In view of color fastness to wet and dry crocking of lac dyed fabrics, good to very good (4, 4-5) was observed for the chitosan untreated samples mordanted with alum, whereas only very poor to poor (1-2) wet crocking and fair to good (3, 3-4) dry crocking was obtained for the corresponding chitosan treated samples with or without alum mordanting. The decrease in the crocking fastness may be due to higher surface dyeing with chitosan treatment. Similar results were noticed for neem tree bark dye, especially on wet crocking of the chitosan treated fabrics, which had the rating scales of poor to fair (2-3), compared to fair to good (3-5) of the untreated fabrics.

As shown in Figures 1 and 2, the stiffness results of dyed fabrics also indicated that the treatment of chitosan on cotton before dyeing caused an increase in stiffness, especially on the warp direction. This could be a result of film formation of chitosan. This increase in stiffness was more pronounced when a crosslinking treatment with Knittex CHN was carried out. In addition, yellowing occurred with chitosan treatment

on cotton fabrics as indicated by a reduction in whiteness index from 57.33 to 50.90.

4. Conclusions

It has been demonstrated that chitosan pretreatment and alum pre-mordanting could be used to enhance the dyeability of cotton fabrics with natural dyes from lac and neem tree bark. Chitosan treated fabrics with alum meta-mordanting produced maximum K/S values for lac dye, while those with alum post-mordanting in case of neem tree bark. Aftertreatment with a crosslinking agent was necessary in order to achieve acceptable wash fastness ratings. Several drawbacks must be concerned in this research, that is, an increased in stiffness and relatively low color fastness to wet crocking of the chitosan treated dyed fabrics.

References

[1] H.T. Deo and B.K. Desai, *J.S.D.C.*, **115** (1999) 224-227.

[2] H.T. Lokhande and V.A. Dorugade, Am. *Dyestuff Reporter*, **88** (1999) 29-34.

[3] S. Lim and S.M. Hudson, *Carbohydr. Res*, **339** (2004) 313-319.

[4] Y. Shin and D.I. Yoo, *J. Appl. Polym. Sci.*, **67** (1998) 1515-1521.

[5] M. Yen, *J. Appl. Polym. Sci.*, **80** (2001) 2859-2864.

[6] A. Abou-Okeil and O.A. Hakeim, *Color. Technol.*, **121** (2005) 41-44.

[7] O.A. Hakeim, A.Abou-Okeil, L.A.W. Abdou and A. Waly, *J. Appl. Polym. Sci.*, **97** (2005) 559-563.

[8] C. Suitcharit, F. Awae, W. Sengmama and K. Srikulkit, *Chiang Mai J. Sci.*, **38** (2011) 473-484.

[9] P. Kampeerapappun, T. Phattararittigul, S. Jittrong and D. Kullachod, *Chiang Mai J. Sci.*, **38** (2010) 95-104.

[10] S. Saxena, V. Iyer, A.I. Shaikh and V.A. Shenai, *Colourage*, **87** (1997) 23-28.

[11] M. Chairat, V. Rattanaphani, J.B. Bremner, S. Rattanaphani and D.F. Perkins, *Dyes Pigm.*, **63** (2004) 141-150.

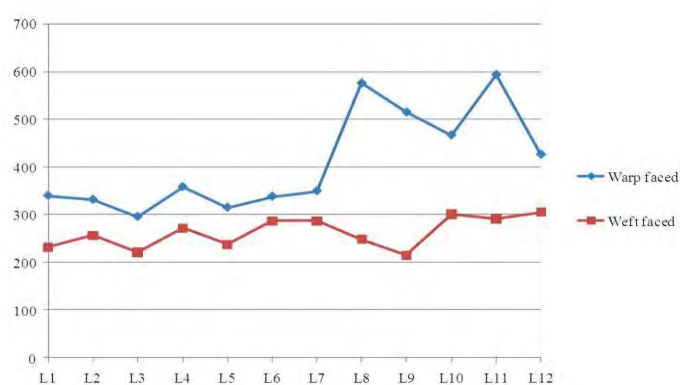[12] http://www.neemfoundation.org/neem-articles/ (Retrieved February 18, 2013).

Figure 1. The stiffness of cotton fabrics dyed with natural dyes from lac: (L1) Blank, (L2) Alum pre-mordanting, (L3) Alum meta-mordanting, (L4) Alum post-mordanting, (L5) Chitosan, (L6) Chitosan + alum pre-mordanting, (L7) Chitosan + alum meta-mordanting, (L8) Chitosan + alum post-mordanting, (L9) Chitosan + Knittex, (L10) Chitosan + alum pre-mordanting + Knittex, (L11) Chitosan + alum meta-mordanting + Knittex, (L12) Chitosan + alum post-mordanting + Knittex.
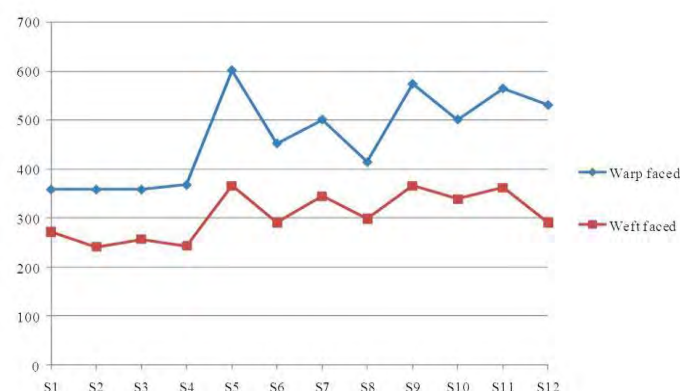

Figure 2. The stiffness of cotton fabrics dyed with natural dyes from neem tree bark: (S1) Blank, (S2) Alum pre-mordanting, (S3) Alum meta-mordanting, (S4) Alum post-mordanting, (S5) Chitosan, (S6) Chitosan + alum pre-mordanting, (S7) Chitosan + alum meta-mordanting, (S8) Chitosan + alum post-mordanting, (S9) Chitosan + Knittex, (S10) Chitosan + alum pre-mordanting + Knittex, (S11) Chitosan + alum meta-mordanting + Knittex, (S12) Chitosan + alum post-mordanting + Knittex

Table 1: *K/S* values and fastness properties of cotton fabrics dyed with natural dye from lac
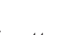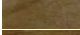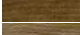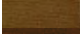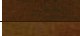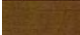
Chitosan treatment	Alum mordanting Methods	After treatment	Sample	*K/S*	Wash fastness			Light fastness	Crocking fastness	
					Color change	Color staining		Color change	Color staining	
						Cotton	Silk		Wet	Dry
-	-	-		0.40	1	4-5	4-5	4	3-4	4-5
-	pre-mordanting	-		1.21	1-2	4-5	4-5	4	4	4
-	meta-mordanting	-		0.21	1-2	4-5	4-5	4	4-5	4-5
-	post-mordanting	-		0.48	1-2	4-5	4-5	4	4-5	4
chitosan	-	-		2.69	1	4-5	4-5	4	1	3
	pre-mordanting	-		5.41	1-2	4-5	4-5	2	2	4
	meta-mordanting	-		6.44	1	4-5	4-5	2	1-2	3
	post-mordanting	-		3.85	1	4-5	4-5	3	1-2	4
chitosan	-			2.47	3-4	4-5	4-5	4	1	2-3
	pre-mordanting	Knittex CHN		5.83	4-5	4-5	4-5	3	1-2	2-3
	meta-mordanting			6.84	2-3	4-5	4-5	3	1-2	3
	post-mordanting			3.85	3	4-5	4-5	3	1-2	2-3

Table 2: *K/S* values and fastness properties of cotton fabrics dyed with natural dye from Siamese neem tree bark

Chitosan treatment	Alum mordanting Methods	After treatment	Sample	*K/S*	Wash fastness			Light fastness	Crocking fastness	
					Color change	Color staining		Color change	Color staining	
						Cotton	Silk		Wet	Dry
-	-	-		1.09	3	4-5	4-5	3	4	4-5
-	Alum pre-mordanting	-		1.19	3-4	4-5	4-5	3	4-5	5
-	Alum meta-mordanting	-		1.72	3	4-5	4-5	3	3	4-5
-	Alum post-mordanting	-		1.46	3-4	4-5	4-5	3	3-4	4-5
chitosan	-	-		2.90	3-4	4-5	4-5	2-3	2-3	4-5
	Alum pre-mordanting	-		3.22	4-5	4-5	4-5	3	2	4-5
	Alum meta-mordanting	-		2.96	2-3	4-5	4-5	3	2	3-4
	Alum post-mordanting	-		3.78	4	4-5	4-5	3	2-3	4-5
chitosan	-			3.39	4	4-5	4-5	3	2-3	4
	Alum pre-mordanting	Knittex CHN		3.49	4-5	4-5	4-5	3	2-3	4-5
	Alum meta-mordanting			3.43	4	4-5	4-5	3-4	2-3	4-5
	Alum post-mordanting			3.91	4	4-5	4-5	3-4	2-3	4

SYNTHESIS AND CHARACTERIZATIONS OF CdS/ZnO NANOCOMPOSITE PHOTOCATALYSTS

Potjanaporn Chaengchawi[1,2], Karn Serivalsatit[1,2], Yoshio Nosaka[3], and Pornapa Sujaridworakun[1,2*]

[1] Research Unit of Advanced Ceramics, Department of Materials Science, Faculty of Science, Chulalongkorn University, Bangkok, 10330, Thailand
[2] Center of Excellence on Petrochemical and Materials Technology, Chulalongkorn University, Bangkok 10330, Thailand
[3] Nagaoka University of Technology, Kamioka, Nagaoka, Niigata 940-2188, Japan

[*] Author for correspondence; *E-mail: pornapa.s@chula.ac.th

ABSTRACT **Visible light responsive CdS/ZnO nanocomposite photocatalysts were successfully synthesized by precipitation method. Firstly, the plate-like ZnO nanoparticles were synthesized by precipitation using $Zn(NO)_3$ and NaOH. Then, the CdS/ZnO nanocomposites were prepared by coating the obtained ZnO with CdS prepared by the use of $Cd(NO_3)_2$ and Na_2S. The nanocomposites were characterized by X-ray Diffraction (XRD), scanning electron microscope (SEM), Brunauer Emmett Teller method (BET), and UV-Vis reflectance spectroscopy. The photocatalytic activity of the nanocomposites was investigated by the photodegradation of methylene blue solution under visible light irradiation. It was shown that the UV-Vis absorbance of the nanocomposites shifted toward higher wavelengths compared with pure ZnO. The photocatalytic activities of CdS/ZnO nanocomposites were compared with the as-prepared CdS and ZnO. The CdS/ZnO nanocomposite with the mole ratio of 1:3 exhibited higher photocatalytic activity than that of pure ZnO and CdS under visible light irradiation.**

1. Introduction

ZnO have been interested due to their widely applications as optical, electrical device, and photocatalyst [1]. ZnO is photocatalyst semiconductor which has widely band gap energy 3.2 eV, high UV absorption, high refractive index, high electron mobility, chemical inert, and non-toxic [2,3]. However, the relatively wide band gap limits its application only in the UV-light region. Moreover, the ZnO photocatalytic activity remains low because of the e-h recombination. Thus it is interesting to develop photocatalyst materials which extend the absorption wavelength into visible-light region. Many approaches have been reported, for example, doping transition metal ions such as Ni, Cr, Fe, and Cu. It was demonstrated that TiO_2 doped by nitrogen [4,5], and Fe(III) doping on WO_3 showed the high activity in visible-light [6]. Another approach is to introduce the composite system by coupling with a narrow band gap semiconductor such as ZnS/ZnO [7], CdS/TiO_2 [8], CdS/ZnO [9-11] and CdSe/ZnS [12].

CdS is a semiconductor which directs band-gap energy 2.4 eV is normally used in visible-light. It is widely applied in various applications for example, solar cell device, gas sensors and light-emitting device [13-15].

In this work, we aimed to synthesis of CdS/ZnO nanocomposite by precipitation method to enhance the the photocatalytic activity in visible light region of ZnO. The obtained samples were investigated for photocatalytic efficiency by the photo degradation of methylene blue solution under visible light irradiation.

2. Materials and Methods

2.1 Preparation of CdS/ZnO nanocomposite

To synthesize ZnO particle, 0.3 M of zinc nitrate $(Zn(NO_3)_2)$ and 5M of sodium hydroxide (NaOH) were used as starting materials. Firstly, the NaOH solution was dropped into $Zn(NO_3)_2$ solution with continuous stirring at 50 ^{o}C for 5h. The obtained precipitant was centrifuged and washed by distilled water and absolute ethanol several times, and dried at 80 ^{o}C for 12 h.

Then, the CdS/ZnO nanocomposite with mole ratio of CdS:ZnO at 1:3 was prepared by dispersing the as-prepared ZnO powders in 30 mL of $Cd(NO_3)_2$ solution for 10 min. After that, 30 mL of Na_2S solution was dropped into the suspension with continuous stirring at room temperature for 2 h. The final product was separated by centrifuged, washed with distilled water and absolute ethanol several times, and dried at 80 ^{o}C for 12 h.

2.2 Characterization of samples

The crystalline phases of samples were investigated by X-ray diffraction (XRD, D8-Advanced, Bruker) was used with Cu-K_α radiation. The morphology of samples were observed by scanning electron microscopy (SEM, JSM 6480LV, JEOL). The specific surface area determined by using Bruner Emmett Teller (BET), and the absorption spectra of samples were record by using UV-VIS-NIR spectrophotometer (SHIMADZU UV–3150).

2.3 Photocatalytic activity measurement

The photocatalytic activity of ZnO, CdS and CdS/ZnO composite were evaluated by photo degradation of methylene blue solution under simulated visible light using fluorescence lamp covered with UV filter. 0.02 g of sample and 20 ml of methylene blue solution with initial concentration of 0.02 mM were used. The suspension was first stirred

in the dark for 2 h to ensure adsorption/desorption equilibrium prior to irradiation. The irradiated suspensions were then centrifuged to separate the powder from the solution, and the clear solution was analyzed by measuring the absorbance at a wavelength of 664 nm using a UV–VIS spectrophotometer (Perkin Elmer instrument, Lambda 35).

3. Results and Discussion

Fig.1 Show XRD patterns of ZnO, CdS and CdS/ZnO composite samples. For pure ZnO, the diffraction peaks could be assigned to Hexagonal Zincite (JCPDS card no. 36-1451), corresponding to the (100), (002), (101), (102), (110), (103), (112) plane. The diffraction peaks of pure CdS could be assigned to Hexagonal Greenockite (JCPDS card no. 41-1049) corresponding to the (101), (110), (112) plane. In case of CdS/ZnO nanocomposite, the peak of ZnO can be assigned to Hexagonal Zincite as pure ZnO, and the peak of CdS can be assigned to Cubic (JCPDS card no. 89-0440) corresponding to the (111), (002), (101) plane. The relative intensity of diffraction peak of ZnO in nanocomposite decreased was due to amount of deposited CdS in nanocomposite.
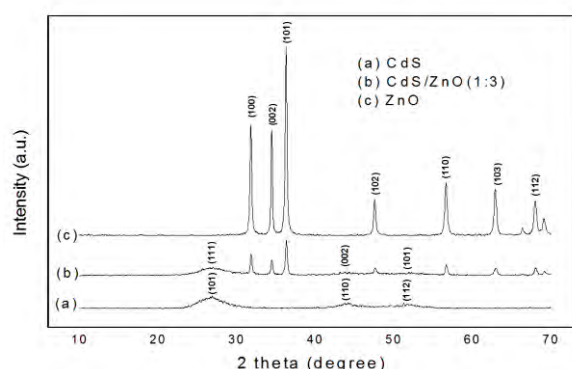
Fig.1 XRD patterns of (a) CdS, (b) ZnO, and (c) CdS/ZnO nanocomposite

Table 1. Shows specific surface area of pure ZnO, pure CdS and CdS/ZnO nanocomposite (1:3 mole ratio) which are 13.39 m^2/g, 93.15 m^2/g and 62.94 m^2/g, respectively. It indicated that CdS has the smallest particle size corresponding with the SEM image and characteristic peaks of XRD. ZnO has large particle with low surface area. When the ZnO particles were deposited by CdS, it resulted in high surface area of nanocomposite compared with that of the pure ZnO.

Table 1: Specific surface area of ZnO, CdS, and CdS/ZnO nanocomposite by BET

Sample	Surface area (m^2/g)
ZnO	13.39
CdS	93.16
CdS/ZnO (1:3)	62.94

Fig.2 shows SEM images of ZnO, CdS and CdS/ZnO nanocomposite, respectively. It was demonstrated in Fig.2a that ZnO particle has plate-like morphology. Fig 2b shows that CdS consisted of small spherical agglomerated particles. Fig.2c shows morphology of CdS/ZnO nanocomposite which mainly composed of plate-like ZnO and small amount of CdS particle deposited on the ZnO surface.
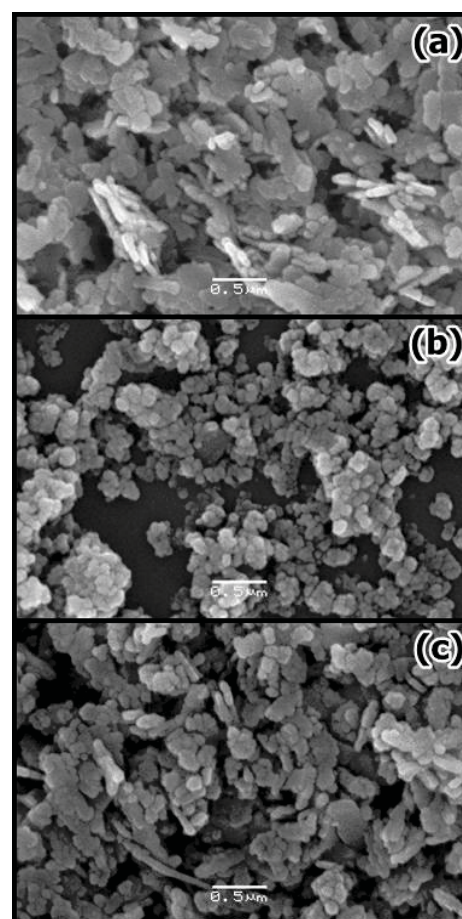
Fig.2 SEM images of of (a) ZnO, (b) CdS, and (c) CdS/ZnO nanocomposite

The UV-vis diffuse reflectance spectra of samples were shown in Fig.3. The spectrum of pure ZnO shows strong absorption of UV-light with wavelength lower than 400 nm and it has no remarkable absorption of visible light with wavelength above 400 nm. Whereas, the pure CdS has strong absorption spectrum in wavelength of visible-light (at about 500 nm.) corresponding to its energy band gap (2.4 eV). The spectrum of CdS/ZnO nanocomposite shows two characteristic absorption edges which could be confirmed that the composite is composed of ZnO and CdS, and the absorption spectra was obviously extended into visible region.
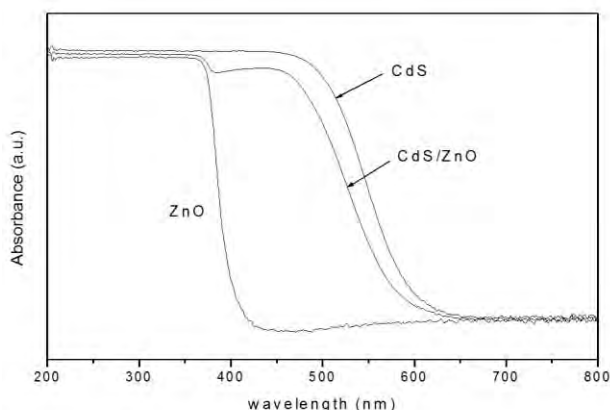
Fig.3 UV-Vis absorption spectra of of ZnO, CdS, and CdS/ZnO nanocomposite

The photocatalytic activity for degradation of methylene blue solution evaluated under visible-light was shown in Fig.4. It is obviously demonstrated that the pure ZnO had no photocatalytic activity, the photocatalytic degradation performance is only 8.07% at final irradiation due to it did not respond for visible light absorption. While, CdS showed photocatalytic activity after visible light irradiation. It can be seen that the maximum photocatalytic performance at 85.6 % was found in CdS/ZnO nanocomposite which was slightly higher than that of CdS with 78.6% of degradation. This could be attributed to the suppression of e-h recombination which has been described by previous reported [10].
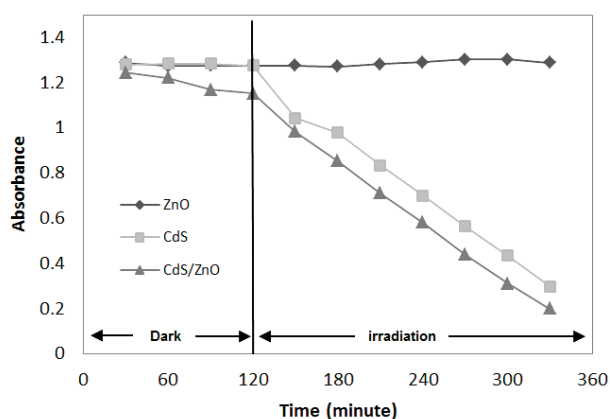
Fig.4 photocatalytic activity of ZnO, CdS, and CdS/ZnO nanocomposite.

The enhancement in photocatalytic efficiency of CdS/ZnO composite under visible light could be described by the charge transfer diagram shown in Fig. 5. When CdS/ZnO composite was activated by visible light, e-h pairs were generated in CdS, the electron in conduction band of CdS could be transferred to the conduction band of ZnO, which suppressed the recombination of e-h pair before they recombine.
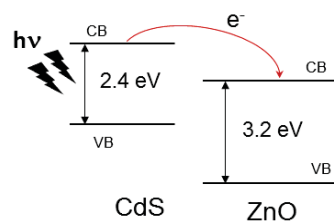
Fig.5 Charge transfer diagram of CdS/ZnO nanocomposite

4. Conclusions

Visible light responsive CdS/ZnO nanocomposite photocatalysts were successfully synthesized by precipitation method. The coupling of ZnO with CdS could extend the absorption of composite into visible wavelength region. The CdS/ZnO (1:3) nanocomposite showed higher photocatalytic activity than that of pure CdS and ZnO under visible light irradiation.

Acknowledgements

References

[1]   A. Moezzi, A. M. McDonaghandM. B. Cortie, *Chem. Eng. J.* **185–186** (2012) 1-22.
[2]   B. LiandY. Wang, *J. Phys. Chem. C* **114** (2009) 890-896.
[3]   X. Su, H. Zhao, F. Xiao, J. JianandJ. Wang, *Ceram. Int.* **38** (2012) 1643-1647.
[4]   D. Nassoko et al., *J. Alloys Compd.* **540** (2012) 228-235.
[5]   H. Diker, C. Varlikli, K. MizrakandA. Dana, *Energy* **36** (2011) 1243-1254.
[6]   A. Hameed, M. A. GondalandZ. H. Yamani, *Catal. Commun.* **5** (2004) 715-719.
[7]   H. X. Sang, X. T. Wang, C. C. FanandF. Wang, *Int. J. Hydrogen Energy* **37** (2012) 1348-1355.
[8]   S. Yamada, A. Y. NosakaandY. Nosaka, *J. Electroanal. Chem.* **585** (2005) 105-112.
[9]   S. Yan et al., *J. Alloys Compd.* **509** (2011) L239-L243.
[10]   B. LiandY. Wang, *J. Phys. Chem. Solids* **72** (2011) 1165-1169.
[11]   T. Bora, H. H. KyawandJ. Dutta, *Electrochim. Acta* **68** (2012) 141-145.
[12]   Z. Wu et al., *Colloids Surf A Physicochem Eng Asp* **350** (2009) 121-129.

[13]   S. Yan et al., *J. Solid State Chem.* **182** (2009)
        2941-2945.
[14]   V. Singh, P. K. SharmaandP. Chauhan,
        Mater. Charact. **62** (2011) 43-52.
[15]   P. Nandakumar et al., *Mater. Sci. Eng., B* **83**
        (2001) 61-65.

SYNTHESIS AND MUTAGENICITY OF SILVER NANOPARTICLES WITH DIFFERENT SIZES AND SHAPES

Karaked Tedsree[1*], Wiranrat Tiyawat[2], Kittiya Ketaram[2], Chatchawin Phetlert[2]

[1]Department of Chemistry, Faculty of Science, Burapha University, Thailand
[2]Department of Biochemistry, Faculty of Science, Burapha University, Thailand
*E-mail: Karaked@buu.ac.th

Abstract: The rapid expansion of nanotechnology promises to have significant benefits to society, thus there is increasing concern that exposure to nanoparticles which may have negative impact on both human and ecology system. Due to well-known bactericide properties of silver nanoparticles, they are nowadays widespread use in consumer products. This research, we aim to study mutagenic effect of silver nanoparticles with different sizes and shapes using Ames/*Salmonella typhimurium* assay without metabolic activation. Ag nanoparticles with two different sizes in range of 10-25 nm and three different shapes (sphere, rod and plate) were obtained and characterized by Transmission electron microscopy (TEM). The mutagenicity test was carried out in the absence and presence of nitrite ion. The results were found to be negative in all tester strains of different sizes and shapes of nanoparticles In addition, dose-dependent manner was not observed in all experiments.

1. Introduction

Nanomaterials are defined as substances with at least one dimension in the 1-100 nm range. Because of their small size and high surface area, these materials can have drastically different properties than their corresponding bulk materials. Therefore, introduction of nanomaterials into the human environment may potentially result in adverse and unpredictable effect. From a regulatory standpoint, it is important to determine toxicity and genotoxicity to evaluate the safety of these nanomaterials.

Silver nanoparticles have emerged as an important class of nanomaterials for a wide range of industrial and medical applications. Their antibacterial activity of silver species has been well known since ancient times. However, the actual bactericide mechanism of silver nanoparticles is not well known. A number of studies have shown the idea that silver ion species released from surface atoms and interact with thiol groups in bacteria proteins, affecting the replication of DNA [1]. Some studies have shown that silver ion including silver nanoparticles can penetrate into cells or sub-cellular compartments and act as catalysts inducing reactive oxygen species (ROS), oxidative stress and DNA damage by direct interaction [2]. There have been reported confirm that the nanoparticle size, surface functionalization and surface structure are major factors that influence toxicity and genotoxicity [3]. The potency of silver in the form of nanoparticles to induce cell damage compared to silver ions is cell type and size-dependent. In addition, the environmental fate of silver nanoparticles will depend upon their surfaces which modified to prevent aggregation. Some types of silver nanoparticles are engineered to remain dispersed in water. These surface modifications can alter nanoparticle properties and their subsequent distribution in the organism. The size-dependent interaction of silver nanoparticles with gram-negative bacteria has been reported by many researchers [3, 4]. However, little is known about how the biological activity of silver nanoparticles changes as the shape of the particles changes. Silver nanoparticles can take many different shapes such as nanosphere, nanorod, nanowire and nanoplate. The shape-dependent interaction with the gram-negative bacterium *Escherichia coli (E. coli)* has been reported [5]. Truncated triangular silver nanoplates with a (111) lattice plane as the basal plane displayed the strongest biocidal action, compared with spherical and rod-shaped nanoparticles and with silver ion (in the form of $AgNO_3$). The combination of nanoscale size and the presence of a (111) plane promote this biocidal property.

There is only a limited amount of data relating to the mutagenicity of nanoparticles when their shape and size are changed. For this reason, we investigated the size and shape dependence on the genotoxicity of silver nanoparticles using the *Salmonella* reverse mutation assay (Ames test). This test utilized 2 different tester strains of *Salmonella typhimurium* (TA98 and TA100) to determine the gene mutation. To our knowledge, this is the first comparative study on the genotoxicity of silver nanoparticles of different shapes.

2. Materials and Methods

2.1 Materials

The metal precursor used to synthesize colloidal silver was silver nitrate ($AgNO_3$). Reagent-grade ethylene glycol (Aldrich) and dimethyl formamide (DMF, Labscan) were used as solvent and reducing agent. Poly(vinylpyrrolidone) (PVP, Aldrich, Mw = 10000) was used as a capping agent. All reagents were used without any further purification.

2.2 Methods

2.2.1 Preparation of PVP-Ag Nanoparticles

Silver nanosphere:
The synthesis was carried out according to a previously reported procedure with some modifications [6]. In general, 0.24 g of PVP and 0.034 g of $AgNO_3$ were dissolved in 30 mL of ethylene glycol under stirring. The solution was heated up to

120 °C at a constant rate of 7 °C per min. A clear yellow solution of colloidal PVP-Ag nanoparticles was obtained after an hour. The colloidal PVP-Ag nanoparticles can be separated by addition of acetone followed by centrifugation.

Silver nanorod:

The synthesis was carried out according to a previously reported procedure with some modifications [7]. Typically, 15 mL of 6×10^{-4} M $FeCl_3$ solution in ethylene glycol was heated to 160 °C for 15 min, and then 15 mL of 6 M $AgNO_3$ in ethylene glycol solution including 0.15g of PVP was poured into the hot solution. The reaction mixture was kept at 160 °C. A gray solution of colloidal PVP-Ag nanorod was obtained after 1.5 h.

Silver Nanoplate:

Silver nanoplates were prepared by using dimethylformamide as a solvent and as a reducing agent. In a typical synthesis, 0.10 g of PVP was dissolved in 25 mL of dimethylformamide then 0.021 g. of $AgNO_3$ was introduced in the solution. The homogenous mixture was refluxed at 130 °C for 1 h. A red solution of colloidal PVP-Ag nanoplates was obtained after 1 h.

2.2.2 Characterization of Ag nanoparticles

The particle size, shape and distribution of silver nanoparticles were determined by transmission electron microscope (TEM) (ECNAI 20, Philips, Japan). The silver nanoparticles were homogeneously dispersed in ethanol, and one drop of the suspension was deposited on a TEM grid and dried at room temperature. UV–visible spectroscopy was performed using a Lambda 45 UV/Vis spectrophotometer (Agilent Technology).

2.2.3 Bacterial tester strains

Salmonella typhimurium tester strains are histidine dependent strains (His⁻) TA98 and TA100 that were capable of detecting the frameshift and base-pair substitution mutations, respectively. Cultures were stored at -80 °C until use. Each overnight culture of TA98 and TA100 isolated from the frozen permanents was inoculated into Oxoid nutrient broth No.2 and was incubated at 37 °C in a shaking water bath. Manipulation of the cultures was performed according to Maron and Ames [8].

2.2.4 Mutagenicity testing

The pre-incubation method was used throughout this study. For the determination of direct mutagenicity, an aliquot of silver nanoparticles with and without $NaNO_2$ was mixed with phosphate buffer, pH 7.4 and fresh overnight culture, and then incubated at 37 °C for 20 min. Later, the molten top agar (45 °C) was added, mixed well and poured onto a minimal glucose agar plate. The plate was incubated at 37^0C for 48 h. Induced His⁺ revertant colonies were counted and compared to the established spontaneous mutation. The positive controls employed for the assay were 1-nitropyrene (1.42 g/plate for TA98 and 0.72 g/plate for TA100). The test compound will be considered to have mutagenic potential if it is able to cause mutations that allow the bacterium to revert back its histidine synthesis ability. For the Ames assay, positive responses required a dose-related increase in the number of revertant colonies/plate at least twice compare to spontaneous mutation. Negative was defined as no dose-related increase in the number of revertant colonies. Three replicates were conducted for each dose group and three independent assays were performed for statistical analysis. Statistical analysis was performed using SPSS program version 11.5. All analyses were two-tailed, and $P < 0.05$ was used to identify statistically significant differences.

3 Results and Discussions

3.1 Synthesis and Characterization

Polymer-protected colloidal silver nanoparticles (PVP-Ag) were synthesized by polyol process. Silver ions as a metal precursor were reduced by ethylene glycol in the presence of PVP. The main role of PVP is preventing silver nanoparticles from aggregation by steric effect arising from the long vinyl chain on the surface of particles [6]. The obtained silver nanoparticles coated with PVP can be homogeneously redispersed in polar solvents such as water and ethanol.

Controlling the size and shape of metal nanostructures is a promising strategy to tailor their physical and chemical properties. Size controlled silver nanoparticles can be synthesized by varying reaction parameters such as reaction temperature, reaction time, concentration of metal precursor and ratio of metal precursor to capping agent [6,9]. In this work, different sizes of silver nanospheres were controlled synthesized by varying the molar ratio of the silver ion precursor to PVP. TEM images of silver nanoparticles obtained at different ratios of silver ion : PVP are shown in Fig. 1
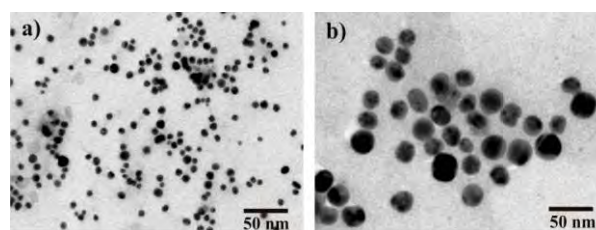
Figure.1 TEM images of different sizes of silver nanospheres prepared with different ratios of Ag+: PVP 1a) 1:20 and 1b) 1:10.

From Fig. 1, the obtained PVP-Ag nanoparticles are near monodispersed with particle size deviation of less than 20%. The amount of capping agent was found to control the final particle size and size distribution of the particle. It is clearly showed that the particle size of nanoparticles increases by decreasing molar ratio of PVP.

Different chemical and physical properties of metallic crystals arise from different crystal surface orientation. Therefore, the controllable preparation of nanocrystals with different shapes and exposed surfaces is very important and challenging. In this work, different shapes of silver nanoparticles were also prepared. TEM images of silver nanorods and nanoplates are shown in Fig. 2
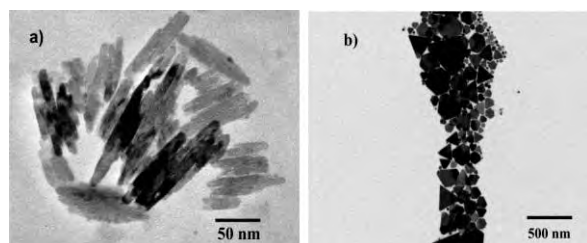

Figure 2. TEM images of silver nanoparticles a) nanorod and b) nanoplate

Nanorods (Fig 2a) were obtained by hot injection method at high temperature (160 °C). At this temperature, silver ions were reduced rapidly to form silver atoms at high rate. According to the thermodynamics growth, face-centered cubic (FCC) crystal structure of silver metal favorably multiply twinned seeds which can further growth to nanorod or nanowires. In addition, adding small amount of $FeCl_3$ was found effect to shape control of silver nanoparticles. Xia and co-workers [10] reported that, Iron ions facilitated the growth of multiply twinned seeds to form nanorod by removing oxygen from the surface of twinned seeds and preventing their dissolution by oxidative etching. Nanoplates were obtained at slower reaction rate. Due to these particles consist of high surface atoms which results in high total surface energy. Thus, the preparation method needs kinetics control. In this work, nanoplates were prepared at lower temperature (130 °C) in the presence of weaker reducing agent (DMF) compared to ethyleneglycol. It was found that the reaction rate could be controlled for the formation of nanoplates with higher yields.

One of the most interesting aspects of Ag nanoparticles is that their optical properties (surface plasmon resonance) depend strongly upon the particle size and shape [11]. Bulk Ag metal is white color in reflecting light while Ag nanoparticle is yellow. In addition, the specific geometrical shapes also give distinct spectral responses. The absorption spectrum of silver nanospheres, nanorods and nanoplates are shown in Fig 3.
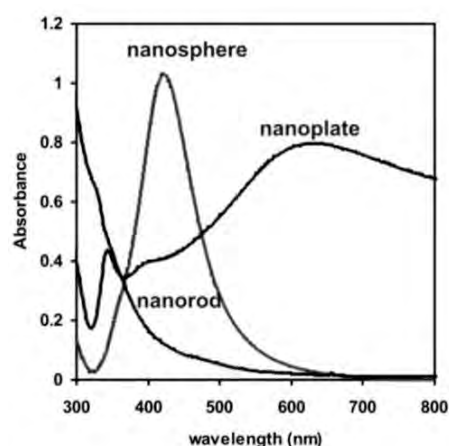
Figure 3. Absorption spectra of silver nanoparticle : nanosphere nanorod and nanoplate.

Table 1: Particle size and optical property of Ag nanoparticles.

PVP-Ag nanoparticles	Color in ethanol	Absorption peak (nm)
Nanosphere (10.0±1.2 nm)	bright yellow	410
Nanosphere (25.3±2.1 nm)	bright yellow	420
Nanorod (50-300 nm)	gray	-*
Nanoplate width 5.3±1.2 nm length 75±10 nm	red-purple	350, 500-600

* no absorption peak in visible range

3.3 Mutagenicity of Silver Nanoparticles

A bulk material should have constant physical and chemical properties regardless of its sizes, but size-dependent properties are often found in nanomaterials. In this work, decreasing the particle size to nanoscale ensuring a significantly large surface area of the particles is in contact with the bacterial effluent. However, the results in Fig. 2 showed that their mutagenic activity did not markedly increase more than twice in comparison to the spontaneous revertants both in *Salmonella typhimurium* TA98 and TA100. Moreover, most nitrite-treated silver nanoparticles did not show the mutagenic effect on both tester strains in the absence of metabolic activation in acidic condition. Dose-dependent manner was not observed in all experiments.

The results from Fig. 2 indicated that decreasing the particle size from 25 nm to 10 nm does not make a significant increase in the His+ revertants. This result was consistent with previous reports indicating that nanoparticles are Ames negative [12] or weakly positive [13]. It has been suggested that the negative results may be due to the inability of the nanomaterials to penetrate the bacterial cell wall so the nanoparticles cannot enter bacterial cells to damage DNA and induce mutations. [14].

Table 2: Mutagenicity of silver nanoparticles with different sizes and shapes in *Salmonella typhimurium* tester strains

Ag nano particle	Dose (µg/plate)	Number of colonies/plate			
		T98		T100	
		without NO₂⁻	*with NO₂⁻	without NO₂⁻	*with NO₂⁻
spontaneous mutation	-	16±2	16±3	67±7	67±7
sphere (10nm)	0.0022	16±3	17±3	65±6	68±4
	0.0220	18±3	18±4	69±9	69±7
	0.2200	16±5	9±1	70±3	71±6
sphere (25nm)	0.0022	18±4	14±6	68±7	71±5
	0.0220	13±2	18±1	66±1	66±0
	0.2200	21±3	13±8	68±6	68±4
rod	0.0022	14±2	12±6	72±4	62±11
	0.0220	17±5	10±5	68±6	71±5
	0.2200	16±4	12±1	65±3	69±6
plate	0.0022	22±2	9±1	57±7	72±5
	0.0220	15±2	14±6	78±1	74±9
	0.2200	16±2	15±1	68±4	64±7
positive control	0.72	-	-	705±11	697±21
	1.42	424±11	417±16	-	-

* 0.1725 g /plate

As the results in Fig. 2, we have not found that silver nanoparticles undergo shape-dependent interaction affected to genotoxicity with the frameshift and base-pair substituted mutations. Although, we expected that silver nanoparticles with different shapes may also have different effective surface areas in terms of active facets. For spherical nanoparticle, generally cubooctahedral shape, their surface contains different (100) and (111) facets with different ratio depend on their sizes. The surfaces of nanorods are bound by (100) and the ends by (111) facets while nanoplates contained (111) on the basal plane. For the FCC crystal structure, (100) plane with surface more unsaturated has higher surface energy than saturated (111) plane. The relationship between shape and mutagenicity could be considered in term of surface energy and surface selectivity. In case of nanoparticles could not penetrate into cells, it was expected that high surface energy of (100) facet in nanorod should has higher potential to get oxidize into silver ion when they come into contact with cells. From the results, the significant difference was not shown in any shapes. In the case of the nanoparticles can penetrate into cells, their surface selectivity to the active element groups on cell components should be concerned. As the result, markedly increase more than twice in comparison to the spontaneous revertants was not found both in *Salmonella typhimurium* TA98 and TA100. However, there has been reported that truncated triangular silver nanoplates with a (111) basal plane displayed the strongest biocidal action, compared with spherical and rod-shaped nanoparticles.[5] Perhaps, it may be necessary to determine the genotoxicity with other methods such as *rec* assay, micronucleus assay, sister chromatid exchange or chromosome aberration in order to confirm our results.

4. Conclusions

Bacterial mutagenicity was assessed in *Salmonella typhimurium* tester strains TA98 and TA 100 for detection of frameshift mutation and base-pair substitution mutation. All different sizes and shapes of silver nanoparticles coated with PVP did not increase the mutant frequencies. Moreover, most nitrite-treated silver nanoparticles did not show the mutagenic effect on both tester strains in the absence of metabolic activation in acidic condition.

Acknowledgements

References

[1] M. Marini, N. de Niederhausern, R Iseppi, M. Bondi, C. Sabia, M. Toselli, F. Pilati, *Biomacromol*. **8** (2007) 1246–1254.

[2] K.B. Holt, A.J. Bard, *Biochem.,* 44 (2005) 13214–13223.

[3] M.V.D.Z. Park, A.M. Neigh, J.P. Vermeulen, L.J.J. de la Fonteyne, H.W. Verharen, J.J. Briede, H.V. Lovern, W.H. de Jong, *Biomat.,* **32** (2011) 9810-9817.

[4] G.A.M. Castan˜o´n, N.N. Martı´nez, F.M. Gutierrez , J.R.M. Mendoza, F. Ruiz, *J. Nanopart. Res*. **10** (2008) 1343–1348.

[5] S. Pal, Y.K. Tak, J.M. Song, *App. Environ. Microbiol*. (2007) 1712–1720.

[6] P.Y. Silvert, R.H. Urbina, N. Duvauchelle, V. Vijayakrishnan, K.T. Elhsissen, *J. Mater. Chem. 6(4)* (1996) 573-577.

[7] J. Jiu, K. Murai, D. Kim, K. Kim, K. Suganuma, *Mat. Chem. Phys*. **114** (2009) 333–338.

[8] D.M. Maron, B.N. Ames, *Mutat. Res.* **113** (1983) 173-215.

[9] P.Y. Silvert, R.H. Urbinab, K.T. Elhsissena, *J. Mater. Chem.* **7(2)** (1996) 573-577.

[10] B. Wiley, Y. Sun, Y. Xia, *Acc. Chem. Res. 40* (2007) 1067–1076

[11] J. Zhang, X. Li, X. Sun, Y. Li. *J. Phys. Chem. B,* **109 (**2005) 12544-12548.

[12] Y. Nakagawa, S. Wakuri, K. Sakamoto, N. Tanaka, *Mutat. Res.* **394** (1997) 125–132.

[13] S. Maenosono, R. Yoshida, S. Saita, J. *Toxicol. Sci.* **34** (2009) 349–354.

[14] R. Landsiedel, M. D. Kapp, M. Schulz, K. Wiench, F. Oesch, *Mutat. Res.* **681** (2009) 241–258.

PHOTOCATALYTIC ACTIVITIES OF TITANIUM DIOXIDE BLENDED WHITE CEMENT COATED ON SUBSTRATE

Pullawit Lousuphap[1], Nuttapun Sirikawinkobkul[1], Withaya Panpa[2], Chatvalee Kalambhaheti[3],Supatra Jinawath [1],Sirithan Jiemsirilers[1, 4], and Dujreutai Pongkao Kashima[1, 4]*

[1] Research Unit of Advanced Ceramics, Department of Materials Science, Faculty of Science, Chulalongkorn University, Patumwan, Bangkok 10330, Thailand.
[2] Faculty of Industrial Technology,Thepsatri Rajabhat University
[3] PTT Research and Technology Institute (PTT RTI), 71 Moo 2, Phaholyothin Rd., Km.78, Sanubtueb, Wangnoi, Ayutthaya 13170, Thailand.
[4] Center of Excellence on Petrochemical and Materials Technology, Chulalongkorn University, Patumwan, Bangkok 10330, Thailand.

*E-mail: dujreutai@gmail.com

Abstract: Coating of titanium dioxide (TiO_2 P-25) on various substrates always encounters a problem about the immobilization of catalyst particles. To overcome this problem and enhance the adhesion of P-25, a gold standard of TiO_2 photocatalyst, on substrate, white cement was selected to blend with P-25. In this research white cement provides a strong bonding between P-25 particles and substrate surface which is resulted from hydradation of the hardened cement, without extra treatments required. Samples were prepared via granulation process by coating of white cement on the substrate as the first layer, then curing in the air for 1 day. After that coating white cement mixed with 25 wt% TiO_2 P-25 was done as the second layer, then curing in air for 1 day and in water for another 3 days. The photocatalytic activities were measured spectrophotometrically through degradation of methylene blue (MB) and cumene hydroperoxide (CHP). The results of UV-Vis spectra indicated that the absorbance of the MB decreased 60%, while HPLC analysis confirmed that CHP concentration approximately decreased 70% after UV irradiation for 3h. This indicates that the prepared photocatalyst can potentially decompose the organic pollutants in wastewater, and is possible for better development.

1. Introduction

Of all the photocatalysts, TiO_2 is a viable photocatalyst in terms of activity, chemical inertness, photostability [1-3] and production cost. Its applications include self-cleaning [4], hydrogen production[5], degradation of organic compounds in wastewater, but in the powder form, it requires filtration to separate for reuse.

In recent years, there are many researchers tried to fixed TiO_2 on different types of supports, such as glass [6], polymers [7] and ceramics [8] by various methods including sol-gel [9], sputtering [10], chemical vapor decomposition [11] and spray pyrolysis [12]. However, the immobilization of TiO_2 on various support was still not strong enough and some methods

required advance technology which was too expensive for commercial purpose.

Therefore, many reserchers had studied mechanical properties, microstructures, and surface of cement mixed TiO_2 for photocatalytic degradation [13-15], but there were still some disadvantages about calcium from cement encountering in the active site of TiO_2.

In this research, white cement with high Al_2O_3 content was introduced to mix with TiO_2 P-25, in order to act as an adhesive between P-25 powder and the substrate. Optimization for appropriate amounts of white cement and P-25 and photocatalytic activity of TiO_2 blended white cement was studied.

2. Materials and Methods

2.1 Materials

White cement (AC, 80% Alumina, KERNEOS), TiO_2-P25 (75% anatase and 25% rutile, Degussa, Germany), Cumene hydroperoxiden (CHP, 80% $C_6H_5C(CH_3)_2OOH$, AR-Grade, Merck Chemical Co.), Methylene blue (MB, Merck Chemical Co.) and porous glass beads (EC, ECOLITE®, diameter ~ 3 mm) were used in this study.

2.2 Preparation of samples

Samples were prepared via granulation process by coating of white cement on the glass substrates as a first layer, then curing in air for 1 day. After that coating white cement mixed with 25 wt% and 50 wt% TiO_2-P25 was done as the second layer, then curing in air for 1 day and in water for another 3 days.

2.3 Sample characterization

Crystalline phases of the sample were identified by X-ray Diffractometer (XRD, Bruker, D8 Advance). The absorbance of MB over the spectrum range of 300-600 nm was determined with a UV-VIS Spectrophotometer (Perkins Elmer, Lambda 35). CHP concentrations were measured by High Performance

Liquid Chromatography (HPLC, HP HEWLETT PACKARD SERIES 1100), and column (Thermoscientific® Hypersil Gold particle size 1.9 μm diameter 3 mm).

2.4 Photocatalytic activity studies

The photocatalytic activities of the samples were measured through the decomposition of MB (0.02 mM, 10 mL) and CHP (initial concentration 230 ppm, 10 mL) under UV irradiation (Lamp: Philips TL-D 18 w). The light intensity between light source and samples was 2 mW/cm^2 and for each test, an average absorbance of 2 samples was taken.

3. Results and Discussion

3.1 XRD pattern of the samples
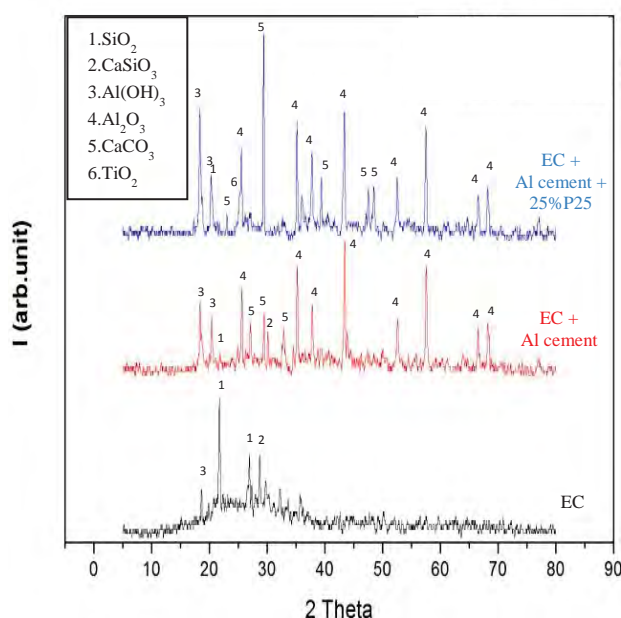
Figure1. XRD of EC glass substrate, coated with Al cement and with 25% TiO$_2$/Al cement.

XRD results of the samples before and after coating with TiO$_2$/Al cement shown in Figure 1 indicated that after coating, no reaction between TiO$_2$ and Al cement found, hence TiO$_2$ still can play a role as the photocatalyst. The peak match in XRD pattern of EC + cement + TiO$_2$ sample showed the phase of TiO$_2$ anatase as marked as number 6 in Figure 1. However, Ca(OH)$_2$ released from cement could react with CO$_2$ from the atmosphere to form CaCO$_3$ on the surface of EC substrate and might interfere with the active sites of the TiO$_2$, finally photocatalytic activity decreased.
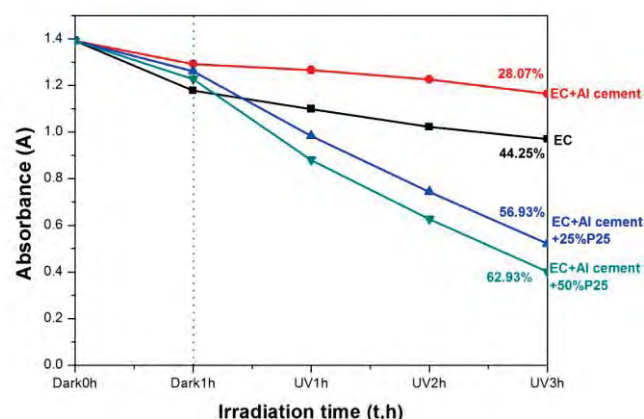
Figure2. The absorbance of MB after photocatalytic activity test of 4 samples EC, EC + Al cement, EC + Al cement + 25% P25, and EC + Al cement + 50% P25 measured by UV- VIS Spectrophotometer.

3.2 The photocatalytic results of MB

Figure 2, The results from UV-VIS spectra revealed that during one hour in the dark (Dark 0h – Dark 1h), the absorbance of MB in all condition slightly decreased by adsorption on the porous surface of the sample, and after UV irradiation for 3 h, the rate of MB still slightly decreased in case of EC substrate and EC coated with Al cement. On the other hand considering of EC substrate which contained P25 (25% and 50%), it revealed that after UV irradiation for 3h, the absorbance of MB suddenly decreased due to the photocatalytic activity of TiO$_2$-P25 on the sample surface. The adsorbing ability of EC substrate to MB was better than the EC substrate which was coated by Al cement. This is because of EC substrate surface contained more open pores than the coated one. Increasing of the amount TiO$_2$-P25 from 25% to 50%, did not promote much higher degradation of MB as clearly observed by the absorbance of MB which was decreased slightly lower than that of 25% TiO$_2$-P25. Mixing TiO$_2$-P25 in Al cement and coated on EC substrate be able to produce photocatalytic activity on the surface of sample and could decompose MB after UV irradiation for 3h up to 62.93%.

3.3 The photocatalytic results of CHP

The standard solution of CHP composed of 230 ppm CHP, 20 ppm dimethyl phenyl carbinol (DMPC) and 2 ppm acetophenone (ACP). The HPLC analyses of CHP concentrations in Figure 3(a) indicated that after subjecting EC substrate 10 samples in 10 ml of standard solution and left in the dark for 1h, the concentration of all compounds did not change even after UV irradiation for 2h and 4h. It is implied that only EC substrate could not decompose CHP. Fig 3(b) indicated that after subjecting EC coated with Al cement 10 samples in 10 ml of standard solution the results showed the similar effect as EC substrate. It can conclude that EC substrate and EC coated with Al cement could not decompose CHP after UV irradiation for 4h but in Fig 3(c) and 3(d) after subjecting of EC

coated with 25% and 50% P25/Al cement 10 samples in 10 ml of standard solution and left in the dark for 1h, the concentration of all compounds did not change but after UV irradiation for 2h and 4h the concentration of CHP decreased because P25 on the sample surface and UV light can promote photocatalysis reaction in order to decompose CHP to DMPC, ACP, Phenol and Acetone. Sample prepared by TiO_2-P25 blended Al cement coating on EC substrate could decompose CHP up to 78.87%, after UV irradiation and CHP changed to lower molecular weight chemical structure such as DMPC, ACP and phenol (as intermediate products). The higher increasing level of acetone (also as an intermediate product) was also detected.
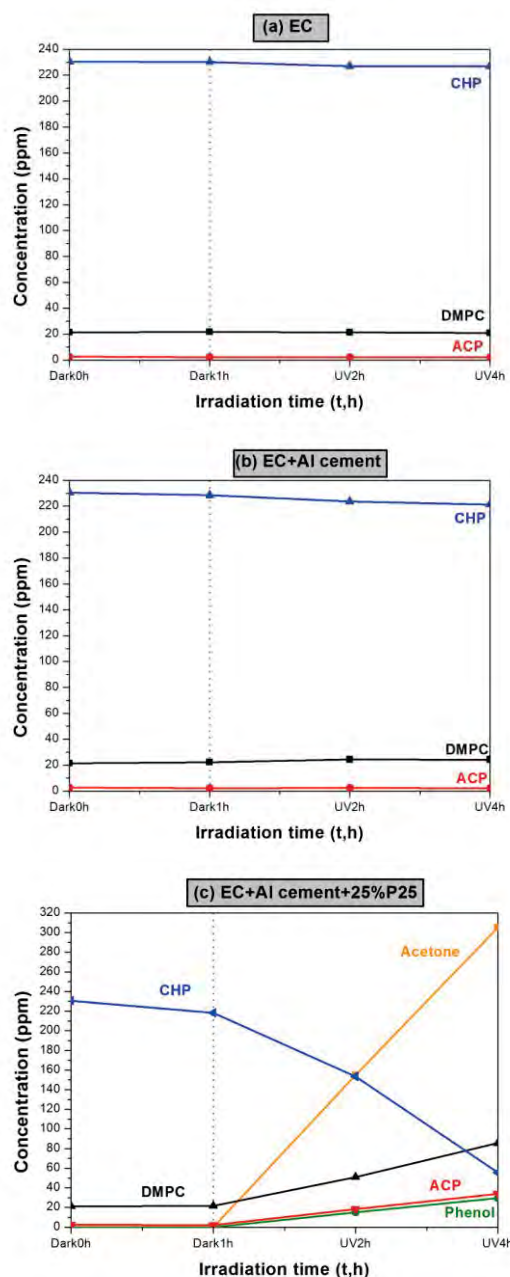
Figure3. Changing in concentrations (measured by HPLC) of CHP, DMPC and ACP in standard solution after subjecting of (a) EC, (b) EC coated with Al cement, (c) EC coated with 25%TiO_2 P25/Al cement, and (d) EC coated with 50% TiO_2 P25/Al cement

4. Conclusions

EC substrate coated with 25-50% TiO_2-P25 blended Al cement by granulation process are able to degrade methylene blue (MB) 56.93-62.93% under UV irradiation for 3 h and decompose cumene hydroperoxide (CHP) 75.94-78.87% under UV irradiation for 4 h. Accordingly, they might potentially decompose organic pollutants which mainly contained CHP in wastewater and it is promising to reuse this materials in wastewater treatment purpose.

References

[1] M.A. Fox, M.T. Dulay, *Chem. Rev.*, **93** (1993) 341-357.
[2] A. Hagfeldt, M. Gratzel, *Chem. Rev.*, **95** (1995) 49–68.
[3] J.C. Zhao, T.X. Wu, K.Q. Wu, K. Oikawa, H. Hidaka, N. Serpone, *Environ. Sci. Technol.*, **32** (1998) 2394–2400.
[4] C.Euvananont, C. Junin, K. Inpor, P. Llimthongkul and C. Thanachayanont, *Ceram. Int.*, **34** (2008) 1067.
[5] R. Dholam, N. Patel, M. Adami, and A. Miotello, *Int. J. Hydrogen Energ.*, **33** (2008) 6896.
[6] M. Karches, M. Morstein, P. Rudolf von Rohr, R.L. Pozzo, J.L. Giombi, M.A. Baltanas, *Catal. Today*, **72** (2002) 267.

[7] T. Kemmitt, N.I. Al-Salim, M. Waterland, V.J. Kennedy, A. Markwitz, *Curr. Appl. Phys*., **4** (2004) 189.

[8] T.L.R. Hewer, S. Suárez, J.M. Coronado, R. Portela, P. Avila, B. Sänchez, *Catal. Today*, **143** (2009) 302.

[9] N. Arconada, A. Durán, S. Suárez, R. Portela, J.M. Coronado, B. Sánchez, Y. Castro, *Appl. Catal. B*: *Environ*., **86** (2009) 1.

[10] C.M. Maghanga, J. Jensen, G.A. Niklasson, C.G. Granqvist, M. Mwamburi, *Sol. Energy Mater. Sol. Cells*, **94** (2010) 75.

[11] P.G. Karlsson, J.H. Richter, M.P. Andersson, M.K.J. Johansson, J. Blomquist, P. Uvdal, A. Sandell, *Surf. Sci*., **605** (2011) 1147.

[12] I. Oja Acik, A. Junolainen, V. Mikli, M. Danilson, M. Krunks, *Appl. Surf. Sci*., **256** (2009) 1391.

[13] T. Meng, Y. Yu, X. Qian, S. Zhan, K. Qian, *Construction and Building Materials.,* **29** (2012) 241-245.

[14] J. Chen, C.S. Poon, *Environ. Sci. Technol.,* **43** (2009) 8948-8952.

[15] A. Folli, I. Pochard, A. Nonat, U. H. Jakobsen, A.M. Shepherd, and D.E. Macphee, *J. Am. Ceram. Soc*., **93** (2010)3360–336.

EXFOLIATED FUNCTIONALIZED PHYLLOSILICATES: SYNTHESIS, CO$_2$ SORPTION AND THERMODYNAMICS EFFECTS

Cléo T. G. V. M. T. Pires[1], Nilton G. de Oliveira Jr.[1], Maurício A. Melo Jr.[1], Claudio Airoldi[1*]

[1] Institute of Chemistry, University of Campinas, UNICAMP, P.O Box 6145, 13084-971 Campinas, SP, Brazil.

* Author for correspondence; E-Mail: airoldi@iqm.unicamp.br, Tel. +55 1935213109, Fax. +55 1935213023

Abstract: Exfoliated nickel phyllosilicates were obtained by ultrasound delamination of previously synthesized ethanolamine (E) and diethanolamine (D) talc-like hybrid materials. Layered precursors nickel silicates were prepared by incorporation of aminoalcohols into 3-glycidoxypropyltrimethoxysilane to give new silylating agents, which were employed in the syntheses of nickel phyllosilicates (Ph), called PhE and PhD by the sol–gel process. Exfoliation process used water, cetyltrimetylamonium bromide (CTAB), tetrabutylamonium hydroxide (TBAOH) and combinations of CTAB-TBAOH and CTAB-KOH aqueous solution and ethanol to achieve materials with different delamination or intercalation levels. Structures have been confirmed by infrared spectroscopy, solid state ^{29}Si and ^{13}C NMR, thermogravimetry, X-ray powder diffraction, nitrogen adsorption at 77 K and electron microscopy. The ^{13}C NMR results showed organic moieties covalently bound on the inorganic framework, while ^{29}Si NMR revealed that silicon only occupies T positions. The materials presented a well-organized trioctahedral structure, indicated by the powder X-ray patterns. Basal spacings of 1.01 and 1.15 nm were found for PhE and PhD. Delaminated materials have up to 1.7 and 2.1 nm of basal space. Nitrogen adsorption showed a surface area increase from about 30 m^2 g^{-1} for PhE and PhD up to 320 m^2 g^{-1} for exfoliated materials. Based on the nitrogen amount, 3.08 and 2.25 mmol g^{-1} of silylating agent were grafted onto the inorganic framework. Measurements of CO$_2$ uptake by the phyllosilicates were performed on a simultaneous dosing gas system coupled with an isothermal calorimeter.

1. Introduction

Layered solid materials are extremely versatile and can be synthesized by various methods and compositions. Within this systematic it is possible to obtain silicates,[1] aluminosilicates[2] and heavy metal oxides,[2] among other compositions, which allows employment in assorted research fields, such as materials for sensors and nanocomposites, in processes of ion exchange, sorption and intercalation.[3]

One way to change the properties of lamellar materials are chemical modification with organic groups on the surface. These modifications were studied in order to meet in a single material the distinct properties that may be associated with many uses of scientific and technological point of view.[4] These new synthesized materials may include, as example, the mechanical stability of the inorganic polymer and the ability to complex cations due to the presence of pendant chains containing Lewis basic centers covalently attached to the main structure.[5] A diversity of applications have been reported in this class of materials, such as in catalysis,[6] chromatographic determinations,[7] and sorbents for pollutants species in solution, such as heavy metals,[8] pesticides,[9] surfactants,[10] and dyes.[11]

A useful method for the specific materials and the desirable properties comes from the application of the sol-gel process[12], which allows organic-inorganic bonding by direct synthesis, with the great advantage of being executable at a low temperature, including copolymerization reactions with alkoxysilanes in organo-substituted base conditions.[13]

The study of sorption processes, especially when accompanied by calorimetric measurements provide a broad understanding of the process, with the main thermodynamic quantified.[14] Diverse possible interactions, such as ion exchange, complexation, hydrogen bonds or precipitation at the surface present enthalpy variation in different ranges.

Among gases, CO$_2$ is reason of strong research at the sorption field due to its excess association with the global warming.[15] Concerns for adsorbent improvements are related with cost, sorption rate, CO$_2$ sorption capacity and thermal stability among others.

This work had evaluated thermodynamical effects for CO$_2$ sorption on functionalized organo-phyllosilicates before and after exfoliation process. Also structural effects for different delayered materials were carefully studied.

2. Materials and Methods

2.1 Layered materials synthesis

The synthesis of nickel phyllosilicates was previously described,[16] Briefly, 7.6 g nickel nitrate were dissolved in 300 cm^3 of deionized water under stirring at 323 K. Then an ethanolic solution of silane was dropped to the nickel solution to form a green suspension. Thus 300 cm^3 aqueous NaOH 0.10 mol dm^{-3} were added. The final suspension was aged at 323 K for two days and then filtered and washed with water until neutral pH.

Exfoliated nickel phyllosilicates were carried out directly into tubes containing 0.40 g of PhE or PhD and 10 cm^3 of liquid, consisting of ethanol, deionized water, CTAB$_{(aq)}$ 10%, TBAOH$_{(aq)}$ 10%, and combinations of 7.5 cm^3 CTAB with 2.5 cm^3 of KOH

1.0 mol dm^{-3} or TBAOH 40%. All dispersions were subjected to ultrasonic bath at room temperature for 3 h, and the final product were filtered and washed with water. The materials derived from PhE were denominated E-EtOH, E-H$_2$O, E-CTA, E-TBA, E-CTA/KOH, and E-CTA/TBA according to the liquid used. Samples derived from PhD were named similarly, changing the E by D.

2.2 Characterization

The materials were analyzed by X-ray diffraction (XRD) on a diffractometer XRD 7000, Bruker, using a radiation source of CuKα 0.154 nm, with a scan rate of 2.0^o 2θ min^{-1} at room temperature. Some samples were analyzed by transmission electron microscopy (TEM). The samples were suspended in isopropyl alcohol, sonicated and deposited on a carbon thin film, the deposited onto a copper grid. The micrographs were taken at the Electron Microscopy Laboratory (LME) of the National Synchrotron Light Laboratory (LNLS), the microscope was used JEM 2100 FEG with accelerating voltage of 200 KV. Different electron collections were used, such as regular TEM images, bright field (BF) and high angle annular dark filed (HAADF). Also energy dispersive spectroscopy (EDS) and electron energy loss spectroscopy (EELS) were performed at the same microscope. The analysis of porosity and surface materials were performed in a volumetric adsorption analyzer ASAP 2010 Micromeritrics to 77 K. For the calculation of area and pore sizes were used BET and BJH methods. The zeta potential was determined by laser Doppler velocimetry using a NanoZetaS (Malvern Instruments LTD., UK). The ζ-potential was estimated from the electrophoretic mobility measurements using the Smoluchowski model.

2.3 CO$_2$ sorption and calorimetry

Experiments on CO$_2$ sorption and equilibrium calorimetry were carried out up to 100 mmHg pressure at a Gas Dosing System coupled to a commercial calorimeter LKB 2277, which allows to obtain simultaneous values for amount sorbed and the energy involved for each sorption.[17] Data treatment used Langmuir formalism to fit all results and calculate the thermodymanic values.[17,18]

3. Results and Discussion

The set of X-ray diffractograms of exfoliated nickel phyllosilicates, and their precursors are shown in Figures 1 and 2. In general the changes observed in the exfoliation processes were very similar for both PhE and PhD phyllosilicates (curves a). Among all liquids used, ethanol presented the lower effect, and there was no significant changes in the XRD patterns (curves b), which is explained by weak interactions of ethanol molecules with the phyllosilicates surface. For samples ultrasounded in all aqueous solutions (curves c-g), a higher exfoliation degree was observed.

The diffractogram of the phyllosilicate PhE, the curve a of Figure 1 shows a double peak centered

at 4.99 and 8.87^o 2θ, which indicate basal distances of 1.77 and 0.99 nm. The smaller distance corresponds to the part that may not be functionalized. This second peak disappeared or decreased in intensity after treatment in ultrasound bath in some aqueous system. Among all the solutions used the mixture CTAB/TBAOH was certainly more efficient because as observed in curve f, the peak for the 001 plane (from JCPDS card number 13-0558) can no longer be observed clearly, by mixing the incoherent scatter at the diffractogram beginning in case of permanence of the same peak. Such an superior outcome to the CTA/TBA system was relatively expected, since this mixture has been used successfully in other exfoliation studies.[19] In peaks related to other plans, which have no relationship to z axis, no significant changes were observed, with functionalization degree of 3.08 and 2.25 mmol g^{-1} for PhE and PhD based samples respectively.

Figure 1. XRD patterns for exfoliated nickel phylossilicates samples modified with ethanolamine PhE (a), E-EtOH (b), E-H$_2$O (c), E-TBA (d), E-CTA (e), E-CTA/TBA (f) e E-CTA/KOH;

For sample PhD the plane indicated by peak 001 centered at 7.72^o 2θ, which corresponds to 1.14 nm distance. The exfoliations modified mainly peaks related with 001 plans reflection for most new materials, varying the intensity and position toward lower values of 2θ, indicating a partial exfoliation.

Results for elemental analysis and NMR spectroscopy showed no meaningful difference before and after exfoliation process. Also only T sites were observed by ^{29}Si NMR after ultrasound treatment, while ^{13}C NMR confirmed the organic structure remain.[16]

In order to investigate structural and morphological aspects of some prepared material scanning and transmission electron microscopy (STEM) was employed as a tool for these purposes. Phyllosilicate PhE micrographs approximately along the axis 001 in Bright Field (BF) and in High Angle Annular Dark Field (HAADF) are shown in Figure 3. In these images are observed changes in gray and white scales depending on the thickness, in the case of overlapped

unordered silicate layers high resolution images (atomic level) were not achieved, because the used conditions the electron beam amorphizes the lamellar silicates if a larger magnification is used, furthermore these types of phyllosilicates have no high crystallinity, as observed by X-ray diffraction. The presence of different textures, as observed in the particle mainly below the image indicate a process of phase change with the electron beam interaction or the prior presence of another phase at smaller amount. In order to clarify this issue, samples were analyzed using data from energy dispersive spectroscopy (EDS) and electron energy loss spectroscopy (EELS), which confirmed the tetrahedral environment for silicon atoms, while nickel are completely octahedral.
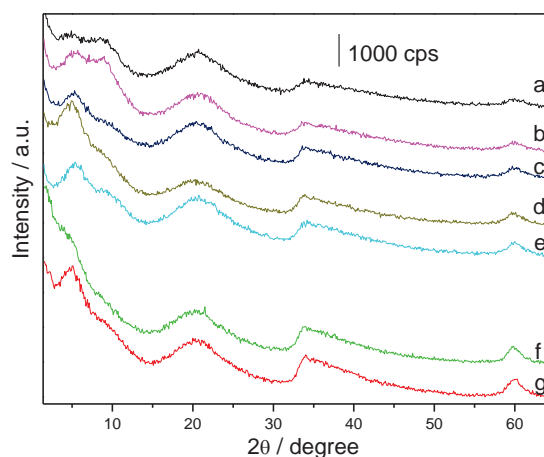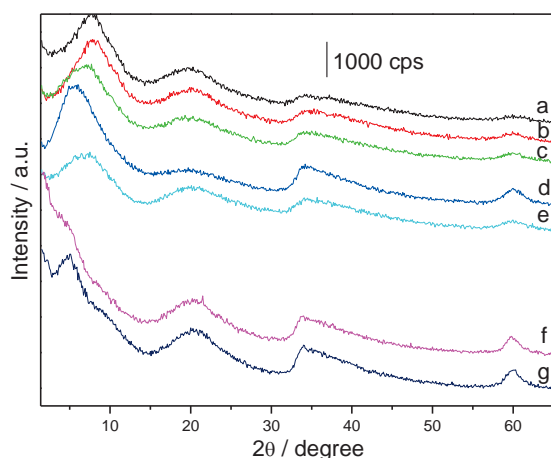

Figure 2. XRD patterns for exfoliated nickel phylossilicates samples modified with diethanolamine PhD (a), D-EtOH (b), D-H_2O (c), D-TBA (d), D-CTA (e), D-CTA/TBA (f) e D-CTA/KOH.

In these images, which are fairly representative, heterogeneity with respect to the particle size can be observed with the dimensions ranging from a few tens of nanometers to more than a micrometer. The stacking of the plates occurs more disordered than in other lamellar silicates such as magadiite and ilerite, as previously reported.[20,21]
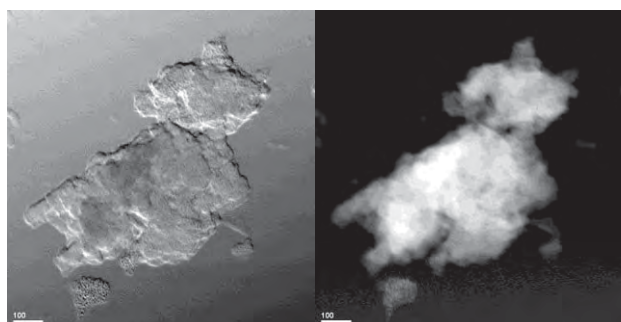
Figure 3. PhE phylosilicate STEM Micrographs at HAADF and BF mode. Scale bar = 100 nm

A TEM image for the exfoliated E-CTA/TBA sample is shown in Figure 4. Generally, there was observed a large thickness difference for the particles, since usually the sample majority is positioned perpendicular to 001 plane, in addition to relatively large heterogeneity typically presented by these organofunctionalized phyllosilicates. However a slight change was observed, with a small decrease in all average particle sizes.
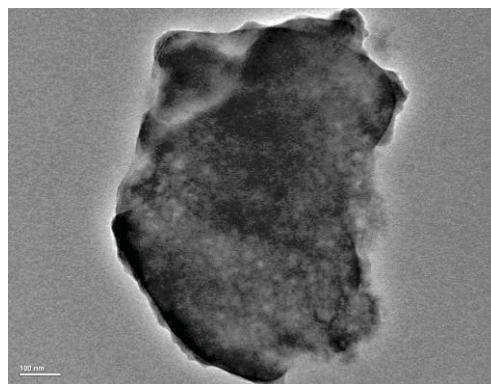
Figure 4. TEM micrograph of the sample E-CTA/TBA. Scale bar = 100 nm.

Results of nitrogen adsorption and desorption at low temperatures were obtained for most samples, however for some samples the results presented complicated features and their fit were not possible. Among the good results were observed the surface area increase after exfoliation, mainly with CTA/TBA, changing the initial area of 18 and 31 m^2 g^{-1} for PhD and PhE, respectively, up to and 94 and 320 m^2 g^{-1} for D-CTA/TBA and E-CTA/TBA. These surface area variation among materials containing diverse organo-groups are directly correlated with the stronger interactions for diethanolamine moieties with adjacent groups, which keep the lamellas fastener.

Other important measures were concerning the zeta potential. Nickel phylosilicate PhE is positively charged with average value of 30.2 mV. The delamination process with CTA/TBA aqueous solution decreased the average value to 20.7 mV. This charge reduction are in agreement with theoretical expectations, because usually layered silicate based materials shows extensively charge misbalance, along their structures.[21,22] Thus, particle thickness reduction for this materials, necessarily gone lead to zeta potential reduction.

CO_2 adsorption on PhE and E-CTA/TBA samples results are shown at Figure 5. Sorbed amounts at the studied pressure range PhE presented a linear behavior, reaching 13.2 mmol g^{-1} at 100 mmHg. On the other hand E-CTA/TBA after 30 mmHg starts decrease the amount adsorbed at each pressure increase, maybe nearing the equilibrium pressure for desorption and presenting CO_2 sorption capacity of 5.3 mmol g^{-1}. These results are related with the gas entrapment allowed for PhE sample, whilst at the exfoliated sample interactions at a single surface, with lower functional group density, are in lower amount. Also regardless the system is dry, the particle charge can be associated with CO_2 sorption capacity, being proportionally correlated.
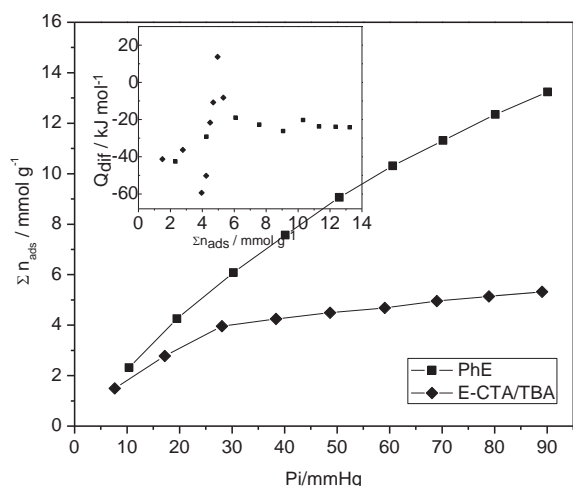
Figure 5. Quantitative and Calorimetric (Inset) CO_2 sorption results for PhE and E-CTA/TBA materials.

The thermal effect for each gas sorption are shown inset Figure 5. Similarly regular is PhE interaction energies and sorbed amounts, presenting an average value of -25.7 KJ mol^{-1}. In contrast, the exfoliated material demonstrates a more complex energy profile, mainly after 40 mmHg, indicating a sort of interactions, more or less favored, in agreement with this materials complexity with smaller probability to occur gas entrapment than at non-functionalized sample.

4. Conclusions

The precursor lamellar materials were synthesized successfully, both nickel phyllosilicates containing two different organic groups. These materials were exfoliated by ultrasound treatment with several liquids. The most efficient media on the exfoliation process was the aqueous solution containing CTABr and TBAOH. The particles observation in electron microscopes are in good agreement with the results obtained by XRD and morphology normally observed for this class of materials. CO_2 sorption was more efficient on PhE material, while the exfoliation process decrease maximum sorption capacity and change the involved energetic.

References

[1] H. Krüger, V. Kahlenberg and R. Kaindl, *Solid State Sci.* **7**, (2005) 1390-1396.

[2] C. Tagusagawa, A. Takagaki, K. Takanabe, K. Ebitani, S. Hayashi and K. Domen, *J. Phys. Chem. C* **113**, (2009) 17421-17427.

[3] F. Feng and K. J. Balkus Jr., *Micropor.Mesopor. Mat.* **69**, (2004) 85-96.

[4] M. Richard-Plouet, S. Vilminot and M. Guillot, *New J. Chem.* **28**, (2004), 1073-1082.

[5] O. G. da Silva, E. C. da Silva Filho, M. G. da Fonseca, L. N. H. Arakaki and C. Airoldi, *J. Colloid Interface Sci.* **302**, (2006) 485-491.

[6] A. S. Amarasekara, A, R, Oki, L. McNeal and U. Uzoezie, *Catal. Commun..* **8,** (2007) 1132-1136.

[7] C. R. Silva, I. C. S. F. Jardim and C. Airoldi, *J. Chromatogr. A.* **987**, (2003), 127-138.

[8] A. A. El-Nasser and R. V. Parish, *J. Chem. Soc., Dalton Trans.* (1999) 3463-3466.

[9] A. M. Faria, L. Maldaner, C. C. Santana, I. C. S. F. Jardim and C. H. Collins, *Anal. Chim. Acta.* **582**, (2007), 34-40.

[10] R. Zhang, C. Liu and P. Somasundaran, *J. Colloid Interface Sci.* **310**, (2007), 377-384.

[11] A. S. O. Moscofian, C. T. G. V. M. T. Pires, A. P. Vieira and C. Airoldi, *RSC Adv.* **2**, (2012), 3502-3511.

[12] C.J. Brinker, G.W. Scherer, Sol–Gel Science — The Physics and Chemistry of Sol–Gel Processing. Boston, Academic Press, 1990.

[13] K. A. Carrado, L. Xu, R. Csencsits and J. V. Muntean, *Chem. Mater.* **13**, (2001), 3766-3773.

[14] T. R. Macedo, G. C. Petrucelli and C. Airoldi, *Thermochim. Acta.* **502**, (2010) 30-34.

[15] C.-H. Yu, C.-H. Huang and C.-S. Tan, *Aerosol Air Qual. Res.* **12**, (2012) 745–769.

[16] M. A. Melo Jr., F. J. V. E. Oliveira and C. Airoldi, *Appl. Clay Sci.* **42**, (2008) 130-136.

[17] N. G. Oliveira Jr. Development of a gas dosing system (SDG) suitable for calorimetric studies of adsorption of gases on solids, Ph.D. Thesis, Unicamp, Campinas, Brazil, 2012.

[18] I. Langmuir, *J. Am. Chem. Soc.* **40**, (1918) 1361-1403.

[19] Y. Bi, J.-F. Lambert, Y. Millot, S. Casale, J. Blanchard, S. Zeng, H. Nie and D. Li *J. Mater. Chem.* **21**, 2011, 18403-18411.

[20] C. T. G. V. M. T. Pires, N. G. Oliveira Jr. and C. Airoldi, *Mater. Chem. Phys.* **135**, (2012), 870-879.

[21] C. T.G.V.M.T. Pires, J. R. Costa and C. Airoldi, *Mi Micropor. Mesopor. Mater.* **163**, (2012) 1–10.

[22] A. Jung, K. Peter, D. E. Demco, D. Jehnichen and M. Moeller, *Macromol. Chem. Phys.* 213, (2012) 389−400.

STUDY THE EFFECT OF BASIC DYES SORPTION ON DIFFERENT CHEMICALLY MODIFIED SBA-15

Khalid Ahmed[1], Cleo T. G. V. M. T. Pires[1*], Ali Riaz[1], Claudio Airoldi[1*]

[1] 1Institute of Chemistry, University of Campinas, UNICAMP, P.O Box 6145, 13084-971 Campinas, Sao Paulo, Brazil

* Authors for correspondence; E-Mail: cleo@iqm.unicamp.br, airoldi@iqm.unicamp.br, Tel. +55 1935213109, Fax. +55 1935213023

Abstract: The aim of this investigation is to study the sorption of basic dye methylene blue from aqueous solution with different chemically modified mesoporous silica SBA-15. Samples were prepared only with pure silicate composition and also containing aluminium in different concentrations. Resultant materials were characterized by different techniques, such as ^{29}Si nuclear magnetic resonance (NMR) in solid state, infrared spectroscopy, thermogravimetry, electron microscopy and small angle X-ray scattering (SAXS). Surface properties variation for different synthesized SBA-15 mesoporous materials resulted on slight different sorption capacities for the dye methylene blue from aqueous solution. The effect of contact time and the sorbent kind was established, as well desorption phenomena was noticed for higher concentration after 24 h, due to the relatively weak interaction between silanol groups and methylene blue molecules.

1. Introduction

The appearance of colored compounds from emerging effluents after diverse industrial activities such as paper manufacturing, dying cloths, leather treatment printing etc into the environment is undesirable. This is not only an unfavourable condition due to the color affect on aquatic plants photosynthesis, but also they contain a substantial amount of organic dye. These organic molecules and their breakdown products may be toxic in nature and their removal from industrial effluents is a major environmental concern [1-5], in fact, many of these dyes have shown hazardous properties and are toxic in nature due to aromatic rings belonging to their chemical structure.

Adsorption has proven to be the most efficient method for quickly lowering the concentration of dissolved dyes in an effluent, and activated carbon is the most widely used adsorbent for removal of dyes from aqueous solution. However, the high cost of production and regeneration make it uneconomical [6]. Therefore, inorganic adsorbents (e.g. zeolites) with high surface areas have been used as alternatives to carbon adsorbents[7, 8]. In recent years, commercial zeolites with unique surface and pore properties have been increasingly studied for the liquid adsorption of dissolved pollutants in water [9]. However, few studies have focused on the adsorption of cationic dyes by synthesized zeolite[9, 10, 11]. Juang et al[12] reported an investigation for removal of a basic dye from aqueous solution using mesoporous zeolite MCM-41, and found that it is an efficient adsorbent because of its large pore space and the strong interaction between the basic dye and surface hydroxyl groups of MCM-41. Also modification of MCM-41 by incorporation of aluminium into the structure has excellent adsorption performance for methylene blue and rhodamine B [13, 14, 15].

In order to systematically change the properties of layered silicate materials, we have investigated the possibility of isomorphous substitution of silicon by aluminium or boron. It is demonstrated that addition of boron and/or aluminium compounds to the reaction mixture leads directly to boron and aluminium containing layered materials in a hydrothermal crystallization process without further treatment. The layered materials obtained were identified as hectorite types, magadiite and kenyaite-like types. The isomorphous substitutions were proven by ^{11}B, ^{27}Al, and ^{29}Si solid state NMR spectroscopy. The chemical composition of the layered material determines not only the final properties of the pillared material, but also affects the pillaring process itself. The probability of introducing pillars into the interlamellar spaces between the layers strongly depends on the charge density of the bulk layers [16]. However, the charge density in an individual structure can only be varied over a very small range.

Isomorphous substitution of silicon by another element, e.g. Al, Fe, or B, has a tremendous effect on the framework charge density and consequently on surface properties. The present work consists on the synthesis of mesoporous SBA-15 silica containing aluminium replacing some silicon sites. Resultant differences on surface acidity were evaluated regarding the sorption of methylene blue dye. Kinetics and thermodynamical parameters were evaluated.

2. Materials and Methods

2.1 Preparation of SBA-15

SBA-15 silicas were synthesized as previously reported by Zhao et al.[17,18] using Pluronic P123 triblock copolymer ($EO_{20}PO_{70}EO_{20}$, Aldrich). Briefly, a 4.0 g Pluronic P123 were dissolved in 30 g of water and 120 g of 2 mol dm^{-3} HCl (Synth) solution. Then, 8.50 g of TEOS (98% Acros Organics) was added drop wise, and the resulting mixture was stirred for 2 h and then kept at 373K for 2 days under static conditions. The solid product was filtered, washed with water and ethanol, dried in an oven for 4 h at

323K, and subsequently calcined in air for 5.5 h at 823K to remove the P123 polymer.

The preparation of SBA-15 containing aluminium was prepared by a similar method as described above, with simple modifications.[19,20] Thus after TEOS addition and ageing for 45 min, 0.46 g or 0.92 g aluminium isopropoxide ($[(CH_3)_2CHO]_3Al$, Merck) were added and than mixed for further 2 hours before hydrothermal treatment. These samples were named [Al]SBA-15 and [2Al]SBA-15.

2.2 Characterization

Nuclear magnetic resonance of the silicon nucleus in the solid state for all synthesized samples was performed on a Bruker 300 MHz Avance spectrometer operating with Larmor frequencies for ^{29}Si at 59.6 MHz and with a probe using a 4 mm zirconium rotor with spinning rate of 10 kHz. The experiment was conducted with 60 s recycle delay.

The small angle X-ray scattering was performed on the D11A-SAXS line, at the National Synchrontron Light Laboratory (LNLS, Campinas, SP, Brazil), for λ = 0.1488 nm, with a sample-detector distance of 453 mm, and a CCD detector. The plane distance $d_{(hkl)}$ at different Miller indices (hkl) were calculated from Bragg's law ($n\lambda = 2d \sin \theta$) and the cubic lattice parameters (a_0) for the samples were calculated by a_0 = $d_{(110)}$ x $2^{0.5}$.

Nitrogen sorption isotherms were measured at 77 K on a Quantachrome NOVA 4200e surface area and pore size analyzer. Before the sorption measurements, all samples were outgassed under vacuum for 12 h at 423 K. The BET surface area was calculated by applying the Brunauer–Emmett–Teller equation to the sorption isotherms over a relative pressure range from 0.05 to 0.30 [21]. The pore volume was estimated using the BJH (Barrett–Joyner–Halenda) method and the pore size distributions (PSDs) determined as the value corresponding to the maximum in the BJH pore size distribution plot.

Transmission electron microscopy images were obtained with a JEM-MSC 2100 microscope operated at 200 kV. For TEM measurements the samples were prepared by dispersing the powder samples in isopropanol, then dispersed and dried on the carbon film in a copper grid. The estimation of pore volume and d_{110} were performed using several images average with Imaje J software and CSI pack.

Fourier transform infrared (FTIR) spectra were obtained on a Bruker Equinox 55 spectrophotometer in the 4000 to 400 cm^{-1} range, with resolution of 4 cm^{-1}. The samples (0.50%) were pressed with KBr, with a pressure of 7 ton cm^{-2}.

The thermogravimetric (TG) data were obtained in a TA Instruments 5100 heating to 1273 K at 0.167 K s^{-1} rate under an oxygen flow of 1.67 cm^3 s^{-1}.

For determination of dye concentrations a Shimadzu spectrophotometer model MultiSpec-1501 TCC-240A was used.

2.3 Sorption

Methylene blue sorption were carried out by the batchwise method with aqueous solutions at 298 ± 1 K. For this purpose samples of approximately 20 mg were suspended in a series of flasks containing dye solutions, varying in concentration from 0.05 to 0.25 mmol dm^{-3}, with deionized water with pH near to 5. Samples were left under stirring for 2.0 or 24 h, centrifuged, filtered and the amount of methylene blue in the supernatant was measured spectroscopically at λ_{max} = 665 nm. The obtained data was adjusted to Langmuir and Freundlich models [19], to estimate the monolayer sorption capacity of each sample.

Also the time influence on the sorptions was determined through a series of flasks with masses near to 20 mg contact with 50.0 cm^3 solution. The flasks were maintained under orbital stirring from 10 to 100 min for methylene blue. After filtration, the final concentrations were also determined as before.

3. Results and Discussion

SBA-15 silica prepared with and without aluminium with exhibited a single strong peak on its SAXS patterns (Figure 1). Similar patterns were recorded for the synthesized without aluminium with aluminium and with double aluminium it shows that the structure of different SBA-15 is same. Two additional peaks were observed, which can be indexed on a hexagonal lattice as (200) and (210) reflections.
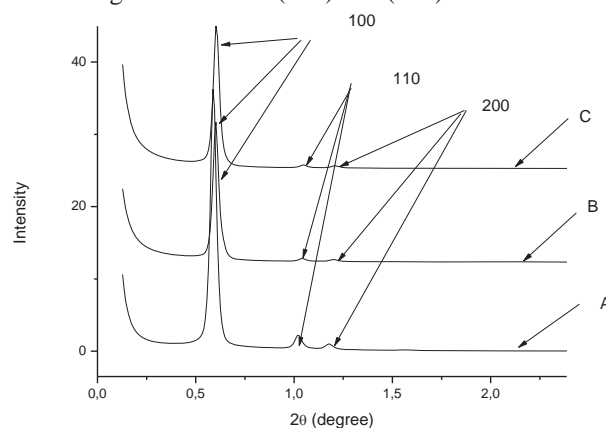
Figure 1: SAXS patterns for different types of SBA-15. Pure silica material (A), [Al]SBA-15 (B) and [2Al]SBA-15 (C).

Relative intensities of (110) and (200) peaks varied as the concentration of aluminium varies. As discussed above, the SBA-15 prepared without aluminium exhibited strong (200) reflection, whereas the (110) reflection was less visible.

The synthesized SBA-15 exhibited about 8 to 10% TGA weight loss at temperatures between 370K and 400K. This weight loss can be attributed primarily to the decomposition and desorption of the polymeric template and, to a smaller extent, to the release of water formed from the condensation of silanols (H_4OSi) in the silica framework. The content of the polymeric template in this SBA-15 sample was similar

to the content of the ionic surfactant template in typical MCM-41 and MCM-48 silicas[20, 21].

FT-IR spectra of SBA-15 present bands at 3439 and 1650 cm^{-1} can be attributed to the stretching vibration of hydroxyl and water, respectively [23]. It has been reported that adsorbed water, which is probably due to humid KBr and incorporated humidity in the process of sample preparation, has two bands around 3439 and 1640 cm^{-1} [24, 25], Moreover, silanol bonds show absorption at 1450 and 1595 cm^{-1} [26], and small crystallites could result in two broad peaks around 3400 and 1650 cm^{-1}[27] Si–O–Al vibration appeared in the range of 400–600 cm^{-1}. The peak at 1104 cm^{-1} corresponded to the asymmetric stretching vibration of Si–O–Si and the bands at 800 and 470 cm^{-1} can be assigned to the symmetric stretching and deformation modes of Si–O–Si [28], respectively. For SBA-15 silica, this peak was attributed to the Si–OH stretching vibration [29]. For [Al]SBA-15 samples, this peak indicated the possibility of formation of bonds of Al–O–Si, and the peak intensity of [Al]SBA-15 was obviously higher than that of pure siliceous material.

^{29}Si NMR spectra for SBA-15 present prominent signals for the Q^3 (Si(OSi)$_3$(OH)) and Q^4 (Si(OSi)$_4$) species around 100 and 110 ppm respectively, with the intensity of the former being higher. It is known that Q^3 is more intense than Q^4 in the mesophases prepared under acidic conditions [30]. A higher intensity of Q^3 indicates a lower degree of condensation of the silicate species. It is also significant that Q^3/Q^4 ratio of SBA-15 samples prepared under hydrothermal condition is higher than that of the same samples prepared under non hydrothermal condition.

The transmission electron microscopy (TEM) image of [Al]SBA-15 is shown at Figure 2. In this micrography is observed the pore channels parallel among each other as different grayscales. The average pore diameter observed by TEM is around 8,7 nm. SBA-15 and [2Al]SBA-15 morphology is very similar to [Al]SBA-15, as well the pore diameter. These results are in agreement with SAXS and nitrogen sorption data. This last one showed 8.5 nm for average pore diameter and surface are ranging from 690 to 810 m^2 g^{-1}.
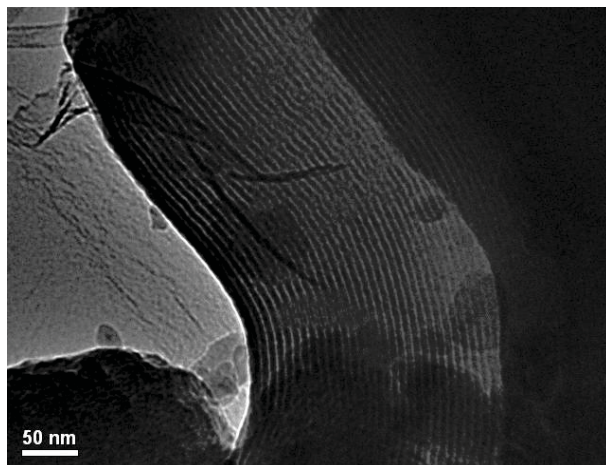
Figure 2: Transmission electron microscopy image of [Al]SBA-15 mesoporous material.

Methylene blue (MB) sorption onto SBA-15 samples results are show at Figures 3-5. The data obtained from the above tests were used to calculate the adsorption capacity, q$_t$ (mmol g^{-1}), of the adsorbent by a mass balance relationship [19]. Figure 3 shows the isotherm measured for methylene blue on SBA-15 materials with time contact of 2h. All samples presented a very similar behavior, which mean a possible multilayer sorption process or the presence of two distinct sorption sites. As shown the adsorption capacity of MB increased with all types of SBA-15 with increasing initial dye concentration because the initial concentration provides a powerful driving force to overcome the mass transfer resistance between the liquid and solid phases [31]. SBA-15 possesses a sorption capacity, about 0.08 mmol.g^{-1}. It also shows that when sorption capacity reaches about 0.04 mmol g^{-1} get little stable and increase again at around 0.08 mmol g^{-1}. Both Langmuir and Freundlich model did not fit well with obtained results, presenting determination coefficients of 0.93 and 0.91 respectively.
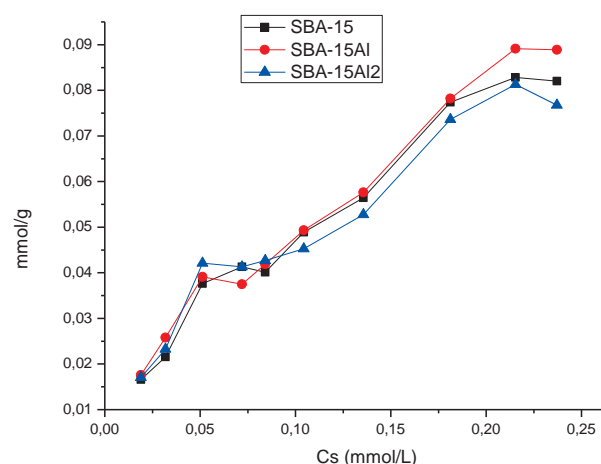
Figure 3: Sorption capacity of SBA-15 samples for methylene blue after 2h stirring.

Figure 4 shows the isotherm measured for methylene blue on SBA-15 materials with time contact of 24h. Once again, all samples presented a very similar behavior. In this case, with a longer time contact an interesting fact were noticed, which consists maximum sorption capacities decreasing with MB concentration increase. Also all values for the sorption capacities are smaller than those observed for the experiment carried out for 2h. This results indicates a desorption process due to the weak interaction between the silanol groups and subsequent MB agglomeration at the solution.

The study of time contact influence for the methylene blue sorption process onto SBA-15 materials is shown in Figure 5. Despite the differences are not so pronounced, a quicker sorption is observed for the samples containing aluminum, possibly with a two steps on the process, which probably complete the

monolayer at early 10 min. Subsequent sorption may correlate with double layers formation and polycondensation, which at longer times initiate an desorption process as observed by comparison between Figures 3 and 4.
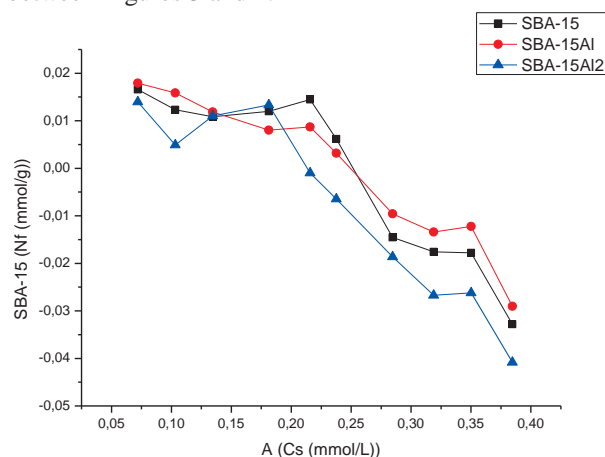
Figure 4: Sorption capacity of SBA-15 samples for methylene blue after 24h stirring.
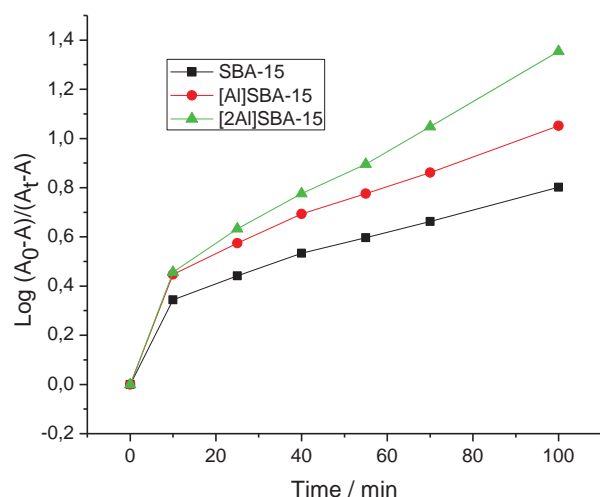
Figure 5: Time influence on the sorption capacity of SBA-15 samples for methylene blue.

4. Conclusions

All mesoporous SBA-15 samples, containing aluminum or not were successfully synthesized and characterized. The resultant surface modifications were evaluated for methylene blue dye sorption. and only slightly difference were observed, nevertheless [Al]SBA-15 is a better sorbent. Aspects concerning the influence of time and dye concentration were studied and a desorption process take a place after several hours.

Acknowledgements

References

[1] A. T. Cooper and D. Y. Goswami, *J. Sol. Energy Eng.* **124**, (2002) 305.

[2] A. H. Gemeay, I. A. Mansour, G. E. Rehab and B. Z. Ahmed, *J. Chem. Technol. Biotechnol.* 79, (2004) 79.

[3] D. F. Ollis, *Compt. Rend. Chem.* **3**, (2000) 405.

[4] S. R. Khan, C. R. Huang and J. W. Bozelli, *Environ. Prog.* **4**, (1985) 229.

[5] G. Mills and M. R. Hoffmann, *Environ. Sci. Technol.* **27**, (1993) 1681.

[6] S. W Blocki, *Environ. Prog.* 12, (1993) 226.

[7] S. B Wang , H. T Li, S. J Xiie, S. L Liu and L. Y Xu, *Chemosphere* 65, (2006) 82.

[8] B. Armagan, O. Ozdemir, Turan and M. S. Mand Celik, *J Chem Technol Biotechnol.* 78, 2003) 725.

[9] A. Metes, D. Kovacevic, D. Vujevic and C. Papic, *Water Res.* **38**, (2004) 3373.

[10] S. Wang, H. Li and L. Xu, *J. Colloid Interface Sci.* 295, (2006) 71.

[11] L. C Juang, C. C Wang, C. K Lee and T. C. Hsu, *J. Environ. Eng. Manag.* 17, (2007) 29.

[12] W. T. Tsai, K. J Hsien and H. C Hsu, *J. Hazard. Mater.* 166, (2009) 635.

[13] D. Wei, H. Wang, X. Feng, W. Chuch, P. Ravikovitch and M. Lyubovsky, *J. Phys. Chem. B.* 103, (1999) 2113.

[14] M. A Zanjanchi and S. Asgari, *Solid State Ionics* 171, (2004) 277.

[15] S. Eftekhari, A. Habibi-Yangjeh and S. Sohrabnezhad, *J. Hazard. Mater.* **178**, (2010) 349.

[16] T. J. Pinnavaia, *Science* 220, (1983) 365.

[17] D. Zhao, Q. Huo, J. Feng, B. F. Chmelka and G. D Stucky, *J. Am. Chem. Soc.* **120**, (1998) 6024.

[18] Z. Wang and T. J. Pinnavaia, *Mater. Chem.* **13**, (2003) 2127.

[19] C. T. G. V. M. T. Pires, J. R. Costa and C. Airoldi, *Micropor. Mesopor. Mater.* **163**, (2012) 1.

[20] C. T. G. V. M. T. Pires, N. G. Oliveira Jr. and C. Airoldi, *Mater. Chem. Phys.* **135**, (2012) 870.

[21] M. Kruk, A. Sayari and M. Jaroniec, *Stud. Surf. Sci. Catal.* **129**, (2000) 577.

[22] M. Kruk, M. Jaroniec, R. Ryoo and S. H. Joo, *Chem. Mater.* **12**, (2000) 1414.

[23] M. Guidotti, N. Ravasio, R. Psaro, G. Ferraris and G. Moretti, *J. Catal.* **214**, (2003) 242.

[24] Y. Suda and T. Morimoto, *Langmuir* **3**, (1987) 786.

[25] K. Tanaka and J. M. White, *J. Phys. Chem.* **86**, (1982) 4708.

[26] S. Klein, S. Thorimbert and W. F. Maier, *J. Catal.* **163**, (1996) 476.

[27] E. Sanchez, T. Lopez, R. Gomez, Bokhimi, A. Morales and O. Novaro, *J. Solid State Chem.* **122**, (1996) 309.

[28] K. Y. Jung and S. B. Park, *Appl. Catal. B* **25**, (2000) 249.

[29] T. Blasco, M. A. Camblor, A. Corma and J. P. Pariente, *J. Am. Chem. Soc.* **115**, (1993) 11806.

[30] S. Che, H. Li, S. Lim, Y. Sakamoto, O. Terasaki and T. Tatsumi, *Chem. Mater.* **17**, (2005) 4103.

[31] W. T. Tsai, K. J. Hsien and H. C.Hsu, *J. Hazard. Mater.* **166**, (2009) 635.

HYDROTHERMAL SYNTHESIS AND CHARACTERIZATION OF POTASSIUM IODIDE (KI)–DOPED MESOPOROUS TiO$_2$ NANOMATERIAL

Malinee Leekrajang[1], Chanatip Samart[1*], <u>Kannikar Kaewpraneet</u>[1],
Wachara Weangkaew[2], Koji Kajiyoshi[3]

[1] Department of Chemistry, Faculty of Science and Technology,
Thammasat University, Klong 1, Klong Luang, Pathumthani, 12121 Thailand
[2] School of Chemical and Biochemical Engineering, Sirinthorn International Institute of Technology,
Thammasat University, Klong 1, Klong Luang, Pathumthani, 12121 Thailand
[3] Research Laboratory of Hydrothermal Chemistry, Faculty of Science,
Kochi University, 780-8520 Japan

[*] Author for correspondence; E-Mail: chanatip@tu.ac.th, Tel. +66 2564 4440 to 59 ext. 2401, Fax. +66 2564 4483

Abstract: Titanium dioxide (TiO$_2$) has been one of the most investigated metal oxides, and it can be used in many applications such as semiconductor in dye-sensitized solar cells (DSSCs), photocatalysis, gas sensors, and so on. Potassium iodide (KI) - doped mesoporous TiO$_2$ nanomaterial was synthesized by a cetyltrimethylammonium bromide (CTAB) - assisted hydrothermal process. The as-synthesized samples were characterized by X-Ray diffraction (XRD), scanning electron microscopy (SEM), and Brunauer-Emmett-Teller (BET) surface area. The effects of synthesis temperature and time, and potassium iodide doping content on structural and physical properties were investigated. The XRD patterns and SEM micrographs showed anatase crystalline phase of mesoporous TiO$_2$. The peaks of excess KI were found from the XRD patterns for the samples with higher content of iodide ion. The N$_2$ sorption isotherm results showed that the surface area and pore volume were affected by different doping degree of KI. The condition with the highest surface area and pore volume was found on the synthesis temperature of 36 ºC and the synthesis time of 48 h with KI/Ti = 1.

1. Introduction

Titanium dioxide (TiO$_2$) is a semiconducting material that can be used in many applications, for example, photocatalysis and solar cells. Because of its low-cost manufacturing and non-toxic property, TiO$_2$ has drawn great attentions from many researchers. However, non-porous TiO$_2$ has some limitations such as small surface area. Compared with non-porous TiO$_2$, mesoporous TiO$_2$ has high specific surface area, ordered pore structure and excellent adsorption property [1]. The synthesized mesoporous anatase TiO$_2$ nanopowder by hydrothermal method showed higher photocatalytic activity than commercial TiO$_2$ nanoparticles [2].

A surfactant-template approach was used to synthesize the mesoporous TiO$_2$ with significantly high surface area [3]. The templates in the preparation of mesoporous materials are removed by high temperature post-treatment. Also, at high temperature, the crystallization of mesoporous materials occurs with an anatase phase that has higher photocatalytic activity than amorphous and rutile phases. However, the mesoporous structure may collapse when these templates are removed in high temperature, which greatly limits the applications of mesoporous TiO$_2$ [4].

Several studies have been fulfilled to further increase photocatalytic activity of mesoporous materials by, for example, co-doping TiO$_2$ with other elements. Iodine-doped TiO$_2$ nanospheres showed higher photocatalytic efficiency compared with iodide-TiO$_2$ nanoparticles even though the latter had much greater surface area [5]. The presence of iodine in iodine-doped TiO$_2$ nanocrystallites expanded the photo-responsive in visible light, and led to enhance the photocatalytic efficiency [6].

In this paper, the synthesis of iodine-doped mesoporous TiO$_2$ by a hydrothermal method at the temperature of 110 °C for 24 h, is presented. To gain the mesoporous TiO$_2$ structure with high surface area, cetyltrimethylammonium bromide (CTAB) is employed as cationic template [7]. Titanium (IV) isopropoxide is the Ti source. Previous studies indicated that iodide ion inhibited the collapse of mesoporous structures by adding potassium iodide (KI) to the preparation of mesoporous materials. Hence, an effect of KI is investigated with synthesis temperature and synthesis time.

2. Materials and Methods

2.1 Synthesis of KI doped mesoporous TiO$_2$

All the reagents used in the experiments are of analytical grade and used without further purification. In a typical synthesis of mesoporous TiO$_2$, 7.29 g of cetyltrimethylammonium bromide (CTAB) was dissolved in 23.9 ml of deionized water and stirred for 30 min under a nitrogen stream. 17.07 g of titanium (IV) isopropoxide was added dropwise into the solution under vigorous stirring for 30 min. 0.72 g of NaOH was slowly added to above solution. A certain amount of KI (the molar ratios of KI/Ti = 1, 3, and 5) was dissolved in the 180.0 ml of deionized water and added slowly to the solution under the fiercely stirring.

The resulting solution was kept in an autoclave and heated at 110 °C for 24 h. The resultant material was filtered off, air-dried at room temperature, and then calcined in air to remove moisture and volatile matter at 540 °C for 6 h.

2.2 Characterization of Materials

X-ray diffraction (XRD) patterns were obtained on an X-ray diffractometer (Bruker AXS) using Cu Kα radiation with wavelength λ = 0.154060 nm. Porous structure and BET surface area were characterized by N_2 adsorption-desorption isotherms on a BET surface area analyzer (Autosorb-iQ Series). Scanning electron microscope (SEM) micrographs were obtained on S-3400N instrument (Hitachi).

3. Results and Discussion

3.1 XRD analysis

The samples were synthesized at 36 °C for 24 h with different KI/Ti molar ratios of 0 (NonKI), 1, 3 and 5. The XRD patterns of the prepared sample after hydrothermal treatment at 110 °C for 24 h and calcination at 540 °C are illustrated in Figure 1. The samples show diffraction peaks (10-80°) at 2θ values of 25.32°, 37.92°, and 47.94° which correspond to anatase (101), (004), and (200) crystal planes. Peaks corresponding to rutile and brookite are not found, which indicates that all the samples of KI-doped porous TiO_2 material are anatase structure after calcination at 540 °C.
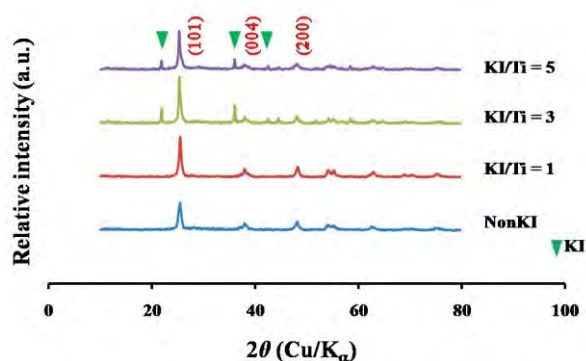
Figure 1. XRD patterns of KI-doped TiO_2 samples synthesized at 36 °C for 24 h

It is revealed from Figure 1 that increasing the amount of iodide ion has small effect on the intensity of diffraction peaks which indicate the crystallinity of TiO_2. Peaks corresponding to an excess of KI are found for the samples with higher content of iodide ions (KI/Ti = 3 and 5).

3.2 SEM analysis

Figure 2 shows the SEM micrographs of TiO_2 particles. In Figure 2a and 2c, rhombic and spherical particles are found on the surface of pure and doped porous TiO_2 samples (KI/Ti = 1), and iodide ions doping has no effect on particle size. In Figure 2b and 2d, it is indicated that iodide ions affect the

morphology of TiO_2 particles by increasing the porosity in TiO_2 particles. The XRD and SEM results confirm the presence of iodide ions in obtained mesoporous TiO_2 with anatase crystalline phase.
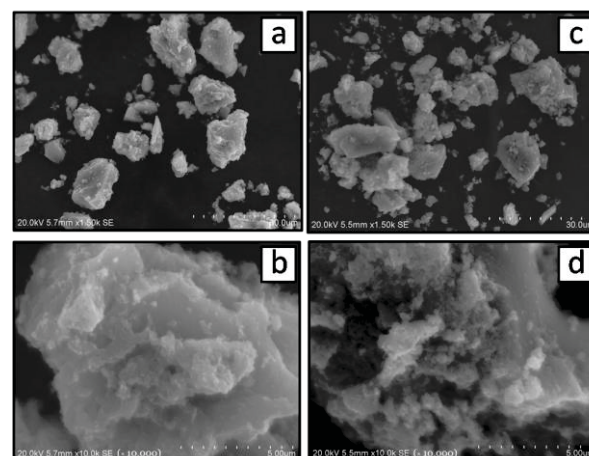
Figure 2. SEM micrographs of TiO_2 particles (a, b) without KI and (c, d) with KI/Ti = 1

3.3 N_2 adsorption-desorption analysis

Figure 3 shows the N_2 adsorption-desorption isotherms and Figure 4 shows the corresponding BJH pore size distributions of different doping degree of KI. The BET specific surface area and BJH pore volume of samples are summarized in Table 1.
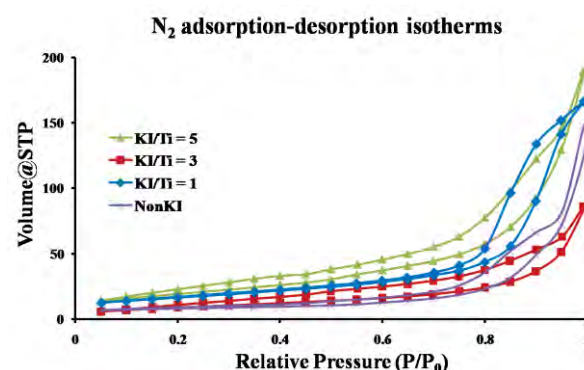
Figure 3. Nitrogen adsorption-desorption isotherms of KI-doped TiO_2 samples synthesized at 36 °C for 24 h

It is revealed from Figure 3 that pure and iodide ion doped TiO_2 samples exhibit adsorption isotherms with hysteresis, which indicate mesopore structures [8], according to IUPAC classification of adsorption isotherms. The curve of pure TiO_2 sample exhibits H2-type hysteresis loop from 0.40 to 0.95 (P/P$_o$), while the curve of iodide ion (KI/Ti = 1) doped sample behaves a hysteresis loop between H1-type and H2-type from 0.70 to 0.95 (P/P$_o$). For KI/Ti = 3 and 5, the doped samples exhibit H2-type hysteresis loop from 0.10 to 0.95 (P/P$_o$). The H1-type hysteresis is associated with porous materials that have narrow distributions of pore size. This indicates that the pore type is cylinder-like. The H2-type hysteresis is also associated with porous

materials that have narrow necks and wide bodies. This indicates that the pore type is ink-bottle. The hysteresis loop of iodide ion doped samples is steeper and moves slightly to lower P/P_o, which indicates that pore size of samples reduces because of iodide ions added. However, the quantity of nitrogen adsorption is much higher than that of pure TiO_2 [4].
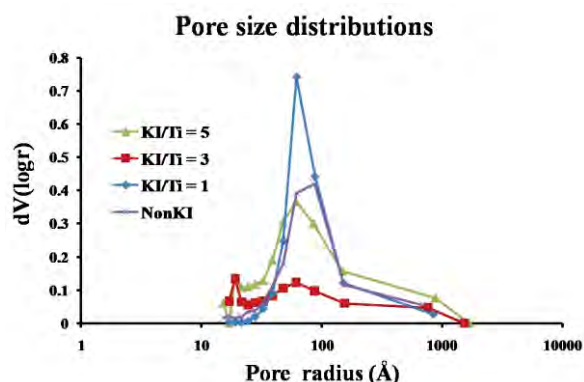
Figure 4. Pore size distributions of KI-doped TiO_2 samples synthesized at 36 °C for 24 h

Table 1. Effects of synthesis conditioning on physical properties of mesoporous TiO_2

	Molar Ratio of KI/Ti 36 °C, 24 h				Synthesis Temperature (°C) KI/Ti = 1, 24 h			Synthesis Time (h) KI/Ti = 1, 36 °C		
	Non KI	1	3	5	36	50	70	24	36	48
Surface area ($m^2 g^{-1}$)	43.4	68.7	41.7	85.7	68.7	78.4	75.1	68.7	62.0	87.7
Pore volume ($cm^3 g^{-1}$)	0.20	0.26	0.13	0.29	0.26	0.27	0.25	0.26	0.24	0.33

The BJH pore size curves show that the pore size distribution of the iodide ion (KI/Ti = 1) doped samples is narrower than that of pure TiO_2. However, for KI/Ti = 3 and 5, the pore size distributions are slightly wider. The excess amount of KI may affect on the pore structure corresponded with the adsorption hysteresis. From Table 1, the specific surface area of KI/Ti = 1 and 5 samples prepared at 36 °C for 24 h, are 68.7 and 85.7 $m^2 g^{-1}$, respectively, which are higher than that of pure TiO_2. However, KI/Ti sample gives lower specific surface area corresponded with the smaller average pore size (see Figure 3). In general, iodide ion inhibits the collapse of mesoporous channels resulting from the overquick dehydration among the free hydroxyl groups and also plays a part in structure-directing to some extent [4].

4. Conclusions

The iodide-doped mesoporous TiO_2 material has been synthesized by a template (CTAB) - assisted hydrothermal method with good surface area. The XRD and SEM results confirm the presence of potassium iodine molecule in obtained material with anatase crystalline phase.

The results of BET and SEM prove that the content of iodide ions has a crucial effect on the mesopore structure and morphology. The BET results showed that the structural properties of as-prepared porous material are affected by different doping degree of KI as follows: the specific surface area and pore volume with KI/Ti = 5 > 1 > Non > 3. The KI-doped mesoporous TiO_2 material prepared at 36 °C for 48 h with KI/Ti = 1 has the highest surface area of 87.7 $m^2 g^{-1}$ and the highest pore volume of 0.33 $cm^3 g^{-1}$.

References

[1] T. Jiang, Q. Zhao, M. Li, and H. Yin, *J. Hazard. Mater.* **159** (2008) 204–209.
[2] S. Pavasupree, J. Jitputti, S. Ngamsinlapasathian, and S. Yoshikawa, *Mater. Res. Bull.* **43** (2008) 149–157.
[3] J.C. Yu, L. Zhang, Z. Zheng, and J. Zhao, *Chem. Mater.* **15** (2003) 2280–2286.
[4] Y. Wang, J. Ren, G. Liu, and P. Peng, *Mater. Chem. Phys.* **130** (2011) 493–499.
[5] Z. He, L. Zhan, F. Hong, S. Song, Z. Lin, J. Chen, and M. Jin, *J. Environ. Sci.* **23** (2011) 166–170.
[6] Y. Ma, J.–W. Fu, X. Tao, X. Li, and J.–F. Chen, *Appl. Surf. Sci.* **257** (2011) 5046–5051.
[7] K. Di, Y. Zhu, X. Yang, and C. Li, *Colloid Surf. A* **280** (2006) 71–75.
[8] O. Carmody, R. Frost, Y. Xi, and S. Kokot, *Surf. Sci.* **601** (2007) 2066–2076.

THE EFFECT OF QUANTITATIVE AND PARTICLE SIZE DISTRIBUTION OF COPPER(II) OXIDE AND COPPER (II) CARBONATE ON THE APPEARANCE OF COPPER METAL IN METALLIC LUSTER GLAZE

Siwat Lawanwadeekul[1], Sakdiphon Thiansem[2]

[1] Department of Metrology and Quality System, Faculty of Industrial Technology, Lampang Rajabhat University, Lampang 52000, Thailand
[2] Department of Industrial Chemistry, Faculty of Science, Chiang Mai University, Chiang Mai 50200, Thailand.

* Author for correspondence: E-Mail: b_siwat@hotmail.com, Tel +66 81 530 7695

Abstract: The purpose of the study was to investigate the optimization of the appearance of copper in metallic luster glazes. Copper(II) oxide and copper(II) carbonate were used in unground and ground forms (ground for 4, 8 and 16 hours) as an additive at 10, 15, 20, 25 and 30 %wt. The specimen was coated with the glaze and fired at 1230°C in a reduced atmosphere. The specimens were tested using optical microscopy (OM), scanning electron microscopy (SEM) and energy dispersive spectrometry (EDS). The results show that the optimum appearance was gained by adding copper(II) oxide at 15% (13.88 µm average particle size) which had been ground for 4 hours.

1. Introduction

Metallic luster is a metal glaze nano-composite applied as a thin layer of copper or silver nanoparticles embedded in a silica-based glassy matrix. The metal particles range from 2-50 nm in size and the whole layer is approximately 100 nm to 1 mm thick [1-3]. The effect of luster is a consequence of the size of the copper nanoparticles, which have special optical properties; in scattered light, the luster acquires a green, brown, ochre or yellow sheen. In specula reflection, the luster acquires a colored metallic shine, usually golden-yellow, blue, and green or pink [4-7].

Copper(II) oxide and copper(II) carbonate are widely used as additives because of their high level of reactivity, their selectivity in oxidation and reduction reactions when fired in different atmospheres (Figure 1). After being fired at a high temperature, these compounds ionize and when they cool down, these ions form into oxides[8]. Copper ions can join with another ionic substance, such as silicon(Si^{4+}), to become copper silicates such as Cu_2SiO_2 and $CuSiO_3$. The reaction depends on several factors including particle size and the quantity of additive. Researchers are therefore interested in studying this to find the optimized parameters for adding copper as a luster.

$$CuCO_3 \longrightarrow CuO + CO_2$$

$$CuO \underset{OF}{\overset{RF}{\rightleftarrows}} Cu_2O \underset{OF}{\overset{RF}{\rightleftarrows}} Cu$$
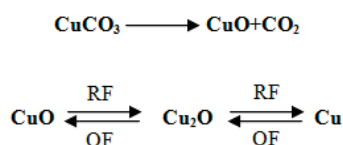
Figure 1. The transition reaction of copper

2. Materials and Methods

The chemical analysis of glaze and clay slip formulations are given in Table 1. The glaze was prepared in a pot mill, and mixed with water (30% vol.) and additives at 10, 15, 20, 25 and 30% wt. The distributions of the particle size of the additives were analyzed by laser diffractometer. The glaze suspensions were coated over specimens with a glaze thickness of 2.4-2.8 mm and the specimens were then fired at 1230°C in a reduction atmosphere and soaking for 30 minutes at maximum temperature. Finally, the specimens were tested by laser diffraction, optical microscopy, scanning electron microscopy and energy dispersive spectrometry.

Table 1: Chemical composition of raw materials.

Sample	Clay slip	Basic glaze
SiO_2	71.69	64.62
Al_2O_3	18.65	13.89
Fe_2O_3	1.30	0.80
TiO_2	0.22	0.10
MnO_2	0.05	0.01
CaO	0.09	7.17
MgO	0.13	0.19
K_2O	2.65	4.16
Na_2O	0.45	2.21
LOI	4.50	6.53

3. Results and Discussion

3.1 Laser diffraction analysis

The distribution of the particle size of copper(II) oxide is both wide and monomodal. Unground Copper(II) oxide has an average particle size of 24.72 µm. When ground for 4, 8 and 16 hours, the average size is 13.88, 10.84 and 5.46 µm respectively.

Unground copper(II) carbonate has a smaller particle size (average of 9.89 µm). When ground for 4, 8 and 16 hours, the average grain size (somewhat bimodal) is 3.60, 2.06 and 1.73 µm respectively. These results show in Figure 2
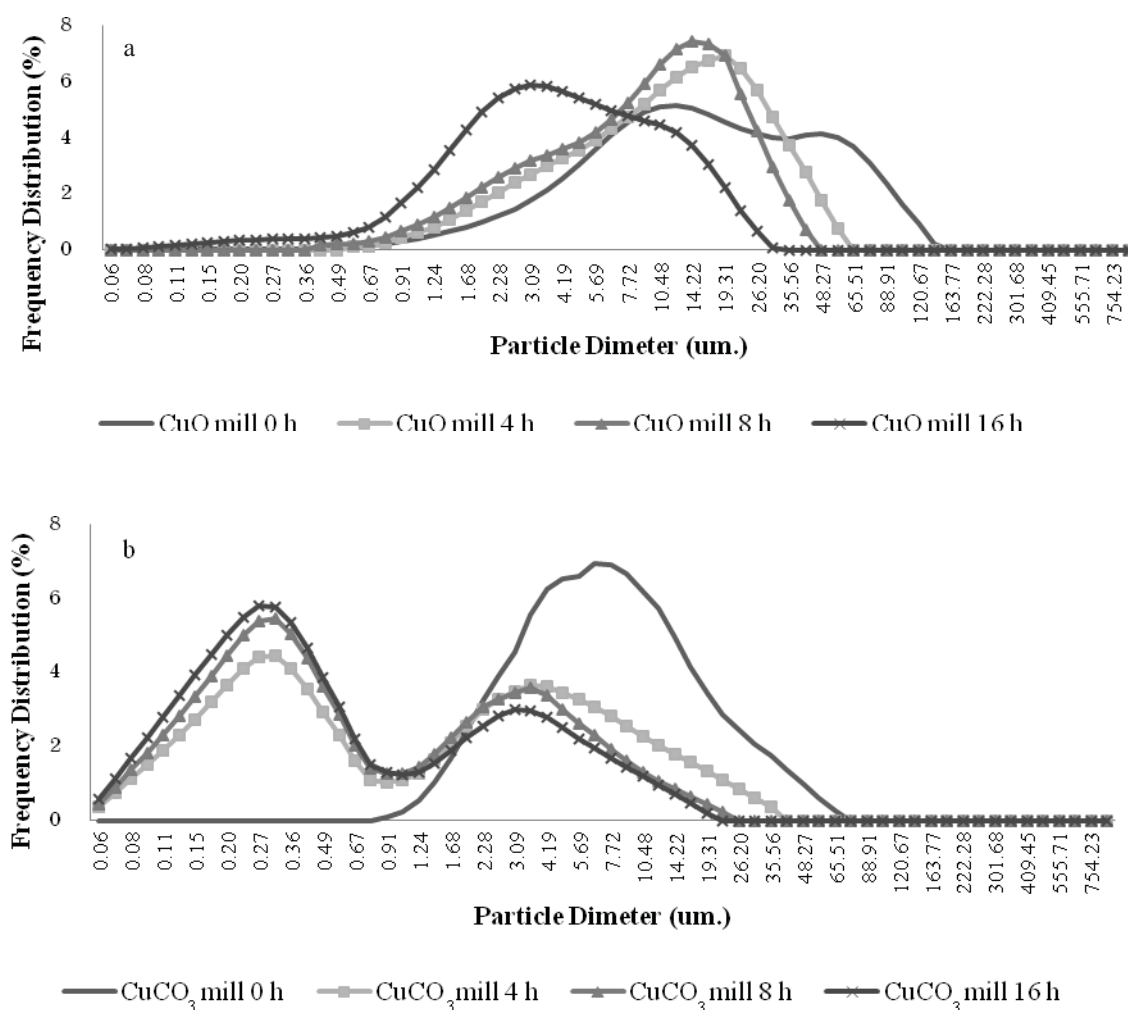
Figure 2. Particle size distributions of 2 additives (a. CuO and b. CuCO₃) after milling at various times.

3.2 Optical microscopy analysis

The composition of the glaze is fundamental to the formation of luster. Analysis of the layers of glaze demonstrated that the composition of the glaze depends on the size of the particles. However, the homogeneous particle size in the glaze, as seen in Figure 3a, does not appear bright. This may be because there is no copper in the glaze, or because the amplification is not high enough. In Figure 3b it can be seen that there is small spot of copper oxide in the sample and at 20x magnification (Figure 3c) the copper can be seen clearly. The color of the coating is different due to the number of ions; if there are +2 ions, the resulting color is green, +1 ion gives a red color and no ions gives a gray color.

3.3 Scanning electron microscope

Similar composition and microstructures are seen in all the lusters, indicating a common production technique. A scanning electron microscopy image of a glaze surface is shown in Figure 4. A sample analysis of the surface, magnified at 85x and 500x respectively, can be seen in Figure 4a and Figure 4b. These samples are composed of 10% copper(II)oxide ground for 4 hours and they were tested by energy dispersive spectrometry (EDS) to determine whether write down result from EDS.

In Figure 4b, EDS shows that carbon deposits may occur when firing in strongly reduced atmospheres, in this case visible as black spots. However, carbon was not the subject of this study. Figures 4c and 4d (SEM of 15% Copper(II)oxide ground for 4 hours at 85x and 500x magnification) show the location of the copper metal. At figures 4c and 4d, the text was 15%.
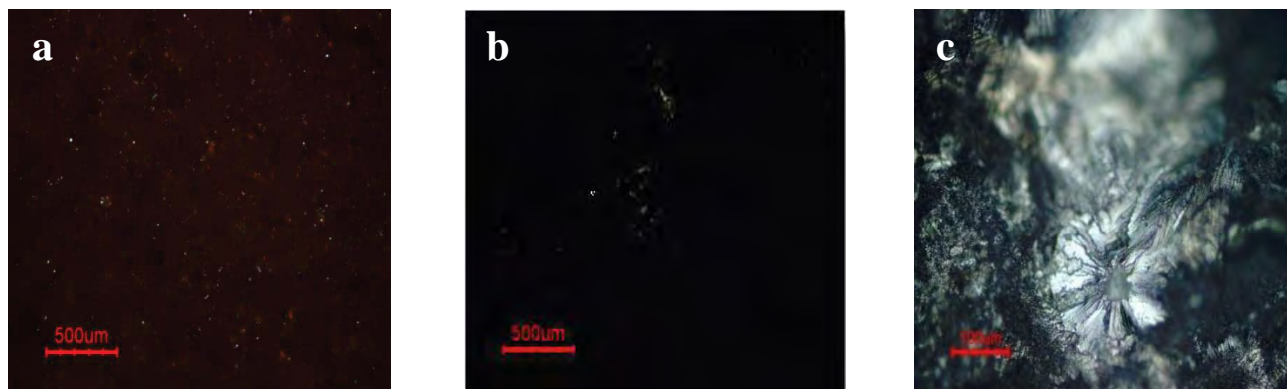
Figure 3. Optical microscopy on glaze surface (a) 10% copper(II) oxide ground for 4 hours at 5x magnification (b) 15% copper(II) oxide ground for 4 hours at 5x magnification and (c) 15% copper(II) oxide ground for 4 hours at 20x magnification.
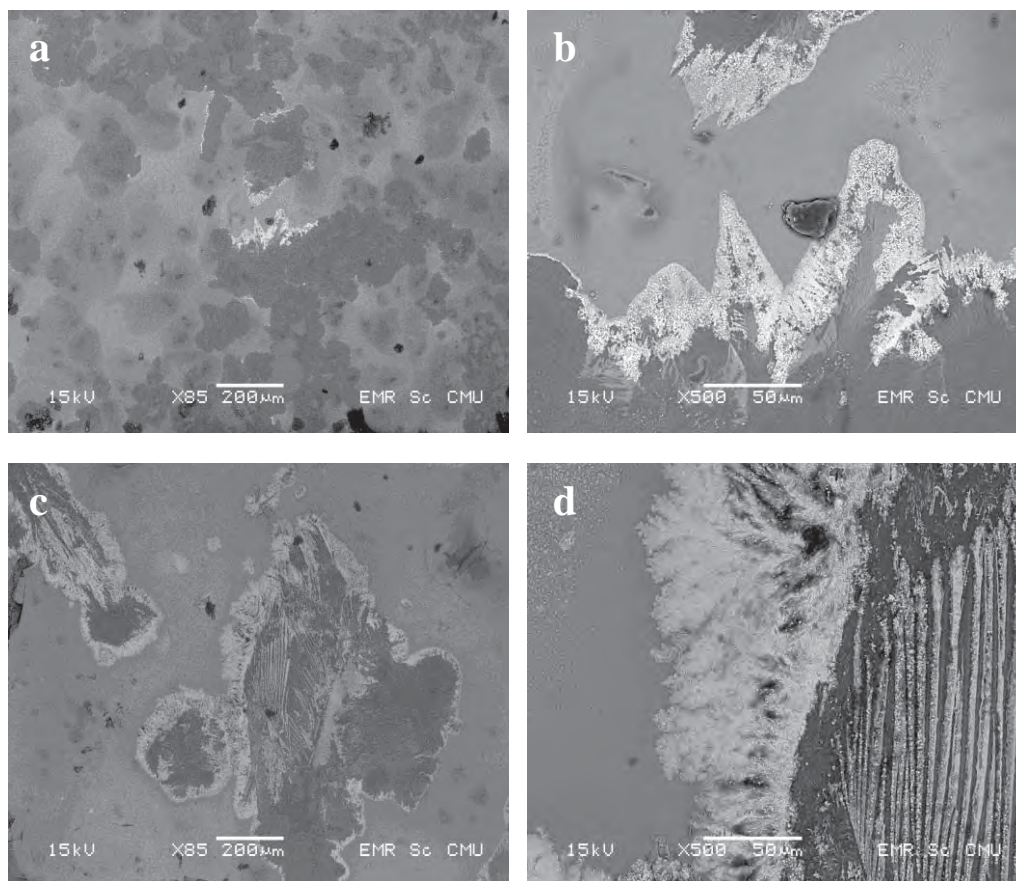
Figure 4. SEM of glaze surface (a) and (b) 10% copper(II) oxide ground for 4 hours (c) and (d) 15% copper(II) oxide ground for 4 hours.

3.4 Energy Dispersive Spectrometry
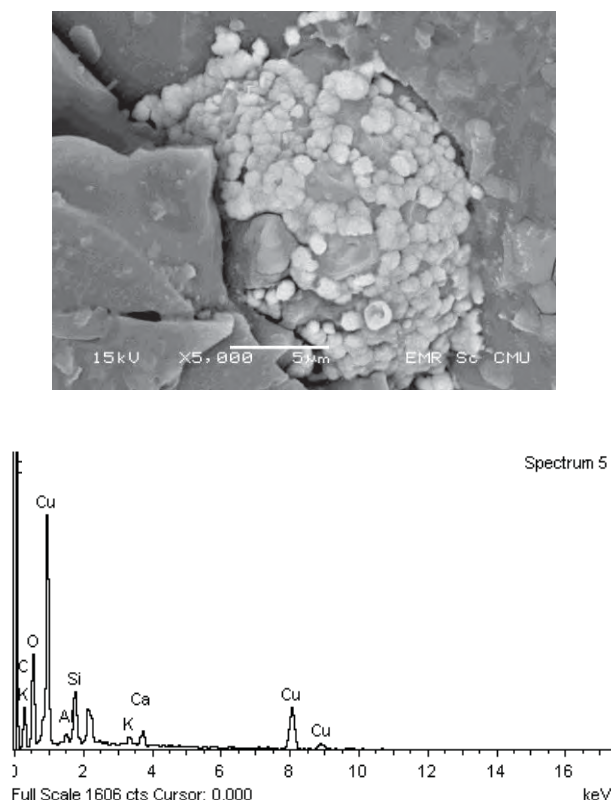
Figure 5. SEM/EDS in areas of copper.

Figure 5 shows the energy dispersive spectrometry analysis of a sample. This can be used to show peaks of copper; the higher the peak, the greater the quantity. Other elements such as silicon, calcium, etc. are present only in low quantities. EDS and SEM of the position shows that the area includes copper. This detail can insert into the figure.

4. Conclusions

The effects of the addition of copper oxide and copper carbonate varied with changes in the proportion of additives used and changes in particle size.

1. The occurrence of copper in the glaze from fired copper(II) oxide and copper(II) carbonate resulted from the strongly reduced atmosphere.
2. Adding copper oxide is more effective than adding copper(II) carbonate.
3. The optimum appearance was gained by using 15% copper(II) oxide, ground for 4 hours (with an average particle size of 13.88 µm).

References

[1] T. Pradell, J. Molera, A.D Smith, A.Climent and S. Michael, *J. cultural heritage*, (2008) e123-e128.
[2] J. Peʹrez-Arantegui, J. Molera, A. Larrea, T. Pradell, M. Vendrell,I. Borgia, B.G. Brunetti, F. Cariati, P. Fermo, M. Mellini, A. Sgamellotti and C. Viti, *J.Am. Ceram Soc.* **84** (2001) 442e446.
[3] P. Sada and Mazzoldi, *J. phys,* **Vol 93**, No. 12 (2003) 10058-10063.
[4] V. Lazic, F. Colao and R. Fantoni*, J. Cultural Heritage4*, (2003), pp. 303s-308s.
[5] J.Roque and J. Molera, *J. Euro Soc*. **26** (2006) 3813–3824.
[6] A. Polvorinos del Rio, J. Castaing and M. Aucouturier, *Nuclear Instruments and Methods in Physics Research B.* **249** (2006) 596–600.
[7] O. Bobin, M. Schvoerer, J.L. Miane and J.F. Fabre, *J. Non-Crystalline Solids.* **332** (2003) 28–34.
[8] A.Paul, 2nd *Chemistry of Glasses*, chapman and hall London, (1990).

Organic Chemistry and Medicinal Chemistry

SYNTHESIS AND CHARACTERIZATION OF 1,8-NAPHTHALIMIDE OPTICAL BRIGHTENERS

Tianchai Chooppawa, Mongkol Sukwattanasinitt, Paitoon Rashatasakhon[*]

Department of Chemistry, Faculty of Science, Chulalongkorn University, Bangkok, Thailand

*Author for correspondence; E-Mail: paitoon.r@chula.ac.th, Tel. +66 22187620

Abstract: A series of 4-alkoxyl or 4-aryloxy-*N*-aryl-1,8-naphthalimides are synthesized and evaluated for their optical properties as well as thermal stabilities. All compounds have absorption wavelengths around 364-368 nm and emission wavelengths of 425-436 nm. Their outstanding thermal stabilities are evident as their 10% decomposition temperatures are in the range of 340-430 °C. Interestingly, it is found that their quantum efficiencies are exclusively dependent on the substituents at the 4-position. It is proposed that the electronic effect of the substituents on the 4-aryloxy groups influences the photo-induced electron transfer (PET) process, which causes a variation in quantum efficiencies.

Keywords Fluorescence; optical brightener; 1,8-naphthalimide; thermal stability; quantum yields

1. Introduction

Optical brighteners or fluorescent brightening agents (FBA) are colorless to weakly colored organic compounds that, in solution or applied to a substrate, absorb ultraviolet light and re-emit most of the absorbed energy as blue fluorescent light between 400 and 500 nm [1]. Materials that evenly reflect most of the light at all wavelengths striking their surface appear white to the human eye. Natural fibers, for example, generally absorb more light in the blue region of the visible spectrum (blue defect) than in others because of impurities (natural pigments) they contain. As a result, natural fibers take on an unwanted, yellowish cast. Synthetic fibers also have this yellowish cast, although not as pronounced.The whiteness in substrates, however, can be improved by either increasing their reflection (reflectance) or compensating their blue defects. Before the advent of fluorescent whitening agents (FBA), the common practice was to apply small amounts of blue or violet dyes (called bluing agents) to boost the visual impression of whiteness. These dyes absorb light in the green-yellow region of the spectrum, thereby reducing brightness. Unlike bluing dyes, FBAs offset the yellowish cast by absorbing the invisible short wavelength radiation and re-emitting the visible blue light, which imparts a brilliant whiteness of the substrate.

Several derivatives of 1,8-naphthalimide have also been reported as FBAs. For examples, Grabchev [2] prepared 1,8-napthalimides containing an isolated double bond and used them in co-polymerization with acrylonitrile. Recently, a new method for the synthesis of 4-allyloxy-1,8-naphthalimide derivatives using phase transfer catalysis was reported in 2001 [3]. Four 4-allyloxy-1,8-naphthalimide fluorescent brighteners were synthesized in good yield and their absorption and fluorescent spectra were determined.

According to patented information [4], the thermal stabilities of fluorescent brighteners can be tuned by incorporating various phenoxy and alkoxygroups into the structures. In this project, we synthesized a series of aryloxy or alkoxy substituted naphthalimides derivatives and investigated their photophysical properties such as absorption, molar absorptivity, emission, and quantum efficiency. The thermal-stabilities will also be examined.

2. Experimental

2.1. Materials

All commercially available chemicals were purchased from Sigma-Aldrich (USA) used without purification. Commercial *n*-hexane, ethyl acetate and methanol were fractionally distilled before use. The ^{1}H NMR were determined on Varian Mercury NMR spectrophotometer (Varian, USA) at 400 MHz with chemical shifts reported as ppm in CDCl$_3$. The ^{13}C NMR was measured on Bruker NMR spectrophotometer (Bruker, Germany, which equipped at 100 MHz with chemical shifts reported as ppm in CDCl$_3$). To investigate their thermal properties, differential scanning calorimeter (DSC) 204 F1 Phoenix (Netzsch) was used to determine their glass transition temperature (T_g), melting temperature (T_m), and crystal temperature (T_c). UV-2550 UV-visible spectrophotometer (SHIMADZU, Japan) was used for absorption study. The emission spectra were acquired by Carry Eclipse Fluorescence Spectrophotometer (Agilent Technologies). The thermal gravimetric analysis (TGA) experiments were conducted at the PTT Company in Wang-Noi, Ayutthaya.

2.2. Synthesis
4-Bromo-*N*-(phenyl)-1,8-naphthalimide (2a)
4-Bromo-1,8-naphthalic anhydride (**1**) (1.0 g, 1.07 mmol), 6 mL glacial acetic acid, and 4Å Molecular sieve (4Å MS) (10 g) were added into a round bottom flask. Then, aniline (0.16 mL, 0.16 g,

1.76 mmol) was added. The mixture was stirred and heated under refluxing conditions overnight. After the reaction mixture was allowed to cool to room temperature, the mixture was poured into 30 g of ice and the resulting precipitate was filtered, washed with cool water, and dried over a steam bath. The white powder was next purified by column chromatography that used hexane/ethyl acetate (10:1) as the eluent to obtain **2a** as white crystalline solid (77%). ^{1}H NMR (CDCl$_3$) δ (ppm) 7.35 (d, J = 7.2 Hz, 2H), 7.50-7.64 (m, 3H), 7.90 (t, J = 8.0 Hz, 1H), 8.10 (d, J = 7.6 Hz, 1H), 8.48 (d, J = 8.0 Hz, 1H), 8.66 (d, J = 8.4 Hz, 1H), 8.73 (d, J = 6.8 Hz, 1H).

1 → a. **56 - 81 %** → **2a-c**

2a: Ar = phenyl
2b: Ar = 4-methoxy-phenyl
2c: Ar = 2,6-diisopropyl-phenyl

b. or c. **16 - 91 %** → **3a-g**

3a: Ar = phenyl
   R = cumylphenyl
3b: Ar = 4-methoxyl-phenyl
   R = cumylphenyl
3c: Ar = 2,6-diisopropyl-phenyl
   R = cumylphenyl
3d: Ar = 2,6-diisopropyl-phenyl
   R = phenyl
3e: Ar = 2,6-diisopropyl-phenyl
   R = butyl
3f: Ar = 2,6-diisopropyl-phenyl
   R = 4-*t*-butyl-phenyl
3g: Ar = 2,6-diisopropyl-phenyl
   R = 4-methoxycarbonyl-phenyl
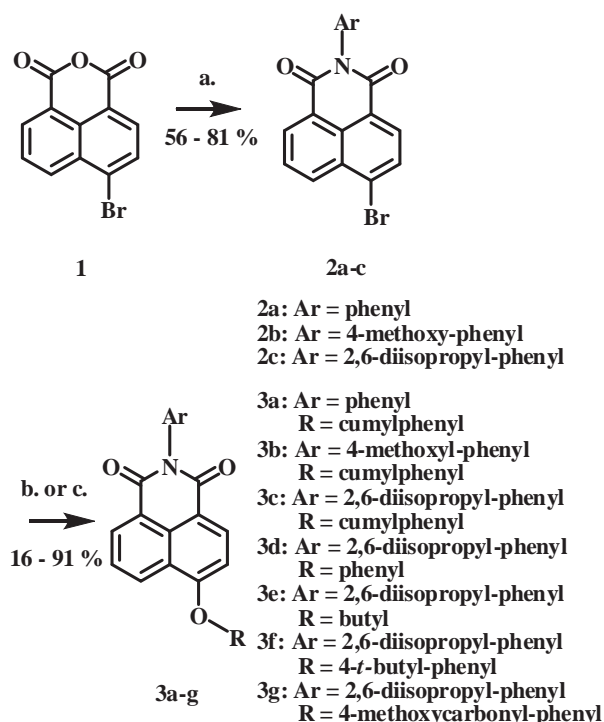
Scheme 1   Synthesis methods: (a) aromatic amine (ArNH$_2$), glacial acetic acid, reflux; (b) phenol or alcohol (ROH), KOH, 18-crown-6, DMF, 70 °C; (c) phenol or alcohol, K$_2$CO$_3$, DMF, 110 °C.

4-Bromo-*N*-(4-methoxy-phenyl)-1,8-naphthalimide (2b)

The synthesis of **2b** was conducted using the procedure described for **2a**. **2b** was obtained as an off-white powder (56%). ^{1}H NMR (CDCl$_3$) δ (ppm): 3.80 (s, 3H), 7.00 (d, J = 8.8 Hz, 2H), 7.15 (d, J = 8.8 Hz, 2H), 7.80 (t, J = 8.0 Hz, 1H), 8.01 (d, J = 8.0 Hz, 1H), 8.39 (d, J = 8.0 Hz, 1H), 8.57 (d, J = 8.4 Hz, 1H), 8.64 (d, J = 7.2 Hz, 1H).

4-Bromo-*N*-(2,6-diisopropyl-phenyl)-1,8-naphthalimide (2c)

The synthesis of **2c** was conducted using the procedure described for **2a**. **2c** was obtained as an off-white powder (81%). ^{1}H NMR (CDCl$_3$) δ (ppm): 1.05 (d, 12H), 2.65 (m, 2H), 7.25 (d, J = 7.6 Hz, 2H), 7.42 (t, J = 7.8 Hz, 1H), 7.85 (t, J = 7.8 Hz, 1H), 8.05 (d, J = 8.0 Hz, 1H), 8.40 (d, J = 8.0 Hz, 1H), 8.59 (d, J = 7.6 Hz, 1H), 8.66 (d, J = 7.2 Hz, 1H).

4-Cumylphenoxy-*N*-(phenyl)-1,8-naphthalimide (3a): Method A

A mixture of **2a** (0.21 g, 0.59 mmol), 4-cumylphenol (0.25 g, 1.19 mmol), KOH (0.05 g, 0.91 mmol), and 18-crown-6 (catalytic amount) in DMF (2 mL) was heated and stirred at 70°C overnight. The mixture was then poured into ice/water and the crude precipitate was collected by vacuum filtration and washed with water. After purification by column chromatography using hexane/ethyl acetate (4:1) as the eluent, **3a** was obtained as a pale powder solid (16%). ^{1}H NMR(CDCl$_3$) δ (ppm): 1.67 (s, 6H), 6.89 (dd, J = 7.6 Hz and 8.4 Hz, 1H), 7.04 (d, J = 8.4 Hz, 2H), 7.12 – 7.34 (m, 9H), 7.42 (d, J = 6.4 Hz, 1H), 7.75 (t, J = 7.6 Hz, 1H), 8.45 (d, J = 8.4 Hz, 1H), 8.63(d, J = 7.2 Hz, 1H), 8.70 (d, J = 8.8 Hz, 1H), 7.50 (d, J = 6.4 Hz, 1H). ^{13}C NMR (CDCl$_3$) δ (ppm): 30.7, 42.8, 110.5, 116.5, 120.2, 122.7, 124.1, 125.9, 126.5, 126.8, 128.5, 128.6, 128.7, 129.3, 129.5, 130.0, 130.1, 130.3, 133.3, 148.4, 150.3, 152.4, 160.3, 164.6.

4-Cumylphenoxy-*N*-(phenyl)-1,8-naphthalimide (3a): Method B

A mixture of **2a** (2.6 g, 7.39 mmol), 4-cumylphenol (3.24 g, 15.26 mmol), anhydrous potassium carbonate (3.03 g, 21.91 mmol) in DMF (120 mL) was heated and stirred at 110 °C overnight. The mixture was then poured into ice/water and the crude precipitate was collected by vacuum filtration and washed with water. After purification by column chromatography using hexane/ethyl acetate (10:1) as the eluent, **3a** was obtained as a pale powder (66%).

4-Cumylphenoxy-*N*-(4-methoxy-phenyl)-1,8-naphthalimide (3b)

This compound was prepared using Method B described for **3a** and was obtained as a yellow powder solid (91%). ^{1}H NMR(CDCl$_3$) δ (ppm): 1.74 (s, 6H), 3.87 (s, 3H), 6.95 (d, J = 8.4 Hz, 1H), 7.06 (d, J = 8.8 Hz, 2H), 7.11 (d, J = 8.8 Hz, 2H), 7.20 – 7.40 (m, 9H), 7.82 (t, J = 8.4 Hz, 1H), 8.50(d, J = 8.4 Hz, 1H), 8.70 (d, J = 8.4 Hz, 1H), 8.76 (d, J = 8.4 Hz, 1H). ^{13}C NMR (CDCl$_3$) δ (ppm): 30.9, 55.5, 110.5, 114.7, 120.2, 125.9, 126.5, 126.7, 128.2, 128.8, 128.9, 129.6, 132.3, 133.2, 148.4, 152.5, 159.5.

4-Cumylphenoxy-*N*-(2,6-diisopropyl-phenyl)-1,8-naphthalimide (3c)

This compound was prepared using Method B described for **3a** and was obtained as a white powder solid (89%). ^{1}H NMR (CDCl$_3$) δ (ppm): 1.08 (d, 12H), 1.67 (s, 6H), 2.67 (m, 2H), 6.80 - 7.30 (m, 12H), 7.39 (t, J = 7.8 Hz, 1H), 7.75 (t, J = 7.8 Hz, 1H), 8.45 (d, J = 8.4 Hz, 1H), 8.64 (d, J = 7.2 Hz, 1H), 8.70 (d, J = 8.4 Hz, 1H), ^{13}C NMR (CDCl$_3$) δ (ppm): 24.0, 29.2, 30.9, 42.9 110.7, 114.8, 120.2, 125.9, 126.8, 128.2, 128.9, 129.4, 132.4, 133.4, 145.8, 148.4, 150.3, 152.6, 160.3, 163.8, 164.5.

4-Phenoxy-*N*-(2,6-diisopropyl-phenyl)-1,8-naphthalimide (3d)

This compound was prepared by Method B described for **3a** using phenol instead of 4-

cumylphenol. It was obtained as a white powder solid (79%). ^{1}H NMR (CDCl$_3$) δ (ppm): 1.20 (d, 12H), 2.80 (m, 2H), 7.00 (d, J = 8.0 Hz, 1H), 7.25 (d, J = 7.6 Hz, 2H), 7.36 (d, J = 7.6 Hz, 3H), 7.53 (dd, J = 6.4 Hz and 7.6 Hz, 3H), 7.85 (t, J = 7.6 Hz, 1H), 8.57 (d, J = 8.0 Hz ,1H), 8.77 (d, J = 7.4 Hz, 1H), 7.50 (t, J = 7.6 Hz, 1H), 8.61 (d, J = 8.0 Hz, 1H), 8.67 (d, J = 6.8 and 7.6 Hz, 1H), 8.83 (d, J = 8.0 Hz, 1H).^{13}C NMR (CDCl$_3$) δ (ppm): 14.2, 24.0, 29.3, 110.9, 115.4, 116.7, 120.8, 122.8, 124.3, 125.7, 126.7, 128.9, 129.5, 130.5, 131.1, 132.5, 133.4, 145.8, 155.0, 160.2, 163.8, 164.5.

4-Butoxy-*N*-(2,6-diisopropyl-phenyl)-1,8-naphthalimide (3e)

A mixture of **2c** (0.14 g, 0.38 mmol) and K$_2$CO$_3$ (0.40 g, 2.92 mmol) was refluxed in *n*-butanol (7.0 ml, 5.67 g, 76.5 mmol). After the evaporation of solvent and purification by column chromatography, **3e** was obtained as white solid in 76%. ^{1}H NMR(CDCl$_3$) δ (ppm): 1.07 (t, 3H), 1.15 (d, 12H), 1.65 (m, 2H), 2.00 (m, 2H), 2.75 (m, 2H), 4.43 (m, 2H), 7.08 (d, J = 8.0 Hz, 1H), 7.26 – 7.33 (m, 2H), 7.49 (t, J = 7.4 Hz, 1H), 7.50 (t, J = 7.6 Hz, 1H), 8.61 (d, J = 8.0 Hz, 1H), 8.67 (d, J = 7.6 Hz, 2H). ^{13}C NMR (CDCl$_3$) δ (ppm): 13.8, 19.4, 24.0, 29.1, 31.0, 105.9, 114.8, 122.5, 123.9, 125.9, 129.0, 129.3, 130.1, 132.0, 134.1, 145.8, 160.7, 164.0, 164.6.

4-(4-*tert*-butyl-phenoxy)-*N*-(2,6-diisopropyl-phenyl)-1,8-naphthalimide (3f)

This compound was prepared by Method B described for **3a** using 4-*tert*-butyl-phenol instead of 4-cumylphenol. **3f** was obtained as a pale powder solid (78%). ^{1}H NMR (CDCl$_3$) δ (ppm): 1.16 (d, 12H), 1.39 (s, 9H), 2.75 (m, 2H), 7.00 (d, J = 8.4 Hz, 1H), 7.25 (d, J = 8.0 Hz, 2H), 7.32 (d, J = 8.0 Hz, 2H), 7.45 – 7.55 (m, 3H), 7.85 (t, J = 8.4 Hz, 1H), 8.52 (d, J = 8.4 Hz, 1H), 8.73 (d, J = 8.4 Hz, 1H), 8.80 (d, J = 8.4 Hz, 1H). ^{13}C NMR (CDCl$_3$) δ (ppm): 24.0, 29.1, 31.5, 34.6, 110.5, 116.4, 120.2, 122.7, 124.0, 124.2, 126.5, 127.3, 128.9, 129.4, 130.4, 131.0, 132.4, 133.4, 133.6, 145.7, 148.7, 152.4, 160.4, 163.8, 164.4.

4-(4-methoxycarbonyl-phenoxy)-*N*-(2,6-diisopropyl-phenyl)-1,8-naphthalimide (3g)

The synthesis of **3g** was carried out using method described for **3a** using methyl 4-hydroxybenzoate instead of phenol. **3g** was obtained as a yellow powder solid (19%). ^{1}H NMR (CDCl$_3$) δ (ppm): 1.15 (d, 12H), 2.74 (m, 2H), 3.95 (s, 3H), 7.10 (d, J = 8.4 Hz, 1H), 7.20 (d, J = 8.8 Hz, 2H), 7.33 (d, J = 7.6 Hz, 2H), 7.48 (t, J = 7.6 Hz, 1H), 7.85 (t, J = 8.4 Hz, 1H), 8.15 (d, J = 8.8 Hz, 2H), 8.57 (d, J = 8.4 Hz, 1H), 8.70 (d, J = 8.4 Hz, 1H), 8.74 (d, J = 8.4 Hz, 1H). ^{13}C NMR (CDCl$_3$) δ (ppm): 24.0, 29.1, 52.3, 112.8, 117.9, 119.5, 122.9, 124.0, 124.6, 127.0, 128.6, 129.5, 130.4, 130.8, 132.2, 132.6, 133.0, 145.7, 158.5, 159.5, 163.6, 164.2, 166.2.

2.3. Photophysical test

Absorption

The stock solutions of each compound were prepared in CH$_2$Cl$_2$ at 10^{-3} – 10^{-5} M, then diluted to more than 5 different concentrations. To obtain the accurate result, all absorbance should not exceed 1.0 arbitrary unit (a.u.). The molar absorptivity (ε) was obtained from the slope of the calibration curve between concentration and absorbance. The λ$_{max}$ was chosen from the wavelength that provides the highest absorbance.

Emission or Fluorescence

To collect the complete fluorescent spectra, all compounds were excited at 364 nm and started to collect at each 10 nm interval with a slit width of 5 nm to prevent the residual absorption band. In this work, the PMT was controlled at 595 volts.

Quantum yield

The quantum yield was determined from the absorbance at λ$_{max}$ and the sum of all fluorescent intensity at all wavelengths. Then, the slope from the plot between sum of fluorescent intensity and absorbance of all compounds were determined and compared to the standard compound. Quinine sulfate in 0.1 M H$_2$SO$_4$ with a quantum yield of 0.54 was used as the standard [5].

3. Results and discussion

3.1. Synthesis of fluorescent brighteners

The synthesis of fluorescent brighteners was successfully conducted as shown in the experimental part. It is worth noting that the substitution of the bromo group by phenoxyl group (second step) using the patented condition [4] did not yield appreciable amount of the expected product. For example, the reaction of **3a** under the patented condition would exclusively resulted in the hydroxyl substituted products. Since the patented condition could generate free hydroxide rapidly; and then, the free hydorxide, which acts as nucleophilic base, might substituted faster than generation of phenoxide. To overcome this problem, we replaced the KOH by a weaker and non-nucleophilic base – potassium carbonate and chose to operate at a high temperature, which resulted in a much greater yield of phenoxyl substituted products (**3a-e**). In fact, the acidic proton at hydroxy group is poor in the case of aliphatic alcohol. Fortunately, the preparation of **3e** could occur; although only this case, 28% recovery of starting material was obtained.

3.2. Photophysical study

The absorption and emission data of **3a-g** were summarized in **Table 1**. The absorption (λ$_{max}$ and ε) and emission properties (λ$_{max}$) of these compounds are insignificantly different, which correspond to their similar photoactive π-conjugate system. These compounds absorbed 365-nm UV light and emitted visible light (420-430 nm) - a desired characteristic

for optical brightener. However, the quantum yields varied drastically depending on the substituent at the

Table 1 The photophysical and thermal properties of **3a-g**.

Cmpd	Absorption		Emission		Td (°C)[f]	Tm (°C)[d]	Tg (°C)[e]	Tc (°C)[d]
	λ_{max} (nm)[a]	log ε (M^{-1} cm^{-1})[a]	λ_{max} (nm)[b]	Φ^c				
3a	364	4.19	433	0.12	430	177	72	142
3b	364	4.15	436	0.005	430	242	72	112
3c	365	4.11	435	0.11	430	192	82	-
3d	364	4.18	425	0.87	375	218	83	-
3e	368	4.22	431	0.92	340	212	-	147
3f	364	4.27	434	0.11				
3g	359	4.30	421	0.55				

[a] measured in diluted CH_2Cl_2 solution, [b] excited at 364 nm, [c] determined by using quinine sulfate in 0.1 M H_2SO_4 as standard, [d] determined by DSC on the first heating cycle with a heating rate of 10 °C/min under N_2, [e] determined by DSC on the second heating cycle with a heating rate of 10 °C/minute under N_2, [f] 10% decomposition temperature obtained from TGA data with a heat rate of 10 °C/min under N_2.

nitrogen (**3a-c**) and the 4-position (**3c-g**). For the nitrogen substituent, the electron-rich group such as the 4-methoxyphenyl in **3b** may lower quantum yield by internal charge transfer (ICT) process having the imide group as the electron-withdrawing fragment. For the substituents at the 4-position, we proposed that they might take part in a photo-induced electron transfer (PET) process, but the effects are variable depending on their energy levels. Compound with phenoxy (**3d**) and *n*-butoxy group (**3e**) exhibited excellent quantum efficiencies (87 and 92%, respectively), whereas those with cumylphenoxy (**3c**), 4-*t*-butylphenoxy (**3f**), and 4-methoxycarbonyl phenoxy (**3g**) showed lower quantum efficiencies. This might indicated that the LUMO of these latter three groups located in between the HOMO and LUMO levels of the naphthalimide unit, thus allow the electron to transfer to the excited fluorophore. In order to prove this hypothesis, we are currently performing computational calculations and the results will be reported in due course.

3.3. Thermal stability test

Data from Differential Scanning Calorimetry (DSC) and Thermo Gravimetric Analysis (TGA) were summarized in **Table 1** as glass transition temperature (T$_g$), melting temperature (T$_m$), crystallization temperature (T$_c$), and 10% decomposition temperature (T$_d$). It is apparent that compounds with a cumylphenoxy group (**3a-c**) are more thermally stable. This may cause by the bulkiness and steric hindrance of the cumylphenyl group. Nevertheless, most compounds (**3a**-**3e**) have glass-transition temperatures in the range of 70-80 °C, which are suitable for application in blending or molding process of thermoplastic.

4. Conclusions

A series of 4-alkoxy or 4-aryloxy-*N*-aryl napthalimides were successfully synthesized and characterized. Based on their absorption and emission maxima, they are suitable for application as optical or fluorescent brighteners. The substitution at the 4-position with cumylphenoxy group resulted in compounds with excellent thermal stability, i.e. 10% decomposition temperature at 430 °C. Interestingly, it is found that their quantum efficiencies or quantum yields are exclusively dependent on the substituents at the 4-position. It is believed that the electronic effect of the substituents on the 4-aryloxy groups influences the photo-induced electron transfer (PET) process, which causes a variation in quantum efficiencies.

References

[1] http://www.mufong.com.tw/Ciba/ciba_guid/optical_brighteners.pdf, available online on 5 September 2011.
[2] Grabchev, I.; Bojinov, V. *Polym. Degrad. Stabil*. **70** (2000) 147-153.
[3] Bojinov, V.; Grabchev, I. *Dyes Pigments*. **51** (2001) 57-61.
[4] Niak, S. N.; Dhalla, A. M.; Chauhan, Y. B. Fluorescent brighteners, methods of preparation thereof, fluorescent brightener compositions, and methods of preparation and uses thereof. *US patent 20070117887A1*.
[5] Melhuish, W. H. *J. Phys, Chem.* **65** (1961) 229-235.

DERIVATIVES OF CARBAZOLE AND TRUXENE AS HOLE-TRANSPORTING MATERIALS IN OLED

Danusorn Raksasorn[1], Mongkol Sukwattanasinitt[2], and Paitoon Rashatasakhon[2*]

[1] Program of Petrochemical and polymer science, Faculty of Science, Chulalongkorn University, Bangkok 10330 Thailand
[2] Organic Synthesis Research Unit, Department of Chemistry, Faculty of Science, Chulalongkorn University, Bangkok 10330 Thailand

[*] Author for correspondence; Email: paitoon.r@chula.ac.th, Tel. +6622817620

Abstract: Two derivatives of carbazole and truxene (compound 1 and 2) are synthesized by iodination of truxene core and Cu-catalyzed C-N coupling with carbazole or 3,6-di(9-carbazolyl) carbazole. All compounds are characterized by ^{1}H-NMR, ^{13}C-NMR and mass spectroscopy. The photophysical properties of compound 1 and 2 are studied using UV-vis and fluorescence spectroscopy. In solution phase, the absorption of two compounds appears very similar with a maximum absorption wavelength at 330 nm. The fluorescence spectra of compound 1 and 2 exhibit a maximum emission wavelength at 367 and 391 nm, respectively, corresponding to the higher degree of geometrical relaxation for 2, which contains more carbazole units. The thermal properties of two compounds are determined by thermogravimetric analysis (TGA) and differential scanning calorimetry (DSC). Compound 1 and 2 possess high thermal stability (Tg = 249 and 293 ºC, respectively) and TGA suggesting that all compounds are thermally stable with 5% weight loss temperature (T_{5d}) at 392 and 371 ºC, respectively.

1. Introduction

Organic light-emitting diodes (OLEDs) have become an attractive technology since the end of 20th century due to their energy-saving nature and abilities to be fabricated flat or flexible displays [1]. In a typical OLED device, there is a thin layer of emitting material (EM) sandwiched between cathode and anode. Upon electrical excitation, a recombination of electron from the LUMO and hole or positive charge at the HOMO of the EM molecule will result in the emission of visible light [2-3]. In order to improve the device efficiency, layer of hole- or electron-transporting material (HTM, or ETM) can be fabricated between EM and electrodes [4]. The most commonly used HTMs are N,N'-diphenyl-N,N'-bis(1-naphthyl)-(1,1'-biphenyl)-4,4'-diamine (NPB) and N,N'-bis(3-methylphenyl)-N,N'-bis(phenyl) benzidine (TPD), which have high hole mobility. However, low glass transition temperature (T_g) of NPB and TPD (100 and 65 °C, respectively) and their low morphological properties leading to degradation of devices. There have been several examples of molecular designs which incorporate emissive and hole-transporting moieties into the same molecules [5-9], which not only gave rise to new optoelectronic materials with superior properties, but also eased multiple fabrications on the electrodes. In out current study, we incorporated highly emissive truxene unit with carbazole fragments with an aim to achieve new OLED materials with a combination properties of EM and HTL. The synthesis and characterization of the new compounds are reported herein.

2. Materials and Methods

2.1 Chemical and instruments

All reagents were purchased from Aldrich, Fluka and used without further purification. All ^{1}H-NMR spectra were recorded on Varian Mercury 400 MHz NMR spectrometer (Varian, USA). ^{13}C-NMR spectra were recorded at 100 MHz on Bruker NMR spectrometer. Mass spectra were recorded on a Microflex MALDI-TOF mass spectrometer (Bruker Daltonics) using doubly recrystallized α-cyano-4-hydroxy cinnamic acid (CCA) as a matrix. Absorption spectra were measured by a Varian Cary 50 UV-Vis spectro photometer. Fluorescence spectra were obtained from a Varian Cary Eclipse spectrofluorometer. Thermal experiments with Differential Scanning Calorimeter (DSC) were performed on Mettler Toledo DSC 822e and Thermogravimetric Analysis (TGA) were studied using Simultaneous Thermal Analyzer Netzsch 409.

2.2 Synthesis

2.2.1 3,6-di(9-carbazolyl) carbazole (5)

The compound was prepared according to the literature method [10].

2.2.2 Truxene (6) [11,12]

A mixture of 3-phenylpropionic acid (10.02 g, 66.72 mmol) and polyphosphoric acid (50 g) was heated at 60 °C for 60 min under nitrogen atmosphere. Water (5 mL) was then added to the reaction and temperature was raised to 160 °C for 3 h. After the reaction was cooled to room temperature, the mixture was poured into ice water and grey powder was filtered and washed with water. The crude product was purified by recrystallization from toluene to yield 6 as light-yellow solid (11.12 g, 49%). ^{1}H NMR (CDCl$_3$): δ 7.92 (d, J = 7.5 Hz, 1H), 7.68 (d, J = 7.3 Hz, 1H), 7.50 (t, J = 7.2 Hz, 1H), 7.39 (t, J = 7.2 Hz, 1H), 4.22 (s, 2H).

2.2.3 5,5,10,10,15,15-hexabutyl-truxene (7)

A solution of truxene (6) (1.00 g, 2.92 mmol) in DMF (50 mL) at 0 °C under nitrogen, NaH (1.19 g,

29.8 mmol) was added and the solution was allowed to warm to room temperature and stirred for 30 min, then n-butyl bromide (3.2 mL) was added for 24 h. The mixture was poured into water and extracted with EtOAc. The combined organic layer was dried over MgSO$_4$, filtered, and concentrated under reduce pressure. The crude product was purified by silica gel column chromatography using hexane as the eluent to yield **7** as white solid (1.48 g, 75%). ^{1}H NMR (CDCl$_3$): δ 8.38 (d, J = 7.4 Hz, 1H), 7.47 (d, J = 5.9 Hz, 1H), 7.43 – 7.31 (m, 2H), 3.09 – 2.88 (m, 2H), 2.20 – 2.00 (m, 2H), 1.02 – 0.79 (m, 4H), 0.61 – 0.35 (m, 10H).

2.2.4 5,5,10,10,15,15-hexabutyl-2,7,12-triiodo-truxene (8)

To a solution of **7** (0.50 g, 0.74 mmol) in 5 ml of solvent mixture (CH$_3$COOH:H$_2$SO$_4$:H$_2$O = 100:40:3) was added 1 mL of CCl$_4$. After adding KIO$_3$ (0.16 g, 0.75 mmol) and I$_2$ (0.94 g, 3.72 mmol), the mixture was heated to 80 °C and stirred for 3 h. The reaction was cooled to room temperature and poured into water. The crude product was obtained by filtration and purified by recrystallization from ethanol to afford white powder (0.65 g, 84%). ^{1}H NMR (CDCl$_3$): δ 8.07 (d, J = 8.4 Hz, 1H), 7.76 (s, 1H), 7.71 (d, J = 8.4 Hz, 1H), 2.91 – 2.77 (m, 2H), 2.08 – 1.95 (m, 2H), 0.99 – 0.78 (m, 4H), 0.59 – 0.30 (m, 10H).

2.2.5 Compound 1

A mixture of **8** (0.11 g, 0.10 mmol), carbazole (0.12 g, 0.73 mmol), Cu bronze powder (0.17 g, 2.69 mmol) and K$_2$CO$_3$ (0.21 g, 1.53 mmol) in degassed nitrobenzene (1 mL) was refluxed for 48 h under N$_2$ atmosphere. The resulting brown solution was allowed to cool to room temperature and extracted with CH$_2$Cl$_2$ (3 × 50 mL). The combined organic layer was dried over MgSO$_4$, filtered, and concentrated under reduce pressure. The crude product was purified by silica gel column chromatography using 4:1 hexane/CH$_2$Cl$_2$ as the eluent to yield **1** (48.6 mg, 41%). ^{1}H NMR (CDCl$_3$): δ 8.60 (d, J = 8.5 Hz, 1H), 8.22 (d, J = 7.8 Hz, 2H), 7.73 (s, 1H), 7.66 (d, J = 8.3 Hz, 1H), 7.59 (d, J = 8.2 Hz, 2H), 7.49 (t, J = 7.2 Hz, 2H), 7.35 (t, J = 7.2 Hz, 2H), 3.15 – 3.02 (m, 2H), 2.27 – 2.15 (m, 2H), 1.13 – 1.01 (m, 4H), 0.77 (dt, J = 23.8, 12.5 Hz, 4H), 0.62 (t, J = 7.3 Hz, 6H). ^{13}C NMR (100 MHz, CDCl$_3$): δ 155.5, 145.6, 140.9, 139.1, 138.1, 136.2, 125.95, 125.77, 124.7, 123.5, 120.8, 120.4, 120.0, 109.9, 56.0, 36.6, 26.7, 22.9, 13.9. MALDI-TOF-MS: found 1173.768 ([M]$^+$ calcd: 1173.69)

2.2.6 Compound 2

A mixture of **8** (0.11 g, 0.10 mmol), **5** (0.18 g, 0.37 mmol), Cu bronze powder (0.13 g, 2.05 mmol) and K$_2$CO$_3$ (0.22 g, 1.56 mmol) in degassed nitrobenzene (1 mL) was refluxed for 48 h under N$_2$ atmosphere. The resulting brown solution was allowed to cool to room temperature and extracted with CH$_2$Cl$_2$ (3 × 50 mL). The combined organic layer was dried over MgSO$_4$, filtered, and concentrated under reduce pressure. The crude product was purified by silica gel column chromatography using 4:1 hexane/CH$_2$Cl$_2$ as the eluent to yield **2** (0.11 g, 50%). ^{1}H NMR (CDCl$_3$): δ 8.80 (d, J = 8.5 Hz, 1H), 8.40 (s, 2H), 8.22 (d, J =

7.5 Hz, 4H), 7.99 (s, 1H), 7.96 – 7.85 (m, 3H), 7.75 (d, J = 8.7 Hz, 2H), 7.48 (q, J = 8.3 Hz, 8H), 7.34 (t, J = 7.1 Hz, 4H), 3.33 – 3.20 (m, 2H), 2.48 – 2.36 (m, 2H), 1.27 – 1.10 (m, 4H), 1.03 – 0.80 (m, 5H), 0.72 (t, J = 7.3 Hz, 6H). ^{13}C NMR (100 MHz, CDCl$_3$): δ 156.2, 146.2, 142.0, 140.9, 139.9, 138.4, 136.0, 130.8, 126.6, 126.3, 126.1, 125.2, 124.4, 123.4, 121.2, 120.5, 120.1, 119.9, 111.5, 109.9, 56.5, 37.0, 27.0, 23.1, 14.2. MALDI-TOF-MS: found 2165.802 ([M]$^+$ calcd: 2164.04)

3. Results and Discussion

3.1 Synthesis of compound **1** and **2**

Upon the preparation of truxene from 3-phenylpropionic acid according to the reported procedure, the methylene units were alkylated by excess amount of *n*-butylbromide to afford **7** in 75%. This hexaalkylated compound exhibit greater solubility in organic solvents, which facilitate not only the purification process of the target and intermediate molecules, but also prevent the aggregation by pi-stacking leading to low quantum efficiency. Treatment of **7** with KIO$_3$ and I$_2$ produced triiodo **8** which reacted with carbazole in the presence of catalytic amount of Cu bronze to afford **1** in moderate yield.
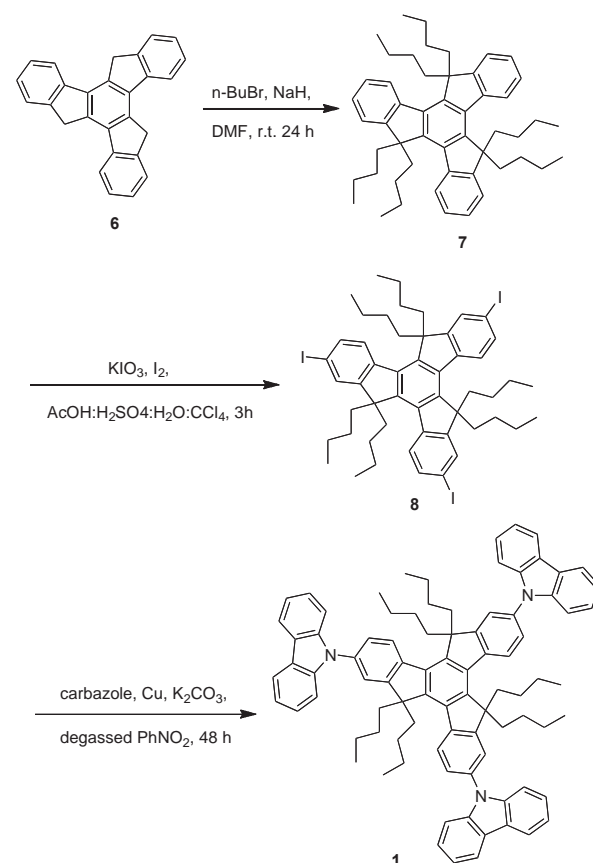
Scheme 1. Synthesis of **1**

In addition, the synthetic process for 3,6-di(9-carbazolyl) carbazole (**5**) was outlined in scheme 2. The target compound **2** was then accomplished by the Cu-catalyzed C-N coupling of **5** with **8**.

Scheme 2. Synthesis of **2**

Figure 1. Normalized absorption and emission spectra of compound **1** and **2** in CHCl$_3$ solution

3.2 Photophysical properties of compound **1** and **2**

The investigation of absorption properties of **1** and **2** in CHCl$_3$ revealed that both compounds had a similar maximum absorption wavelength (Table 1 and Figure 1). However, the molar absorptivity of **2** was slightly higher than that of **1** due to higher number of photoactive carbazole units. For the fluorescence properties, the emission band of **2** appeared at a longer wavelength which probably due to a higher degree of geometrical relaxation upon excitation. This is also evident by the lower quantum efficiency of **2** (0.10) as compared to that of **1** (0.22) [13].

Table 1. Photophysical properties of compound **1** and **2**.

Cpd.	Absorption		Emission	
	λ_{max} (nm)	log ε (M^{-1}cm^{-1})	λ_{max} (nm)	Φ_F [a]
1	331	4.95	367	0.22
2	330	5.05	391	0.10

[a] 2-aminopyridine in 0.1 M H$_2$SO$_4$ (Φ_F = 0.60) was the reference.

3.3 Thermal properties

The thermal properties of **1** and **2** were studied by differential scanning calorimetry (DSC) and thermogravimetric analysis (TGA). The results are summarized in Table 2. From TGA data suggested that all compounds were thermally stable with 5% weight loss (T$_{5d}$) at 392 and 371 ^{o}C, respectively. From the second heating cycle on DSC, compound **1** showed only an endothermic peak at 249 ^{o}C due to glass transition temperature (T$_g$) and no signal for melting and crystallization temperature was observed. For compound **2**, an endothermic baseline shift due to the glass transition temperature (T$_g$) at 293 ^{o}C was observed. These results suggested that all compound could form molecular glass with high T$_g$.

Table 2. Thermal properties of compound **1** and **2**

Cpd.	Mp^c (^{o}C)	T$_g^a$ (^{o}C)	T$_d^b$ (^{o}C)
1	>300	249	392
2	>300	293	371

[a] Obtained from DSC measurements on the second heating cycle with a heating rate of 10 ^{o}C/min under N$_2$ atmosphere.
[b] Obtained from TGA measurements with a heating rate of 10 ^{o}C/min under N$_2$ atmosphere.
[c] Obtained from scientific melting point.

4. Conclusions

Two derivatives of carbazole and truxene were successful synthesized by iodination of truxene core and Cu-catalyzed C-N coupling with carbazole or 3,6-di(9-carbazolyl) carbazole. With 6 *n*-butyl groups substituted on the truxene core preventing aggregation by pi-stacking, the compounds were well-soluble in organic solvents. In addition, both **1** and **2** were thermally stable and could form molecular glass with high T$_g$.

References

[1] N.T. Kalyani, S.J. Dhoble, *Renew. Sust. Energ. Rev.* **16** (2012) 2696-2723.

[2] F. Hide, M.A. Diaz-Garcia, B.J. Schartz, A.J. Heeger, *Accounts Chem. Res.* **30** (1997) 430–436.

[3] J.H. Burroughes, D.D.C. Bradley, A.R. Brown, R.N. Marks, K. Mackey, R.H. Frien, P.L. Burns, A.B. Holmes, *Nature* **347** (1990) 539-541.

[4] C. W. Tang, S.A. VanSlyke, *Appl. Phys. Lett.* **51** (1987) 913–915.

[5] T. Kumchoo, V. Promarak, T. Sudyoadsuk, M. Sukwattanasinitt, P. Rashatasakhon, *Chem.-Asian J.* **5** (2010) 2162-2167.

[6] J. Li, D. Liu, Y. Li, C.-S. Lee, H.-L. Kwong, S. Lee, *Chem. Mater.* **17** (2005) 1208-1212.

[7] V. Promarak, M. Ichikawa, T. Sudyoadsuk, S. Saengsuwan, S. Jungsuttiwong, T. Keawin, *Synthetic Met.* **157** (2007) 17–22.

[8] V. Promarak, M. Ichikawa, T. Sudyoadsuk, S. Saengsuwan, S. Jungsuttiwong, T. Keawin, *Thin Solid Films.* **516** (2008) 2881–2888.

[9] Z. Yang, B. Xu, J. He, L. Xue, Q. Guo, H. Xia, W. Tian, *Org. Electron.* **10** (2009) 954–959.

[10] A. Kimoto, J.-S. Cho, M. Higuchi, K. Yamamoto, *Macromolecules.* **37** (2004) 5531-5537.

[11] Yuan MS, Fang Q, Liu ZQ, Guo JP, Chen HY, Yu WT, et al. *J. Org. Chem.* **71** (2006) 7858-7861.

[12] N. Earmrattana, M. Sukwattanasinitt, P. Rashatasakhon, *Dyes Pigments.* **93** (2012) 1428-1433.

[13]Lacowicz, J.R., *Principles of Fluorescence Spectroscopy [3rd] Ed,* Springer Science, New York (2006), pp. 1 – 25.

SILICONE TUBE WITH DRUG RELEASE PROPERTY

Jiratchaya Mokkaphan[1*], Supason Wanichwecharungruang[2], Premsuda Sombuntham[3]

[1] Department of Petrochemical and Polymer Science, Chulalongkorn University, Pathumwan, Bangkok, 10330 Thailand
[2] Department of Chemistry, Faculty of Science, Chulalongkorn University, Bangkok 10330, Thailand
[3] Department of Otolaryngology Head and Neck surgery, Faculty of Medicine, Chulalongkorn University, Bangkok 10330, Thailand

* Author for correspondence; E-Mail: Mokkaphan_555@hotmail.com, Tel. +66 22187634, Fax. +66 22 541309

Abstract: In medication, tracheostomy tube, made from polydimethylsiloxane (PDMS), is used in patients with chronic obstructive pulmonary disease (COPD) to provide an airway and to remove secretions from the lungs. However, after intubation, inflammation may occur. Thus polysiloxane tube that possesses anti-inflammatory activity should help solving the problem. The goal of this study is, therefore, to fabricate polysiloxane tube that can slowly release budesonide, an anti-inflamatory drug, into the contacted environment. Here budesonide was first encapsulated into ethylcellulose polymeric nanoparticles by solvent displacement method. The budesonide-loaded particles were then grafted on to the polysiloxane tube. In vitro release of budesonide from the polysiloxane modified tube at 37°C, pH 5.8 was studied. The result indicated prolonged release of budesonide for at least 10 days.

1. Introduction

Silicone (PDMS) tracheal tubes have been used widely in patients with COPD due to its specific mechanical properties softness, low toxicity, and relatively good blood compatibility [1-6]. The most common indication for tracheotomy is patients requiring long-term mechanical ventilation. Patients with chronic obstructive lung disease, with poor control of airway secretions may require tracheotomy not only to prevent aspiration of particulates but also to allow their removal by frequent airway suctioning [7]. However, tracheotomy may cause tracheal injury, an increased of bacterial contamination of the airway in patients with tracheotomy, suggesting a potential increased risk of lower airway infections. The gram-negative bacilli that have a major impact on patient outcome whenever deep-seated infections occur [8-11].

Budesonide is an anti-inflammatory drug. It blocks the inflammatory cell influx and inhibits inflammatory mediator release by inhibition of the arachidonic acid pathway. Budesonide is one of the corticosteroids representing the cornerstone of asthma management, an intranasal budesonide has been proven very effective for a long time [12-16]. Thus we purpose here to incorporate budesonide into the PDMS tube in order to make the tubing with anti-inflammatory activity for lessening the inflammation problem during tracheostomy.

Here budesonide was first loaded into nanoparticles made of ethyl cellulose polymers (EC) then the budesonide loaded particles were covalently linked to the surface of the silicone tube. The release of the budesonide from the tube was then evaluated.

2. Materials and Methods

2.1 Materials

Poly(dimethyl siloxane) (PDMS) tubes were from Koken (Tokyo, Japan). Ethylcellulose (EC, Ethyl 48% w/w ethoxy content, viscosity 300 cp) and 1-hydroxybenzotriazole (HOBt) were purchased from Sigma Aldrich (Steinheim, Germany). Budesonide (MW 430.5, analytical grade) was purchased from Fluka (Seelze, Germany). Succinic anhydride (analytical grade), 3-aminopropyltriethoxysilane (γ-APS) and 1-Ethyl-3-(3-dimethylaminopropyl) carbodiimide (EDCI) were purchased from Acros Organics (Geel, Belgium). Rhodamine B Sulfonyl Chloride was purchased from Invitrogen (USA).

2.2 Instruments

High performance liquid chromatography (HPLC) was performed with a Waters 1525 Binary HPLC (pump), connected to a Waters 2489 (UV/VIS detector). UV–Vis spectroscopy was obtained from UV-2550 (SHIMADZU, Japan). Scanning electron microscope (SEM) photographs were obtained from JEM-6400 (JEOL, Japan). Size distribution was obtained with Zetasizer nano series instrument (Zs, Malvern Instruments, USA). Contact angle was obtained from Ramé-hart, Model 200, Standard Contact Angle Goniometer, Succasunna (NJ, USA). Surface topography was observed through confocal laser scanning fluorescence microscopy (CLFM), Nikon Digital Eclipse C1si Confocal Microscope system (Tokyo, Japan).

2.3 Preparation of chemically functionalized PDMS surface

The oxygen-plasma-treated PDMS tubes were refluxed with γ-APS in toluene (2:100 % v/v) at 110 °C for 3 h under N_2 atmosphere. Triethanolamine (TEA) served as the catalyst was added to a reaction mixture (Scheme 1a-1b). Then the tubes were rinsed with distilled water followed with excess hexane and ethanol, then washed and annealed at room temperature for 24 h. The obtained γ-APS-modified PDMS tubes were dipped in solution of succinic anhydride in DMF in a presence of catalytic amount of

pyridine. The mixture was stirred at 80 °C overnight under N$_2$ atmosphere (Scheme 1b-1c).

2.4 Surface characterization

The Kaiser reaction was used to confirm the presence of primary amino terminal groups on the tube [17]. The activated surface by oxygen plasma was analysed by contact angle using deionized water (Millipore water). The particle-grafted-PDMS tubes were subjected to SEM and CLFM analyses.

2.5 Nanoparticles formation

Budesonide was encapsulated into the EC at budesonide to polymer weight ratios of 1:1 by solvent displacement method [18, 19]. Budesonide (500 mg) and EC (500 mg) were dissolved in ethanol to give EC and budesonide concentrations of 5,000 ppm each. The mixture (50 mL) was dialyzed against distilled water (CelluSep T4, MWCO 12,000–14,000, Membrane Filtration Products, Seguin, TX, USA). The obtained budesonide encapsulated particles in aqueous suspension were subjected to SEM analysis. The amounts of budesonide encapsulated into polymeric particles and in the dialysate water were determined using UV/VIS absorption spectroscopy at 246 nm, with the aid of a calibration curve. The encapsulation efficiency (% EE) and loading capacity were calculated from the following equations:

Encapsulation efficiency (%) = (A/B)×100
Loading (%)   = [A/(B+C)]×100

Whereas A = weight of encapsulated budesonide = weight of budesonide used - weight of budesonide found in dialysate; B = weight of budesonide used; C = weight of polymer used.

2.6 Preparation of budesonide particles grafted PDMS tube

The budesonide particles grafted PDMS tube was carried out through esterification reaction using EDCI and HOBt as coupling agents. Budesonide-loaded particles (aqueous suspension, 50 ml, 500 mg budesonide, 500 mg EC) were put into a round bottom flasks and HOBt (0.88 g, 0.65 mol, dissloved in 5 ml ethanol) was added. Then the functionalized tubes (0.5 mol, 2.51 cm^2 surface area on each tube, 30 tubes) and EDCI (1.25 g, 0.65 mol) were put in and the mixture was stirred in ice bath at 0 °C under N$_2$ atmosphere overnight (Scheme 1c-1d). Then tubes were rinsed with distilled water, and repeatedly washed with excess ethanol. Topography of the tube and nanoparticles were examined with SEM and CLSM.

2.7 Preparation of fluorescence labeled particles

The fluorophore Rhodmine B (Lissamine rhodamine B sulfonyl chloride) was first covalently linked to the EC by adding 1% of Rhodmine B into aqueous EC particle suspension under light-proof and N$_2$ atmosphere and the mixture was stirred at room temperature overnight. The Rhodamine B-labeled EC polymer was then purified from free Rhodamine B by dialysis under light-proof condition and the obtained polymer was used to prepare particles as described

above. The obtained labelled particles were grafted onto the PDMS tube as previously described and the product was subjected to CLFM analysis.

2.8 Determination of release profiles

Seven tubes (2.51 cm^2 for each tube) were soaked in phosphate buffer saline (PBS) solution (1.55 mM, pH 5.8, 5 ml) at 37°C. Aliquots of the release medium (500 µL each) were transferred into 1.5 ml tube, at the indicated times (0, 1, 2, 5, 7, 10, 13, 17 and 21 days) and were subjected to budesonide quantification. During each time the volume of the suspension was kept constant by adding PBS as required (500 µL each). The withdrawn aliquot was filtered by nylon syringe filters (13 mm, 0.2µm, 100/PK), then added with 200 µL ethyl acetate and the ethyl acetate layer was subjected to budesonide quantification using HPLC analysis with the aid of a calibration graph constructed from freshly prepared standard budesonide solutions. The stationary phase was 100 mm × 4.6 mm column packed with Hypersil C18 and the mobile phase consisting of ethanol : acetonitrile : 25 mM phosphate buffer pH 3 (2:30:15, v/v/v). The flow rate was set at 1.5 mL/min and the detection by UV detection at 240 nm. The experiment was repeated three times.

3. Results and Discussion
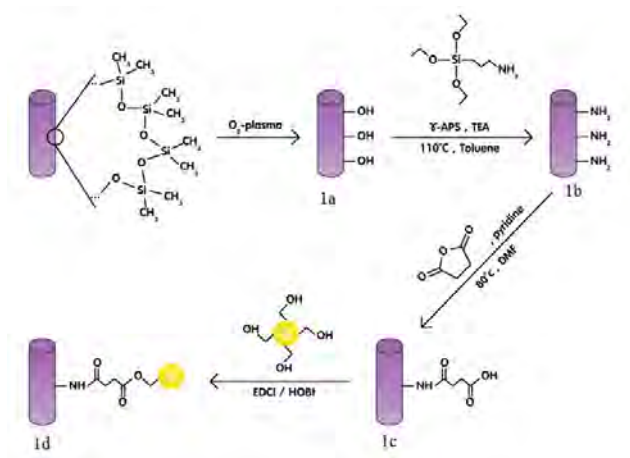
Scheme 1. Surface functionalization of the PDMS tube and grafting of budesonide-loaded nanoparticles onto the surface of the functionalized PDMS tube.

3.1 Synthesis and characterizations of chemically functionalized PDMS surface

3.1.1 Treatment of the PDMS surface by Oxygen-plasma

Modification of PDMS tube surface could be confirmed by contact angles measurement; water contact angles of untreated and treated PDMS surfaces were 99.94 ± 1.2° and 86.9 ± 2.9°, respectively (Figure 1), indicating the change in surface functionality by the O$_2$ plasma treatment to a more hydrophilic surface.

3.1.2 γ-APS-grafted plasma-treated PDMS

Plasma-treated PDMS was grafted with γ-APS and the presence of amino groups could be confirmed through a deep violet color from Kaiser test (Figure 2).

3.1.3 Coupling reaction of γ-APS-grafted PDMS with succinic anhydride

The change from amino groups into succinamide moieties resulted in the fading of violet color from Kaiser test (Figure 3).

a   b
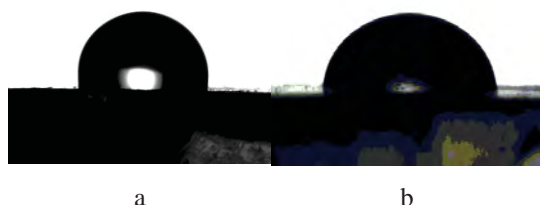
Figure 1. Contact angles of a) untreated PDMS and b) O_2-plasma-treated PDMS surface.
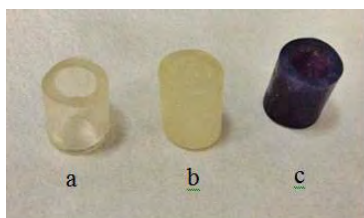
Figure 2. Colorimetric revelation of the amine a) is the reference PDMS b) is the aminopropylsilanized PDMS and c) tube b after Kaiser test.

a   b
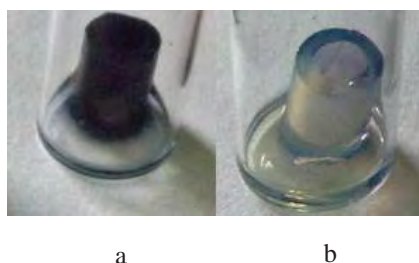
Figure 3. Colorimetric (Kaiser test) revelation of the amine in a) aminopropylsilanized PDMS and b) PDMS succinamide.

3.2 Nanoparticles formation

Budesonide-loaded EC showed 24.5% loading capacity and the encapsulation process gave 49% encapsulation efficiency.

The SEM images indicated nanospherical morphology of budesonide-loaded particles with the dry size of approximately 350 - 380 nm (Figure 4). In water, approximately 370 nm of the hydrodynamic diameter was obtained from the DLS analysis with a narrow size distribution (PDI of 0.303).

a   b
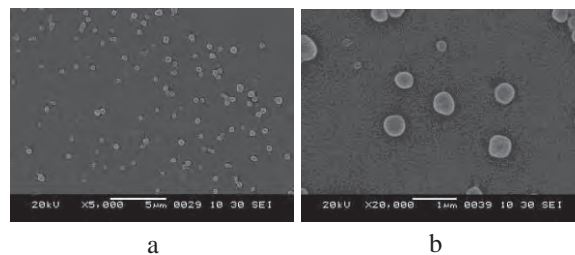
Figure 4. Representative SEM images of nanoparticles a) ×5,000 and b) ×20,000

3.3 The particle-grafted-PDMS tube

The budesonide-loaded particles were grafted onto the PDMS tube through the esterification between hydroxyl groups of the particles and carboxyl groups on the functionalized surface tube (Scheme 1c-1d). SEM images clearly indicated the presence of particles on the surface of tube (Figure 5).

a   b
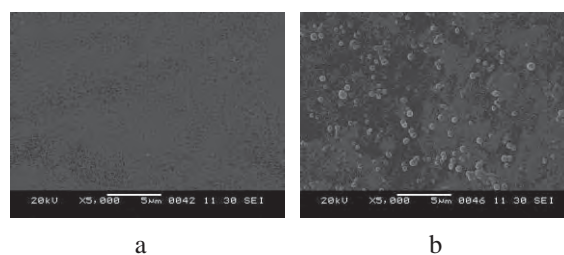
Figure 5. SEM images of the surface of a) PDMS tube and b) the budesonide-loaded particles-grafted-PDMS tube.

3.4 Distribution of fluorescence-labeled particles onto the surface of the PDMS tube

To track the location of particles on the surface of the PDMS tube, fluorophore Rhodamine B was covalently linked to the EC polymeric chains. Rhodamine-labeled EC nanosparticles were prepared and grafted on to the tube and the distribution of the particles on the surface of tube could be obtained from fluorescent images (Figure 6). The fluorescent signals from Rhodamine-labeled EC nanoparticles confirmed that the EC nanoparticles were well distributed on the PDMS tube surface.

a   b   c
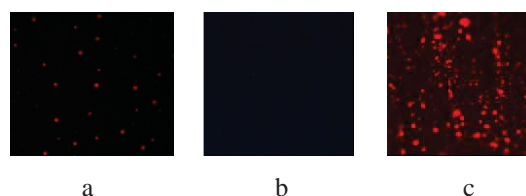
Figure 6. Fluorescent images of a) Rho-labeled EC nanoparticles, b) PDMS tube and c) Rho-labeled EC nanoparticles on PDMS tube.

3.5 Release of the budesonide

As shown in Figure 7, in vitro drug release study indicated sustained release of budesonide from the tube, indicated prolonged release of budesonide for

more than 10 days, with 85% budesonide being released by the end of the third week.
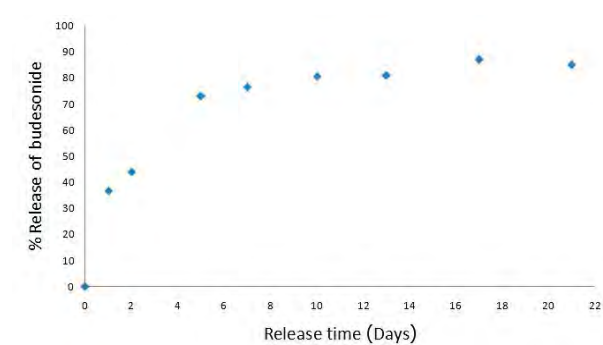
Figure 7. Release profile of budesonide from the surface of the PDMS tube.

4. Conclusions

Here we present a novel PDMS tube which can slowly release budesonide. The tube was prepared through surface functionalizing the PDMS tube with budesonide-loaded nanoparticles, reported here in on their preparation. The grafted tubes showed prolonged release of budesonide for more than 10 days.

Acknowledgements

References

[1] S. Backman, G. Björling, U.B. Johansson, M. Lysdahl, A. Markström, U. Schedin, R.E. Aune, C. Frostell and S. Karlsson, *Laryngoscope* **119** (2009) 657-664.

[2] T. Goto, Y. Oyamada, M. Wakaki and R. Kato, *Interactive Cardio Vascular and Thoracic Surgery* **10** (2009) 107-109.

[3] I. Takanami, T. Abiko and H. Kurihara, *The Journal of Thoracic and Cardiovascular Surgery* **134** (2007) 1362-1363.

[4] T. Shiraishi, K. Kawahara, T. Shirakusa, K. Inada, K. Okabayashi and A. Iwasaki, *The Society of Thoracic Surgeons* **66** (1998) 1925-1929.

[5] R. Kato, T. Kobayashi, M. Watanabe, M. Kawamura, K. Kikuchi, K. Kobayashi and T. Ishihara, *The Annals of Thoracic Surgery* **51** (1991) 327-329.

[6] C. Lenfant and N. Khaltaev, Global Strategy for the Diagnosis, Management and Prevention of Chronic Obstructive, *National Heart, Lung and Blood Institute,* (2001), pp. 45-56.

[7] http://circ.ahajournals.org/ (Retrieved November 29, 2005).

[8] J.E. Heffner, *ArtIfIcial Airyski PatIents Receiving Mechanical MntIIatIon* **96** (1989) 186-190.

[9] C.C. Meinesz, J. Mouroux, J. Cosson, P. Huitorel and B. Blaive, *European Respiratory Journal* **11** (1998) 330-333.

[10] R.K. Dilip, G.M. Dilip and V.M. Kalpana, *Respiratory mucus pH*, **18**(1990) 699-701.

[11] W. Pornputtapitak, N. El-gendy and C. Berkland, *Pharmaceutical Sciences* **101** (2012) 1063-1072.

[12] E.S. Brett, *Clin Therapeutics* **26** (2004) 473-92.

[13] N.S. Mohanad, D. Yusrida, K.K. Peh and T.F.T. Yvonne, *Pharmacy and Pharmacology* **4** (2010) 878-884.

[14] R. Nave, R. Fisher and N. McCracken, *Respiratory Research* **8** (2007) 65.

[15] F.L. Mota, A.P. Carneiro, A.J. Queimada, S.P. Pinho and E.A. Macedo, *Pharmaceutical Sciences* **37** (2009) 499-507.

[16] H. Shuguang, H. Michael and R.B. Peter, *Pharmaceutical and Biomedical Analysis* **24** (2001) 371-380.

[17] E.T. de Givenchy, S. Amigoni, C.D. Martin, G. Andrada, L. Caillier, S. Géribaldi and F.D.R. Guittard, *Langmuir* **25** (2009) 6448-6453.

[18] C.P. Reis, R.J. Neufeld, A.J. Ribeiro and F. eiga, *Nanomedicine: Nanotechnology, Biology, and Medicine* **2** (2006) 8-21.

[19] S.K. Sahoo and V. Labhasetwar, *Drug Discovery Today* **8** (2003) 1112-1120.

CHEMICAL COMPOSITIONS AND ANTIBACTERIAL ACTIVITY OF *PLECTRANTHUS ROTUNDIFOLIUS* EXTRACTS

Chalida Phungpanya[1], Theeraphan Machan[1*], Patcharee Pripdeevech[1], Chalermporn Thongpoon[2], Kanlaya Jumpatong[3]

[1] Program of Applied Chemistry, School of Science, Mae Fah Luang University, Chiang Rai 57100, Thailand
[2] Program of Chemistry, Faculty of Sciences and Technology, Pibulsongkram Rajabhat University, Phitsanulok 65000, Thailand
[3] Department of Chemistry, School of Science, University of Phayao, Phayao 56000, Thailand

[*] Author for correspondence; E–Mail: t.machan@sci.mfu.ac.th, Tel. +66 53 916769, Fax. +66 53 916776

Abstract : This work reported the study of chemical compositions and antibacterial activity of the extracts from aerial part and tubers of *Plectranthus rotundifolius*. The chemical constituents of both extracts were analyzed by GC–MS technique. Five major components of aerial extract were γ-muurolene (21.68%), α-humulene (12.68%), *E*-caryophyllene (5.67%), *n*-dodecane (5.55%), and 1-octen-3-ol (4.63%) while the main components in tuber extract were *epi-α*-cadinol (15.52%), sesquicineole (9.36%), cyperene (4.88%), *epi-α*-bisabolol (3.00%), and α-santalene (2.25%). The aerial hexane extract showed antibacterial activity in microtiter plates with two–fold serial dilution assay against *Bacillus subtilis*, *Escherichia coli*, and *Staphylococcus aureus* with MIC values of 10.00, 1.25, and 1.25 mg/mL, respectively. The hexane extract of tubers also showed significant antibacterial activity in paper disc diffusion method against *Bacillus subtilis*, *Pseudomonas aeruginosa*, and *Staphylococcus aureus* with MIC values of 75.00, 125.00, and 500.00 mg/mL, respectively.

1. Introduction

        P. rotundifolius (Poir.) Spreng (synonyms: *P. tuberosus* Blume, *Coleus dysentericus* Buk., *C. rotundifolius* (Poir.) A. Chev. & E. Perrot, *C. parviflorus* Benth., and *Solenostemon rotundifolius* (Poir.) J.K. Morton) [1] is a green perennial aromatic herb that belongs to the family Lamiaceae (Labiatae) and locally known in Thai as "Man Khi–Nu" and "Man Nu". This plant is widely distributed in Asia and tropical areas, especially in the Southern part of Thailand [2]. Leaves of the plant present a lighten scent. Tubers can be eaten as vegetable and often used in Southern Thai cuisine such as curry and grill. The tubers can also be fermented to the alcoholic beverages [3,4]. In addition, this plant is used in the traditional medicine for treatment of dysentery, blood in the urine as well as eye disorders [5]. There have no reports on an organic solvent extraction except the hydrodistillation method from this plant. In this study, the aerial part and tubers of *P. rotundifolius* are extracted by hexane, moreover, then analyzed by GC–MS technique, the identification of components, and the

investigation of antibacterial activity are also the highlight of this study.

2. Materials and Methods

2.1 Plant Materials

        Fresh aerial part and tubers were collected from Surat Thani, Thailand in July, 2011. The plant was identified and deposited at CMU herbarium, Faculty of Science, Chiang Mai University, Chiang Mai, Thailand. Mixtures of *n*–alkanes (C_8–C_{22}) analogue were purchased from Merck (Darmstadt, Germany).

2.2 Extraction

        The 1.10 kg of aerial part and tubers were chopped into small pieces and then separately macerated in 1.50 L hexane for 3 days at room temperature in 2 times, afterwards, solvent removal under reduced pressure was evaporated to obtain 0.048 and 0.19% of aerial and tuber hexane extracts, respectively.

2.3 Gas Chromatography–Mass Spectrometry (GC–MS)

        The hexane extracts of both parts of the plant were analyzed by a Hewlett Packard model HP6890 gas chromatograph (Agilent Technologies, Palo Alto, CA, USA). The HP–5MS (5% phenylpolymethylsiloxane) capillary column (30 m × 0.25 mm i.d., film thickness 0.25 μm ; Agilent Technologies, USA) was equipped and interfaced to an HP model 5793 mass–selective detector. The oven temperature was initially held at 60°C and then increased by 3°C/min to 250°C. The injector and detector temperatures were 250°C and 280°C, respectively. Purified helium was used as the carrier gas at a flow rate of 1 mL/min. EI mass spectra were collected at 70 eV ionization voltages over the range of *m/z* 29–300. The electron multiplier voltage was 1150 V. The ion source and quardrupole temperatures were set at 230°C and 150°C, respectively. The identification of hexane extracts were performed by comparison of their Kovats retention indices, relative to C_8–C_{22} *n*–alkanes, and comparison of the mass spectra of individual components with the

reference mass spectra in the NIST 98 and Wiley 275 databases at the present quality match greater than 90%. The relative quantity of the components of all samples was determined directly from the GC peak areas. The percentage compositions of hexane extracts of *P. rotundifolius* were reported in **Table 1**.

Table 1 Chemical compositions of fresh aerial part and tuber hexane extracts from *P. rotundifolius*

Chemical compounds	%RA[a]		RI[d]	RI[e]
	AH[b]	TH[c]	(Exp)	(Lit)
Acyclic monoterpene				
Myrcene	0.56		998	990
Limonene	0.36		1025	1029
Cyclic monoterpene				
α-Thujene	tr		931	930
ρ-Cymene		tr	1021	1024
β-Phellandrene		tr	1026	1029
Oxygenated monoterpene				
Camphor	1.51	tr	1141	1146
Menthol		tr	1170	1171
Eugenol		0.20	1355	1359
Acyclic sesquiterpene				
Z-β-Farnesene		0.73	1438	1442
Cyclic sesquiterpene				
α-Copaene	0.91	tr	1371	1376
β-Elemene	0.98	0.38	1387	1390
Cyperene		4.88	1387	1390
Sibirene		tr	1394	1398
α-Gurjunene		0.74	1409	1409
E-Caryophyllene	5.67		1414	1419
α-Santalene		2.25	1415	1417
α-trans-Bergamotene		0.98	1431	1438
α-Humulene	12.68		1448	1454
cis-Muurola-3,5-diene		1.24	1466	1450
Oxygenated sesquiterpene				
Sesquicineole		9.36	1511	1516
E-Nerolidol		0.13	1560	1563
trans-Sesquisabinene hydrate		0.48	1576	1579
α-Acorenol		tr	1629	1633
epi-α-Cadinol		15.52	1641	1640
epi-α-Bisabolol		3.00	1681	1684
trans-Muurola-3,5-diene		0.34	1458	1453
β-Chamigrene		0.35	1469	1477

Table 1 (Cont.) Chemical compositions of fresh aerial part and tuber hexane extracts from *P. rotundifolius*

Chemical compounds	%RA[a]		RI[d]	RI[e]
	AH[b]	TH[c]	(Exp)	(Lit)
β-Bisabolene		0.31	1505	1505
γ-Cadinene	tr		1511	1513
δ-Cadinene	0.31		1518	1523
α-Cadinene		tr	1533	1538
Cyclic diterpene				
3E-Cembrene A		0.24	1952	1948
Oxygenated diterpene				
Phytol	3.18		2112	2111
Acyclic hydrocarbon				
n-Nonane	0.20		897	900
n-Decane	2.37		997	1000
n-Dodecane	5.55	0.42	1196	2000
n-Tridecane	0.62	tr	1295	1300
n-Tetradecane	3.59		1395	1400
n-Pentadecane	1.01		1494	1500
n-Hexadecane	1.87	0.20	1594	1600
n-Heptadecane	0.65	tr	1694	1700
n-Octadecane	0.67		1793	1800
n-Nonadecane	0.67		1893	1900
n-Eicosane	0.83		1993	2000
n-Docosane	0.51		2194	2200
Aromatic hydrocarbon				
1,2,4-Trimethylbenzene	0.29		1020	1025
Naphthalene	0.24		1180	1181
Alcohol				
2Z-Hexenol	0.25	tr	884	867
1-Octen-3-ol	4.63		976	979
Benzyl alcohol		tr	1034	1031
Phenylethyl alcohol		0.11	1113	1116
ρ-vinyl-Guaiacol		0.15	1313	1309
Phenylpropene				
Elemicin		tr	1554	1557
Ketone				
Cyperotundone		0.30	1689	1695
Ester				
cis-2-tert-butyl-Cyclohexanol acetate	0.58		1289	1293
Myrtenyl acetate		tr	1321	1326
Methyl-o-anisate		tr	1338	1337
Benzyl salicylate		0.56	1863	1865
Methyl hexadecanoate	0.47	0.43	1921	1921

Table 1 (Cont.) Chemical compositions of fresh aerial part and tuber hexane extracts from *P. rotundifolius*

Chemical compounds	%RA[a]		RI[d] (Exp)	RI[e] (Lit)
	AH[b]	TH[c]		
Methyl linoleate		0.50	2094	2095
(Z,Z,Z)-9,12,15-Octadecatrienoic acid, methyl ester	1.05		2098	2105

%RA[a], Relative peak area (raw peak area relative to total peak area)

AH[b], Aerial part hexane extract of *P. rotundifolius*

TH[c], Tuber hexane extract of *P. rotundifolius*

RI (Exp)[d], Programmed temperature retention indices as determined on HP–5MS column using a homologous series of *n*–alkanes (C_8–C_{22}) as internal standard and H_2 as a carrier gas

RI (Lit)[e], Values from literature data using He as a carrier gas

tr[f], Trace amount (%RA < 0.10)

2.4 Antibacterial activity

The aerial hexane extract was used to determine the MIC inhibition by microtiter plates with two–fold serial dilution assay against *Bacillus subtilis*, *Bacillus cereus*, *Escherichia coli*, *Staphylococcus aureus*, *Salmonella typhimurium*, *Pseudomonas aeruginosa*, *Pseudomonas fluorescens*, and *Micrococcus luteus* whereas disc diffusion assay was tested for tuber hexane extract against *Bacillus subtilis*, *Escherichia coli*, *Staphylococcus aureus*, *Salmonella thyphimurium*, *Pseudomonas aeruginosa*, *Micrococcus luteus*, and Methicillin–resistant *Staphylococcus aureus* (MRSA). The results were presented as follows in **Table 2**.

Table 2 The MIC of antibacterial activitiy of crude extracs from *P. rotundifolius*

Bacteria	MIC of *P. rotundifolius* (mg/mL)	
	AH[a]	TH[b]
B. subtilis	10.00	75.00
B. cereus	10.00	-[c]
E. coli	1.25	ND[d]
S. aureus	1.25	500.00
MRSA	-	ND
S. typhimurium	ND	ND
Ps. aeruginosa	ND	125.00
Ps. fluorescens	ND	-
M. luteus	ND	ND

AH[a], Aerial hexane extract of *P. rotundifolius*

TH[b], Tuber hexane extract of *P. rotundifolius*

ND[c], Not detected

-[d], Not tested

3. Results and Discussion

The aerial and tuber hexane extracts of *P. rotundifolius* were analyzed and identified the chemical components by GC–MS technique. Five major compounds of aerial hexane extract were *γ*-muurolene (21.68%), *α*-humulene (12.68%), *E*-caryophyllene (5.67%), *n*-dodecane (5.55%), and 1-octen-3-ol (4.63%) while *epi*-*α*-cadinol (15.52%), sesquicineole (9.36%), cyperene (4.88%), *epi*-*α*-bisabolol (3.00%), and *α*-santalene (2.25%) were also five main components of tuber hexane extract. From the results, the chemical components of both parts were significantly difference presented chemotypes, although there were in same major groups (cyclic sesquiterpene and oxygenated sesquiterpene group).

In antibacterial activity study, three microbes, *B. subtilis*, *E. coli*, and *S. aureus*, were exhibited by aerial hexane extract with MIC values of 10.00, 1.25, and 1.25 mg/mL, respectively. The tuber hexane extract inhibited the growth of *B. subtilis*, *Ps. aeruginosa*, and *S. aureus* with MIC values of 75.00, 125.00, and 500.00 mg/mL, respectively. From these results, major compositions of the extracts were monoterpenes and sesquiterpenes and they could be the compounds that showed antibacterial activity against bacteria and fungi [6].

4. Conclusions

In this present study, the aerial part and tubers of *P. rotundifolius* were extracted with hexane, analyzed by GC–MS technique, and investigated the MIC of antibacterial activity. The most abundant group of major compounds were cyclic sesquiterpenes in an aerial extract while the oxygenated sesquiterpenes were the major group of compounds in the tuber extract. In addition, terpenoid compositions in both crude extracts had ability to inhibit some microbes in this study.

References

[1] C.W. Lukhoba, M.S.J. Simmonds and A.J. Paton, *J. Ethnopharmacol.* **103** (2005) 1–24.

[2] S. Yuenyongsawad and S. Tewtrakul, *Songklanakarin J. Sci. Technol.* **27** (2005) 497–502.

[3] D. Pasternak and A. Schlissel, *Combinating Desertification with Plants*, Kluwer Academic/Plenum Publishers, USA (2001).

[4] L.J. Rice, G.J. Brits, C.J. Potgieter and J. Van Staden, *S. Afr. J. Bot*. **77** (2011) 947–959.

[5] G.J.H. Grubben and O.A. Denton, *Plant Resources of Tropical Africa 2: Vegetables*, PROTA Foundation, Netherlands (2004).

[6] A. Vijayakumar, V. Duraipandiyan, B. Jeyaraj, P. Agastian, M. Karunai Raj and S. Ignacimuthu, *Asian Pac. J. Trop. Med*. **2** (2012) 190–199.

α-GLUCOSIDASE INHIBITORS FROM RHIZOMES OF GINGER (*ZINGIBER OFFICINALE*)

Vutcharaporn Vongsungyang[1,2], Preecha Phuwapraisirisan[2*]

[1] Program in Biotechnology, Faculty of Science, Chulalongkorn University, Bangkok 10330, Thailand
[2] Department of Chemistry, Faculty of Science, Chulalongkorn University, Bangkok 10330, Thailand

* Author for correspondence; E-Mail: preecha.p@chula.ac.th, Tel. +66 22187624, Fax. +662 2187598

Abstract: Type II Diabetes mellitus (T2DM) is a metabolic disorder characterized by high blood glucose levels (hyperglycemia). Intensive control on blood glucose level is critical not only to halt T2DM development but also alleviate micro- and macrovascular complications. One therapeutic approach to decrease hyperglycemia is to retard absorption of glucose using antidiabetic drugs possessing α-glucosidase inhibitory effect such as acarbose and voglibose. However, they have side effects such as flatulence and diarrhea. Therefore, it is of interest to search for drugs from new sources, including Thai herbs that can minimize the side effects. Ginger is an underground rhizome of the plant *Zingiber officinale* belonging to the family Zingiberaceae. *Z. officinale* possessed hypoglycemic effect in rat, but active components responsible for this effect have not been identified. In this study, the methanol extract of ginger rhizomes was assayed for inhibitory activity against α-glucosidase and purified using column chromatography, leading to 6-gingerol, 10-gingerol, 6-shogaol, acetoxy-8-gingerol. Of isolated compounds, 10-gingerol showed potent inhibitory effect againt yeast α-glucosidase, maltase and sucrase with IC_{50} values of 2.82, 4.8 and 4.11 mM, respectively.

1. Introduction

Type II Diabetes mellitus (T2DM) is a metabolic disorder characterized by high blood glucose levels, typically recognized as prosprandial hyperglycemia. It is estimated that patients with type 2 diabetes will likely increase [1]. Intensive control on blood glucose level is critical not only to halt T2DM development but also alleviated micro- and macrovascular complications [2]. One therapeutic approach to decrease prosprandial hyperglycemia is to retard absorption of glucose via inhibition of α-glucosidase. Delaying glucose absorption after meals is known to be beneficial in therapy disease [3]. α-Glucosidase inhibitors are used as drugs for diabetes therapy (acarbose and voglibose). However, they have side effects such as flatulence and diarrhea. Therefore, it is of interest to search for drugs from new sources, including Thai herbs, with can minimize the side effects.

Z. officinale (commonly known as ginger) is a widespread herbal medicine mainly used for the treatment of gastrointestinal (GI) disorders including: dyspepsia, nausea and diarrhea [4]. Ginger is an underground rhizome of the plant *Zingiber officinale* belonging to the family Zingiberaceae. *Z. officinale*, a commonly used spice in the Indian kitchen, is known by several names Ardharakam, Adrak, Adu, Ala, etc.

The juice of *Z. officinale* possess a potential antidiabetic activity in type I diabetic rats, possibly involving 5-HT receptors. Treatment with *Z. officinale* produced a significant increase in insulin levels and a decrease in fasting glucose levels also caused a decrease in serum cholesterol, serum triglyceride and blood pressure in diabetic rats [5]. Phytochemicals present in *Z. officinale* may play an important role in suppressing the elevated tissue lipids in diabetic rats. Hence, *Z. officinale* may be useful in the treatment of diabetes [6]. Extract of *Z. officinale* can protect the tissues from lipid peroxidation. The extract also exhibit significant lipid lowering activity in diabetic rats. thus indicating the potential of *Z. officinale* in diabetic dyslipidaemia [7].

2. Materials and Methods

2.1 Materials

Ginger rhizomes were purchased from Khlong Toei Market, in April 2012. α-Glucosidase from baker's yeast, rat intestinal acetone powder, *p*-nitrophenyl-α-D-glucopyranoside (*p*NPG) and glu-kit were supplied by Sigma Aldrich Co. (USA).

2.2 Preparation of extracts

Ginger rhizomes crude (289 g) were extracted with methanol for two days at room temperature, and this procedure was repeated three times. Metanolic extract was evaporated in rotary evaporator, yielding yellow sticky paste.

2.3 Isolation and identification of α-glucosidase inhibitor

The methanol extract (21.9 g) was isolated by quick column chromatography and then eluted with CH_2Cl_2 containing increasing amounts of MeOH (100:0, 95:5, 90:10, 80:20, 70:30 and 50:50 v/v, 500 mL) to give six main fractions. Each fraction was then evaporated under reduced pressure at 40 °C to dryness before biological evaluation against α-glucosidase. The fractions showing high inhibitory activity were further purified by column chromatograpy.

Fractions 2 was purified by sephadex LH-20 and eluted with 1:9 MeOH- CH_2Cl_2, to afford four major fractions; the third fraction is 6-Gingerol (**1**, 190 mg).

The second fraction was further purified on silica gel CC eluted with 2:8 EtOAc- hexane to obtain 6-shogaol (**2**, 59 mg), 10-gingerol (**3**, 54 mg), acetoxy-8-gingerol (**4**, 39 mg).

6-Gingerol (**1**); yellow oil; ^{1}H NMR (CDCl$_3$, 400 MHz) δ 6.82 (d, J = 8.0 Hz, 1H , H-5′), 6.67 (s, 1H, H-2′), 6.64 (dd, J = 8.0, 2.0 Hz, 1H, H-6′), 4.02 (m, 1H, H-5), 3.86 (s, 3H, OCH$_3$), 2.81 (brd, J = 6.8 Hz, 2H, H-1), 2.72 (brd, J = 6.8 Hz, 2H, H-2), 2.54 (d, J = 4.0 Hz, 1H, H-4b), 2.51 (d, J = 8.4 Hz, 1H , H-4a), 1.27-1.48 (m, 8H, H-6~H-9), 0.88 (t, J = 6.8 Hz, 3H, H-10) ^{13}C NMR (CDCl$_3$, 100 MHz) δ 211.4, 146.5, 144.0, 120.8, 114.5, 111.1, 67.7, 55.9, 49.4, 45.4, 36.5, 31.7, 29.3, 25.1, 22.8, 14.0; ESIMS, m/z 317.1 [M+Na]$^+$ (C$_{17}$H$_{26}$NaO$_4$).

6-Shogaol (**2**); brown oil; ^{1}H NMR (CDCl$_3$, 400 MHz) δ 6.76 (d, J = 7.6 Hz, 1H, H-5′), 6.63 (s, 1H, H-2′), 6.62 (d, J = 8.0 Hz, 1H, H-6′), 6.61 (d, J = 16.0 Hz, 1H, H-5), 6.02 (d, J = 16.0 Hz, 1H, H-4), 3.80 (s, 3H, OCH$_3$), 2.78 (m, 4H, H-1 and H-2), 2.17 (m, 2H, H-6), 1.53 (m, 2H, H-7) 1.2-1.38 (m, 4H, H-8 and H-9), 0.82 (t, J = 6.8 Hz, 3H, H-10); ^{13}C NMR (CDCl$_3$, 100 MHz) δ 198.7, 146.8, 142.9, 132.3, 129.3, 119.8, 113.3, 110.1, 54.9, 41.0, 31.4, 30.3, 28.9, 26.8, 21.6, 13.0; ESIMS, m/z 275.2 [M-H]$^-$ (C$_{17}$H$_{23}$O$_3$).

10-Gingerol (**3**) yellow oil; ^{1}H NMR (CDCl$_3$, 400 MHz) δ 6.82 (d, J = 8.0 Hz, 1H, H-5'), 6.67 (s, 1H, H-2'), 6.66 (d, J = 8.0 Hz, 1H, H-6'), 4.02 (m, 1H, H-5), 3.87 (s, 3H, OCH$_3$), 2.83 (dd, J = 16.0, 8.0 Hz, 2H, H-1), 2.73 (dd, J = 12.0, 8.0 Hz, 2H, H-2), 2.44-2.58 (m, 2H, H-4), 1.37 (m, 2H, H-6) 1.25-1.60 (m, 14H, H-7~H-13), 0.87 (t, J = 6.4 Hz, 3H, H-14) ^{13}C NMR (CDCl$_3$, 100 MHz) δ 211.3, 146.5, 144.0, 132.7, 120.8, 114.4, 111.0, 67.7, 55.9, 49.4, 45.4, 36.5, 31.9, 29.3, 25.4, 22.7, 14.1 ; ESIMS, m/z 349.2 [M-H]$^-$ (C$_{21}$H$_{33}$O$_4$).

Acetoxy-8-gingerol (**4**) oil; ^{1}H NMR (CDCl$_3$, 400 MHz) 6.75 (d, J = 8.0 Hz, 1H, H-5'), 6.60 (dd, J = 8.0, 4.0 Hz, 1H, H-6'), 6.59 (s, 1H, H-2'), 4.87 (m, 1H, H-5), 3.82 (s, 3H, OCH$_3$), 2.75 (brd, J = 8.0 Hz, 2H, H-1), 2.68 (brd, J = 8.0 Hz, 2H, H-2), 2.44-2.60 (m, 2H, H-4), 1.99 (s, 3H, OAc), 1.93 (s, 3H, OAc), 1.44 (m, 2H, H-6), 1.18-1.26 (m, 10H, H-7~H-11), 0.80 (t, J = 8.0 Hz, 3H, H-12) ^{13}C NMR (CDCl$_3$, 100 MHz) δ 209.0, *170.7*, *170.6*, 146.4, 143.8, 133.2, 120.9, 114.3, 111.0, *71.2*, *70.9*, 55.9, 47.6, 45.8, 38.5, 35.9, 34.2, 31.6, 31.2, 29.3, 24.7, 22.5, *21.2*, *21.1*, 13.9; ESIMS, m/z 364.2 [M] (C$_{23}$H$_{36}$O$_5$). *Italic values are those of its enantiomer.

2.4 Baker's yeast α-glucosidase inhibitory activity

Assay was performed according to a slightly modified method of Hwang *et.al* [8]. Briefly, 10 µL of sample dissolved in DMSO (0.1, 1 and 10 mg/mL) was added to 0.1 M phosphate buffer (pH 6.9, 50 µL) and α-glucosidase (0.1 U/mL, 40 µL). After pre incubated at 37 °C for10 min, 50 µL of 1 mM *p*NPG prepared in the same buffer was added. The reaction mixture was incubated for additional 20 min, and terminated by adding 100 µL of 1 M Na$_2$CO$_3$. The enzymatic hydrolysis of the *p*NPG was monitored

based on the amount of *p*-nitrophenol released into the reaction mixture by Bio-Rad microplate reader model 3550 UV using a 405 nm absorbance (Fig 1). The percentage inhibition of activity was calculated as follows:

$$\% \text{ inhibition } = [(A_0\text{-}A_1)/A_0] \times 100$$

Where A_0 is the absorbance without the sample, and A_1 is the absorbance with the sample. Acarbose was used as positive control and the experiment was performed in triplicate.
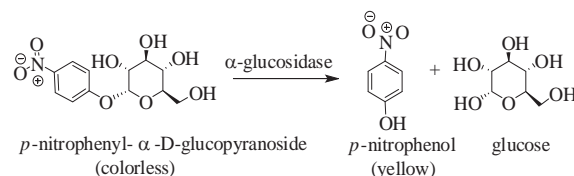
Fig 1. Hydrolysis of *p*NPG by α-glucosidase from baker's yeast

2.5 Rat intestinal α-glucosidase inhibitory activity

assay was performed according to a slightly modified method of Jo et.al [9]. The crude enzyme solution prepared from rat intestinal acetone powder was used as a source of maltase and sucrase. Rat intestinal acetone powder (1.0 g) was resuspended in 30 mL of 0.9 % NaCl solution. After centrifugation (12,000×g, 30 min), supernatant was used for the assay. A 10 µL of sample (0.1, 1 and 10 mg/mL in DMSO) was preincubated with the crude enzyme solution (as maltase, 20 µL; as sucrase, 20 µL, respectively) at 37 °C for 10 min. The substrate solution (maltose: 0.58 mM, 20 µL; sucrose: 20 mM, 20 µL, respectively) in 0.1 M phosphate buffer (pH 6.9) was then added to the reaction mixture and incubated for additional 40 min. The mixture was heated in an oven at 80 °C for 15 min to stop the reaction. The concentration of glucose released from the reaction mixture was determined by the glucose oxidase method using a glu-kit (Sigma–Aldrich, USA) (Fig 2). The percentage inhibition of activity was calculated using above expression. Enzymatic activity was quantified by measuring absorbance at 540 nm. The experiment was performed in triplicate.
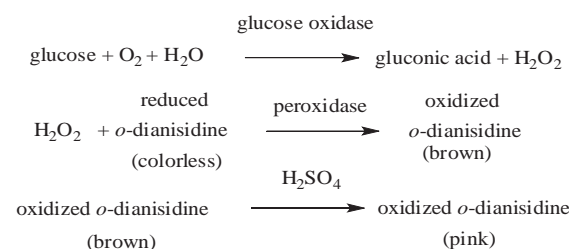
Fig 2. The schematic reaction of glucose oxidase in the glu-kit.

3. Results and Discussion

3.1 Identification of the α-glucosidase inhibitory substance

The isolated compounds from ginger rhizomes were characterized by NMR data as 6-gingerol (**1**), 6-shogaol (**2**), 10-gingerol (**3**), acetoxy-8-gingerol (**4**). Chemical structures of **1**-**4** are shown in Fig 3.

Fig 3. Chemical structures of **1**-**4**

Fig 4. Inhibitory effect of isolated compounds on rat intestine against sucrase [**A**], maltase [**B**] and baker's yeast [**C**]
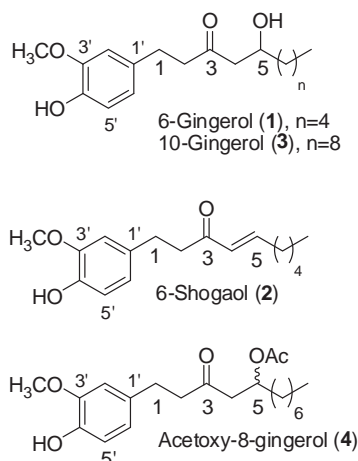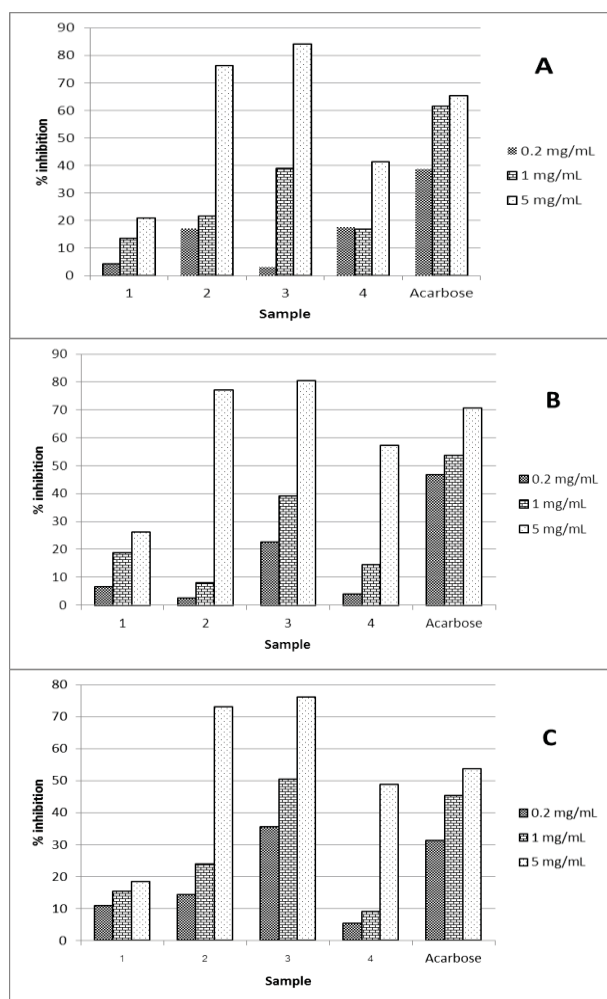
Table 1: α-glucosidase inhibitory activity of isolated compounds

compounds	IC$_{50}$[a] (mM)		
	yeast α-glucosidase	maltase	sucrase
1	NI[b]	NI	NI
2	11.32	12.21	10.85
3	2.82	4.86	4.11
4	NI	NI	NI
Acarbose	3.13	0.75	0.36

[a] The IC$_{50}$ value is defined as the inhibitory concentration to inhibit 50% of enzyme activity
[b] No inhibition, less than 60% inhibition at 5 mg/mL

3.2 Inhibitory activity of **1**-**4** against α-glucosidase

α-Glucosidase inhibitory activity of **1**-**4** are demonstrated in Table 1. Of isolated compounds, **2** and **3** displayed high α-glucosidase inhibitory activity with IC$_{50}$ values in range of 2-12 mM. However, **3** showed potential inhibition, which was 2- 4 folds greater than **2**. For gingerol type **1** and **3**, the increase of hydrophobicity by four methylene units in **3** remarkably resulted in potent inhibition. Given identical chain length (n=4) in **1** and **2**, the presence of α, β- unsatuated ketone in **2** instead of β- hydroxy ketone in **1** led to improved activity. Therefore, the presence of α, β- unsatuated ketone with increase hydrophobicity by alkyl chain is likely to promote enzyme inhibition.

4. Conclusions

The isolated compounds from ginger rhizomes were identified as gingerol- and shogaol-type compounds. They are active against α-glucosidase from baker's yeast and from rat intestine (maltase and sucrase). Among four compounds, **3** had the highest inhibitory activity, thus indicating that it would be responsible for antidiabetic activity previously reported. The presence of α, β- unsatuated ketone in **2** and increase hydrophobic alkyl chain in **3** possibly plays an important role in enzyme inhibition.

References
[1] I. Heydari, V. Radi, S. Razmjouv and A. Amiri, *Int. J. Diabetes Mellit.* **2** (2010) 61–63.
[2] P. Zimmet, K. G. M. M. Alberti, J. Shaw, *Nature.* **414** (2001) 782.
[3] K.Y. Kim, K.A. Nam, H. Kurihara and S.M. Kim, *Phytochemistry.* **69** (2008) 2820-2825.
[4] M. Minaiyan, A. Ghannadi and A. Karimzadeh, *Daru* **14** (2006) 97-101.

[5] S. P. Akhani, S.L. Vishwakarma and R. K. Goyal, *Journal of Pharmacy and Pharmacology*. **56** (2004) 101–105.

[6] S. K. Ramudu, K. Mallikarjuna and S. R. Kesireddy, *Int. J. Diabetes Dev. Ctries* **31** (2011) 97–103.

[7] U. Bhandari, R. Kanojia and K.K. Pillai, *Journal of Ethnopharmacology* **97** (2005) 227–230.

[8] I. Guk Hwang, H. Young Kim, K. Sik Woo, J. Tae Hong, B. Yeon Hwang, J. Kyung Jung, J. Lee and H. Sang Jeong, *Food Chem*. **127** (2011) 122-126.

[9] S-H. Jo, E-H. Ka, H-S. Lee, E. Apostolidis, H-D. Jang and Y-I. Kwon, *Int. J. Appl. Res. Nat. Prod* . **2** (2010) 52-60.

DESIGN AND SYNTHESIS OF CHROMONE DERIVAITVES AS PLASMEPSIN II INHIBITORS

Pradith Lerdsirisuk[1], Jiraporn Ungwitayatorn[1*]

[1] Department of Pharmaceutical Chemistry, Faculty of Pharmacy, Mahidol University, 447 Sri-Ayuthya Road, Ratchathewi, Bangkok 10400, Thailand

[*] E-Mail: pyjuw@mahidol.ac.th

Abstract: Plasmepsin II (Plm II) is an aspartic protease which involves in the hemoglobin degradation inside the food vacuole during the erythrocytic phase of the parasite's life cycle. This enzyme has received considerable attention as a promising target for antimalarial drug design. Since HIV-1 protease (HIV-1 PR) is known as an aspartic protease and several HIV-1 PR inhibitors exhibit activity against Plm II and antimalarial activity against *P. falciparum*. These findings indicate that HIV-1 PR inhibitors may aid in the removal of plasmodium parasites and used as antimalarial drugs. The preliminary screening of Plm II inhibitory activity of the previous forty-six synthesized chromones with HIV-1 PR activities were performed by employing a docking study. Results from docking simulation technique using AutoDock program, some chromone derivatives showing good binding energy with Plm II together with high HIV-1 PR inhibitory activity (more than 70% inhibition) were selected to evaluate for their antimalarial activity against *P. falciparum* (K1) using the microculture radioisotope method. Chromone 35 was found to be the most active compound with IC_{50} value of 0.95 μM while primaquine possessed IC_{50} value of 2.41 ± 0.10 μM. Based on docking study of chromone core structure, a series of designed chromones were synthesized as Plm II inhibitors. The synthetic route was mainly divided into two parts. Firstly, the chromone core structure was prepared by Baker-Venkataraman rearrangement and subsequent intra-molecular cyclization with a catalytic amount of strong acid. These reactions were practical and economical methods for synthesis of the chromone structure. Secondly, the esterification at positions 6 and 7 of the chromone structure was performed to provide the designed chromone derivatives. All of the new compounds in this study were biologically evaluated for their antimalarial activity.

1. Introduction

Plasmepsin II (Plm II), a member of aspartic protease enzyme inside the digestive food vacuole of malaria parasite, is a crucial drug target to search the new drugs for antimalarial chemotherapy [1]. Plm II is involved in the initial step of human hemoglobin degradation process that digest the human hemoglobin as a source of amino acids for growth and maturations during the erythrocytic phase of its life cycle [2]. This enzyme makes the first strategic cleavage of hemoglobin at α-chain between Phe33 and Leu34 in the hinge region, which is highly conserve and responsible for the stability of hemoglobin tetramer, resulting in protein unfolding [3]. Plm II has received considerable attention as a promising target for antimalarial drug design because the inhibition of Plm II results in the starvation of the malaria parasite.

Since HIV-1 protease (HIV-1 PR) is also an aspartic protease enzyme, several HIV-1 PR inhibitors exhibit activity against Plm II, *e.g*., pepstatin A, the known potent peptidomimetic aspartic proteases inhibitor, can inhibit HIV-1 PR, Plm II and cultured malaria parasites [4]. HIV-1 PR inhibitors currently used in AIDS patients such as saquinavir, ritonavir and lopinavir can directly inhibit Plm II and the *in vitro* growth of both drug-sensitive and drug-resistant *P. falciparum* strains. These findings indicate that HIV-1 PR inhibitors may aid in the removal of Plasmodium parasite and used as antimalarial drugs [5-6]. However, peptidomimertic inhibitors normally exhibit low bioavailability due to their high molecular weight, poor solubility and synthesis difficulties. Therefore, the non-peptido-mimetic inhibitors are more interesting for developing the new aspartic protease inhibitors. In our search for new potent aspartic protease inhibitors, we concentrate on flavonoids or chromone compounds (Figure 1).
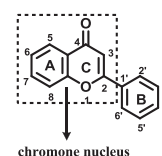
Figure 1. General flavonoid structure.

Flavonoids, a ubiquitous group of secondary metabolites compounds with a wide distribution in fruits and vegetables [7], have been reported that they can exhibit the antimalarial activity against *P. falciparum* [8]. Luteolin and some of naturally occurring flavonoids have been reported that they can exhibit the antimalarial activity against *P. falciparum* [8-9]. The previous study of chromone derivatives as HIV-1 PR inhibitors, forty-six chromone derivatives have been previously synthesized and evaluated the *in vitro* inhibitory activity against HIV-1 PR [10]. The three most potent inhibitors showed IC_{50} = 0.34, 0.65 and 2.53 μM, respectively. Therefore, these chromone derivatives were selected to investigate their inhibitory activity against Plm II.

In this study the chromone derivatives were designed and synthesized as non-peptidomimetic Plm II inhibitors. The preliminary screening of Plm II inhibitory activity of the previous forty-six synthesized chromones with HIV-1 PR inhibitory activities were performed by docking study using AutoDock program [11]. Chromone compounds which showed good binding energy with Plm II from docking study and high HIV-1 PR inhibitory activity

(more than 70 % inhibition) were selected to evaluate for their antimalarial activity against *P. falciparum* using the microculture radioisotope method [12]. Moreover, a new series of chromone derivatives were designed based on docking simulation results. The designed chromone derivatives were synthesized using the commercially available 2,4,5-trimethoxyacetophenone as starting material. The synthesis route of chromone derivatives was divided into two major parts. First part was the preparation of chromone core structure (**49**). Second part was the esterificaition at positions 6 and 7 of the chromone structure to obtain the designed chromone derivatives (**49a-49h**). These chromone compounds were also tested for their antimalarial activity against *P. falciparum*.

2. Materials and Methods

2.1 Molecular modeling experiments

The molecular structures of all chromone compounds were modelled with SYBYL 8.0 molecular modelling program (Tripos Associates, Saint Louis, MO) on an Indigo Elan workstation (Silicon Graphics Inc., Mountain View, CA) using the sketch approach. Firsly, each structure was energy minimized using the standard Tripos force filed (Powell method and 0.05 kcal/mole.Å energy gradient convergence criteria) and electrostatic charge was assigned by the Gasteiger-Hückel method. These conformations were used as starting conformations to perform docking. The crystal structures of Plm II complexed with inhibitor (1SME) were obtained from the Brookhaven Protein Database (PDB). The inhibitor structures were firstly removed from the complex structures, and added polar hydrogen parameters. The grid maps representing the protein in the actual docking process were calculated with AutoGrid. The docking calculations were performed using AutoDock program version 4.0. The docking study was carried out using the Lamarckian genetic algorithm, applying a standard protocol, with an initial population of 150 randomly placed individuals, a mutation rate of 0.02, and a crossover rate of 0.80. One hundred independent docking runs were carried out for each ligand. Results differing by less than 2.0 Å in positional root mean-square deviation (rmsd) were clustered together and represented by the results with the most favorable free energy of binding.

2.2 Synthesis

The chromone derivatives were synthesized via one-pot cyclization reaction as shown in scheme 1.
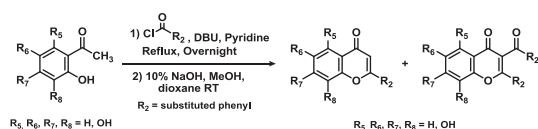
Scheme 1. Synthesis of chromone derivatives via one-pot cyclization reaction [10].

The new designed chromone derivatives were synthesized using the commercially available 2,4,5-trimethoxyacetophenone as starting material. The synthesis route of the designed chromone derivatives was

divided into two main parts, *i.e.*, (i) the preparation chromone **49** as a core structure and (ii) the addition of the steric groups at positions 6 and 7 of the core structure.

Part I: Preparation of chromone core structure (chromone **49**) (scheme 2)
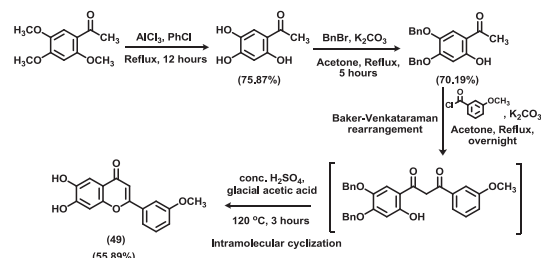
Scheme 2. Synthesis route of chromone **49** [13-16].

Part II: Esterification of chromone **49** by substituted benzoyl chloride (scheme 3)
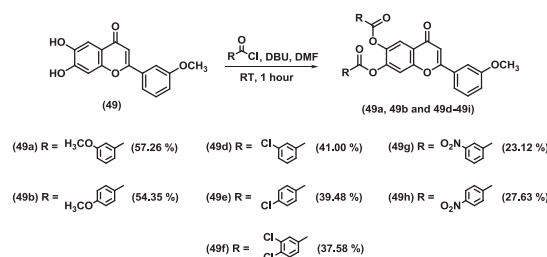
Scheme 3. Esterificaion of chromones **49a**, **49b** and **49d-49h**.

Esterification of chromone **49** and substituted benzoic acid could also be performed by using EDAC.HCl and HOBt as coupling reagents (scheme 4)
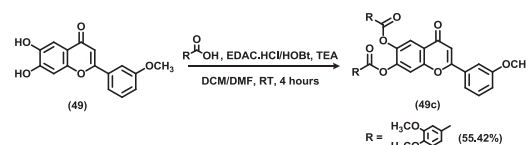
Scheme 4. Esterification of chromones **49c** [17].

All of synthesized chromone compounds were elucidated by spectroscopic techniques. The characterization data of chromone **49c** was shown as the representative of newly synthesized compounds.

Chromone **49c**: White solid; m.p. 188-189 °C; ^{1}H-NMR: δ 3.78 (s, 3H, OCH$_3$), 3.86 (s, 3H, OCH$_3$), 3.92 (s, 3H, OCH$_3$), 3.94 (s, 3H, OCH$_3$), 3.96 (s, 3H, OCH$_3$), 6.83-6.86 (m, 1H, H5″), 6.86 (s, 1H, H3) 6.88 (d, *J* = 8.50 Hz, 1H, H5‴), 7.10-7.13 (m, 1H, H4′), 7.44-7.49 (m, 2H, H2′, H5′), 7.52-7.54 (m, 2H, H6′, H2″), 7.58 (d, *J* = 2.00 Hz, 1H, H2‴), 7.75 (dd, *J* = 8.48, 1.97 Hz, 1H, H6″), 7.79 (s, 1H, H8), 7.80 (dd, *J* = 8.50, 2.00 Hz, 1H, H6‴), 8.21 (s, 1H, H5); MS m/z 635.1557 [M+Na]$^+$.

2.3 *In vitro* antimalarial activity assay

The *in vitro* antimalarial activity was evaluated against the parasite *Plasmodium falciparum* (K1, multi-drug resistant strain), which was cultured continuously according to the method of Trager and Jensen [18].

Quantitative assessment of antimalarial activity *in vitro* was determined by the microculture radioisotope technique based upon the method described by Desjardins *et al* [12]. The levels of incorporated radioactive labeled hypoxanthine, indicating parasite growth, were determined using the TopCount NXT Microplate Scintillation and Luminescence Counters (Perkin Elmer, USA). The percentage of parasite growth was calculated using the signal count per minute of treated (CPM_T) and untreated conditions (CPM_U) from duplicate experiment of each concentration, by this formula.

$$\% \text{ parasite growth} = CPM_T/CPM_U \times 100$$

The inhibition concentration (IC_{50}) represents the concentration which indicate 50% reduction in parasite growth. The standard sample was dihydroartremisinine (DHA) and mefloquine (MEF). This assay was carried out from the Bioassay laboratory of the National Center of Genetic Engineering and Biotechnology (BIOTEC).

3. Results and Discussion

3.1 Molecular modeling

The docking results of previous forty-six chromone derivatives were ranked by their binding energy against Plm II and were filtered with % inhibition against HIV-1 PR. Twenty chromone compounds which showed good binding energy with Plm II from docking study and high inhibitory activity against HIV-1 PR (more than 70 % inhibition) were selected for evaluating the antimalarial activity against *P. falciparum* (K1 multi-drug resistant strain). The selected chromone compounds could be classified into 2 series; there are 3-rings system series and 4-ring system series. The binding energy of selected chromone compound in 4-rings system series (-10.56 to -13.24 kcal/mole) showed better than chromone compounds in 3-rings system series (-7.35 to -8.93 kcal/mole).

Based on docking study, new chromone derivatives (**47**-**52**), which have hydroxyl groups at positions 6 and 7 of chromone structure, were designed and performed docking against Plm II. The results of docking simulation of chromones **47**-**52** showed the slightly better binding energy than the chromone compounds in the 3-rings system series. Therefore, chromones **47**-**52** were subjected to structural modification by adding the steric groups at the both hydroxyl groups to gain the better binding energy. The structural modification of unmodified chromones **47**-**52** led to the better binding energy than the unmodified chromones and pepstatin A. However, the binding energies of modified chromones were slightly different. Therefore, only eight modified chromone derivatives (**49a**-**49h**) were chosen to synthesize due to the modified chromone**s** **49** (R_2 = 3'-(OCH$_3$)-phenyl) were easier and less cost for synthesis. The binding modes of modified chromone derivatives (**49a**-**49h**) were analyzed. It was found that the alignments of all chromones were fit in the pocket of Plm II template and aligned in the same orientation as shown in Figure 2.
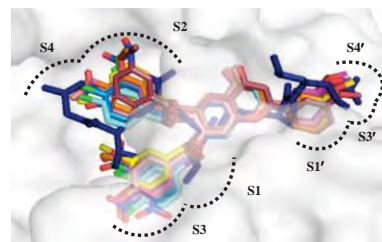

Figure 2. The binding mode of modified chromone compounds comparing with the pepstatin A (navy blue color).
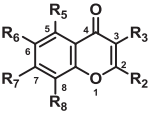
3.2 Synthesis

Chromone **49** was synthesized according to Scheme 2. As seen from the preparation of chromone core structure, all steps of the synthesis pathway were practical and economical methods for the synthesis. The Baker-Venkataraman rearrangement and subsequent intra-molecular cyclization with a catalytic amount of strong acid were used because only simple reagents and solvent were required and the desired chromone (**49**) was provided as the major product with % yield more than 50 %. The esterification reaction was preformed to yield the modified chromone derivatives. Seven of them (**49a**, **49b** and **49d**-**49h**) were synthesized via esterification of chromone **49** by alcoholysis and substituted benzoyl chloride under basic condition as seen in Scheme 3. Chromone **49c** was synthesized via esterification of chromone **49** and substituted benzoic acid using EDAC.HCl and HOBt as coupling reagents (Scheme 4). Triethylamine should be added as catalyst into the reaction to increase rate of the reaction. All of these modified chromone compounds were obtained in low to moderate % yield.

3.3 *In vitro* antimalarial activity assay

As discussed earlier, the preliminary activity screening of chromone derivatives was carried out using docking study against Plm II. However the direct Plm II inhibitory activity test is unavailable during this study period, the antimalarial against *P. falciparum* was evaluated *in ivtro* by microculture radioisotope method. Twenty chromones compounds from the docking study and the newly designed chromones **49** and **49a**-**49h** were evaluated against *P. falciparum* (K1 multi-drug resistant strain). The results of the antimalarial activity of these chromone compounds were shown in Table 1. The three most potent compounds were chromones **35**, **38** and **44** with IC_{50} = 0.95, 4.87, 5.46 μM, respectively. Although the three most potent compounds exhibited the activity lower than the standard compounds (DHA and MEF), these chromone compounds showed the potency better than the antimalarial drugs currently used in patients, *i.e.*, primaquine (IC_{50} = 2.41 ± 0.10 μM) and tafenoquine (IC_{50} = 1.95 ± 0.06 μM) [19]. Apart from being the most potent antimalarials in this study (IC_{50} = 0.95 μM), results from previous study showed that chromone **35** was also potent HIV-1 PR inhibitor with 92.24 % inhibition [10]. All of these newly synthesized compounds were also evaluated for their antimalarial activity.

Table 1. The antimalarial activity of twenty selected chromone compounds and chromone **49**.

Chromone	R_2	R_3	R_5	R_6	R_7	R_8	IC_{50} (μM)
3	Benzyl	H	H	H	OH	OH	9.43
4	Phenyl	H	H	H	OH	OH	19.66
16	4′-(t-butyl)-Phenyl	H	H	H	OH	H	11.41
17	3′-(CF_3)-Phenyl	H	OH	H	OH	H	11.07
18	4′-(F)-Phenyl	H	OH	H	OH	H	Inactive
19	3′,4′-(diF)-Phenyl	H	OH	H	OH	H	Inactive
20	4′-(t-butyl)-Phenyl	H	OH	H	OH	H	9.15
23	3′-(Cl)-Phenyl	H	OH	H	OH	H	13.83
24	3′,4′-(diCl)-Phenyl	H	OH	H	OH	H	11.25
25	4′-(OCH_3)-Phenyl	H	OH	H	OH	H	Inactive
26	3′-(OCH_3)-Phenyl	H	OH	H	OH	H	Inactive
27	3′-(OCH_3)-Phenyl	H	H	OH	H	H	13.23
31	3′-(CF_3)-Phenyl	3″-(CF_3)-Benzoyl	H	H	OH	OH	Inactive
34	4′-(F)-Phenyl	4″-(F)-Benzoyl	H	H	OH	OH	Inactive
35	4′-(NO_2)-Phenyl	4″-(NO_2)-Benzoyl	H	H	OH	OH	0.95
37	3′,4′-(diF)-Phenyl	3″,4″-(diF)-Benzoyl	H	H	OH	H	12.40
38	3′-(CF_3)-Phenyl	3″-(CF_3)-Benzoyl	H	H	OH	H	4.87
42	4′-(NO_2)-Phenyl	4″-(NO_2)-Benzoyl	H	H	OH	H	9.85
44	4′-(t-butyl)-Phenyl	4″-(t-butyl)-Benzoyl	H	H	OH	H	5.46
46	4′-(NO_2)-Phenyl	4″-(NO_2)-Benzoyl	OH	H	OH	H	5.91
49	3′-(OCH_3)-Phenyl	H	H	OH	OH	H	13.94
DHA							2.02 nM
MEF							0.0301

Chromone **49** was found to be active compound with IC_{50} = 13.94 μM while the modified chromones **49a-49h** were inactive.

4. Conclusions

In this study the preliminary screening of Plm II inhibitory activity of the previous chromones with HIV-1 PR inhibitory activities were performed by docking simulation technique. Chromone compounds which showed good binding energy with Plm II and high HIV-1 PR inhibitory activity were selected to evaluate for their antimalarial activity against *P. falciparum*. The most active chromone **35**, which exhibited high potency against HIV-1 PR, showed better antimalarial activity than the currently used drugs, *i.e.* primaquine and tafenoquine. Based on docking results, a series of newly designed chromones were synthesized as Plm II inhibitors. The synthesis pathways of these chromones were practical and economical method.

References

[1] S.E. Francis, D.J. Jr. Sullivan and D.E. Goldberg, *Annu. Rev. Microbiol.* **51** (1997) 97-123.
[2] R. Banerjee, J. Liu, W. Beatty, L. Pelosof, M. Klemba and D.E. Goldberg, *Proc. Natl. Acad. Sci. USA.* **99** (2002) 990-995.
[3] D. Gupta, R.S. Yedidi, S. Varghese, L.C. Kovari and P.M. Woster, *J. Med. Chem.* **53** (2010) 4234-4247.
[4] T.M. Martins, A. Demingos, C. Berry and D.M. Wyatt, *Acta. Trop.* **97** (2006) 212-218.
[5] S. Parikh, J. Liu, P. Sijwali, J. Gut, D.E. Goldberg and P. Rosenthal, *Antimicrob. Agents. Chemother.* **50** (2006) 2207-2209.
[6] S. Parikh, J. Gut, E. Istvan, D.E. Goldberg, D.V. Havlir and P. Rosenthal, *Antimicrob. Agents. Chemother.* **49** (2005) 2983-2985.
[7] A. Scalebert and G. Williamson, *J. Nutr.* **130** (2000) 2073S-2085S.
[8] A.M. Lehane and K.J. Saliba, *BMC. Res. Notes.* **1** (2008) 26.
[9] C. Yenjai, K. Prasanphen, S. Daodee, V. Wongpanich and P. Kittakoop, *Fitoterepia.* **75** (2004) 89-92.
[10] J. Ungwitayatorn, C. Wiwat, W. Samee, P. Nunthanavanit and N. Phosrithong, *J. Mol. Struct.* **1001** (2011) 152-161.
[11] G.M. Morris, R. Huey, W. Lindstrom, M.F. Sanner, R.K. Belew, D.S. Goodsell, *et al*, *J. Comput. Chem.* **30** (2009) 2785-2791.
[12] R.E. Desjardins, C.J. Canfield, J.D. Haynes and J.D. Chulay, *Antimicrob. Agents. Chemother.* **16** (1979) 710-718.

[13] G. Bringmann, T.F. Noll, T. Gulder, M. Dreyer, M. Grune and D. Moskaru, *J. Org. Chem.* **72** (2007) 3247-3252.

[14] S. Saito and J. Kawabata, *Tetrahedron* **61** (2005) 8101-8108.

[15] H. Gao and J. Kawabata, *Biosci. Biotechnol. Biochem.* **68** (2004) 1854-1864.

[16] C. Riva, C.D. Toma, L. Donadel, C. Boi, R. Pennini, G. Motta, *et al*, *Synthesis* (1997) 195-201.

[17] K.S. Babu, T.H. Babu, P.V. Srinivas, B.S. Sastry, K.H. Kishore, U.S.N. Murty, *et al*, Bioorg. Med. Chem. Lett. **1** (2005) 3953-3956.

[18] W. Trager and J.B. Jensen, *Science.* **193** (1976) 673-675.

[19] P.G. Bray, S. Deed, E. Fox, M. Kalkanidis, M. Mungthin, L.W. Deady, *et al*, *Biochem. Pharmacol.* **70** (2005) 1158-1166.

DENDRON-CHOLESTEROL CONJUGATE FOR DNA DELIVERY

Surasak Kheawchaum, Apichart Suksamrarn, Boon-ek Yingyongnarongkul[*]

Department of Chemistry and Center of Excellence for Innovation in Chemistry, Faculty of Science, Ramkhamheang University, Bangkapi, Bangkok 10240, Thailand. [*] E-mail: boonek@ru.ac.th

Abstract: Gene therapy is an approach to treat genetic disorders and other acquired genetic defects. In recent years much effort has been focused on the development of a variety of non-viral DNA carriers. Cationic liposome and cationic polymer, for example; dendrimer, have been shown to achieve efficient transfection for various animal and human cells. These carriers hold great promise as a safe and non-immunogenic approach to gene delivery. Base on the structures of both carriers, new cationic lipids were designed and synthesized. In this study, three dendron-cholesterol conjugates of first, second and third generations, which are termed DC-G1, DC-G2 and DC-G3, respectively were synthesized and characterized using spectroscopic means.

1. Introduction

Gene therapy is an approach that aims to cure inherited and acquired diseases by correcting the overexpression or underexpression of defective genes. The success of gene therapy is largely dependent upon the development of a vector that delivers and efficiently expresses a therapeutic gene in a specific cell population[1]. The following two methods are available for gene deliver, i.e. viral vectors and non-viral vectors. Viral vectors have been intensively investigated and have demonstrated high transfection efficiencies, although safety risks such as immunogenicity, oncogenicity and potential virus recombination[2]. Therefore, non-viral vector have been considered as potential alternatives. They do have certain advantages: non-viral vectors readily form complexes with pDNA, they are not limited by gene sized, and can be vested through structural modification with the ability to carry pDNA to the target cells[3].

Non-viral vectors can be divided into two main classes: cationic lipids and cationic polymers. In both case, cationic charge is required to effectively bind and condense the nucleic acid, which is a polyanion. Cationic polymers have high charge due to their polymeric nature; however this can lead to adverse toxicity[4].

Dendrons also called dentritic wedges, are nanometric trees constituted of numerous branches linked to the core. This versatile class of dentritic molecules processes the advantage to have functional groups (generally different) both at the level of the core and at the end of the branches. Such feature is particularly interesting to elaborate special and complex dendritic architectures. However, this advantage is often more theoretical than practical, due to the necessity for one type of these functions to be non reactive during the synthetic process; either the functions located at the surface for dendrons built by a convergent process, or the function located at the core for dendrons built by a divergent process[5]. The advantages of the divergent process are the rapid growth of the dendrons series, the rapid increase of the size of the dendritic species, and the better overall yield of the dendrons products. However, the limiting features of this method are the possibility of generating molecular imperfection at higher generations and the difficulty in selectively modifying the peripheral functionality. On the other hand, the convergent process offers attractive features such as greater control of the dendrons growth and easy placement of specific peripheral functionality. Nonetheless, the limitations of this method are: the dentritic growth is slow, the branching reaction is highly susceptible to steric inhibition at the focal point, and lower overall yield of the target products[6].

In this study, three dendron-cholesterol conjugates of first, second and third generations, which are termed DC-G1, DC-G2 and DC-G3, respectively were synthesized by divergent process, (Figure 1).
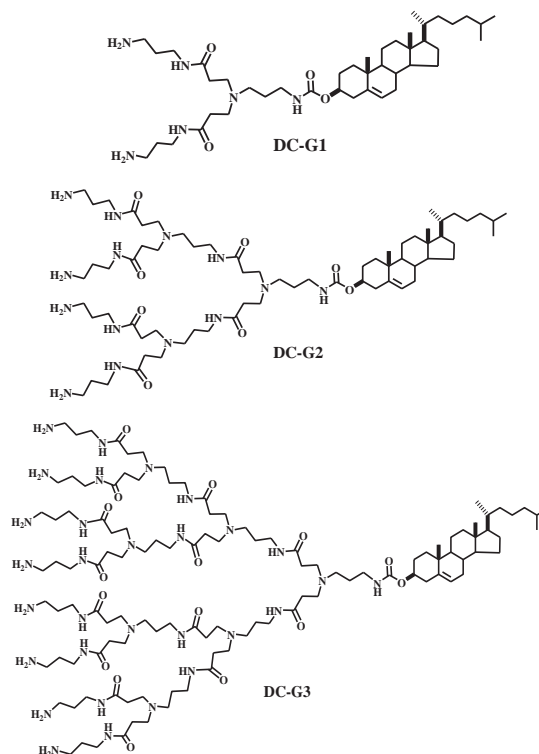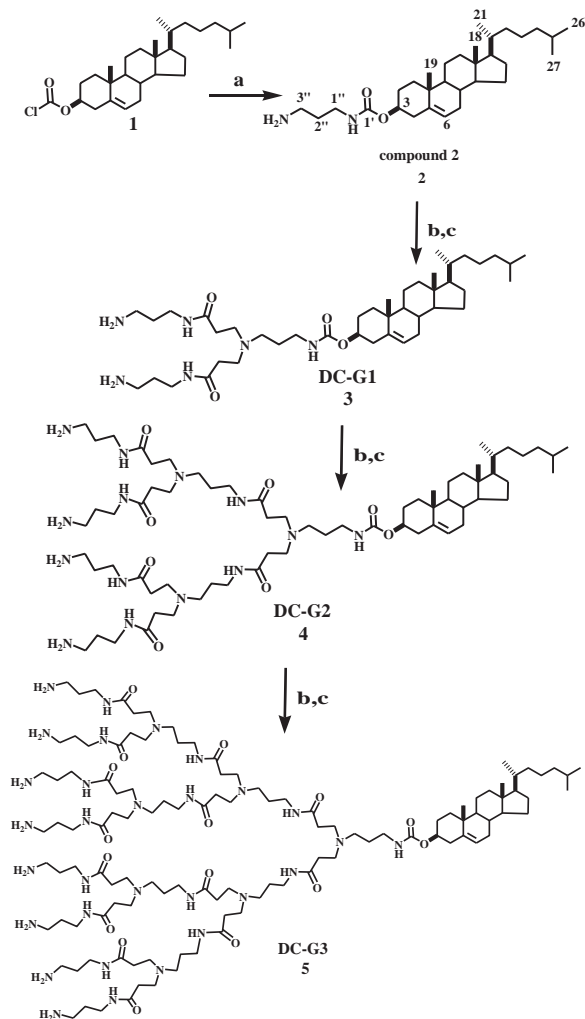

Figure 1. Structures of dendron-cholesterol conjugates.

2. Materials and Methods

2.1 Material

Cholesteryl chloroformate, methyl acrylate and 1,3-diaminopropane were purchased from Sigma Aldrich (Steinheim, Germany). CH_2Cl_2 and MeOH are analytical grade.

2.2 Synthesis of DC-G1 (1), DC-G2 (2), DC-G3 (3).

Scheme 1. Reagents and conditions: (a) 1,3-diaminopropane, CH_2Cl_2, rt; (b) methyl acrylate, MeOH, rt; (c) 1,3-diaminopropane, MeOH, rt.

Compound 2. Cholesteryl chloroformate (2.0 g, 4.45 mmol) was dissolved in 200 mL of CH_2Cl_2 and slowly dropwise into stirred solution of 1,3-diaminopropane (3.3 g, 44.5 mmol) in 100 mL of CH_2Cl_2. The reaction mixture was stirred at room temperature and poured into water and extracted with EtOAc (3 x 150 mL). The organic phase was dried over anhydrous Na_2SO_4 and concentrated under vacuum. The crude extracted was purified by column chromatography on silica gel using CH_2Cl_2/MeOH (96/4) as eluting solvent to give compound 2 (1.8 g, 92%). IR : ν_{max} 3357, 2938, 2870, 1690 cm^{-1}; ^{1}H NMR (400 MHz, CDCl$_3$): δ 0.64 (3H, s, 18-CH$_3$Chol), 0.83 (2 x 3H, d, J = 5.6, 26-CH$_3$Chol,

27-CH$_3$Chol), 0.88 (3H, d, J = 6.1, 21-CH$_3$Chol), 0.97 (3H, s,19-CH$_3$Chol), 2.77(2H, br m, NH$_2$CH_2-), 3.22 (2H, br m, -CH_2NHCOOChol), 4.55 (1H, s, 3-CH Chol), 5.33 (1H, s, 6-HChol); ^{13}C NMR, (100 MHz, CDCl$_3$): δ 11.7 (18-CH$_3$Chol), 18.63 (21-CH$_3$Chol), 19.1 (19-CH$_3$Chol), 22.4, 22.0 (26-CH$_3$Chol, 27-CH$_3$Chol), 39.4 (-CH$_2$NHCOO-), 49.9 (NH$_2$CH$_2$-), 157.4 (-NH COOChol-); MS (ES$^+$) C$_{31}$H$_{54}$N$_2$O$_2$: calculated, 486; found, 487 [M+H]$^+$.

DC-G0.5 A stirred solution of **2** (200 mg, 0.41 mmol) in 6 mL of MeOH was added with methyl acrylate (0.11 mL, 1.23 mmol) and continually stirred at room temperature for 24 hr. The unreacted methyl acrylate was removed under vacuum. The obtained compound was purified by column chromatography on silica gel using CH_2Cl_2/MeOH (100/4) as eluting solvent to give DC-G0.5 (260.0 mg, 95%). IR : ν_{max} 3379, 2948, 2807, 1720, 1690, 1247, 1029 cm^{-1}; ^{1}H NMR (400 MHz, CDCl$_3$): δ 0.64 (3H, s, 18-CH$_3$Chol), 0.83 (2 x 3H, d, J = 5.6, 26-CH$_3$ Chol, 27-CH$_3$Chol), 0.88 (3H, d, J = 6.1, 21-CH$_3$ Chol), 0.97 (3H, s, 19-CH$_3$Chol), 2.50 (4H, br t, ((-CH$_2$)$_2$NCH$_2$-), 2.50 (2H, br t, ((-CH$_2$)$_2$NCH$_2$-), 2.78 (4H, br t, ((-CH$_2$ CH$_2$))$_2$ NCH$_2$-), 3.16 (2H, br t, -CH$_2$NHCOO-) 3.65 (6H, s, 2 x CH$_3$O); ^{13}C NMR, (100 MHz, CDCl$_3$): δ 11.7 (18-CH$_3$Chol), 18.63 (21-CH$_3$Chol), 19.1 (19-CH$_3$ Chol), 22.4, 22.0 (26-CH$_3$ Chol, 27-CH$_3$Chol), 31.8 ((-CH$_2$)$_2$ NCH$_2$-), 38.9 (-CH$_2$COO), 49.1 ((-CH$_2$CH$_2$)$_2$NCH$_2$-), 51.3((-CH$_2$)$_2$NCH$_3$O), 51.7 (2 x CH$_3$O), 156.2(-NH COOChol), 173.0 (2 x CH$_3$OCO-); MS (ES$^+$) C$_{39}$H$_{66}$N$_2$O$_6$: calculated, 658; found, 659 [M+H]$^+$.

DC-G1 A stirred solution of DC-G0.5 (235.7 mg, 0.36 mmol) in 10 mL of MeOH was added with 1,3-diaminopropane (0.60 mL, 7.2 mmol) and continually stirred at room temperature for 48 hr. The unreacted 1,3-diaminopropane was removed under vacuum and obtained compound was purified by sephadex LH-20 column using MeOH as eluting solvent to give DC-G1 (**3**) (147.0 mg, 75%). IR: ν_{max} 3286, 2935, 2867, 1690, 1693 cm^{-1}; ^{1}H NMR (400 MHz, CDCl$_3$): δ 0.64 (3H, s, 18-CH$_3$Chol),0.83 (2 x 3H, d, J = 5.6, 26-CH$_3$Chol, 27-CH$_3$Chol), 0.88 (3H, d, J = 6.1, 21-CH$_3$Chol), 0.97 (3H, s, 19-CH$_3$Chol), 2.30 (4H, br t, ((-CH$_2$)$_2$NCH$_2$-), 2.39 (2H, br t, ((-CH$_2$)$_2$NCH$_2$-), 2.65 (4H, br t, ((-CH$_2$-CH$_2$))$_2$NCH$_2$-), 2.80 (2H, br t, H$_2$N CH$_2$-), 3.10 (2H, br t,-CH$_2$NHCOO-), 3.25 (2H, br t, CH$_2$NHCOCH$_2$-), 7.78 (6H, br s, NH$_3^+$); ^{13}C NMR, (100 MHz, CDCl$_3$): δ 11.7 (18-CH$_3$Chol), 18.63 (21-CH$_3$Chol), 19.1 (19-CH$_3$Chol), 22.4, 22.0 (26-CH$_3$ Chol, 27 CH$_3$Chol), 34.1 ((-H$_2$N)$_2$NCH$_2$-), 36.5 (-CH$_2$ NHCOCH$_2$-), 38.4 (H$_2$NCH$_2$-), 38.6 (-CH$_2$NHCOO-), 50.0 ((-CH$_2$CH$_2$)$_2$-NCH$_2$-), 51.0((-CH$_2$ CH$_2$)$_2$NCH$_2$-), 156.7 (-NHCOO-Chol), 173.4(2 x NHCOCH$_2$-); MS (ES$^+$) C$_{43}$H$_{78}$-N$_6$O$_4$: calculated, 743; found, 744 [M+H]$^+$.

DC-G1.5 A stirred solution of DC-G1 (**3**) (115.3 mg, 0.16 mmol) in 5 mL of MeOH was added with methyl acrylate (0.14 mL, 1.60 mmol) and continually stirred at room temperature for 48 hr. The unreacted methyl acrylate was removed under vacuum and obtained compound was purified by column

chromatography on silica gel using CH_2Cl_2/MeOH (93/7) as eluting solvent to give DC-G1.5 (151.7 mg, 87%). IR: ν_{max} 3312, 2948, 2866, 1732, 1690, 1646, 1247, 1032 cm^{-1}; ^{1}H NMR (400 MHz, CDCl$_3$): δ 0.64 (3H, s, 18-CH$_3$Chol), 0.83 (2 x 3H, d, J = 5.6, 26-CH$_3$-Chol, 27-CH$_3$Chol), 0.88 (3H, d, J = 6.1, 21 CH$_3$-Chol), 0.97 (3H, s, 19-CH$_3$Chol), 2.44 (18H, br t, ((-CH_2)$_2$NCH$_2$), (6H, br t, (-CH$_2$)$_2$NCH_2-), 2.72(12H, br t,((-CH$_2$CH_2)$_2$ NCH$_2$-)), 3.18 (6H, br t, (-CH_2 NH CO-), 3.63 (12H, s, CH_3O-); ^{13}C NMR, (100 MHz, CDCl$_3$): δ 11.7 (18-CH$_3$Chol), 18.63 (21-CH$_3$Chol), 19.1 (19-CH$_3$Chol), 22.4, 22.0 (26-CH$_3$Chol, 27 CH$_3$ Chol) 36.9 (-CH_2 NH CO-), 38.5 (-CH_2NH COO-), 48.9 ((-CH_2CH$_2$)$_2$N CH_2-)), 49.1 ((-CH$_2$CH_2)$_2$ NCH$_2$-), 51.0 ((-CH$_2$CH$_2$)$_2$ NCH$_2$-), 51.6 (CH_3O-), 156.4 (-NH COO-), 171.4 (2 x (-NHCOCH_2-), 173.0 (CH$_3$ OCO-); MS (ES$^+$) C$_{59}$H$_{102}$N$_6$O$_{12}$: calculated, 1087; found, 1088 [M+H]$^+$.

DC-G2 A stirred solution of DC-G1.5 (120 mg, 0.11 mmol) in 3 mL of MeOH was added with 1,3 diaminopropane (4.2 mL, 50 mmol) and continually stirred at room temperature for 72 hr. The unreacted 1,3-diaminopropane was removed under vacuum and obtained compound was purified by sephadex LH-20 column using MeOH as eluting solvent to give DC-G2 (**4**) (97.0 mg, 70%). IR: ν_{max} 3284, 2935, 2867, 1690, 1632 cm^{-1}; ^{1}H NMR (400 MHz, CDCl$_3$): δ 0.64 (3H, s, 18-CH$_3$Chol), 0.83 (2 x 3H, d, J = 5.6, 26-CH$_3$Chol, 27-CH$_3$Chol), 0.88 (3H, d, J = 6.1, 21-CH$_3$Chol), 0.97 (3H, s, 19-CH$_3$Chol), 2.30 (12H, br t, ((CH_2)$_2$NCH$_2$-), 2.39 (6H, br t, ((-CH$_2$)$_2$NCH_2-), 2.65 (12H, br t, ((-CH_2CH$_2$)$_2$NCH$_2$-), 2.80 (8H, br t, H$_2$NCH_2-), 3.10 (2H, br t, -CH_2NHCOO-), 3.25 (6H, br t, -CH_2NH-COCH$_2$-), 7.78 (12H, br s, NH$_3^+$); ^{13}C NMR, (100 MHz, CDCl$_3$): δ 11.7 (18-CH$_3$Chol), 18.63 (21-CH$_3$-Chol), 19.1 (19-CH$_3$Chol), 22.4, 22.0 (26-CH$_3$Chol, 27-CH$_3$Chol) 34.1((-H$_2$N)$_2$N CH$_2$-), 36.5 (-CH_2NH-COCH$_2$-), 38.4 (H$_2$NCH_2-), 38.6(-CH_2 NHCOO-), 50.0 ((-CH_2CH$_2$)$_2$NCH$_2$-), 51.0 ((CH$_2$CH$_2$) $_2$NCH_2-), 156.7 (-NHCOOChol), 173.4 (2 x (-NH COCH$_2$-); MS (ES$^+$) C$_{67}$H$_{126}$N$_{14}$O$_8$: calculated, 1255; found, 1256 [M+H]$^+$.

DC-G2.5 A stirred solution of DC-G2 (**4**) (65 mg, 0.05 mmol) in 2 mL of MeOH was added with methyl acrylate (4.5 mL, 50 mmol) and continually stirred at room temperature for 60 hr. The unreacted methyl acrylate was removed under vacuum and obtained compound was purified by column chromatography on silica gel using CH_2Cl_2/MeOH (80/20) as eluting solvent to give DC-G2.5 (72.3 mg, 74%). IR: ν_{max} 3285, 2948, 2867, 1733, 1690, 1642, 1247, 1033 cm^{-1}; ^{1}H NMR (400 MHz, CDCl$_3$): δ 0.64 (3H, s, 18-CH$_3$ Chol), 0.83 (2 x 3H, d, J = 5.6, 26-CH$_3$Chol, 27-CH$_3$-Chol), 0.88 (3H, d, J = 6.1, 21-CH$_3$Chol), 0.97 (3H, s, 19-CH$_3$Chol), 2.44 (28H, br t, ((-CH_2)$_2$ NCH$_2$), (14H, br t, (-CH$_2$)$_2$NCH_2-), 2.72 (28H, brt, (-CH_2CH$_2$)$_2$-NCH$_2$-), 3.18 (14H, br t, (-CH_2NHCO), 3.63 (24H, s, CH_3O-); ^{13}C NMR, (100 MHz, CDCl$_3$): δ 11.7 (18-CH$_3$Chol), 18.63 (21-CH$_3$Chol), 19.1 (19-CH$_3$Chol), 22.4, 22.0 (26-CH$_3$Chol, 27 CH$_3$Chol) 36.9 (-CH_2NH-CO-), 38.5 (-CH_2NHCOO), 48.9 ((CH$_2$CH$_2$)$_2$ NCH$_2$-)), 49.1((CH$_2$CH_2)$_2$NCH$_2$), 51.0 ((-CH$_2$CH$_2$)$_2$ NCH$_2$-), 51.6 (CH_3O-), 156.4 (-NHCOO-), δ 171.4 (2 x (-NH-COCH$_2$-)), 173.0 CH$_3$OCO-); MS (ES$^+$) C$_{99}$H$_{174}$-N$_{14}$O$_{24}$: calculated, 1943; found, 1944 [M+H]$^+$.

DC-G3 A stirred solution of DC-G2.5 (50 mg, 0.03 mmol) in 2 mL of MeOH was added with 1,3-diaminopropane (2.5 mL, 30 mmol) and continually stirred at room temperature for 80 hr. The unreacted 1,3-diaminopropane was removed under vacuum and obtained compound was purified by sephadex LH-20 column using MeOH as eluting solvent to give DC-G3 (**5**) (43.5, 63%). IR: ν_{max} 3285, 2934, 2867, 1690, 1644 cm^{-1}; ^{1}H NMR (400 MHz, CDCl$_3$): δ 0.64 (3H, s,18-CH$_3$Chol), 0.83 (2x3H, d, J = 5.6, 26-CH$_3$-Chol, 27-CH$_3$Chol), 0.88 (3H, d, J = 6.1, 21-CH$_3$-Chol), 0.97 (3H, s, 19-CH$_3$ Chol), 2.30 (28H, br t, ((-CH_2)$_2$NCH$_2$), 2.39 (18H, br t, ((-CH$_2$)$_2$NCH_2-), 2.65 (28H, br t, ((-CH_2CH$_2$))$_2$ NCH$_2$-), 2.80 (16H, br t, H$_2$NCH_2-), 3.10 (2H, br t, -CH_2NHCOO-), 3.25 (28H, br t, CH_2NHCOCH$_2$-), 7.78 (24H, br s, NH$_3^+$); ^{13}C NMR, (100 MHz, CDCl$_3$): δ 11.7 (18-CH$_3$Chol),18.63 (21-CH$_3$Chol), 19.1 (19-CH$_3$Chol), 22.4, 22.0 (26-CH$_3$Chol, 27 CH$_3$Chol) 34.1 ((-H$_2$N)$_2$NCH$_2$-), 36.5 (-CH_2NHCOCH$_2$-), 38.4 (H$_2$NCH_2-), 38.6 (-CH$_2$ NH-COO-), 50.0 ((-CH_2CH$_2$)$_2$NCH$_2$-), 51.0 ((-CH$_2$ CH$_2$)$_2$ NCH_2-), 156.7 (-NHCOOChol), 173.4 (2 x (-NHCO-CH$_2$-)); MS (ESI) C$_{115}$H$_{222}$N$_{30}$O$_{16}$: calculated, 2281; found, 1141 [M+2H]$^{2+}$.

3. Results and Discussion

Cationic lipid, non-viral vector, is the chemical transfection agent for delivery of nucleic acids which hold great promise as a save and non-immunogenic approach to give delivery. Several cationic lipids having various cationic headgroups, linkers, and hydrophobic tails were reported. Cholesterol was often used as a lipid anchor because of its lipid bilayer stabilizing activity and minimal toxicity to the treated cells. Cholesterol-based cationic lipids with variation of headgroups, mono-, di-, and polyvalent, have been synthesized and tested for their transfection efficiency. To our knowledge, dendron-cholesterol conjugate has not been reported. We report here the synthesis of dendron-cholesterol conjugates of first, second, and third generation. The synthetic route is shown in Scheme 1. The cholesteryl chloroformate (**1**) was reacted with 1,3-diaminopropane using high dilution method to afford **2** in 92% yield for chromatography. The primary amine of **2** was used as a starting point for constructing of dendron unit. The first generation of dendron-cholesterol conjugate, DC-G1 (**3**), was synthesized by two step reactions. Thus, compound 2 was reacted with methyl acrylate to give DC-G0.5 in 95% yield after column chromatography. From the ^{1}H NMR spectra, the peak of methyl ester of DC-G0.5 was found at 3.65 ppm. The DC-G0.5 was then reacted with 1,3-diaminopropane to give DC-G1 (**3**) in 75%. The resonances from the methyl ester at 3.65

ppm are no longer visible, confirming complete conversion of the ester groups. A similar synthetic, purification and characterization procedure was used for the remaining dendron-cholesterol conjugates **4** and **5**, yield of 70 and 63% were obtained, respectively.

DC-G0.5

CH₃O- ⟶
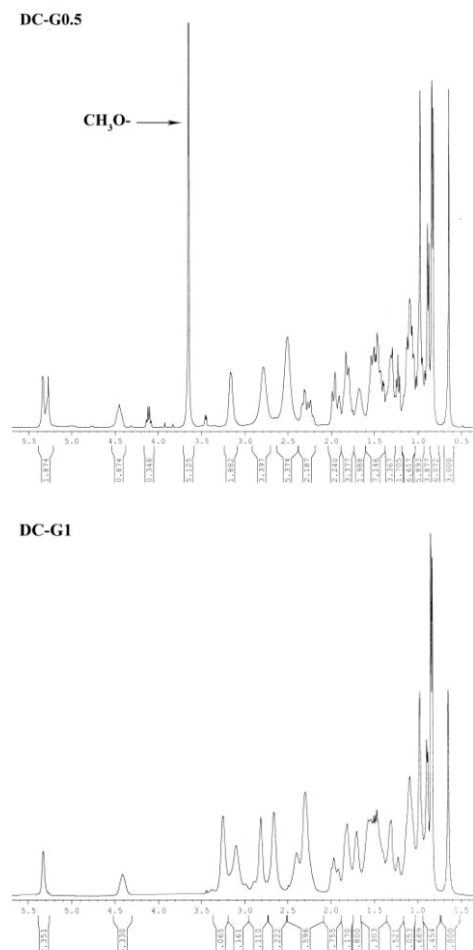
DC-G1

4. Conclusions

The dendron-cholesterol conjugates of first, second and third generation could be successfully synthesized for the first time. The IR, NMR and MS supported the desired structures of DC-G1, DC-G2 and DC-G3. The novel structure of this conjugate should be a capable material in the transfection applications.

Acknowledgements

References

[1] M. Nishikawa and L. Hung, *Hum Gene ther.* **12** (2001) 861–870.

[2] M. Thomas and A.M. Klibanov, *Appl. Microbiol. Biotechnol.* **62** (2003) 27–34.

[3] F.D. Ledley, *Hum. Gene Ther.* **6** (1995) 1129–1144.

[4] H. Lv, S. Zhang, B. Wang, S. Cui, *J. Controlled Releasa.* **114** (2006) 100–109.

[5] A. Inma, T. Cédric-Olivier, L. Régis, M. Valéric, S. Paul, R. Oriol, S. Miquel, C. Anne-Marie and M. Jene-Pierre, *J. Organ. Chem.* **692** (2002) 1928.

[6] Z. Xu, M. Kahr, K. L. Walker, C. L. Wilkins, J. S. Moore, *Am. Chem. Soc.* **116** (1994) 4537.

SYNTHESIS AND CHARACTERIZATION OF CLICKABLE β-CYCLODEXTRIN

Thawinda Kongprathet[1*], Supason Wanichwecharungruang [1]

[1] Department of Chemistry, Faculty of Science, Chulalongkorn University, Pathumwan, Bangkok, Thailand

[*] Author for correspondence; E-Mail: kthawinda@gmail.com

Abstract: β-Cyclodextrin (β-CD) is a well-known host that can form inclusion complexes with various guest molecules, and therefore helps improving solubility, stability and serves as a sustained release carrier for many bioactive molecules. Conjugation of β-CD with polymer is another approach to enhance and open up new applications for β-CD. Because of high efficiency and ease of synthesis, thiol-ene reaction, one of well-known click reactions, can be used to graft β-CD on polymers with thiol functionality. Therefore, β-CD with terminal alkene functionality will be needed. Here, the synthesis and the characterization of alkenyl functionalized β-CD are reported. Demonstration of the grafting of the functionalized β-CD on polymer was carried out on hydrolyzed keratin, a polymer with high cystine level. The encapsulation and controlled release of guest molecule from the grafted polymer was then investigated using a model guest molecule, 1-anilinonaphthalene-8-sulfonic acid (1,8-ANS), by fluorescence spectroscopy.

1. Introduction

Cyclodextrin (CDs) are cyclic oligosaccharides, consisting of a variable number of alpha-1,4-linked D-glucopyranosyl units. However, composing of 6, 7 and 8 units naturally occur as α -, β-, and γ-CD respectively. Due to their hydrophobic cavity in the torous shape of CDs, they can form inclusion complexes with a variety of bioactive molecules, as host-guest interaction, to significantly increase aqueous solubility and stability of the guest molecules and also serve as a control release carrier [1-2]. Among the commercially available CDs, β-CD is the cheapest with an appropriate cavity size, and is used in many applications.

The effective and reliable reaction to join small units together via carbon-hetero atom bonds is described as "Click chemistry" [3]. Although, numerous organic reactions have been referred as click reaction, Cu(I) catalyzed Huisgen 1,3-dipolar cycloaddition is the most well-known. However, the metal residue contenting in the final product causes the limitation for biological applications [4]. Therefore, one of well-known click reactions, thiol-ene reaction, has attracted our interest due to its metal-free condition.

The coupling of thiols with enes generally occurs via two routes; (i) anti-Markovnikov radical addition and (ii) base catalyzed Michael addition [5]. In the latter case, mild reaction condition, minimal by-products and high conversion are its characteristics [4]. We, therefore, direct our research toward this route.

In most cases, sustained release of guest molecules from CD cannot be controlled much. The interaction between the two is one of the important factors. Here we propose that by attaching CD onto polymer can help retarding the release of the guest molecules due to the steric from the polymer chain. The loading of the guest molecules could be done at elevated temperature and if the system is to be used at lower temperature, more sustained release should be observed.

It would be ideal if β-CD could be covalently attached with polymer with ease. Hence, in the present work, we report the synthesis and characterization of β-CD with clickable property, alkenyl functionalized β-CD, to couple with thiol functionality of polymer via thiol-ene click reaction. Hydrolyzed keratin with high cystine level was chosen as an example polymer for the CDs grafting. We also investigated the encapsulation and controlled release property of the β-CD-grafted polymer using 8-anilino-1-naphthalenesulfonic acid (1,8-ANS) as a model molecule. 1,8-ANS is known to be a fluorescence probe for exploring hydrophobic regions due to its fluorescence quenching property in water but not in hydrophobic environment such as the cavity of β-CD [6].

2. Materials and Methods

2.1 Materials

β-cyclodextrin (β-CD, Wako, Japan), methacrylic anhydride (Sigma Aldrich, Germany), hydroquinone (Acros Organics, Belgium), pyridine (Carlo Erba, Italy), triethylamine (TEA, Carlo Erba, Italy), Tris (2-carboxyethyl) phosphine hydrochloride (TCEP·HCl, Acros Organics, Belgium), hydrolysed keratin (MW$_{avg}$ = 125,000 Da, Croda, UK), and 1-anilinonaphthalene-8-sulfonic acid (1,8-ANS, Sigma Aldrich, Germany) were used as receive. Commercial dichloromethane was fractionally distilled before use. Dialysis tubing cellulose membrane (MWCO = 10322, avg flat width 76 mm (3.0 in.), Sigma Aldrich, Germany).

2.2 Synthesis and characterization of alkenyl functionalized β-CD (alkenyl β–CD)

The synthesis of alkenyl β–CD was carried out based on the method of Saito and Yamaguchi [7] with a slight modification. To achieve the introduction of one vinyl group, β–CD (1 g, 0.88 mmol), hydroquinone (0.01 g, 0.091 mmol), and methacrylic anhydride (130 μL, 0.88 mmol) were used and dissolved in pyridine (20 mL). Briefly, β–CD and hydroquinone were firstly dissolved in pyridine. Methacrylic anhydride was then slowly added. The solution was refluxed at 50°C for 5h. However, due to the resemblance in the polarity, the product was irremovable from the leftovers of β–CD at this step. Thus, the mixture, white powder, was obtained by precipitation in dichloromethane (100 mL) and, then, subjected to ^{1}H-NMR and ATR-FTIR analysis. The number of vinyl groups introduced to β–CD was determined by ESI-MS.

^{1}H-NMR (D$_2$O, 400 MHz, δ ppm): 5.04 (C(1)H of β-CD), 3.93-3.78 (C(3,5,6)H of β-CD), 3.63-3.52 (C(2,4)H of β-CD), 1.90 (CH$_3$ in mathacryloyl), 5.74 (CH$_2$=C in methacryloyl) and 6.12 (CH$_2$=C in methacryloyl).

ATR-FTIR (cm^{-1}): 3296 (O-H stretching), 2918 (C-H stretching), 1706 (C=O stretching of ester), 1589 (C=C stretching) and 1153 (C-O stretching).

ESI-MS (positive ion mode, [M+Na]$^+$]): 1157.3589 (β-CD), 1225.37 (alkenyl β-CD with one vinyl group per ring) and 1293.41(alkenyl β-CD with two vinyl groups per ring)

2.3 Click reaction

In the typical reaction, hydrolysed keratin (500 μL, 20% w/v) was firstly reduced by TCEP·HCl in deionized water for 2-3 h at room temperature to generate free thiol groups. The excess amount of the reducing agent was removed by excess dialysis against deionized water. Alkenyl β–CD (10 mg), the white mixture powder from the first step, and TEA (catalyst amount) were added afterwards and the reaction was carried out for one day at room temperature. To purify and collect β–CD-grafted keratin, excessive dialysis against deionized water was used and the product was freeze dried. Any residues of free β–CD from the first step was also removed in this purification method. The obtained yellowish product was subjected to ^{1}H-NMR and gel permeation chromatography (GPC, Shimadzu, RID-10A, Waters 600E Series generic pump, PL aquagel-OH 50 8um column, refractive index detector, calibrated with pollulans as standard (Mw 4.9–805 kDa)). Deionized water was used as the solvent to dissolve all samples and as the mobile phase, at a flow rate of 1 mL/min at 40 °C.

2.4 Controlled release study

Fluorescence of aqueous 1,8-ANS solutions in the presence of alkenyl β-CD, keratin and β-CD-grafted keratin were observed using a thermal controlled fluorescence spectrophotometer. All samples were stirred for 30 min and kept to equilibrium for 10 min at room temperature before data collection. For scan

mode, the excitation wavelength was set at 370 nm, while the emission wavelength was scanned from 370 to 600 nm. For thermal mode, the temperature range was 20-60 °C with a scan rate of 10°C/min.

3. Results and Discussion

3.1 Synthesis and characterization of alkenyl functionalized β-CD (alkenyl β–CD)

The esterification of hydroxyl groups of β-CD with methacrylic anhydride could be achived, using pyridine as both catalyst and solvent, and hydroquinone as radical scavenger preventing the polymerization of methacrylic anhydride. The success of synthesis was confirmed by ATR FT-IR, ^{1}H NMR (Figures 1, 2a) and ESI-MS.

New peaks at 1706 and 1589 cm^{-1} assigned to ester and vinyl group in the IR spectrum indicated that the methacrylate was formed (Figure 1b). This result also conformed to ^{1}H-NMR spectrum, showing proton peaks of vinyl and methyl of methacryloyl. However, due to the mixing of products and left over β-CD, integration of proton in ^{1}H-NMR spectrum and also % yield of alkenyl β-CD could not be calculated at this step. Nevertheless, according to the intensity of mass peaks found in ESI-MS result, product composition could be approximated as 1: 0.2: 0.05 (by mole) for β-CD: alkenyl β-CD with one vinyl group per ring: alkenyl β-CD with two vinyl groups per ring.
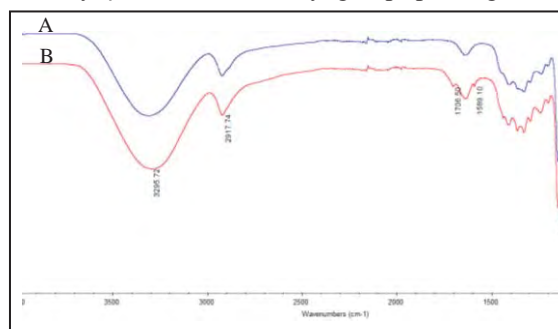

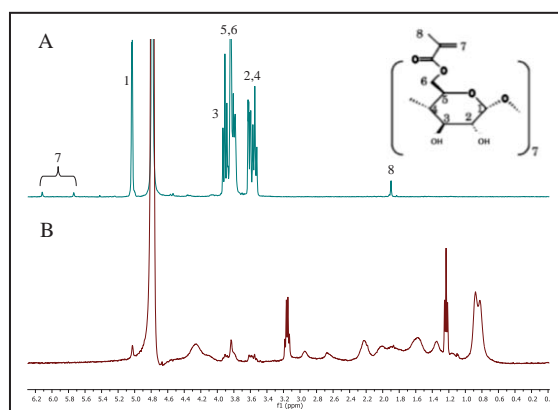Figure 1. ATR FT-IR spectrum of (a) β–CD and (b) alkenyl β–CD

Figure 2. 1H-NMR spectra of (a) alkenyl β–CD, and (b) β-CD-grafted keratin.

3.2 Synthesis and characterization of β-CD-grafted keratin

To couple alkenyl β–CD with thiol groups on the keratin via base catalysed thiol-ene click reaction, reduction of disulfide was firstly carried out using TCEP·HCl, a phosphine compound, as a reducing agent in an excess amount. According to Li *et al.* [4], TCEP could serve as an effective catalyst in this click reaction.

The success of grafting β–CD on keratin was confirmed by ^{1}H-NMR spectrum (Figure 2 b). The presence of proton peaks of β–CD and the absence of proton peak of vinyl group indicated successful click reaction. The increase in weight average molecular weight (M_w) of β-CD-grafted keratin (130 kDa) comparing to keratin (125 kDa), determined by GPC, also assured this success.

3.3 Controlled release study of β–CD-grafted keratin with a model molecule (1,8-ANS)

The inclusion complex between 1,8-ANS and β-CD cavity could be disturbed by the increase in temperature. However, keratin might act as polymer network to control the release of 1,8-ANS into hydrophilic environment or/and help increasing the number of encapsulated molecules. To confirm this assumption, controlled release property of β–CD-grafted keratin with 1,8-ANS was investigated by thermal controlled fluorescence spectrophotometer, comparing the result with β-CD and keratin systems.

The emission wavelengths of ANS in the presence of keratin, β-CD-grafted keratin, and alkenyl β-CD were 473, 476, 502 nm, respectively. The blue shift of emission peaks and the increase in intensity of ANS mean that 1,8-ANS was surrounded by hydrophobic environment.
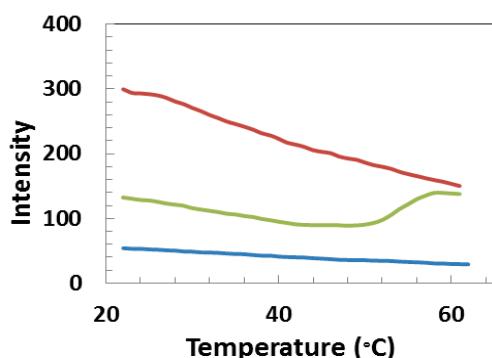
.
Figure 3. Fluorescence intensity of 1,8-ANS at various temperature in the presence of (red) keratin, (green) β-CD-grafted keratin, and (blue) alkenyl β-CD.

Fluorescence intensity of the ANS/keratin system decreased rapidly with the increase in temperature ranging from 25 to 60 °C (Figure 3). On the other hand, for both ANS/alkenyl β-CD and ANS/alkenyl β-CD-grafted keratin systems, their intensities changed insignificantly. This means that CD could serve as a sustain carrier for the ANS, even when being grafted on polymer.

Explanation on the blue shift of ANS fluorescent signal in the presence of ungrafted ketratin is that the keratin probably forms self-assembled structure [8] which could encapsulate the 1,8-ANS, and protecting it from direct contact with water molecules. This resulted in the observed blue shift. However, as shown in the red line of Figure 3, keratin could not hold 1,8-ANS very well as the fluorescent intensity decreased rapidly when the temperature increased. In contrast, β-CD could hold the 1,8-ANS better as the intensity of the fluorescent signal did not change much when the temperature increased (blue line). In the case of β-CD-grafted keratin, the release of 1,8-ANS was faster than from the β-CD but slower than from the keratin. We speculated that the release of 1,8-ANS was from keratin at the beginning and the released 1,8-ANS then got into the very nearby CD cavity. At the temperature of around 53 °C, the increased of the slope indicated 1,8-ANS molecules ought to move into hydrophobic environment. We speculated that the dissociation from keratin was probably almost complete and the released 1,8-ANS moved into the nearby CD cavity effectively.

4. Conclusions

β-CD with clickable property was successfully synthesized. Its application on natural polymer was also demonstrated.

Acknowledgements

References

[1] A. Vyas, S. Saraf and S. Saraf, *J. Incl. Phenom. Macrocycl. Chem.* **62** (2008) 23-42.
[2] A. L. Laza-Knoerr, R. Gref and P. Couvreur, *J. Drug Target.* **18** (2010) 645–656.
[3] H. C. Kolb, M. G. Finn and K. B. Sharpless, *Angew. Chem. Int. Ed.* **40** (2001) 2004-2021.
[4] G. Z. Li, R. K. Randev, A. H. Soeriyadi, G. Rees, C. Boyer, Z. Tong, T. P. Davis, C. R. Becer and D. M. Haddleton, *Polym. Chem.* **1** (2010) 1196-1204.
[5] C. E. Hoyle and C. N. Bowman, *Angew. Chem. Int. Ed.* **49** (2010) 1540-1573.
[6] B. D. Wagner and S. J. Fitzpatrick, *J. Incl. Phenom. Macrocycl. Chem.* **38** (2000) 467-478.
[7] R. Saito and K. Yamaguchi, *Macromolecules.* **36** (2003) 9005-9013.
[8] J. G. Rouse and M. E. Van Dyke, *Materials*, **3** (2010) 999-1014.
[9] T. Nozaki, Y. Maeda, K. Ito and H. Kitano, *Macromolecules.* **28** (1995) 522-524.

CHEMICAL CONSTITUENTS FROM THE TWIGS OF *MANGIFERA FOETIDA* LOUR

Ratanaporn Sompong[1], Kanda Panthong[1,2*]

[1]Department of Chemistry and Center of Excellence for Innovation in Chemisty, Faculty of Science, Prince of Songkla University, Hat Yai, Songkhla 90112, Thailand
[2]Natural Products Research Center, Faculty of Science, Prince of Songkla University, Hat Yai, Songkhla 90112, Thailand
*E-mail address: kanda.p@psu.ac.th, Tel. +66 74288433, Fax. +66 74 558841

Abstract: Three known flavonoids, quercetin (1), 2(*S*)-5,7,3',5'-tetrahydroxyflavanone (2) and garbanzol (3), together with one chromone, 5,7-dihydroxychromone (4), were isolated from the acetone extract of the twigs of *Mangifera foetida* Lour. Their structures were determined by 1D and 2D NMR spectroscopic data and compared with those reported in the literatures.

1. Introduction

Mangifera foetida Lour. is a plant belonging to Anacardiaceae family. The genus *Mangifera* contains about 70 species. Twenty species have been found in Thailand (Eiadthiong, et al., 2000). *M. foetida,* commonly called the horse mango, is distributed throughout western Malaysia and has been introduced into Myanmar and Indo-China (Kostermans and Bompard, 1993). *M. foetida* has various local names: "mamuit" (มะมุด), "maachang" (มาจัง), "malamuit" (มะละมุด), and "macha" (มาแจ) (Orwa et al., 2009).

According to the information from SciFinder Scholar database and ScienceDirect, benzenoids, coumarins, flavonoids, flavonols, monoterpenes, sesquiterpenes, triterpenes, steroids, and xanthones, were chemical constituents found in *Mangifera* genus. *M. foetida*, *M. odorata* and *M. pajang* showed a high value of total phenolic content (TPC) (221-2665 mg GAE/100 g) (Ikram et al., 2009). Based on SciFinder Scholar database and ScienceDirect, the leaves of *M. foetida* showed anti-tumor promoting activity (Murakami et al., 1995), antibacterial activity (Grosvenor et al., 1995) and medicinal use in Indonesia (Grosvenor et al., 1995). The fruits of *M. foetida* showed antioxidant activity (Ikram et al., 2009). Phytochemical examination and biological activity on the twigs of *M. foetida* have not yet been reported. In addition, the acetone extract of the twigs of *M. foetida* exhibited moderate antioxidant activity with an IC_{50} value of 0.61 mg/ml (using DPPH*). These prompted us to investigate its chemical constituents in order to isolate the chemical constituents from this plant.

In this paper, we report the isolation and structural elucidation of three known flavonoids, quercetin (**1**) 2(*S*)-5,7,3',5'-tetrahydroxyflavanone (**2**) and garbanzol (**3**) together with one chromone, 5,7-dihydroxychromone (**4**).

2. Materials and Methods

2.1 General Experimental Procedure

Dry column vacuum chromatography (DCVC), column chromatography (CC), flash column chromatography (FCC) and Sephadex LH-20 column were carried out on silica gel 60 GF$_{254}$ (Merck), silica gel 100 (70-230 mesh ASTM, Merck), silica gel 60 (230-400 mesh ASTM, Merck), and Sephadex LH-20 (GE Healthcare), respectively. Thin layer chromatography (TLC, thickness 200 μm) and precoated thin layer chromatography (PLC, thickness 250 μm) of silica gel 60 GF$_{254}$ (Merck) were used. Solvents for extraction and chromatography were distilled at their boiling ranges prior to use. The IR spectra were measured with a Perkin-Elmer FT-IR spectrophotometer. ^{1}H and ^{13}C Nuclear magnetic resonance spectra were recorded on a Bruker FT-NMR Ultra Shield^{TM} 300 and 500 MHz spectrometer. Spectra were recorded in acetone-d$_6$ and recorded as δ values in ppm downfield from TMS (internal standard δ 0.00). The Ultraviolet spectra were measured with UV-160A spectrophotometer (SHIMADZU).

2.2 Plant material

The twigs of *M. foetida* Lour. were collected from Sichon, Nakhonsithammarat province, in the South of Thailand, in June 2010. The plant was identified by Asst. Prof. Dr. Charan Leerativong and a voucher specimen (Kanda 001) has been deposited at the Herbarium of the Department of Biology, Faculty of Science, Prince of Songkla University, Songkhla, Thailand.

2.3 Extraction and Isolation

The air-dried twigs of *M. foetida* Lour. (3.42 kg) were immersed in acetone (17.5 L) successively three times over a period of 5 days at room temperature. Filtration and evaporation of the solvent under reduced pressure gave a crude acetone extract as a dark brown gum (53.16 g). The acetone extract was subjected to DCVC eluting with a gradient of hexane, acetone-hexane, acetone-methanol and finally with methanol to give 9 fractions (A1-A9). Fraction A5 was separated by Sephadex LH-20 CC eluting with MeOH:CH$_2$Cl$_2$ (1:1, v/v) to give 7 subfractions (F1-F7). Subfraction F6 was separated by PLC using acetone-benzene

(2:98, v/v 5 runs) to give **4** (0.4 mg). Fraction A7 (1.75 g) was separated by Sephadex LH-20 CC eluting with MeOH:CH$_2$Cl$_2$ (1:1, v/v) to give 6 subfractions (B1-B6). Subfraction B4 (947.8 mg) was separated by CC eluting with acetone-hexane (3:7, v/v) to give 5 subfractions (C1-C5). Subfraction C3 (322.2 mg) was separated by FCC eluting with acetone-hexane (3:7, v/v) to give 9 subfractions (D1-D9). Subfractions D3 and D5 were recrystallized from a mixture of acetone and hexane to give **1** (3.6 mg) and **2** (0.7 mg), respectively. Subfraction B3 (206.2 mg) was separated by CC eluting with acetone-hexane (3:7, v/v) to give 8 subfractions (E1-E8). Subfraction E3 give **3** (2.5 mg).

Quercetin (1): a yellow solid; mp: 317.0-318.9 °C (decompose); UV (MeOH) λ_{max} (nm) (log ε): 372 (3.49), 311 (3.04), 256 (3.48), 240 (3.31); IR (neat): 3304, 1605 cm^{-1}; ^{1}H NMR (Acetone-d$_6$, 300 MHz): δ_H 12.20 (*s*, 5-OH, 1H), 7.81 (*d*, *J* = 2.1 Hz, H-2′, 1H), 7.69 (*dd*, *J* = 8.4, 2.1 Hz, H-6′, 1H), 6.99 (*d*, *J* = 8.4 Hz, H-5′, 1H), 6.52 (*d*, *J* = 1.8 Hz, H-8, 1H), 6.26 (*d*, *J* = 1.8 Hz, H-6, 1H); ^{13}C NMR (Acetone-d$_6$, 75 MHz): δ_C 175.7 (C-4), 164.3 (C-7), 161.4 (C-5), 156.9 (C-9), 147.5 (C-4′), 146.2 (C-2), 145.0 (C-3′), 135.8 (C-3), 122.8 (C-1′), 120.5 (C-6′), 115.2 (C-5′), 114.8 (C-2′), 103.2 (C-10), 98.3 (C-6), 93.6 (C-8).

2(*S*)-5,7,3',5'-Tetrahydroxyflavanone (2): a yellow solid; mp: 262.5-263.1 °C; [α]$_D^{27.6}$ +4.9 (*c*, 1.0, MeOH); UV (MeOH) λ_{max} (nm) (log ε): 403 (3.17), 335 (3.54), 287 (4.16) and 222 (4.23); IR (neat): 3255, 1638 cm^{-1}; ^{1}H NMR (Acetone-d$_6$, 300 MHz): δ_H 12.17 (*s*, 5-OH, 1H), 9.73 (*br s*, OH, 1H), 8.15 (*br s*, OH, 1H), 7.04 (*s*, H-4′, 1H), 6.87 (*d*, *J* = 1.2 Hz, H-2′, H-6′, 2H), 5.96 (*d*, *J* = 2.1 Hz, H-8, 1H), 5.95 (*d*, *J* = 2.1 Hz, H-6, 1H), 5.39 (*dd*, *J* = 12.6, 3.0 Hz, H-2, 1H), 3.14 (*dd*, *J* = 17.1, 12.6 Hz, H-3b, 1H), 2.72 (*dd*, *J* = 17.1, 3.0 Hz, H-3a, 1H); ^{13}C NMR (Acetone-d$_6$, 75 MHz): δ_C 197.8 (C-4), 167.9 (C-7), 165.9 (C-5), 164.9 (C-9), 147.5 (C-5′), 146.6 (C-3′), 132.2 (C-1′), 119.8 (C-2′), 116.6 (C-6′), 115.3 (C-4′), 103.8 (C-10), 97.4 (C-6), 96.5 (C-8), 80.6 (C-2), 44.2 (C-3).

Garbanzol (3): yellow solid; mp: 209.3-210.8 °C; [α]$_D^{27.4}$ +23.0 (*c*, 0.25, MeOH); UV (MeOH) λ_{max} (nm) (log ε): 276 (3.64), 251 (3.22) and 213 (3.95); IR (neat): 3271, 1669 cm^{-1}; ^{1}H NMR (Acetone-d$_6$, 500 MHz): δ_H 9.70 (*br s*, OH, 1H), 8.59 (*s*, OH, 1H), 7.73 (*d*, *J* = 8.5 Hz, H-5, 1H), 7.44 (*d*, *J* = 8.5 Hz, H-2′, H-6′, 2H), 6.90 (*d*, *J* = 8.5 Hz, H-3′, H-5′, 2H), 6.63 (*dd*, *J* = 8.5, 2.5 Hz, H-6, 1H), 6.40 (*d*, *J* = 2.5 Hz, H-8, 1H), 5.05 (*d*, *J* = 12.0 Hz, H-2, 1H), 4.57 (*dd*, *J* = 12.0, 3.0 Hz, H-3b, 1H), 4.39 (*d*, *J* = 3.0 Hz, 3-OH, 1H); ^{13}C NMR (Acetone-d$_6$, 125 MHz): δ_C 193.2 (C-4), 165.8 (C-7), 164.7 (C-9), 158.9 (C-4′), 130.3 (C-2′,C-6′), 129.8 (C-5), 129.4 (C-1′), 115.9 (C-3′,C-5′), 113.1 (C-10), 111.8 (C-6), 103.7 (C-8), 84.9 (C-2), 74.0 (C-3).

5,7-Dihydroxychromone (4): a brownish solid; mp: 249.0-251.2 °C; UV (MeOH) λ_{max} (nm) (log ε): 257 (3.56), 236 (3.34); IR (neat): 2922, 1615 cm^{-1}; ^{1}H

NMR (Acetone-d$_6$, 300 MHz): δ_H 12.60 (*s*, 5-OH, 1H), 7.93 (*d*, *J* = 6.0 Hz, H-2, 1H), 6.26 (*d*, *J* = 2.1 Hz, H-8, 1H), 6.13 (*d*, *J* = 2.1 Hz, H-6, 1H), 6.09 (*d*, *J* = 6.0 Hz, H-3, 1H); ^{13}C NMR (Acetone-d$_6$, 75 MHz): δ_C 181.8 (C-4), 164.4 (C-7), 162.5 (C-5), 158.3 (C-9), 156.7 (C-2), 110.7 (C-3), 105.2 (C-10), 99.0 (C-6), 93.9 (C-8).

3. Results and Discussion

Quercetin (1) was isolated as a yellow solid. The UV spectrum exhibited the absorption bands at 372, 311, 256 and 240 nm. The IR spectrum showed absorption bands for a carbonyl group at 1605 cm^{-1} and a hydroxyl group at 3304 cm^{-1}. The ^{1}H NMR spectrum showed one chelated hydroxyl signal [δ_H 12.20 (*s*, 1H], two *meta*-coupled aromatic signals [δ_H 6.52 (*d*, *J* = 1.8 Hz, 1H) and 6.26 (*d*, *J* = 1.8 Hz, 1H)] and characteristic signals of a 1,3,4-trisubstituted aromatic ring [δ_H 7.81 (*d*, *J* = 2.1 Hz, 1H), 7.69 (*dd*, *J* = 8.4, 2.1 Hz, 1H) and 6.99 (*d*, *J* = 8.4 Hz, 1H)]. The ^{13}C NMR spectrum showed fifteen carbons: five methine carbons [δ_C 120.5, 115.2, 114.8, 98.3 and 93.6] and ten quaternary carbons [δ_C 175.7, 164.3, 161.4, 156.9, 147.5, 146.2, 145.0, 135.8, 122.8 and 103.2]. The chelated hydroxyl proton (δ_H 12.20) was located at C-5. The *meta*-coupled aromatic protons at δ_H 6.26 (*d*, *J* = 1.8 Hz, 1H) showed correlations with C-5 (δ_C 161.4), C-7 (δ_C 164.3) and C-8 (δ_C 93.6), of δ_H 6.52 with C-6 (δ_C 98.3), C-7, C-9 (δ_C 156.9) and C-10 (δ_C 103.2), indicating that the *meta*-coupled aromatic protons were located at C-6 and C-8 and the substitutents at C-5 and C-7 to be hydroxyl groups. The 1,3,4-trisubstituted aromatic protons at δ_H 7.81 (H-2') showed correlations with C-2 (δ_C 146.2), C-3' (δ_C 145.0), C-4' (δ_C 147.5) and C-6' (δ_C 120.5), of δ_H 7.69 (H-6') with C-2, C-2' (δ_C 114.8) and C-4' and of δ_H 6.99 (H-5') with C-1', C-3' and C-4', suggesting the connection of 1,3,4-trisubstituted benzene ring at C-2 and the substitutents at C-3' and C-4' to be hydroxyl groups. From the spectral data and comparison with quercetin (Sinha et al., 2012), **1** was identified as 3,5,7,3',4'-pentahydroxyflavone or quercetin.

2(*S*)-5,7,3',5'-Tetrahydroxyflavanone (2) was isolated as a yellow solid. The UV spectrum exhibited the absorption bands at 403, 335, 287 and 222 nm. The IR spectrum showed absorption bands for a carbonyl group at 1638 cm^{-1} and a hydroxyl group at 3255 cm^{-1}. The ^{1}H NMR spectrum showed one chelated hydroxyl signal [δ_H 12.17 (*s*, 1H)], two nonchelated hydroxyl signals [δ_H 9.73 (*br s*, 1H) and 8.15 (*br s*, 1H)], two *meta*-coupled aromatic signals [δ_H 5.96 (*d*, *J* = 2.1 Hz, 1H) and 5.95 (*d*, *J* = 2.1 Hz, 1H)], one oxymethine proton [δ_H 5.39 (*dd*, *J* = 12.6, 3.0 Hz, 1H)], nonequivalent methylene protons [δ_H 3.14 (*dd*, *J* = 17.1, 12.6 Hz, 1H) and 2.72 (*dd*, *J* = 17.1, 3.0 Hz, 1H)] and characteristic signals of a 1,3,5-trisubstituted aromatic ring [δ_H 6.87 (*d*, *J* = 1.2 Hz, 2H) and 7.04 (*s*, 1H)]. The chelated hydroxy proton (δ_H 12.17) showed HMBC correlations with C-5 (δ_c 165.9), C-6 (δ_c 97.4) and C-10 (δ_c 103.8), indicating that it was located at a

peri-position (C-5) to a carbonyl group (δ_c 197.8). The *meta*-coupled aromatic protons at δ_H 5.95 showed HMBC correlations with C-5, C-7 (δ_c 167.9) and C-8 (δ_c 96.5) and of δ_H 5.96 with C-6, C-9 (δ_c 164.9) and C-10, indicating that they were located at C-6 and C-8, respectively and the substituent at C-7 to be a hydroxyl group. The nonequivalent methylene protons (δ_H 3.14) showed HMBC correlation with C-2 (δ_C 80.6), C-4 (δ_C 197.8) and C-1' (δ_C 132.2) and of δ_H 2.72 with C-4, indicating that the nonequivalent methylene protons and oxymethine proton were located at C-3 and C-2, respectively. The 1,3,5-trisubstituted aromatic protons at δ_H 6.87 (H-2' and H-6') showed correlations with C-2, C-1', C-3' (δ_C 146.6), C-5' (δ_C 147.5) and C-6' (δ_C 116.6), and of δ_H 7.04 with C-4' (δ_C 115.3) and C-5', suggesting the connection of a 1,3,5-trisubstituted benzene ring at C-2 and the substituents at C-3' and C-5' to be hydroxyl groups. Comparison of its optical rotation ($[\alpha]_D^{27.6}$ +4.9, c = 1.0, MeOH) with that of 2(*S*)-5,7,3',5'-tetrahydroxyflavanone ($[\alpha]_D^{20}$ +8.4, c = 1.0, MeOH) (Lee et al., 2011), indicated that the absolute configuration at C-2 of **2** was *S*. From the spectral data and comparison with 2(*S*)-5,7,3',5'-tetrahydroxyflavanone (Nessa et al., 2004), **2** was assigned as 2(*S*)-5,7,3',5'-tetrahydroxyflavanone.

Garbanzol (3) was isolated as a yellow solid. The UV spectrum exhibited the absorption bands at 276, 251 and 213 nm. The IR spectrum showed absorption bands for a carbonyl group 1669 cm⁻¹ and a hydroxyl group at 3271 cm⁻¹. The ¹H NMR spectrum showed three nonchelated hydroxyl signals [δ_H 9.70 (*br s*, 1H), 8.59 (*s*, 1H) and 4.39 (*d*, *J* = 3.0 Hz, 1H)], characteristic signals of a 1,2,4-trisubstituted aromatic ring [δ_H 7.73 (*d*, *J* = 8.5 Hz, 1H), 6.63 (*dd*, *J* = 8.5, 2.5 Hz, 1H) and 6.40 (*d*, *J* = 2.5 Hz, 1H), two oxymethine protons [δ_H 5.05 (*d*, *J* = 12.0 Hz, 1H) and 4.57 (*dd*, *J* = 12.0, 3.0 Hz, 1H)] and a 1,4-disubstituted aromatic ring [δ_H 7.44 (*d*, *J* = 8.5 Hz, 2H) and 6.90 (*d*, *J* = 8.5 Hz, 2H)]. The ¹³C NMR spectrum showed 13 signals for 15 carbons: seven signals for methine carbons [δ_c 130.3 (2C), 129.8, 115.9 (2C), 111.8, 103.7, 84.9 and 74.0] and six quaternary carbons [δ_c 193.2, 165.8, 164.7, 158.9, 129.4 and 113.1]. The 1,2,4-trisubstituted aromatic proton (δ_H 7.73) showed cross peaks with C-4 (δ_c 193.2), C-7 (δ_c 165.8) and C-9 (δ_c 164.7), of δ_H 6.63 with C-8 (δ_c 103.7) and C-10 (δ_c 113.1) and of δ_H 6.40 with C-6 (δ_c 111.8), C-7, C-9 and C-10, indicating that they were located at C-5, C-6 and C-8, respectively and the substituent at C-7 to be a hydroxyl group. The location of H-2 (δ_H 5.60) was suggested by its HMBC correlations with C-3 (δ_c 74.0), C-4 (δ_c 193.2), C-1' (δ_c 129.4) and C-2' (δ_c 130.3). A 1,4-disubstituted aromatic protons (δ_H 7.44) resonating at the lowest field gave cross peaks with C-2 (δ_c 84.9) and C-4' (δ_c 158.9), other aromatic proton (δ_H 6.90) showed cross peaks with C-1' and C-4' and a hydroxy proton (δ_H 8.59) showed cross peaks with C-3' and C-5' (δ_C 115.9), indicating the attachment of the 1,4-disubstituted aromatic ring at

C-2 and a hydroxyl group at C-4'. Comparison of its optical rotation ($[\alpha]_D^{27.4}$ +23.0, c = 0.25, MeOH) with that of (2*R*,3*R*)-2,3-*trans*-7,4'-dimethoxydihydroflavonol ($[\alpha]_D^{24}$ +12.8, c = 0.25, MeOH) (Benavides et al., 2007), indicated that the absolute configurations at C-2 and C-3 of **3** were both *R*. By comparison of the NMR data with those garbanzol (Lee et al., 2005), **3** was identified as garbanzol (*trans*-3,7,4'-trihydroxyflavanone).

5,7-Dihydroxychromone (4) was isolated as a brownish solid. The UV spectrum exhibited the absorption bands at 257 and 236 nm. The IR spectrum showed absorption bands for a carbonyl group at 1615 cm⁻¹ and a hydroxyl group at 2922 cm⁻¹. The ¹H NMR spectrum showed one chelated hydroxy signal [δ_H 12.60 (1H, *s*)], two *meta*-couple aromatic signals [δ_H 6.26 (*d*, *J* = 2.1 Hz, 1H) and 6.13 (*d*, *J* = 2.1 Hz, 1H)] and two *cis* olefinic signals [δ_H 7.93 (*d*, *J* = 6.0 Hz, 1H) and 6.09 (*d*, *J* = 6.0 Hz, 1H)]. The ¹³C NMR spectrum showed nine carbons: four methine carbons [δ_c 156.7, 110.7, 99.0 and 93.8] and five quaternary carbons [δc 181.8, 164.4, 162.5, 158.3 and 105.2]. The chelated hydroxy proton [δ_H 12.60 (1H, s)] showed cross peaks with C-5 (δ_c 162.5), C-6 (δ_c 99.0) and C-10 (δ_c 105.2) in the HMBC experiment, indicating that it was located at a *peri*-position (C-5) to a carbonyl group (δ_c 181.8). The *meta*-coupled aromatic protons (δ_H 6.13) showed cross peaks with C-5, C-7 (δ_c 164.4), C-8 (δ_c 93.9) and C-10, of δ_H 6.26 with C-6, C-7, C-9 (δ_c 158.3) and C-10, suggesting that they were located at C-6 and C-8, respectively, and the substituent at C-7 to be a hydroxyl group. The olefinic proton (δ_H 7.93) showed cross peaks with C-3 (δ_c 110.7), C-4 and C-9, and of δ_H 6.09 with C-2 (δ_c 156.7) and C-10 in the HMBC experiment, indicating that they were located at C-2 and C-3, respectively. From the spectral data and comparison with 5,7-dihydroxychromone (Simon et al., 1994), **4** was assigned as 5,7-dihydroxychromone.

4. Conclusion

Three known flavonoids, quercetin (**1**), 2(*S*)-5,7,3',5'-tetrahydroxyflavanone (**2**) and garbanzol (**3**) together with one chromone, 5,7-dihydroxychromone (**4**), were isolated from the twigs of *M. foetida* Lour. by chromatographic techniques.
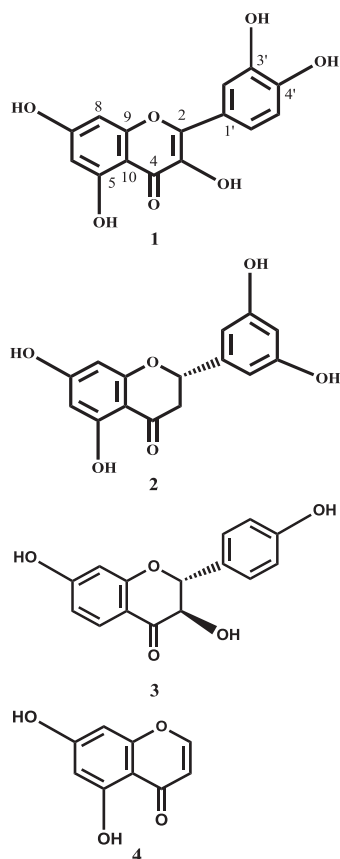
Fig. 1 The structure of compounds **1-4**

References

[1] A. Benavides, C. Bassarello, P. Montoro, W. Vilegas, S. Piacente and C. Pizza, Flavoniods and isoflavonoids from *Gynerium sagittatum*, *Phytochemistry* **68** (2007) 1277-1284.

[2] A. Murakami, S. Jiwajinda, K. Koshimizu and H. Ohigashi, Screening for in vitro anti-tumor promoting activityes of edible plants from Thailand, *Cancer. Lett*. **95** (1995) 139-146.

[3] A. Simon, A.J. Chulia, M. Kaouadji and C. Delage, Quercetin 3-[triacetylarabinosyl(1➔6)galactoside] and chromones from *Calluna vulgaris*, *Phytochemistry* **36** (1994) 1043-1045.

[4] A.J.G.H. Kostermans and J.M. Bompard. 1993. The mangoes; their botany, nomenclature, horticulture and utilization. IBPGR Academic Press, London.

[5] C. Orwa, A. Mutua, R. Kindt, R. Jamnadass, R. Anthony, S. 2009 Agroforetree Database: a tree referent and selection guide version 4.0 (http://www.worldagro-forestry.org/sites/treedbs/freedatabases).

[6] E.H.K. Ikram, K.H Eng, A.M.M. Jalil, A. Ismail. S. Idris, A. Azlan, H.S.M. Nazri, N.A.M. Diton and R. A. M. Mokhtar Antioxidant capacity and total phenolic content of Malaysian underutilized fruits, *J. Food Compos. Anal*. **22** (2009) 388-393.

[7] F. Nessa, Z. Ismail, N. Mohamed and M.R.H.M. Haris, Free radical-scavenging activity of organic extracts and of pure flavonoids of *Blumea balsamifera* DC leaves, *Food Chemistry*. **88** (2004) 243-252.

[8] I.-C. Lee, J.-S. Bae, T. Kim, O.J. Kwon and T.H. Kim, Polyphenolic constituents from the aerial parts of *Thymus quinquecostatus* var. *japonica* collected on Ulleung Island, *J. Korean Soc. Appl. Biol. Chem*. **54** (2011) 811-816.

[9] P.W. Grosvenor, A. Supriono and D.O. Gray, Medicinal plants from Riau Province, Sumatra, Indonesia. Part 2: antibacterial and antifungal activity, *J. Ethnopharmacol.* **45** (1995) 97-111.

[10] R. Sinha, M.K. Gadhwal, U.J. Joshi, S. Srivastava and G. Govil, Modifying effect of quercetin on model biomembranes: studied by molecular dynamic simulation, DSC and NMR, *Int. J. Curr. Pharm. Res.* **4** (2012) 70-79.

[11] T.-H. Lee, J.-L. Chiou, C.-K. Lee, and Y.-H. Kuo, Separation and determination of chemical constituents in the roots of *Rhus javanica* L. var. *roxburghiana*, *J. Chin. Chem. Soc*. **52** (2005) 833-841.

[12] W. Eiadthong, K. Yonemori, A. Sugiura, A. Utsunomiya and S. Subhadrabandhu, Records of *Mangifera* species in Thailand, *Acta Hort*. **509** (2000) 223-231.

[13] http://www. komchadluek.net/detail/20091023/33881 /33881.html (Retrieved November 29, 2011).

SYNTHESIS OF RUTHENIUM COMPLEXES AND PHOTOINDUCED ELECTRON-TRANSFER STUDY IN NONAQUEOUS SOLUTION

Narumon Boonyavong[1], Potjanart Suwanruji[1], Licheng Sun[2], Supa Hannongbua[1], Pattraporn Saiwattanasuk[1] and Thitinun Karpkird[1*]

[1] Department of Chemistry, Faculty of Science, Kasetsart University,Chatuchak, Bangkok, Thailand
[2]Department of Chemistry, School of Chemical Science and Engineering, Royal Institute of Technology (KTH), Stockholm, Sweden

[*]Author for correspondence;E-Mail:fscitnm@ku.ac.th, Tel. +6625625555 ext 2134

Abstract: Two dinuclear complexes, the Ru(bpy)$_3$-viologen-Ru(dcbpy)$_2$(bpy) (1) and the Os(bpy)$_3$-viologen-Ru(dcbpy)$_2$(bpy) (2) were synthesized and isolated in nonaqueous solution. The complexes were characterized by ^{1}H-NMR, MS and Infrared spectroscopy. Photoinduced intramolecular electron transfer of the Ru or Os moiety to viologen (V^{2+}) was observed by UV-Vis spectrometry in acetonitrile solution. With the addition of an external electron donor, triethanolamine (TEOA), light-driven formation of a viologen radical (V$^{+\bullet}$) was observed at 398 and 605 nm. Molecular oxygen quenching of the V$^{+\bullet}$ reversed to the original V^{2+} form. Electrochemical properties of these compounds will be further studied. This system is useful for designing and synthesis of photo molecular devices.

1. Introduction

In the near future, fossil fuel resources might run out from the earth. With this concern, renewable energies such as solar energy, biogas, etc. are in the world's interest as alternative resources. Solar energy is a very attractive choice because it is clean and not exhaust. Solar energy can be converted to electrical energy.

Recently, the synthesis of dinuclear complexes such as diruthenium complexes which ligandsdo not havecarboxyl groups were studied by Monhaphol and co-workers.[1]The photochemistry property of these molecules has been studied for design and construction of molecular devices. One of the most important photoreactions to convert light to electricity is the photoinduced intramolecular electron transfer between an electron donor and an acceptor. Ruthenium (II) polypyridine and viologen[2]is a general couplefor studying the photoinduced electron transfer process and accordingly for construction of a similar charge separated state in artificial systems for solar-energy conversion. In addition, the bipyridyl ligand which was substituted by 4,4'-dicarboxy-2,2'-bipyridine (dcbpy)playsan important role as anchoring ligands.It can increase broadening of absorptionband.[3] The complex which bipyridyl ligandhas carboxyl groupscan give higher efficiency when it was used as dye sensitized molecule.

In this work, complexes**1** and **2**weresynthesized as shown in Scheme1. Their structures were confirmed by ^{1}H-NMR, MS and Infrared spectroscopy.
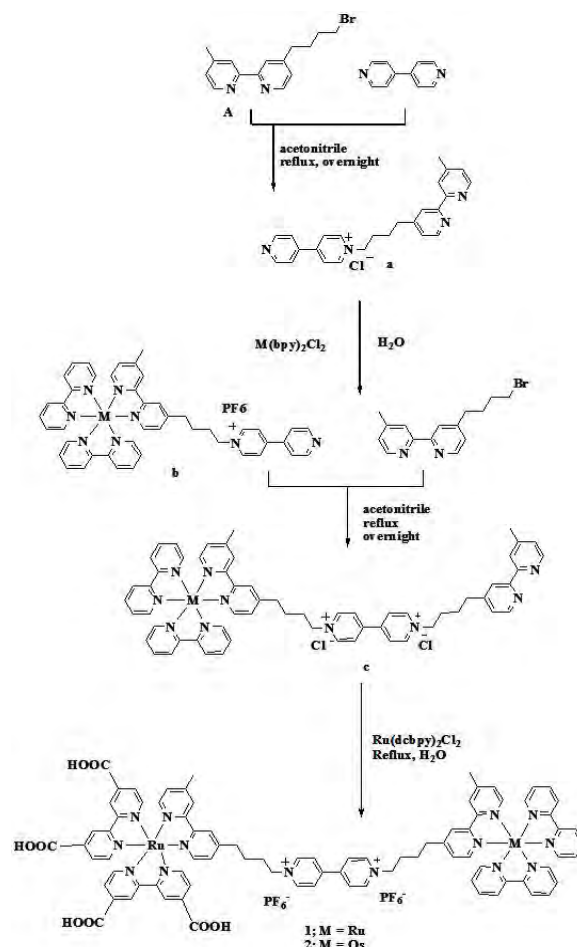
Scheme1. Synthesis pathway of complexes **1** and**2**.

The formation of viologen radical ($V^{+\bullet}$) when the light has been irradiated in non-aqueoussolution was also investigated.

2. Materials and Methods

2.1 Instruments and Materials

HRMS: High-resolution mass spectrometry was carried out using a QTofmicromass spectrometer (Micromass, Inc., Manchester, England)

UV/Visabsorption spectroscopy: UV/Vis absorption spectra were measured using aJasco V-670 spectrophotometer (JASCO International.Co., Ltd.,Tokyo)

Infrared spectroscopy: IR spectra were measured using a system 2000 FT-IR (Perkin Elmer, Beaconsfield bucks.)

Nuclear Magnetic Resonance:^{1}H-NMR spectra were measured using a VARIAN INOVA NMR Spectrometer 400 MHz.

Photochemistry: Samples were prepared byusing the complexes **1** and **2** to dissolve in acetonitrile (0.08 mM).Epson LCD projector Model: EMP-821 (SEIKO EPSON CORP., Beijing) was used asalight source.

Materials:Compounds**A**,**a** and Ru(bpy)$_3$-viologen-Ru(bpy)$_3$ (**RuMVRu**) were synthesized according to Monhaphol et.al.[1] Os(bpy)$_2$Cl$_2$was synthesized accordingto Kober et.al.[4]Ru(dcbpy)$_2$Cl$_2$was synthesized accordingto literature procedures.[6-7]Other materials and solvents employed were commercially available.

2.2 Synthesis

*Os(bpy)$_3$-viologen (2b·3PF$_6^-$):*Compound **a** 0.50 g (0.95 mmol) andOs(bpy)$_2$Cl$_2$ 0.46g (0.79 mmol) were refluxed in 30 ml of (1:1, v/v) ethanol/water under N$_2$ atmosphere at 110°Cfor 24 hours. After that saturated aqueous solution of ammonium hexafluorophosphate (NH$_4$PF$_6$) was added in the cooled reaction mixture and isolated by filtration. The crude product was purified by column chromatography using silica gel and a mixture of CH$_3$CN/sat.KNO$_3$/H$_2$O as an eluent.The dark green solid was obtained (0.44 g, yield 63%).^{1}H-NMR (400 MHz, CD$_3$CN) δ ppm 8.86 (dd, 2H,*J*=4.5Hz,*J*=1.7Hz),8.77 (d,2H,*J* = 6.7Hz),8.46 (dd,4H,*J*= 7.9Hz, *J*=2.9Hz),8.35 (s, 1H),8.33 (s, 1H)8.32 (s, 2H),7.84 (t,4H,*J*=7.9Hz,*J*=7.9 Hz),7.80 (dd,2H,*J*=4.5Hz, *J*=1.7Hz),7.67 (m, 4H),7.45 (dd,2H,*J*=13.1Hz, *J*=5.9Hz),7.34 (m, 4H),7.16 (d,2H, *J*=5.9Hz),4.59 (t,2H,*J*=7.5Hz, *J*=7.5Hz),2.93 (m, 2H),2.60 (s, 3H),2.08 (m, 2H),1.83 (m, 2H) ; ESI-MS: m/z found : [M^{3+}/3, 295.1180], [M^{3+}+PF$_6^-$/2, 515.1345]and[M^{3+}+2PF$_6^-$/1, 1175.1862].

*Os(bpy)$_3$-viologen-bpy (2c·4PF$_6^-$):*Compound**2b·3PF$_6^-$** 142.00 mg (0.11 mmol) andcompound**A** 130.00 mg (0.43 mmol) were refluxed in acetonitrile under N$_2$ atmosphere at 90°Cfor5-6 days. The crude product was changed to PF$_6^-$ and then purified by column chromatography using Sephadex LH20 and acetonitrile as an eluent.The dark green

solid was obtained (151.00 mg, yield 83%).^{1}H-NMR (400 MHz, CD$_3$CN) δ ppm 8.90 (dd, 4H, *J*=2.0Hz, *J*=7.0Hz), 8.66 (d, 1H, *J*=5.4Hz), 8.61 (d, 1H, *J*=5.4Hz), 8.46 (dd, 4H, *J*=3.4Hz, *J*=8.3Hz), 8.39 (d, 4H, *J*=6.5Hz), 8.35 (s, 2H), 8.33 (s, 1H), 8.29 (s, 1H), 7.83 (t, 4H, *J*=7.9Hz), 7.63 (m, 6H), 7.47 (d, 1H, *J*=6.0Hz), 7.43 (d, 1H, *J*=5.9Hz), 7.29 (m, 4H), 7.16 (t, 2H, *J*=4.2Hz), 4.65 (m, 4H), 2.92 (m, 4H), 2.61 (s, 3H), 2.60 (s, 3H), 2.12 (m, 4H), 1.82 (m, 4H); ESI-MS: m/z found:[M^{4+}+PF$_6^-$/3, 418.4577] and [M^{4+}+2PF$_6^-$/2, 697.6472].

Ru(bpy)$_3$-viologen (1b·3PF$_6^-$): Compound **a**1.25 g (2.30mmol) and Ru(bpy)$_2$Cl$_2$ 1.20 g (2.30mmol) were refluxed in 20 ml of water under N$_2$ atmosphere at 90°C for 3 hours. After that, saturated aqueous solution of NH$_4$PF$_6$ was added in the cooled reaction mixture and isolated by filtration. The crude product was purified by column chromatography using silica gel and a mixture of CH$_3$CN/sat.KNO$_3$/H$_2$O as an eluent. The red solid was obtained (0.65 g, yield 30%).^{1}H-NMR (400 MHz, CD$_3$CN)δ ppm 8.85 (dd, 2H, *J*=1.7Hz, *J*=4.5Hz), 8.78 (d, 2H, *J*=7.0Hz), 8.49 (d, 4H, *J*=8.2Hz), 8.35 (dd, 4H, *J*=8.6Hz, *J*=15.9Hz), 8.04 (m, 4H), 7.83 (dd, 2H, *J*=1.7Hz, *J*=4.5Hz), 7.71 (t, 4H, *J*=5.8Hz), 7.54 (dd, 2H, *J*=5.8Hz, *J*=13.5Hz), 7.39 (m, 4H), 7.23 (d, 2H, *J*=5.9Hz), 4.60 (m, 2H), 2.86 (m, 2H), 2.52 (s, 3H), 2.07 (m, 2H), 1.78 (m, 2H); ESI-MS: m/z found : [M^{3+}/3, 265.0995], [M^{3+}+PF$_6^-$/2, 470.1072] and [M^{3+}+2PF$_6^-$/1, 1085.1273].

*Ru(bpy)$_3$-viologen-bpy (1c·4PF$_6^-$):*Compound**1b·3PF$_6^-$**100.80 mg (0.11mmol) and A 130.00 mg (0.43 mmol) were refluxed in acetonitrile under N$_2$ atmosphere at 90°Cfor5-6 days. After that, the most of acetonitrile was removed by a rotary evaporator. Then acetone was added to the reaction mixture forprecipitation. The orange solid was filteredand washed by small amount of acetone. The orange solid was obtained (154.40 mg, yield 90%).^{1}H-NMR (400 MHz, CD$_3$CN) δ ppm 8.90 (d, 4H, *J*=6.3Hz), 8.62 (d, 2H, *J*=5.1Hz), 8.57 (s, 1H), 8.56 (s, 1H), 8.49 (d, 4H, *J*=8.1Hz), 8.38 (d, 4H, *J*=9.0Hz), 8.30 (s, 1H), 8.27 (s, 1H), 8.04 (t, 4H, *J*=7.9Hz), 7.73 (d, 4H, *J*=5.8Hz), 7.57 (d, 1H, *J*=5.8Hz), 7.53 (d, 1H, *J*=5.8Hz), 7.48 (t, 2H, *J*=4.4Hz), 7.39 (m, 4H), 7.24 (t, 2H, *J*=6.0Hz), 4.66 (dt, 4H, *J*=3.0Hz, *J*=7.8Hz), 2.90 (d, 2H, *J*=7.1Hz), 2.86 (d, 2H, *J*=7.2Hz), 2.54 (s, 3H), 2.52 (s, 3H), 2.11 (m, 4H), 1.83 (m, 4H); ESI-MS: m/z found : [M^{4+}/4, 255.0758], [M^{4+}+PF$_6^-$/3, 388.4272] and [M^{4+}+2PF$_6^-$/2, 655.1365].

*Ru(bpy)$_3$-viologen-Ru(dcbpy)$_2$(bpy)(1·6PF$_6^-$):*Ru(dcbpy)$_2$Cl$_2$24.20 mg (0.04 mmol) and compound **1c·4PF$_6^-$**33.40 mg (0.03 mmol), which was changed to**1c·4Cl$^-$**by using tetrabutyl ammoniumchloride (Bu$_4$NCl$^-$),were dissolved in 10 ml of water. Then the mixture was heated at 90°C under N$_2$ atmosphere for 2 days. The product was changed to PF$_6^-$ and recrystallized by using acetone and dichloromethane. The red solid (complex **1**) was isolated from solution by centrifugation. The red solid was obtained (43.50

mg, yield 57%).^{1}H-NMR (400 MHz, CD$_3$CN)δ ppm 8.91 (s, 4H), 8.60 (s, 4H), 8.49 (d, 4H, J=8.1Hz), 8.39 (m, 8H), 8.04 (t, 4H, J=7.5Hz), 7.85 (m, 8H), 7.72 (m, 4H), 7.57 (d, 2H, J=5.8Hz), 7.53 (d, 2H, J=5.8Hz), 7.40 (m, 4H), 7.24 (m, 4H), 4.61 (m, 4H), 2.87 (m, 4H), 2.65 (s, 3H), 2.53 (s, 3H), 2.12 (m, 4H), 1.81 (m, 4H); FT-IR: cm^{-1} found : [O-H stretch, 3475], [C=O, 1735], [C-O, 1217], [C=C, 1603], [C=N, 1637 and 1654], [C-N, 1354] and [C-H bend of aromatic, 841].

*Os(bpy)$_3$-viologen-Ru(dcbpy)$_2$(bpy)(**2·6PF$_6^-$**):*This complex was synthesized fromRu(dcbpy)$_2$Cl$_2$ 10.00 mg (0.02 mmol) and compound **2c·4PF$_6^-$** 19.30 mg (0.02 mmol) and then purified by the same method as complex **1**. The dark green solid was obtained (12.00 mg, yield 31%).^{1}H NMR (400 MHz, CD$_3$CN)δ ppm 9.01 (d, 2H, J=6.1Hz), 8.90 (d, 2H, J=6.9Hz), 8.46 (dd, 4H, J=3.4Hz, J=8.3Hz), 8.39 (d, 4H, J=6.6Hz), 8.35 (s, 2H), 8.33 (s, 2H), 7.92 (t, 4H, J=4.7Hz), 7.86 (m, 4H), 7.81 (m, 4H), 7.63 (m, 4H), 7.47 (d, 2H, J=5.8Hz), 7.43 (d, 2H, J=5.9Hz), 7.28 (m, 8H), 7.16 (m, 4H), 4.65 (m, 4H), 2.87 (m, 4H), 2.60 (s, 3H), 2.53 (s, 3H), 2.10 (m, 4H), 1.81 (m, 4H) ; FT-IR: cm^{-1} found : [O-H stretch, 3489], [C=O, 1736], [C-O, 1216], [C=C, 1590], [C=N, 1637 and 1655], [C-N, 1354] and [C-H bend of aromatic, 839].

3. Resultsand Discussion

Light-induced formation of complexes 1 and 2 with an external electron donor, TEOA

Figure 1 shows the broad absorption of metal-to-ligand charge-transfer (MLCT) transition of Ru(bpy)$_3$ moiety at 450 nm and the strong π→π* ligand-centered band absorption at 280 nm.[8,9] The absorption of heteronuclear **2** shows the similar absorption spectrum to homonuclear **1** and **RuMVRu**. The anchor carboxylic acid groups have no effect to the absorption spectrum. To observe the viologen radical formationof complexes**1** and **2**, the acetonitrile solution of these compounds were irradiated in the presence of an external electron donor, triethanolamine(TEOA), and saturated with Nitrogen.**RuMVRu** from the previous work was used for the comparison.[1]When the viologen radical formed,the solution color changed from orange to green for complex **1** and from light green to dark green for complex **2**. The two absorption peaks at 398 and 605 nm (Figure 1), the characteristic peaks ofthe V$^{+•}$, were observed after15 and 20min of irradiationfor complexes**1** and **2**, respectively. The peak intensityincreased withtheprolonged irradiation time.Complex **2** gavestronger absorptionintensity than that of complex **1** indicating that complex **2** gives more stable viologen radical than that of complex **1**. The viologen radicals of **1** and **2**took longer time to form than that of **RuMVRu** indicating that V$^{+•}$ of **RuMVRu** is easier to form than those of **1** and **2**.In the presence of oxygen in the solution, the absorption spectra and the solution color restored to the

initial.The degradation didnot happen during the irradiation of the complexes**1** and **2**.
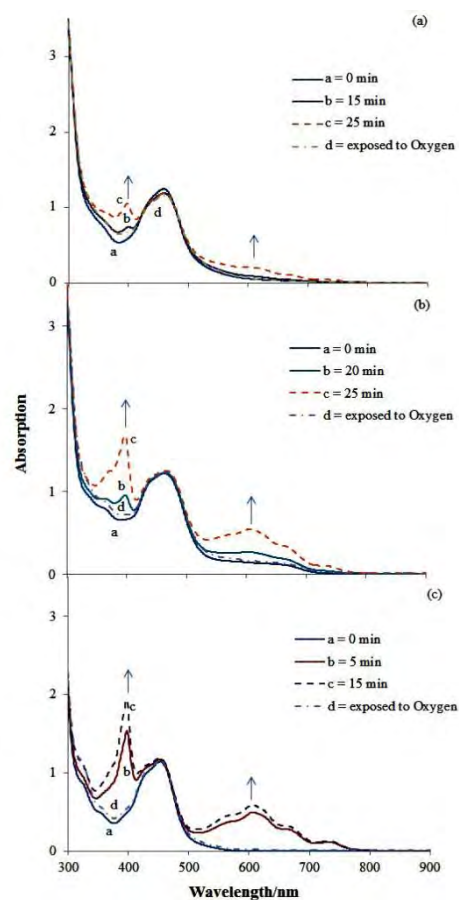
Figure1. Absorption spectra of photochemical reaction of a)**1**,b) **2**, and c)**RuMVRu** (0.08 mM) in the presence of TEOA in acetonitrile.
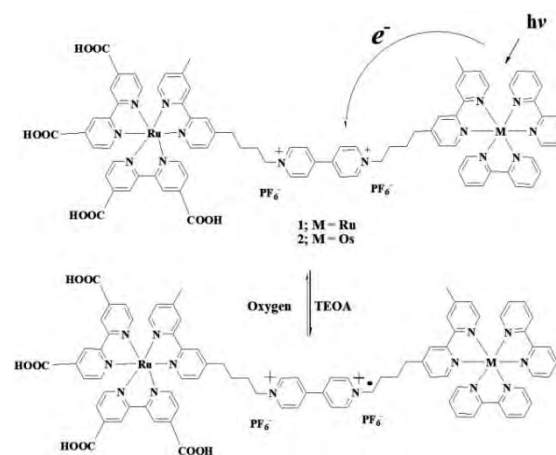
Scheme2. The viologen radicalof complexes**1** and **2** were formed after photoinduced electron transfer.

The mechanism for the photoinducedelectron transfer processes is shown in Scheme2. Under the irradiation of light, the ruthenium complex **1**was excited to the excited state *Ru(II)(bpy)$_3$-V^{2+}-Ru(II)(dcbpy)$_2$(bpy), which can transfer an electron of

Ru(II) intramolecular to the V^{2+} moiety, generating Ru(III) and the $V^{+\bullet}$, Ru(III)(bpy)$_3$-V$^{+\bullet}$-Ru(II)(dcbpy)$_2$(bpy). Nevertheless, the back electron transfer from $V^{+\bullet}$ to the Ru(III) is very fast.[5] with the addition of TEOA, Ru(III) can be reduced to Ru(II) by oxidation of TEOA, and therefore the back electron transfer from $V^{+\bullet}$ to Ru(III) is inhibited; thus a stable $V^{+\bullet}$ radical is formed. In the case of heteronuclear complex **2**, the photo-induce electron transfer mechanism might be proposed similar to the homonuclear **1**. However, heteronuclear complex **2** shows the greater stability viologen radical probably due to a lower oxidation potential of a third-row metal ion relative to that of metal in the second-row.[10-12]

4. Conclusions

The Ru(bpy)$_3$-viologen-Ru(dcbpy)$_2$(bpy) (**1**)and the Os(bpy)$_3$-viologen-Ru(dcbpy)$_2$(bpy) (**2**)have beensuccessfully synthesized and isolated from nonaqueous solution. Their chemical structures werecharacterized by ^{1}H-NMR, MSand Infrared spectroscopy. Theabsorption peaks of the viologen radical of complexes**1** and **2** were observed at398 and 605 nm, respectively.The results indicated that the viologen radical of complex **1**was easily formed than that of complex **2** butthe $V^{+\bullet}$ of complex **2**was more stable than that of complex **1**. The absorption spectra and the solution color can be convertedto the initial in the presence of oxygen, indicating that the whole process is repeatable.

Acknowledgements

References

[1]T.K. Monhaphol, S. Andersson and L. Sun, *Chem. Eur. J.***17** (2011) 11604 – 11612.

[2] a) L.A. Kelly and M.A.J. Rodgers, *J. Phys. Chem.* **99** (1995) 13132 – 13140; b) R. Lomoth, T. Häupl, J. Olof and L. Hammarström, *Chem. Eur. J.***8** (2002) 102 – 110; c) N. Terasaki, T. Akiyama, S. Yamada, *Langmuir***18**(2002) 8666 –8671.

[3] J.J. Kim, H.B. Choi, S.H. Paek, C.W. Kim, K.I. Lim, M.J. Ju, H.S Kang, M.S. Kang and J.J. Co, *Inorg. Chem.***50** (2011) 11340–11347.

[4]E.M. Kober, J.V. Caspar, B.P. Sullivan and T.J. Meyer, *Inorg. Chem.* **27**(1988) 4587-4598.

[5]D. Zou, S. Andersson, R. Zhang, S. Sun, B.R. Åkermark and L. Sun, *J. Org. Chem.***73** (10) (2008) 3775-3783.

[6] V.Shklover, M.K. Nazeeruddin, S.M. Zakeeruddin, C. Barbe´, A. Kay, T. Haibach, W. Steurer, R. Hermann, H.U. Nissen and M. Gra¨tzel, *Chem. Mater.* **9** (1997) 430-439.

[7] W.J. Youngblood, S.H.A. Lee, Y. Kobayashi, E.A. Hernandez-Pagan, P.G. Hoertz, T.A. Moore, A.L. Moore, D. Gust and T.E. Mallouk, *J. Am. Chem. Soc.* **131** (2009) 926–927.

[8] a) E.H. Yonemoto, G.B. Saupe, R.H. Schmehl, S.M. Hubig, R.L. Riley, B.L. Iverson and T.E. Mallouk, *J. Am. Chem. Soc.***116**(1994) 4786 – 8795; b) E.H.Yonemoto, R.L. Riley, Y. II Kim, S. J. Atherton, R. H. Schmehl and T E. Mallouk, *J. Am. Chem. Soc.***114** (1992) 8081 – 8087; c) E. H. Yonemoto, R.L. Riley, Y.II Kim, S.J. Atherton, R.H. Schmehl and T.E. Mallouk, *J. Am. Chem. Soc.***115**(1993), 5348; d) E. H. Yonemoto, Y.II Kim, R.H. Schmehl, J.O. Wallin, B.A. Shoulders, B.R. Richardson, J.F. Haw and T.E. Mallouk, *J. Am. Chem. Soc.***116** (1994) 10557 –10563.

[9] a)P. Zanello, *Inorganic Electrochemistry: Theory, Practive and Application, Royal Society of Chemistry*, (2003), pp. 100 –110; b) W.R.Brownea, R. Hageb and J.G. Vos,*Coord. Chem. Rev.***250**(2006) 1653 –1668.

[10] S. Baitalik, U. Flörke and K. Nag, *Inorg. Chim. Acta.***337**(2002) 439- 449.

[11] P.J. West, T. Schwich, M.P. Cifuentes and M.G. Humphrey,*J. Organomet.Chem.***696** (2011) 2886-2893.

[12] J.L. Chen, Y. Chi and K. Chen, *Inorg. Chem.***49** (2010) 823–832.

TOWARD THE SYNTHESIS OF (±)-CLADONIAMIDE G

Sarochar Soonkit, Paiboon Ngernmeesri[*], Boonsong Kongkathip

Department of Chemistry and Center of Excellence for Innovation in Chemistry, Faculty of Science,
Kasetsart University, Bangkok 10900, Thailand

[*] Author for correspondence; E-Mail: fscipbn@ku.ac.th, Tel. +66 2 5625555 ext 2202, Fax. 66 2 5793955

Abstract: Dioxo-bisindole is the key intermediate for the synthesis of the analogs of (±)-cladoniamide G. The key features of the synthetic strategy include Dieckmann condensation followed by decarboxylation to form one of the indole fragments, Suzuki-coupling reaction to join the two indole fragments together, and nucleophilic addition of the resulting bisindole with oxalyl chloride. This key intermediate was synthesized in 11 steps with 15% overall yield from commercially available methyl 2-aminobenzoate.

1. Introduction

Cladoniamide G is a member of the cladoniamide family of secondary metabolites which were isolated from cultures of *Streptomyces uncialis*, located on the surface of the lichen *Cladonia uncialis* collected near Pitt River, British Columbia [1]. The alkaloid skeletons of the cladoniamides are novel although they appear to be structurally similar to staurosporine and rebeccamycin, which are potent inhibitors of protein kinases and DNA topoisomerase-1, respectively. Because of these biological activities, both compounds have become high-profile lead compounds for the development of anticancer drugs. Both staurosporine and rebeccamycin use C(2) and C(3) of each indole unit to form a six-membered ring to link the two indole units whereas cladoniamides use C(2) and C(3) of one indole unit and N(1) and C(2) of the other to form a linker. The absolute stereochemistry of cladoniamide G was deduced from an X-ray diffraction analysis of cladoniamide A since these compounds appear to be biosynthetically related. In addition, cladoniamide G has been found to possess cytotoxicity against human breast cancer MCF-7 cells *in vitro* at 10 µg/mL (23 µM).
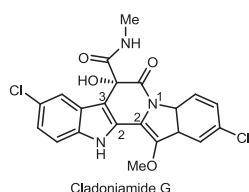
Cladoniamide G

Despite its novel structural features and significant biological activities, the synthesis of the analogs of (±)-cladoniamide G, or even other members in the family, has not been reported. Herein, we report the synthesis of the key intermediate for the synthesis of an analog of cladoniamide G, dioxo-bisindole, from commercially available methyl 2-aminobenzoate and methyl bromoacetate.

2. Results and Discussion

2.1. Retrosynthetic analysis of an analog of (±)-cladoniamide G.

Based on our retrosynthetic analysis below (**Figure 1**), cladoniamide G and its analog **1**, which lacks Cl at C5 of both indole units, would be synthesized in a similar manner. Therefore, we would attempt to synthesize the analog first since its starting materials are much cheaper.

It is envisioned that the tethered amide of **1** could be formed from a nucleophilic addition to the carbonyl ketone of dioxo-bisindole **2** followed by functional group transformations of the attacking nucleophile. Dioxo-bisindole **2** could be constructed via double nucleophilic addition of bisindole **3** and oxalyl-chloride. The two indole units of **3** could be joined by a Suzuki cross-coupling reaction of bromoindole **4** and indolyl boronic acid **5**. Bromoindole **4** could be derived from commercially available methyl 2-amino benzoate (**6**) and methyl bromoacetate (**7**). In addition, boronic acid **5** could be derived from indole (**8**).
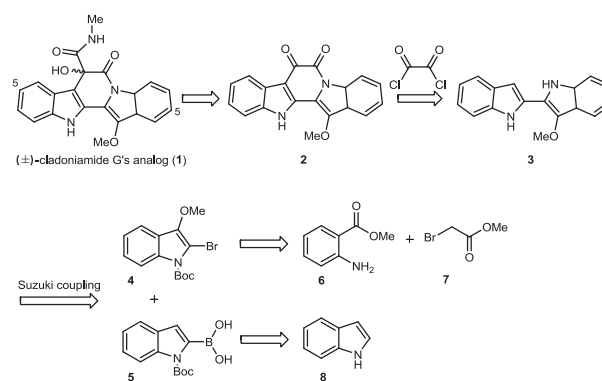

Figure 1. Retrosynthetic analysis of an analog of (±)-cladoniamide G.

2.2. Synthesis of the 2-bromo-3-methoxy indole **4**.

Synthesis of **4** commenced with a nucleophillic substitution of the bromide of methyl bromoacetate (**7**) with methyl 2-aminobenzoate (**6**) following the

method described by Dropinski [2] to give α-amino ester **9** in 83% yield (**Figure 2**). Treatment of **9** with NaOMe in MeOH at reflux generated 3-hydroxy indole **10** in 79% yield. Initial attempts (following the known method) to treat **9** with NaOEt in EtOH [3] resulted in a mixture of ethyl 3-hydroxyindole-2-carboxylate and the corresponding methyl ester **10** since transesterification did not go to completion even after heating for several hours. Fortunately, this problem could be solved easily by using NaOMe as a base in MeOH, and only methyl ester **10** was obtained in 79% yield. Subsequent treatment of **10** with excess dimethyl sulfate [4] gave methoxyindole **11** in 91% yield, and no *N*-methylation was observed. The ester group of **11** was then hydrolyzed by aq. NaOH in MeOH at reflux, and the resulting carboxylic acid was decarboxylated by Cu powder in quinoline at 200 $^{\circ}$C [5] to generate the desired 3-methoxyindole (**12**) in 88% yield.
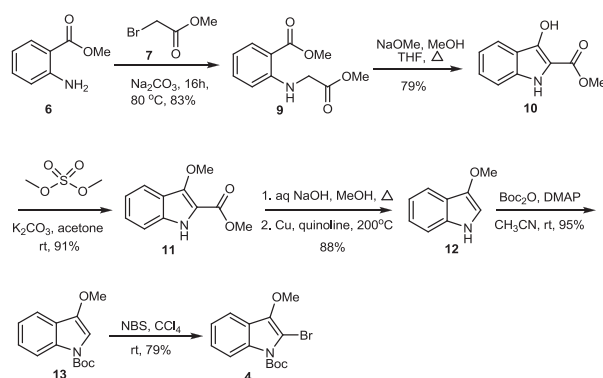

Figure 2. Synthesis of the 2-bromo-3-methoxy indole **4**

Subsequent bromination of 3-methoxy indole **12** with NBS in CCl$_4$ at room temperature [5] resulted in the recovery of most of the starting material after 1 h or complete decomposition after 3 h. When the reaction was carried out at 0 $^{\circ}$C for 1 h, most of the starting material still remained and no desired product was observed. Surprisingly, when the NH group of 3-methoxy indole was protected as the corresponding *t*-butyl carbamate, bromination of this compound went to completion in less than an hour at room temperature to give bromoindole **4**. Although TLC analysis showed that **4** was formed almost exclusively, this compound is not very stable. Purification by chromatography on SiO$_2$ became problematic as some (or all in some run) of the desired product decomposed and no more than 60% yield of this compound could be isolated. Fortunately, the yield was improved to 79% when basic Al$_2$O$_3$ was used instead of SiO$_2$.

2.3. Synthesis of an analog of (±)-cladoniamide G **1**.

We next investigated an approach to the dioxo-bisindole **2**, the key synthon for preparing an analog of (±)-cladoniamide G. Suzuki coupling [6] of bromo indole **4** and indolyl boronic acid [7] **5** generated bisindole **14** in 73% yield. To reveal the NH groups

and increase the nucleophilicity to C3 of one of the indoles, the Boc protecting groups were removed with TFA to afford unprotected bisindole **3** in 90 % yield. Nucleophilic addition of the non-substituted C3 of one indole unit and the NH of the other with oxalyl chloride furnished the desired framework **2** with all the rings in place to complete the synthesis of an analog of cladoniamide G. Finally, if protecting the NH group of **2** is necessary, it could be protected as *t*-butyl carbamate to furnish *N*-Boc dioxo-bisindole **15** in 71% yield.
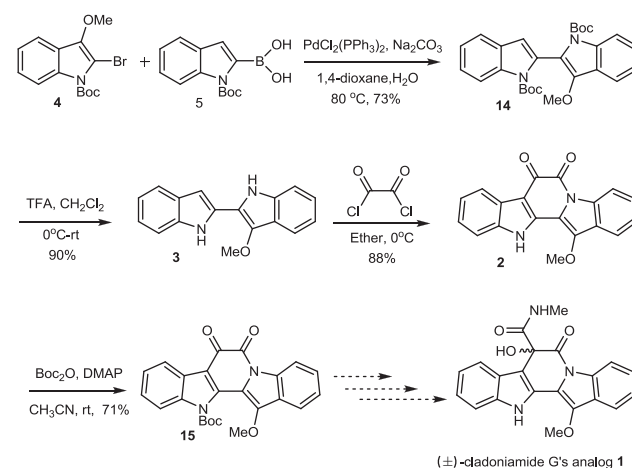
Figure 3. Synthesis of an analog of (±)-cladoniamide-G **1**.

3. Experimental Section

3.1. General

All reactions were carried out in dried glassware under a nitrogen atmosphere employing standard techniques in handling air sensitive materials with stirring by a magnetic stir bar. Tetrahydrofuran (THF) and diethyl ether were dried by distillation from sodium with benzophenone ketyl as an indicator under a nitrogen atmosphere. Dichloromethane and aceto-nitrile were dried by distillation from calcium hydride under a nitrogen atmosphere. Methanol was dried by distillation from magnesium under a nitrogen atmosphere. Acetone (AR grade), 1,4 dioxane (AR grade) and carbon tetrachloride (AR grade) were dried over molecular sieves of 3Å or 4Å. All other commercially obtained reagents were used as received. Flash chromatography was performed on 32-63 μm silica gel or basic alumina (particle size 0.05-0.15 mm, pH 9.5 ± 0.5). ^{1}H and ^{13}C-NMR spectra were recorded on a VARIAN^{UNITY} INOVA 400 spectrometer. Chemical shifts of ^{1}H NMR spectra are reported in ppm relative to CDCl$_3$ (δ 7.26) or DMSO (δ 2.49). Data are presented as follows: multiplicity (s = singlet, d = doublet, t = triplet, q = quartet, m = mutiplet, br = broad, dd = doublet of doublet), coupling constant (J/Hz) and integration. ^{13}C NMR spectra are reported in ppm relative to CDCl$_3$ (δ 77.0) or DMSO-d$_6$ (δ 39.5). Infared spectra were recorded on Perkin-Elmer 2000 Fourier transform infared spectrometer. Absorp-

tions are given in wavenumbers (cm^{-1}). Mass spectra were obtained on an Agilent Technology 1100 series LL/MSD Trap; the first number denoted m/z value and the ion assignment and abundance are given in parentheses and on a GCMS-QP-5050QA spectrometer in electrospray ionization mode (ESI$^+$). Accurate masses (HRMS) were recorded on JEOL JMS-700 Mstation and JEOL JMS-T100LP with FAB and ESI high.

3.1.1. Methyl 3-Hydroxy-1*H*-indole-2-carboxylate (10)

Anhydrous methanol (15 mL) was added to a flask containing sodium (2.95 g, 128 mmol) at 0°C and the suspension was stirred until sodium completely dissolved. This solution was then cannulated to a solution of α-amino ester **9** (14.28 g, 64 mmol) in THF (45 mL). The resulting solution was heated at reflux for 2 h. The reaction mixture was allowed to cool to room temperature and water (30 mL) was added. The mixture was extracted with ether (2 x 30 mL). Dry ice was added to the aqueous phase until a precipitate formed (pH~8). The precipitate was collected by filtration through a fritted funnel and washed several times with water. This off-white solid was dissolved in EtOAc (200 mL), dried over Na$_2$SO$_4$ and concentrated to dryness under reduced pressure to give the desired product as a pale purple/brown solid (9.71 g, 79% yield). IR (KBr) 3429, 3314, 1696 cm^{-1}; ^{1}H NMR (400 MHz, CDCl$_3$) δ 7.85 (br s 2H), 7.75 (dd, J = 0.4, 8.1 Hz, 1H), 7.35 (ddd, J = 1.2, 6.9, 8.4 Hz, 1H), 7.26 (d, J = 8.4 Hz, 1H), 7.10 (ddd, J = 1.0, 6.9, 8.1 Hz, 1H), 3.96 (s, 3H); ^{13}C NMR (100 MHz, CDCl$_3$) δ 163.6 135.3, 127.3, 120.15, 120.12, 119.7, 117.7, 111.9, 107.9, 51.6; HRMS (ESI) [M+H]$^+$ calcd for C$_{10}$H$_{10}$NO$_3$ 192.0661, found 192.0659.

3.1.2. Methyl 3-Methoxy-1*H*-indole-2-carboxylate (11)

To a mixture of hydroxyindole **10** (2.26 g, 11.8 mmol) and K$_2$CO$_3$ (1.80 g, 1.26 mmol) was added acetone (60 mL) followed by dimethyl sulfate (3.4 mL, 35.7 mmol). The reaction mixture was stirred at room temperature for 18 h, and then concentrated to dryness under reduced pressure. The crude residue was dissolved in EtOAc (50 mL) and poured into water (50 mL). The organic layer was separate and aqueous layer was extracted with EtOAc (2 x 30 mL) The organic extracts were combined, dried over Na$_2$SO$_4$ and concentrated to dryness under reduced pressure. The crude product was purified by flash chromatography on SiO$_2$ (1:4 and 1:2 ether/hexanes) to give the desired product as a white solid (2.20 g, 91% yield). IR (KBr) 3292, 1675 cm^{-1}; ^{1}H NMR (400 MHz, CDCl$_3$) δ 9.00 (br s 1H), 7.75 (dd, J = 0.8, 8.2 Hz, 1H), 7.32-7.25 (m, 2H), 7.07 (ddd, J = 1.3, 6.6, 8.1 Hz, 1H), 4.12 (s, 3H), 3.94 (s, 3H); ^{13}C NMR (100 MHz, CDCl$_3$) 161.8, 145.1, 134.3, 126.2, 120.5, 120.3, 120.0, 114.2, 112.1, 62.3, 51.9; LRMS(ESI) m/z (relative intensity) 228.1 (100%, M+Na$^+$); HRMS (ESI) [M+H]$^+$ calcd for C$_{11}$H$_{12}$NO$_3$ 206.0817, found 206.0817.

3.1.3. 3-Methoxyindole (12)

To a solution of methoxy-indole **11** (700 mg, 3.41 mmol) in MeOH was added 1 M aq. NaOH solution (6.8 mL, 6.8 mmol). The reaction mixture was heated at reflux for 1 h. It was then allowed to cool to room temperature, dilute with EtOAc (20 mL) and poured in to ice cold 1M HCl (10 mL). The organic layer was separated and the aqueous layer was extracted with EtOAc (20 mL). The organic extracts were combined, dried over Na$_2$SO$_4$ and concentrated to dryness under reduced pressure to give a white solid. To this solid was added Cu powder (28 mg, 0.44 mmol) followed by distilled quinoline (1.7 mL). The reaction mixture was heated to 200 ^{o}C for 1 h. It was then allowed to cool to room temperature, dilute with EtOAc (50 mL) and poured in to ice-cooled 1 M HCl (50 mL) The organic extracts were combined, dried over Na$_2$SO$_4$ and concentrated to dryness under reduced pressure. The crude residue was purified by flash chromatography on SiO$_2$ (1:4, 1:3 and 1:2 ether/ hexanes) to give the desired product as a brown liquid (440 mg, 88% yield over 2 steps). IR (neat) 3414 cm^{-1}; ^{1}H NMR (400 MHz, CDCl$_3$) δ 7.65 (dd, J = 0.8, 7.9, Hz, 1H), 7.33 (br s, 1H), 7.61 (s, 1H), 7.17-7.10 (m, 2H), 7.05 (ddd, J = 1.7, 6.4, 8.0 Hz, 1H), 7.39 (s, 3H); ^{13}C NMR (100 MHz, CDCl$_3$) δ 141.7, 134.2, 122.6, 119.3, 118.7, 117.7, 111.2, 104.2, 58.0; LRMS(ESI) m/z (relative intensity) 148.1 (88%, M+H$^+$).

3.1.4. *N*-Boc-3-Methoxyindole (13)

To a solution of 3-methoxyindole (6) (299 mg, 2.03 mmol) in CH$_3$CN (10 mL) was added DMAP (25 mg, 0.20 mmol) followed by Boc$_2$O (532 mg, 2.44 mmol). The reaction mixture was stirred at room temperature for 1 h. It was concentrated to dryness and the crude residue was purified by flash chromate graphy on SiO$_2$ (1-3% ether in hexanes) to give the desired product as a clear and coloress oil (475 mg, 95% yield). IR (neat) 1723 cm^{-1}; ^{1}H NMR (400 MHz, CDCl$_3$) δ 8.09 (br s, 1H), 7.57 (d, J = 7.8 Hz, 1H), 7.30 (t, J = 7.6 Hz, 1H), 7.19 (t, J = 7.5 Hz, 1H), 6.95 (br s, 1H), 3.85 (s, 3H), 1.64 (s, 9H); ^{13}C NMR (100 MHz, CDCl$_3$) δ 149.9, 144.6, 133.7, 125.1, 123.7, 122.1, 117.9, 115.1, 103.1, 83.0, 54.7, 28.1; LRMS(ESI) m/z (relative intensity) 270.1 (100%, M+Na$^+$)

3.1.5. *N*-Boc-2-Bromo-3-Methoxyindole (4)

To a solution of *N*-Boc-3-methoxyindole **13** (2.40 g, 9.70 mmol) in CCl$_4$ (25 mL) was added NBS (2.20 g, 12.13 mmol). The resulting suspension was stirred at room temperature under N$_2$ for 15 min. The reaction mixture was filtered through a pad of celite and washed with CCl$_4$ (5 mL) The filtrate was concentrated to ~2 mL under reduced pressure. This solution was purified by flash chromatography on basic Al$_2$O$_3$ (5% ether in hexanes) to give the desired product as a clear and colorless oil (2.5 g, 79% yield). IR (neat) 1734 cm^{-1}; ^{1}H NMR (400 MHz, CDCl$_3$) δ 8.13 (d, J = 8.3 Hz, 1H), 7.56 (d, J = 7.7 Hz, 1H), 7.29 (t, J = 7.7 Hz, 1H), 7.22 (t, J = 7.5 Hz, 1H), 4.00 (s, 3H), 1.69 (s,

9H); ^{13}C NMR (100 MHz, CDCl$_3$): δ 149.3, 143.2, 135.0, 124.9, 123.1, 122.8, 117.0, 115.6, 99.1, 84.9, 61.2, 28.2; LRMS(ESI) *m/z* (relative intensity) 348.5 (91%, M+Na$^+$).

3.1.6. 3-Methoxy-*N,N′*-diBoc-2,2'-biindole (14)

A Schlenk flask containing indolyl boronic acid **5** (2.88 g, 11.03 mmol), PdCl$_2$(PPh$_3$)$_2$ (519 mg, 0.74 mmol) and Na$_2$CO$_3$ (1.56 g, 14.70 mmol) was evaculated under high vacuum and then filled with N$_2$ A solution of bromoindole **4** (2.40 g, 7.35 mmol) in 1,4 dioxane (54 mL) was added to the Schlenk flask followed by deoxygenated water (11 mL) The reaction mixture was heated at reflux for 1 h. It was then allowed to cool to room temperature and poured into ice water (100 mL) The mixture was extracted with ether (3x100 mL). The organic extract was dried over Na$_2$SO$_4$ and concentrated to dryness under reduced pressure. The crude residue was purified by flash chromatography on SiO$_2$ (1-5% ether in hexanes) to give the desired product as a colorless oil (2.46 g, 73% yield). IR (KBr) 1727 cm^{-1}; ^{1}H NMR (400 MHz, CDCl$_3$) δ 8.25-8.21 (m, 2H), 7.51 (d, *J* = 7.7 Hz, 1H), 7.47 (d, *J* = 7.6 Hz, 1H), 7.27-7.22 (m, 2H), 7.16-7.12 (m, 2H), 6.58 (s, 1H), 3.64 (s, 3H), 1.12 (s, 9H), 1.08 (s, 9H); ^{13}C NMR (100 MHz, CDCl$_3$) δ 150.1, 149.9, 142.8, 137.1, 134.4, 128.9, 128.8, 125.6, 124.8, 123.4, 122.8, 122.5, 120.7, 117.7, 115.8, 115.7, 112.5, 83.1, 83.0, 61.1, 27.72, 27.69; LRMS(ESI) *m/z* (relative intensity) 485.2 (100%, M+Na$^+$); HRMS (ESI) [M+Na]$^+$ calcd for C$_{27}$H$_{30}$NaN$_2$O$_5$ 485.2052, found 485.2054.

3.1.7. Dioxo Bisindole (2)

To a solution of *N,N′*-unprotected bisindole **3** (78 mg, 0.30 mmol) in diethyl ether (5 mL) was added dropwise oxalyl chloride (50 μL, 0.58 mmol) at 0 $^{\circ}$C. A red/brown precipitate formed immediately. The reaction mixture was stirred in an ice bath for 1 h. Hexane (10 mL) and ether (10 mL) were added to the reaction mixture and the liquid phase was carefully removed. This process was repeated two more times to leave the desired product as a red solid (83 mg, 88% yield). IR (KBr) 3429, 1694, 1644, 1614, cm^{-1}; ^{1}H NMR (400 MHz, DMSO-d$_6$) δ 12.13 (s, 1H), 8.40 (d, *J* = 8.2 Hz, 1H), 8.00 (d, *J* = 8.0 Hz, 1H), 7.97 (d, *J* = 7.8 Hz, 1H), 7.59 (d, *J* = 8.0 Hz, 1H), 7.49 (dt, *J* = 1.0, 7.8 Hz, 1H), 7.33 (dt, *J* = 0.9, 7.7 Hz, 1H), 7.31 (dt, *J* = 1.4, 7.6 Hz, 1H), 7.24 (dt, *J* = 1.1, 7.5 Hz, 1H) 4.38 (s, 3H); ^{13}C NMR (100 MHz, DMSO-d$_6$) δ 170.4, 155.9, 144.8, 138.8, 137.3, 137.0, 128.9, 125.0, 124.9, 123.9, 123.1, 122.8, 121.8, 120.6, 116.2, 113.0, 112.3, 110.9, 60.9; LRMS(ESI) *m/z* (relative intensity) 339.2 (100%, M+Na$^+$); HRMS (ESI) [M+H]$^+$ calcd for C$_{19}$H$_{13}$N$_2$O$_3$ 317.0926, found 317.0924.

3.1.8. *N*-Boc Dioxo Bisindole (15)

To a suspension of dioxo-bisindole **2** (500 mg, 1.10 mmol) in CH$_3$CN (100 mL) was added DMAP (13.44 mg, 0.11 mmol) followed by Boc$_2$O (1.43 g, 6.57 mmol). The reaction mixture was stirred at room temperature for 48 h. The resulting red/brown solution was concentrated to dryness and the crude residue was purified by flash chromatography on SiO$_2$ (1:1 EtOAc/hexanes) to give the desired product as a orange solid (475 mg, 71% yield). IR (KBr) 1763, 1716, 1655 cm^{-1}; ^{1}H NMR (400 MHz, CDCl$_3$) δ 8.61 (dt, *J* = 0.7, 8.3 Hz, 1H), 8.31 (ddd, *J* = 0.6, 2.6, 6.5 Hz, 1H), 7.88 (ddd, *J* = 0.6, 2.4, 7.0 Hz, 1H) 8.61 (dq, *J* = 0.6, 8.0 Hz, 1H) 7.47 (ddd, *J* = 1.1, 2.4, 7.9 Hz, 1H) 7.40 (m, 2H), 7.15 (ddd, *J* = 1.0, 7.6, 8.8 Hz, 1H), 4.29 (s, 3H), 1.70 (s, 9H); ^{13}C NMR (100 MHz, CDCl$_3$) δ 172.3, 155.3, 148.9, 147.0, 138.0, 138.3, 129.7, 126.7, 125.2, 124.7, 123.3, 122.3, 122.2, 121.5, 117.6, 116.0, 113.7, 113.3, 109.7, 86.2, 60.8, 28.0; LRMS(ESI) *m/z* (relative intensity) 417.0 (100%, M+H$^+$); HRMS (ESI) [M+Na]$^+$ calcd for C$_{24}$H$_{20}$Na N$_2$O$_5$ 439.1270, found 439.1269.

4. Conclusions

In conclusion, the synthesis of dioxo bisindole **15**, a precursor for the synthesis of an analog of (±)-cladoniamide G, was accomplished in 11 steps with 15% overall yield from commercially available methyl 2-aminobenzoate and methyl bromoacetate. Efforts to complete the synthesis of cladoniamide G's analog, along with cladoniamide G, are underway.

References

[1] D. E. Williams, D. Julian, O. P. Brian, B. Helen, T. Tamsin, R. Michel and J. D. Raymond, *Org. Lett.* **10** (2008) 3501-3504.

[2] J. F. Dropinski, T Akiyama, M. Einstein, B. Habulihaz, T. Doebber, J. P. Berger, P. T. Minke and G. Q. Shi, *Bioorg. Med. Chem. Lett.* **15** (2005) 5035-5038.

[3] M. BÖs, F. Jenck, J. R. Martin, J. L. Moreau, V. Mutel, A. J. Sleight, U. Widmer, *Eur. J. Med. Chem.* **32** (1997) 253-261.

[4] P. C. Unangst, T. C. David, S. R. Stabler, J. W. Robert, E. C. Mary, A. K. John, O. T. David,C. C. James, L. A. Richard and M. C. Conroy, *J. Med. Chem.* **32** (1989) 1360-1366.

[5] R Liu, Z. Puwen, G. Tong and M. C. Jame, *J. Org. Chem.* **62** (1997) 7447-7456.

[6] F. Narjes, B. Crescenzi, M. Ferrara, C Ercolani, I. Conte, J Habermann, S. Colarusso, M. R. Ferreira, I Stansfield, A. C. Mackay and S, Zaramella, *J. Med. Chem.* **54** (2011) 289-301.

[7] A. Yamabuki, F. Hikohito, C. Tominari, T. Shigeo, M. Kohji, O. Kana, N. Junko and H. Satoshi, *Tetrahedron Lett.* **47** (2006) 5859-5861.

ANTIBACTERIAL CONSTITUENTS FROM *RHODOMYRTUS TOMENTOSA* LEAVES

Channarong Suaisom[1], Sukanlaya Leejae[2], Saowanee Kumpun[3], Supayang P. Voravuthikunchai[2], and Boon-ek Yingyongnarongkul[1,*]

[1]Department of Chemistry and Center of Excellence for Innovation in Chemistry, Faculty of Science, Ramkhamhaeng University, Bangkok, 10240 Thailand

[2]Department of Microbiology and Natural Products Research Center, Faculty of Science, Prince of Songkla University, Songkhla 90112, Thailand

[3]Department of Chemistry, Faculty of Science and Technology, Suan Sunandha Rajabhat University, Bangkok 10300, Thailand

*E-mail: boonek@ru.ac.th, +66-2-3191900

Abstract: Chemical investigation of an acetone extract of *Rhodomyrtus tomentosa* leaves has resulted in the isolation of rhodomyrtone (1), 5,4′-dihydroxy-3,7,3′,5′-tetramethoxyflavone (2), rhodomyrtonedimer (3), phlorisovalerophenone (4), 3-*O*-cis-*p*-coumaroyl maslinic acid (5), 3-*O*-trans-*p*-coumaroyl maslinic acid (6), 3-*O*-methylellagic acid 3′-*O*-α-rhamnopyranoside (7) and megastigman-7-ene-3,5,6,9-tetraol-9-*O*-β-D-glucopyranoside (8). The structures of these constituents were elucidated by spectroscopic techniques including 1D and 2D NMR and mass spectrometry. Rhodomytronedimer (3) was identified to be a new compound whereas 2, 5, 6, 7 and 8 were isolated from this plant for the first time. Rhodomyrtone (1) exhibited strongest antibacterial activity against *Staphylococcus aureus* with MIC and MBC values of 0.5 µg/ml.

1. Introduction

Rhodomyrtus tomentosa (Aiton) Hassk. is an evergreen shrub belonging to the family Myrtaceae and widely distributed throughout Southeast Asia and often used in traditional Thai medicine. Several biological activities have been reported for extracts of this plant, and some have exhibited antibacterial and antihepatitis properties [1-3]. Previous work on the antibacterial activities showed that an ethanolic extract demonstrated good activity against several types of Gram-positive bacteria [4]. In addition, it is used in formulation of skin-whitening anti-aging and skin-beautifying agents [2]. Acylphloroglucinol, flavonoids, tannins and triterpenes [5-7] have been identified from this plant. We are therefore interested in characterizing their chemical constituents. As a part of this project, we have examined the chemical constituents of acetone extract of the leaves of *R. tomentosa*.

2. Materials and Methods

2.1 Plant material

The aerial parts of *R. tomentosa* were collected from Trad province, Thailand, in October 2009.

2.2 General experimental procedures

The IR spectra were obtained using a Perkin-Elmer FT-IR spectrum 400 spectrometer (ATR). The ^{1}H and ^{13}C NMR spectra were recorded with a Bruker AVANCE 400 MHz spectrometer. Eletrospray mass spectra (ESMS) were determined on Finnigan LC-Q mass spectometer. Column chromatography (CC) and TLC were carried out using Merck silica gel 60 (>230 mesh) and precoated silica gel 60 F_{254} plates, respectively. Plates of silica gel PF_{254}, thickness 1.25 mm, were utilized for preparative TLC. Spots on TLC were visualized under UV light and by spraying with anisaldehyde-H_2SO_4 reagent followed by heating.

2.3 Antimicrobial agents and chemicals

The following commercially available compounds were purchased from indicated manufacturers: Mueller-Hinton agar (MHA) and Mueller-Hinton broth (MHB) from Difco; Tryptic soy broth (TSB) from Bacto; dimethylsulphoxide (DMSO) and glycerol from Sigma-Aldrich and NaCl from Fisher Scientific. All standard chemicals were of analytical grade.

2.4 Tested bacterial strains and growth conditions

Staphylococcus aureus ATCC 29213 and *Escherichia coli* ATCC 25922 were used in this study. The microorganisms were maintained in TSB containing 20% glycerol at -80°C until required. The organisms were precultured on MHA at 37°C for 18 h. An inoculum of 100 µl of the culture was inoculated into 3 ml of MHB and incubated at 37°C until mid-exponential growth phase was obtained.

2.5 Extraction and isolation

The air-dried ground leaves (2.3 kg) of *R. tomentosa* were successively extracted at room temperature with acetone (3 × 6 l, each 3 days) and evaporation of the solvent gave acetone extract

(235.40 g). The acetone extract was isolated by CC on silica gel and eluted with a hexane-EtOAc to EtOAc-MeOH gradient system. The eluted fractions were combined into fractions A−K on the basis of their TLC characteristics. Fraction C (12.83 g) was subjected to CC on silica gel eluting with EtOAc−hexane gradient system to give six fractions (C1-C6). Fraction C3 (5.63 g) was then purified by CC on silica gel using EtOAc−hexane (10:90) as an eluent to give compound **1** (3.24 g). Fraction D (9.65 g) was subjected to CC on silica gel and eluted with gradient system of EtOAc−hexane (10:90 to 100:0) to give fractions D1−D6. Fraction D3 (312 mg) was rechromatographed on silica gel column to give compound **4** (115 mg) using EtOAc−hexane (10:90) as a mobile phase. Fraction E (23.04 g) was conducted gradiently with CH_2Cl_2 –MeOH 100:0 to 80:20 by CC on silica gel to afford nine fractions (E1-E9). Fraction E3 (3.56 g) was rechromatographed on silica gel to afford compounds **2** (8.9 mg) and **3** (6.2 mg). Compounds **5** (30.4 mg) and **6** (85.5 mg) was purified through a CC from fraction F (15.73g) using EtOAc−hexane (10:90) as a mobile phase. Fraction H (25.45g) was subjected to CC on silica gel eluting with CH_2Cl_2 –MeOH gradient solvents system to give eleven fractions (H1-H11). Repeated column chromatography of fraction H6 (23.21 g) eluted with gradient system of CH_2Cl_2 – MeOH (10:90 to 30:70) to give compounds **7** (265 mg) and **8** (28.5 mg). All compounds were identified by comparison of their spectroscopic data (NMR) with those reported in the literature. ^{1}H- and ^{13}C-NMR data of compound **3**, which have not previously been published, are also reported in this paper.

5,4′-Dihydroxy-3,7,3′,5′-tetramethoxyflavone (**2**) [11]. Orange stickiness oil; R_f = 0.60 (80:20, Hexane-Ethyl acetate), positive-ion ES-MS *m/z* (rel. int.%): 375.2 [M+H]$^+$ (100) corresponded to the molecular formula $C_{19}H_{18}O_8$.

Phlorisovalerophenone (**4**) [9]. Orange sticky oil; R_f = 0.48 (90:10, Hexane-Ethyl acetate), negative-ion ES-MS *m/z* (rel. int.%): 209.3 [M-H]$^-$ (100) corresponded to the molecular formula $C_{11}H_{14}O_4$.

3-*O*-cis-*p*-Coumaroyl maslinic acid (**5**) [13]. White needles; R_f = 0.56 (94:6, Dichlorometane-Methanol), positive-ion ES-MS *m/z* (rel. int.%): 619.4 [M+H]$^+$ (100) corresponded to the molecular formula $C_{39}H_{45}O_6$.

3-*O*-trans-*p*-Coumaroyl maslinic acid (**6**) [13]. White amorphous powder; R_f = 0.53 (94:6, Dichlorometane-Methanol), positive-ion ES-MS *m/z* (rel. int.%): 619.1 [M+H]$^+$ (100) corresponded to the molecular formula $C_{39}H_{45}O_6$.

3-*O*-Methylellagic acid 3′-*O*-α-rhamnopyranoside (**7**) [12]. Yellowish white amorphous powder; R_f = 0.41 (80:20, Dichlorometane-Methanol), negative-ion ES-MS *m/z* (rel. int.%): 461.5 [M+H]$^-$ (100) corresponded to the molecular formula $C_{21}H_{18}O_{12}$.

Megastigman-7-ene-3,5,6,9-tetraol-9-*O*-β-D-glucopyranoside (**8**) [10]. Yellowish white amorphous powder; R_f = 0.51 (90:10, Dichlorometane-Methanol)

Negative-ion ES-MS *m/z* (rel. int.%): 405.5 [M+H]$^-$ (100) corresponded to the molecular formula $C_{19}H_{34}O_9$.

Rhodomyrtone (**1**) [8]. Pale yellow solid; R_f = 0.65 (94:6, Hexane-EtOAc); m.p. 184-185 ^{o}C, negative-ion ES-MS *m/z* (rel. int.%): 441 [M+H]$^-$ solid(100) corresponded to the molecular formula $C_{26}H_{34}O_6$. ^{1}H NMR (400 MHz, CDCl$_3$): δ_H 13.41 (1H, s, 8-OH), 8.41 (1H, s, 6-OH), 6.18 (1H, s, H- 5), 4.28 (1H, t, *J* = 5.4 Hz, H-9), 2.98 (2H, dd, *J* = 6.7, 15.7 Hz, H-2′), 2.26 (1H, m, H-3′), 1.37, 1.40 (6H, s, 2-CH$_3$), 1.42, 1.54 (6H, s, 4-CH$_3$), 0.95 (6H, d, *J* = 6.6 Hz, H-4′,5′), 0.82 (6H, d, *J* = 5.7 Hz, H-3″, 4″), 1″ ,2″-H Overlapped with CH$_3$. ^{13}C NMR (100 MHz, CDCl3): δ_C 212.4 (C-3), 206.8 (C-1′), 198.6 (C-1), 167.7 (C-4a), 162.9 (C-8), 158.7 (C-6), 155.6 (C-10a), 114.3 (C-9a), 107.7 (C-7), 106.3 (C-8a), 94.7 (C-5), 56.0 (C-2), 53.2 (C-2′), 24.2 (C-2″), 47.2 (C-4), 45.8 (C-1″), 25.2 (C-9), 25.1 (C-3′), 24.5 (CH$_3$ at C-2), 24.7 (CH$_3$ at C-4), 22.8 and 23.2 (C-4′,C-5′), 22.7 and 23.5 (C-3″, C-4″)

Rhodomyrtonedimer (**3**). Yellow sticky oil; R_f = 0.54 (90:10, Hexane-EtOAc), negative-ion ES-MS *m/z* (rel. int.%): 952.7 [M+H]$^-$ (100) corresponded to the molecular formula $C_{57}H_{76}O_{12}$. ^{1}H NMR (400 MHz, CDCl$_3$): δ_H 14.13 (2H, s, 8-OH), 6.01 (2H, s, H-5), 4.26 (2H, t, *J* = 5.0 Hz, H-9), 4.07 (4H, m, H-1‴), 2.93 (4H, dd, *J* = 7.4, 11.4 Hz, H-2′), 2.24 (2H, m, H-3′), 1.99 (4H, m, H-2‴), 1.76 (2H, m, H-3‴), 1.34, 1.37 (12H, s, 2-CH$_3$), 1.41, 1.53 (12H, s, 4-CH$_3$), 0.94 (12H, d, *J* = 6.6 Hz, H-4′,5′), 0.81 (6H, d, *J* = 5.4 Hz, H-3″), 0.84 (6H, d, *J* = 5.7 Hz, H-4″), H-1″, 2″ Overlapped with CH$_3$. ^{13}C NMR (100 MHz, CDCl3): δ_C 212.1 (C-3), 206.0 (C-1′), 197.4 (C-1), 166.5 (C-4a), 163.9 (C-8), 160.1 (C-6), 156.0 (C-10a), 114.4 (C-9a), 108.4 (C-7), 107.4 (C-8a), 90.6 (C-5), 68.7 (C-1‴), 56.1 (C-2), 53.6 (C-2′), 47.1 (C-4), 45.8 (C-1″), 28.9 (C-2‴), 25.2 (C-9), 25.1 (C-3′), 23.3 (C-3‴), 24.6, 24.7 (CH$_3$ at C-2), 24.6, 24.8 (CH$_3$ at C-4), 22.7 and 23.8 (C-4′, C-5′), 23.2 and 23.4 (C-3″ , C-4″)

3. Results and Discussion

Phytochemical investigation of an acetone extract of *Rhodomyrtus tomentosa* leaves led to the isolation of one new compound named rhodomyrtonedimer (**3**) together with seven know compounds (**1**-**2**, **4**-**8**).

Rhodomyrtone (**1**) [8]. Pale yellow solid; R_f = 0.65 (94:6, hexane-EtOAc); m.p. 184-185 ^{o}C, Negative-ion ES-MS *m/z* (rel. int.%): 441 [M+H]$^-$ (100) corresponded to the molecular formula $C_{26}H_{34}O_6$. ^{1}H NMR spectrum showed the presence of three downfield signals; two for OH groups at δ_H 13.41, 8.14 (each 1H, s), and one aromatic proton at δ_H 6.18 (1H, s, H-5), in addition to one methine proton at δ_H 4.28 (1H, t, *J* = 5.4 Hz, H-9). Furthermore, the spectrum exhibited characteristic signals for an isovaleryl group at δ_H 3.02 (1H, dd, *J* = 6.7, 15.5 Hz, H-2′a), 2.95 (1H, dd, *J* = 6.7, 15.5 Hz, H-2′b), 2.26 (1H, m, H-3′), and 0.95 (6H, d, *J* = 6.6 Hz, two methyls at C-3′). On other hand, the ^{1}H NMR

spectrum revealed the presence of isobutyl group at δ_H 1.45 (2H, m, H-1″), and 0.82, 0.84 (each 3H, d, J = 5.7 Hz, two methyls at C-2″), and in addition to four singlet signals for four methyl groups at δ_H 1.37, 1.40, 1.42 and 1.54. ^{13}C and DEPT NMR spectra indicated the presence of eight methyls, two methylenes, four methines and twelve quaternary carbon atoms, three of the quaternary carbon atoms were assigned to three keto groups at δ_C 212.4 (C-3), 206.8 (C-1′) and 198.6 (C-1). The presence of isovaleryl and isobutyl groups was confirmed from ^{13}C signals at δ_C 206.8, 53.2, 25.1, 23.2 and 22.8 and at δ_C 45.8, 24.2, 23.5 and 22.7, respectively. COSY data showed correlations of the methylene at δ_H 2.98 (H-2′), methine at δ_H 2.26 (H-3′) and two geminal methyls at δ_H 0.95 (2 methyls at C-3′) corresponding to the isovaleryl group and methine proton at δ_H 4.28 (H-9), which further correlated with methine proton (overlapped with methyls) which gave a cross peak with two geminal methyl signals at δ_H 0.82 (2 methyls at C-2″) corresponding to the isobutyl group, respectively. The molecular weight and NMR data of compound **1** were very similar to those reported for rhoydomyrtone [8].

Rhodomyrtonedimer (**3**). Yellow sticky oil; R_f = 0.54 (90:10, hexane-EtOAc), negative-ion ES-MS m/z (rel. int.%): 952.7 [M+H]$^-$ (100) corresponded to the molecular formula $C_{57}H_{76}O_{12}$. In comparison with **1**, compound **3** showed new signals at δ_H 4.07 (4H, m), 1.99 (4H, m) and 1.76 (2H, m), indicating the presence of a 1,5-dioxypentyl unit in **3**. ^{13}C and DEPT NMR spectrum showed the presence of additional five methylenes carbon atoms at δ_C 68.7 (C-1‴), 28.9 (C-2‴) and 23.3 (C-3‴). The OH signal at C-6 of compound **3** was absent and the HMBC spectrum showed correlation of the H-1‴ (δ 4.07) with C-6 (δ 160.1). From this data, it could be concluded that rhodomyrtonedimer (**3**) was linked with pentyl chain at C-6. To the best of our knowledge compound **3** is a new natural product and was named as rhodomyrtonedimer.

The known compounds were identified by analysis of the spectroscopic data (1D, 2D NMR and MS) and comparison of their data with those in the literature to be: Rhodomyrtone (**1**) [8], 5,4′-dihydroxy-3,7,3′,5′-tetramethoxyflavone (**2**) [11], phlorisovalerophenone (**4**) [9], 3-O-cis-p-coumaroyl maslinic acid (**5**) [13], 3-O-trans-p-coumaroyl maslinic acid (**6**) [13], 3-O-methylellagic acid 3′-O-α-rhamnopyranoside (**7**) [12] and megastigman-7-ene-3,5,6,9-tetraol-9-O-β-D-glucopyranoside (**8**) [10]. Compounds **2, 5, 6, 7** and **8** were isolated for the first time from the plant.
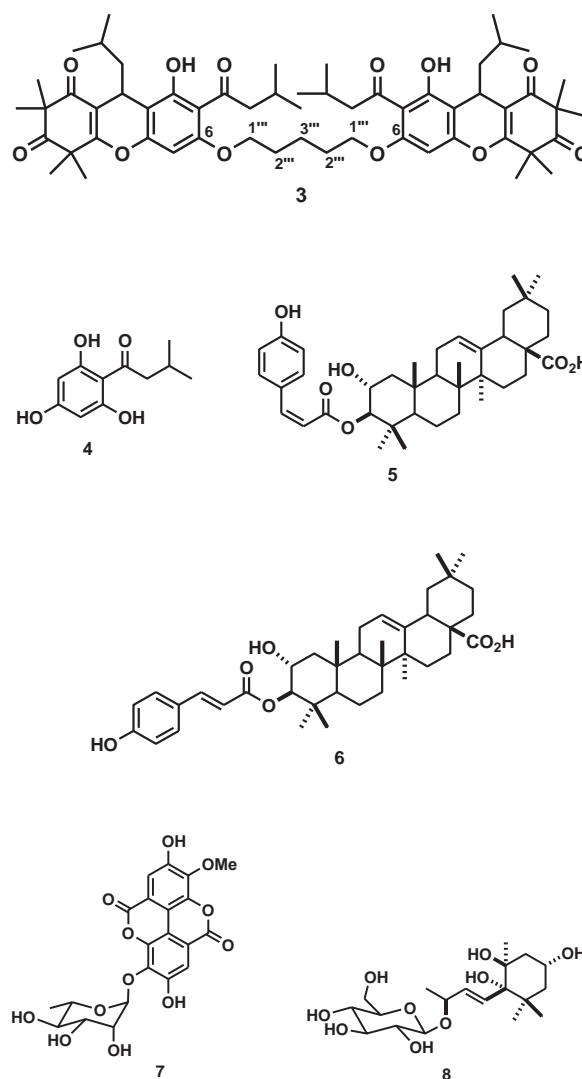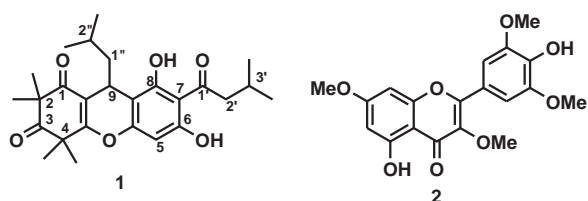
Figure 1. Structure of compounds **1**-**8**.

Table 1. Minimal inhibitory concentration (MIC) and minimal bactericidal concentration (MBC) of pure compounds isolated from acetone extract of *Rhodomyrtus tomentosa* leaves against *Staphylococcus aureus* ATCC 29213 and *Escherichia coli* ATCC 25922.

Sample	MIC/MBC (µg/ml)	
	S. aureus	*E. coli*
1	0.5/0.5	>32/NA
2	>128/NA	>32/NA
3	>32/NA	>32/NA
4	128/>128	>32/NA
5	32/>128	>32/NA
6	128/>128	>32/NA
7	128/>128	>32/NA
8	>128/NA	>128/NA
vancomycin	0.5/1	NA

NA: not applicable.

Eight compounds were tested for antibacterial activity against *S. aureus* ATCC 29213 and *E. coli* ATCC 25922. Compound **1** displayed good antibacterial activity against Gram-positive bacteria. It possessed remarkable activity against *S. aureus* with MIC/MBC values of 0.5/0.5 μg/ml. However, this compound exhibited low antibacterial activity against E. coli with MIC value of >32 μg/ml. Notably, rhodomyrtone showed stronger antibacterial activity than the reference antibiotic vancomycin. Rhodomyrtonedimer (**3**) exhibited low antibacterial activity against both Gram-positive and Gram-negative bacteria. This might be due to the introduction of alkyl chain to the hydroxyl group at C-6.

4. Conclusions

Chemical investigation of an acetone extract of *Rhodomyrtus tomentosa* leaves has resulted in the isolation of one new compound (**3**) together with seven know compounds. Rhodomyrtone (**1**) exhibited highest antibacterial activity against *Staphylococcus aureus* with MIC and MBC values of 0.5 μg/ml

Acknowledgements

References

[1] T. Nguyen Huu, D. Yan, C. Eun Mi, K. Phan Van, M. Chan Van and K. Young Ho, *Arch. Pharm. Res.* **32** (2009) 515-520.

[2] H. Asadhawuut, M. Wilawan, R. C. Anthony, D. Sandra and M.A. Vicky, *J. Org. Chem.* **77** (2012) 680-683.

[3] H. Asadhawuut and M. Wilawan, *Tetrahedron* **64** (2008) 11193–11197.

[4] L. Surasak, T. N. Erik, K. R. H. M. Thijs, P. Sjouke, H. Asadhawut, M. Wilawan, V. P. Supayang, V. D. Jan Maaten and K. Oliver, *Phytomed.* **16** (2009) 645–651.

[5] A. J. Hou, Y. J. Wu and Y. Z. Liu, *Zhongcaoyao.* **30** (1999) 645; *Chem. Abstr.* **132** (1999) 234270.

[6] R. Dachriyanus, Fahmi, M.V. Sargent, B.W. Skelton, Arta Crystallogr., E; Struct. Rep. Online **E60** (2004) 80.

[7] Y. Z. Liu, A. J. Hou, C. R. Ji and Y. J. Wu, *Chem. Abstr.* **130** (1998) 136542.

[8] M. A. Gamal and I. R. M. Sabrin, *ARKIVOC.* **15** (2007) 281-291.

[9] B. Gregor, G. Clarissa, K. Jutta, Z. Josef and B. Hans, *J. Nat. Prod.* **68** (2005) 1545-1548.

[10] Y. Qian, M. Katsuyoshi, O. Hideaki and T. Yoshio, *Chem. Pharm. Bull.* **53** (2005) 800-807.

[11] J. B. Harborne, M. Boardley and H.P. Lindlert, *Phytochem.* **24** (1985) 272-278.

[12] A. Elkhateeb, K. Takahashi, H. Matsuura, M. Yamasaki, O. Yamato, Y. Maede, K. Katakura, T. Yoshihara and K.Nabeta, *Phytochem.* **66** (2005) 2577-2580.

[13] D. Jing-Zhen, R. S. Shelley and H. M. Sidney, *Bioorg. Med. Chem.* **8** (2000) 247-250.

INVESTIGATION OF BIOACTIVE COMPOUNDS FROM FLOWERS OF *MURRAYA PANICULATA* (RUTACEAE)

Samreang Bunteang[1], Sakchai Hongthong[1], Chutima Kuhakarn[1], Thaworn Jaipetch[2], Vichai Reutrakul[1*]

[1]Department of Chemistry and Center of Excellence for Innovation in Chemistry, Faculty of Science, Mahidol University, Bangkok 10400, Thailand
[2]Department of Science and Liberal Art, Mahidol University (Kanchanaburi Campus), Siyok Kanchanaburi 71150, Thailand
E-mail:vichai.reu@mahidol.ac.th

Abstract: The chemical investigation of the methanol extract from flowers of *Murraya paniculata* (Rutaceae) led to the isolation of three known coumarins, namely scopolin (**1**), scopoletin (**2**), scopoletin 7-*O*-(6-*O*-feruloyl-β-D-glucopyranoside) (**3**) and compound **4** which remained to be identified. The chemical structures were elucidated by means of spectroscopic methods and confirmed with the previously reported data in the literatures. Compound **3** was reported for the first time from this plant. The crude extract, fractions and isolated pure compounds were evaluated for their cytotoxicity against a panel of mammalian cancer cell lines.

1. Introduction

The genus *Murraya* (Rutaceae) comprises about 12 species worldwide. In Thailand, three species, namely *M. paniculata*, *M. siamensis* and *M. koenigii*, have been identified [1]. *M. paniculata*, orange jasmine, is a small shrub or evergreen tree growing up to 7 m tall with the flowers throughout the year.

In the previously reported works, various parts of *M. paniculata* have been examined for its biological activities such as antidiarrhoeal, antinociceptive and anti-inflammatory activities [2 and 3]. Even though the flower parts of *M. paniculata* were used to make an essential oil, their biological activities are less explored [4]. Additionally the literature reviews on the topic of the chemical constituents of *M. paniculata* revealed that it comprises coumarins, flavonoids and alkaloids [5-8].

The objectives of this study were to further isolate and identify the chemical compositions of the methanol extract from the flowers of *M. paniculata* as well as to evaluate the cytotoxic activity of the isolated pure compounds.

2. Materials and Methods

2.1 General

Melting points (uncorrected) were recorded in ºC and measured on a digital Electrothermal IA 9000 series apparatus. The IR spectra were recorded on a Perkin Elmer EX FT-IR system spectrometer. Major bands (ν_{max}) were recorded in wave number (cm^{-1}). Ultraviolet (UV) absorption spectra were recorded in ethanol solutions using JASCO V-530 spectrophotometer. Principle bands (λ_{max}) were reported as wavelengths (nm) and log ε. Optical rotations were measured on a JASCO DIP-370 digital polarimeter by using a 50 mm microcell (1 mL). High resolution mass spectra were recorded on a Bruker Micro-mass model VQ-Tof 2 spectrometer. The high resolution nuclear magnetic resonance 500 MHz ^{1}H-NMR spectra together with 125 MHz ^{13}C-NMR spectra were performed on a Bruker AV 500 spectrometer. Spectra were recorded in deuterochloroform, tetradeuteromethanol and hexadeuterodimethyl sulfoxide solution and recorded as δ values in ppm down field from tetramethylsilane (TMS, $\delta = 0.00$) or residual non-deuterated solvent peaks as internal standard. Solvents for extraction, chromatography and crystallization were distilled at their boiling point ranges prior to use. Precoated Silica gel plates (Kieselgel 60 F$_{254}$, 0.20 mm, Merck) were employed for analytical TLC and the compounds were visualized by ultraviolet light (254 and 366 nm) and/or spraying 12% H$_2$SO$_4$ in ethanol/or anisaldehyde solution and Dragendorff's reagent. Silica gel plates (Kieselgel 60 F$_{254}$, 1.25 mm, Merck), activated at 120 ºC for 2 h, were used for preparative TLC. Bands were visualized by ultraviolet light at 254 and 366 nm. Column chromatography was performed by using Silica gel 60 (70-230 mesh, Merck).

2.2 Plant Material

The air-dried flowers (3.0 kg) of *M. paniculata* (Coll. J.F. Maxwell Det.) were collected from Bangkok, Thailand in 2011. A voucher specimen (BKF 151503) was deposited at the Herbarium, Royal Forest Department in Bangkok.

2.3 Extraction and isolation

The air-dried flowers were extracted by distilled methanol (32 liters) using Accelerated Solvent Extractor 300 (ASE®300) at room temperature. After filtration and removal of the solvents under reduced pressure (aspirator), the crude methanol extract (718.3 g) was obtained. This crude methanol extract was diluted in methanol leading to precipitation. After filtration, the solid (98.6 g) was obtained and its structure was assigned as scopolin (**1**). The methanol mother liquor (619.7 g) was subjected to column chromatography over silica gel providing fractions A1-A8. All fractions

were submitted to biological activity screenings. Fraction A2 (38.1 g) was rechromatographed by silica gel to yield fractions B1-B5. Fraction B2 (26.6 g) was further purified by recrystallization to afford compound **2** (135.9 mg). Fraction A6 (2.4 g) was recrystallized to afford compound **3** (53.0 mg). Fraction A5 (12.9 g) was rechromatographed by silica gel to yield fractions C1-C6. Fraction C4 (2.3 g) was further purified by recrystallization to give compound **4** (238.3 mg). The structures of isolated compounds **1**-**3** were elucidated on the basis of spectroscopic techniques (NMR, IR, UV-Vis and MS) and by comparison of their spectroscopic data with those previously reported in the literatures. The analytically pure compounds were submitted to biological activity testings.

3. Results and Discussion

The chromatographic isolation of the methanol extract of the flowers of *M. paniculata* yielded coumarin derivatives whose structures are shown in Figure 1. Isolated pure compounds were identified as scopolin (**1**) [9], scopoletin (**2**) [10], by comparison of their spectral data (^{1}H-NMR and ^{13}C-NMR) with those previously published data; see Tables 2 and 3.

The spectral data of the isolated scopoletin 7-*O*-(6-*O*-feruloyl-β-D-glucopyranoside) (**3**) were compared with those of **3** previously isolated from *Hapolophyllum obtusifolium* (Rutaceae) in 1982 [11].

To the best of our knowledge, compound **3** was isolated for the first time from the *Murraya* genus and its completed spectroscopic assignment were summarized in Table 4.

At present, the chemical structure of compound **4** could not be precisely assigned due to the complexity of its ^{1}H-NMR and ^{13}C-NMR signals. Additional characteristics of its IR spectrum are the O-H, N-H and C=O stretching at 3335, 3218 and 1620 cm^{-1}, respectively. Furthermore, the TLC spot of compound **4** gave positive test with Dragendorff's reagent. The complete assignment of the structure of compound **4** is under investigation.

The results of the cytotoxic activity assay of extract, fractions and compounds **1**-**3** are summarized in Table 1. Fractions A1 and A2 were found active only in P-388 cell line while fraction A3 showed positive activity in all tested cell lines. Unfortunately, compounds **1**-**3** were found inactive in all tested cell lines.
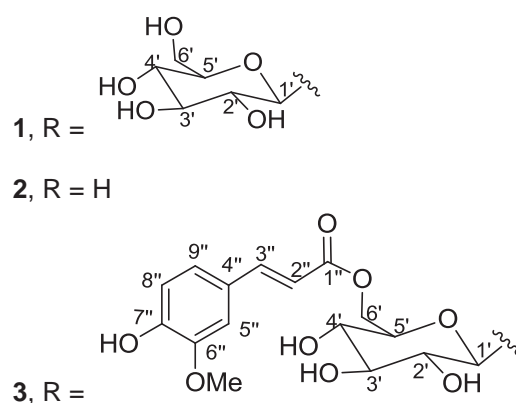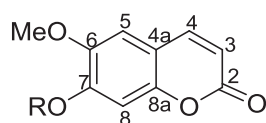
Figure 1. Isolated compounds **1**-**3**

Table 1. Cytotoxic activity of the crude methanol extract, its fractions (A1-A8) and compounds **1**-**3**

crude/ fractions/ pure compounds	cell lines (ED$_{50}$, μg/mL)					
	P-388	KB	Col-2	MCF-7	Lu-1	ASK
MeOH extract	>20	>20	>20	>20	>20	>20
A1	11.48	>20	>20	>20	>20	>20
A2	13.81	>20	>20	>20	>20	>20
A3	11.52	11.38	15.21	12.54	12.98	15.03
A4	>20	>20	>20	>20	>20	>20
A5	>20	>20	>20	>20	>20	>20
A6	>20	>20	>20	>20	>20	>20
A7	>20	>20	>20	>20	>20	>20
A8	>20	>20	>20	>20	>20	>20
scopolin (**1**)	>20	>20	>20	>20	>20	>20
scopoletin (**2**)	>20	>20	>20	>20	>20	>20
compound **3**	>20	>20	>20	>20	>20	>20

Results are expressed as ED$_{50}$ (μg/mL): ED$_{50}$ < 20 μg/mL is considered active for crude or fraction, ED$_{50}$ >20 μg/mL is considered inactive for crude or fraction and < 4 μg/mL is considered active for pure compound. P-388 = murine lymphocytic leukemia, KB = human nasopharyngeal carcinoma, Col-2 = human colon cancer, MCF-7 = human breast cancer, Lu-1 = human lung cancer, ASK = cell line from rat glioma

Table 2. ^{13}C- and ^{1}H-NMR spectroscopic data of scopolin (**1**) (DMSO-d_6+D$_2$O)

position	scopolin (**1**)	
	δ_C	δ_H (mult., J (Hz))
2	160.6	-
3	113.3	6.28 (d, 9.5)
4	144.2	7.91 (d, 9.5)
4a	112.3	-
5	109.8	7.23 (s)
6	146.0	-
7	149.9	-
8	103.1	7.08 (s)
8a	148.9	-
6-OCH$_3$	56.1	3.77 (s)
1'	99.7	5.07 (d, 7.4)
2'	73.1	3.31 (dd, 8.0, 7.4)
3'	76.7	3.29 (dd, 8.0, 8.0)
4'	69.7	3.14 (dd, 8.7, 8.0)
5'	77.1	3.44 (ddd, 8.7, 4.3, 4.1)*
6'	60.7	3.67 (dd, 14.3, 4.3)*,
		3.44 (dd, 14.3, 4.1)*

*The chemical shifts and coupling values were determined from ^{1}H-^{1}H decoupling technique.

Table 3. ^{13}C- and ^{1}H-NMR spectroscopic data of scopoletin (**2**) (a mixture of CD$_3$OD : CDCl$_3$, 1:1)

position	scopoletin (**2**)	
	δ_C	δ_H (mult., J (Hz))
2	163.3	-
3	112.0	6.17 (d, 9.4)
4	144.9	7.67 (d, 9.4)
4a	111.6	-
5	108.7	6.87 (s)
6	146.0	-
7	151.6	-
8	103.6	6.78 (s)
8a	150.4	-
6-OCH$_3$	56.5	3.87 (s)

Table 4. ^{13}C- and ^{1}H-NMR spectroscopic data of scopoletin 7-*O*-(6-*O*-feruloyl-β-D-glucopyranoside) (**3**) (DMSO-d_6)

position	scopoletin 7-*O*-(6-*O*-feruloyl-β-D-glucopyranoside) (**3**)		
	δ_C	δ_H (mult., J (Hz))	HMBC
2	160.5	-	-
3	113.4	6.26 (d, 9.4)	112.4 (C-4a), 160.5 (C-2)
4	144.1	7.90 (d, 9.4)	102.9 (C-8), 109.8 (C-5), 112.4 (C-4a)
4a	112.4	-	-
5	109.8	7.26 (s)	56.0 (6-OCH$_3$), 102.9 (C-8), 112.4 (C-4a)

position	scopoletin 7-*O*-(6-*O*-feruloyl-β-D-glucopyranoside) (**3**)		
	δ_C	δ_H (mult., J (Hz))	HMBC
6	146.0	-	-
7	149.6	-	-
8	102.9	7.17 (s)	109.8 (C-5), 112.4 (C-4a), 144.1 (C-4)
8a	148.9	-	-
6-OCH$_3$	56.0	3.78 (s)	109.8 (C-5), 146.0 (C-6), 149.6 (C-7)
1'	99.3	5.19 (d, 7.3)	73.0 (C-3'), 73.8 (C-2'), 76.5 (C-5'), 149.6 (C-7)
2'	73.8	3.82 *	63.3 (C-6'), 69.8 (C-4'), 76.5 (C-5'), 99.3 (C-1')
3'	73.0	3.30-3.33 (m)	76.5 (C-5'), 99.3 (C-1')
4'	69.8	3.27-3.22 (m)	63.3 (C-6'), 73.8 (C-2'), 76.5 (C-5')
5'	76.5	3.30-3.33 (m)	69.8 (C-4'), 73.0 (C-3')
6'	63.3	4.40 (d, 11.5), 4.17 (d, 11.5)	69.8 (C-4'), 166.5 (C-1'')
1''	166.5	-	-
2''	114.0	6.38 (d, 15.9)	125.4 (C-4''), 145.4 (C-3''), 166.5 (C-1'')
3''	145.4	7.46 (d, 15.9)	111.2 (C-5''), 114.0 (C-2''), 123.1 (C-9''), 125.4 (C-4''), 166.5 (C-1'')
4''	125.4	-	-
5''	111.2	7.21 (d, 1.8)	116.0 (C-8''), 123.1 (C-9''), 145.4 (C-3''), 147.9 (C-7''), 149.4 (C-6'')
6''	147.9	-	-
6''-OCH$_3$	55.7	3.79 (s)	111.2 (C-5''), 145.4 (C-3''), 147.9 (C-7'')
7''	149.4	-	-
8''	116.0	6.74 (d, 8.2)	111.2 (C-5''), 125.4 (C-4''), 147.9 (C-7''),

position	scopoletin 7-O-(6-O-feruloyl-β-D-glucopyranoside) (3)		
	δ_C	δ_H (mult., J (Hz))	HMBC
9″	123.1	7.00 (dd, 8.2, 1.8)	149.4 (C-6″) 111.2 (C-5″), 114.0 (C-2″), 116.0 (C-8″), 145.4 (C-3″), 149.4 (C-6″)
7″-OH	149.4	9.63 (br s)	116.0 (C-8″), 147.9 (C-7″)
3xOH	-	5.48 (d, 4.9), 5.28 (d, 4.4), 5.38 (d, 5.4)	-

*Overlapping signal

Scopolin (1)

White solid (MeOH); m.p. 221.3-223.3 °C (lit. [9] 224-226 °C); UV (EtOH) λ_{max} (log ε) 228 (3.99), 250 (3.45), 290 (3.56) and 341 (3.75) nm; IR (KBr) ν_{max} 3467 (OH), 1706 (C=O), 1569, 1517 (C=C) and 1281 (C-O) cm^{-1}. HRMS-ESI-TOF ([M+Na]$^+$) at m/z 354.0952 (calcd. 354.0951 for $C_{16}H_{18}O_9Na$).

Scopoletin (2)

Yellow solid (MeOH/CH$_2$Cl$_2$); m.p. 204.5-205.4 °C (lit. [10] 203-204 °C); UV (EtOH) λ_{max} (log ε) 229 (3.07), 253 (3.62), 262 (3.57), 297 (3.63) and 346 (4.01) nm; IR (KBr) ν_{max} 3338 (OH) 1703 (C=O), 1566, 1510 (C=C) and 1291 (C-O) cm^{-1}. HRMS-ESI-TOF ([M+Na]$^+$) at m/z 215.0341 (calcd. 215.0321 for $C_{10}H_8O_4Na$).

Scopoletin 7-O-(6-O-feruloyl-β-D-glucopyranoside) (3)

White solid (MeOH); m.p. 207.4-209.3 °C (lit. [11] 206-208 °C); UV (EtOH) λ_{max} (log ε) 227 (3.28), 248 (3.01), 294 (3.11) and 328 (3.27) nm; IR (KBr) ν_{max} 3384 (OH), 1705 (C=O), 1569, 1515 (C=C) and 1275 (C-O) cm^{-1}. HRMS-ESI-TOF ([M+Na]$^+$) at m/z 553.1416 (calcd. 553.1322 for $C_{26}H_{26}O_{12}Na$).

4. Conclusion

Three known compounds, scopolin (1), scopoletin (2), scopoletin 7-O-(6-O-feruloyl-β-D-glucopyranoside) (3) were isolated from the methanol extract of the flowers of *M. paniculata*. All compounds did not show cytotoxicity against mammalian cancer cell lines, P-388, KB, Col-2, MCF-7, Lu-1, and ASK.

Acknowledgements

References

[1] T. Smitinand, *Thai Plant Names*, Revised edition by The Forest Herbarium, Royal Forest Department. Bangkok: Pra Cha Chon Co., Ltd; (2001), pp. 368.

[2] S.Md. Sharker, I.J. Shahid and Md. Hasanuzzaman, *Braz. J. Pharmacogn.* **19** (2009) 746–748.

[3] Md.A. Rahman, Md. Hasanuzzaman, N. Uddin and IZ. Shahid, *Pharmacologyonline* **3** (2010) 768–776.

[4] P.K. Rout, Y.R. Rao, A. Sree and S.N. Naik, *Flavour Fragr. J.* **22** (2007) 352–357.

[5] T.-S. Wu, M.-J. Liou and C.-S. Kuoh, *Phytochemistry* **28** (1989) 293–294.

[6] J.-K. Lin and T.-S. Wu, *J. Chin. Chem. Soc.* **41** (1994) 213–216.

[7] Y. Zeng, L. Xu and Y. Peng, *Yingyong Yu Huanjing Shengwu Xuebao* **10** (2004) 699–702.

[8] T.-S. Wu, Y.-Y. Chan, Y.-L. Leu and S.-C. Huang, *Phytochemistry* **37** (1994) 287–288.

[9] H. Tsukamoto, S. Hisada and S. Nishibe, *Chem. Pharm. Bull.* **33** (1985) 396–399.

[10] F. Shafizadeh and A.B. Melnikoff, *Phytochemistry* **9** (1970) 1311–1316.

[11] E. Kh. Batirov, A. D. Matkarimov, V. M. Malikov and E. Seitmuratov, *Khim. Prir. Soedin.* **6** (1982) 691–695.

DIARYLHEPTANOIDS OF *CURCUMA COMOSA* FROM PRACHIN BURI

Nilubon Sornkaew[1], **Ailian Zhang**[2], **Ratchanaporn Chokchaisiri**[3], **Xiaozhen Chen**[4], **Kanjana Wongkrajang**[1], **Apichart Suksamrarn**[1]*

[1] Department of Chemistry, Faculty of Science, Ramkhamheang University, Bangkok 10240, Thailand
[2] School of Forestry and Bio-technology, Zhejiang Forestry University, Lin'an, Zhejiang, China
[3] Division of Chemistry, School of Science, Phayao University, Phayao 56000, Thailand
[4] Chengdu Institute of Biology, Chinese academy of science, Chengdu, Sichuan, China
* E-mail: s_apichart@ru.ac.th, Tel. +66 23191900

Abstract: Investigation of ethanol extract of the rhizome of *Curcuma comosa* from Prachin Buri province led to the isolation of four new diarylheptanoids, a 1.2:1 mixture of (3*S*)- and (3*R*)-1-(4-hydroxyphenyl)-7-phenyl-(4*E*,6*E*)-4,6-heptadien-3-ol (**1a** and **1b**), a mixture of (3*S*)- and (3*R*)-1-(4-hydroxyphenyl)-3-methoxy-7-phenyl-(4*E*,6*E*)-4,6-hepta-diene (**2a** and **2b**), a 2:1 mixture of (3*S*)-and (3*R*)-1-(3-methoxyl-4-hydroxyphenyl)-7-phenyl-(4*E*,6*E*)-4,6-heptadien -3-ol (**3a** and **3b**), (1*R*,2*R*,5*S*)-1,5-epoxy-2-hydroxy-1-(4-hydroxyphenyl)-7-phenylheptane (**4**), together with four known diarylheptanoids, 1-(4-hydroxyphenyl)-7-phenyl-(4*E*,6*E*)-4,6-heptadien-3-one (**5**), 3,5-dihydroxy-1,7-diphenylheptane (**6**), a 3:1 mixture of (3*S*)- and (3*R*)-1-(4-hydroxyphenyl)-7-phenyl-(6*E*)-6-hepten-3-ol (**7a** and **7b**), a 1:1 mixture of (3*S*)- and (3*R*)-1(3,4-dihydroxyphenyl)-7-phenyl-(6*E*)-6-hepten-3-ol (**8a** and **8b**). The absolute stereochemistry of the isolated compounds has also been determined using the modified Mosher's method. The structures of the new compounds were elucidated by spectroscopic techniques, whereas those of known compounds were identified by comparison of spectroscopic data with those of the reported compounds.

1. Introduction

Curcuma comosa, a member of Zingiberaceae, is widely distributed in tropical and subtropical regions of Asia, especially Thailand, Indonesia, and Malaysia. The rhizome of *C. comosa* has been used extensively in indigenous medicine in Thailand as an anti-inflammatory agent for the treatment of postpartum uterine bleeding. It has also been widely used as an aromatic stomachic. Previous phytochemical investigations of this plant yielded diarylheptanoids [1].

2. Materials and Methods

2.1 General procedures

Optical rotations were measured on a JASCO-1020 polarimeter. ^{1}H and ^{13}C NMR were recorded on a Bruker AVANCE 400 FT-NMR spectrometer operating at 400 (^{1}H) and 100 (^{13}C) MHz. ES-TOFMS and ES-MS spectra were measured with a Bruker microTOF and a Finnigan LC-Q mass spectrometer, respectively. Column chromatography (CC) was carried out using Merck silica gel 60 (finer than 0.063 mm) and Pharmacia Sephadex LH-20. For TLC, Merck precoated silica gel 60 F_{254} plates were used. Spots on TLC were detected under UV light and by spraying with anisaldehyde-H_2SO_4 reagent followed by heating.

2.2 Plant Material

The rhizomes of *C. comosa* were collected from Prachin Buri Province, Thailand, in January, 2008 and the plant species was identified by Dr. Thaya Jenjittikul, Mahidol University. A voucher specimen (Apichart Suksamrarn, No. 074) is deposited at the Faculty of Science, Ramkhamhaeng University.

2.3 Extraction and isolation

The rhizomes of *C. comosa* (5.80 kg) were sliced, air-dried, milled and macerated successively with *n*-hexane and EtOH to yield, after evaporation of the solvents under reduced pressure, the *n*-hexane (335.07 g) and EtOH (322.04 g) extracts, respectively.

The EtOH extract (300.0 g) was fractionated by column chromatography (Merck silica gel 60 PF$_{254}$, 520 g), using a gradient solvent system of *n*-hexane, *n*-hexane–EtOAc, EtOAc, EtOAc–MeOH and MeOH with increasing amounts of the more polar solvent. The eluates were examined by TLC and 11 combined fractions (E1-E11) were obtained. Fraction E4 (2.83 g) was subjected to column chromatography on silica gel using *n*-hexane–CH_2Cl_2 (50:50) to afford 2 subfractions. Subfraction 2 (310.0 mg) was separated on Sephadex LH-20 column, eluting with MeOH to give 3 subfractions. Subfraction 2 was then subjected to column chromatography on silica gel using *n*-hexane–EtOAc (80:20) to give a mixture of compounds **2a**, **2b** (37.3 mg). Fraction E7 (8.88 g) was chromatographed, eluting under isocratic condition of *n*-hexane–EtOAc (80:20) followed by Sephadex LH-20, eluted with MeOH, to yield compound **5** (393.2 mg). Fraction E9 (14.30 g) was subjected to column chromatography eluted with *n*-hexane–CH_2Cl_2 (50:50) to give 5 subfractions. Subfraction 2 was chromatographed using *n*-hexane–EtOAc (80:20) followed by Sephadex LH-20, eluted with MeOH and rechromatographed eluting under isocratic condition with CH_2Cl_2-MeOH (100:1) to afford a mixture of compounds **3a**, **3b** (18.1 mg). Subfraction 3 was purified by Sephadex LH-20 using MeOH to give compound **6** (3.8 mg). Subfraction 4 was separated on Sephadex LH-20 column, eluting with MeOH followed by silica column chromatography, eluting with CH_2Cl_2–MeOH (100:1) to furnish a mixture of compounds **7a**, **7b** (84.3 mg) and a mixture of

compounds **1a**, **1b** (15.9 mg). Fraction E11 (12.72 g) was subjected to column chromatography using CH$_2$Cl$_2$–MeOH (100:1) to give 5 subfractions. Subfraction 5 was chromatographed using *n*-hexane–acetone (80:20) followed by Sephadex LH-20, eluted with MeOH to afford compound **4** (12.5 mg) and a mixture of compounds **8a**, **8b** (230.0 mg) were separated on Sephadex LH-20 column, eluting with MeOH followed by silica column chromatography, eluting with CH$_2$Cl$_2$:MeOH (100:1).

2.3.1 Compound **1a** and **1b**

White needles; $[\alpha]_D^{29}$ -3.8° (*c* 1.37, EtOH); ^{1}H NMR (CDCl$_3$, 400 MHz): δ 1.87 (m, 2H, H-2), 2.65 (m, 2H, H-1), 4.21 (m, 1H, H-3), 5.82 (dd, *J* = 15.1, 6.8 Hz, 1H, H-4), 6.37 (dd, *J* = 15.1, 10.6 Hz, 1H, H-5), 6.54 (d, *J* = 15.6 Hz, 1H, H-7), 6.76 (partially overlapping, 1H, H-6), 6.74 (d, *J* = 8.2 Hz, 2H, H-3′,H-5′), 7.05 (d, *J* = 8.2 Hz, 2H, H-2′, H-6′), 7.22 (m, 1H, H-4″), 7.30 (br t, *J* = 7.5 Hz, 2H, H-3″, H-5″), 7.38 (br d, *J* = 7.5 Hz, 2H, H-2″,H-6″); ^{13}C NMR (CDCl$_3$, 100 MHz): 30.7 (C-1), 38.9 (C-2), 72.0 (C-3), 115.2 (C-3′, C-5′), 126.3 (C-2″, C-6″), 127.6 (C-4″), 128.1 (C-6), 128.6 (C-3″, C-5″), 129.5 (C-2′, C-6′), 131.0 (C-5), 132.8 (C-7), 133.8 (C-1′), 136.1 (C-4), 137.1 (C-1″), 153.7 (C-4′); HMBC correlation: H-1 (C-2, C-3, C-1′, C-2′/C-6′), H-2 (C-1, C-3), H-3 (C-1, C-2, C-4, C-5), H-4 (C-2, C-3, C-6), H-5 (C-3, C-6, C-7), H-6 (C-5, C-7, C-1″), H-7 (C-5, C-1″, C-2″/C-6″); ESMS (-ve): *m/z* 279 [M-H]$^-$; HR-TOFMS (ES$^-$): m/z 279.1385 [M-H]$^-$; calcd for C$_{19}$H$_{20}$O$_2$-H, 279.1385.

2.3.2 Compound **2a** and **2b**

Pale yellow oil; $[\alpha]_D^{29}$ -0.9° (*c* 1.81, EtOH); ^{1}H NMR (CDCl$_3$, 400 MHz): 1.77, 1.94 (m, 2H, H-2), 2.61, (m, 2H, H-1), 3.28 (s, 3H, 3-OMe), 3.60 (m, 1H, H-3), 5.65 (dd, *J* = 15.1, 8.0 Hz, 1H, H-4), 6.33 (dd, *J* = 15.1, 10.8 Hz, 1H, H-5), 6.54 (d, *J* = 15.6 Hz, 1H, H-7), 6.74 (d, *J* = 7.6 Hz, 2H, H-3′, H-5′), 6.78 (dd, *J* = 15.6, 10.8 Hz, 1H, H-6), 7.03 (d, *J* = 7.6 Hz, 2H, H-2′, H-6′), 7.23 (m, 1H, H-4″), 7.30 (br t, *J* = 7.2 Hz, 2H, H-3″, H-5″), 7.38 (br d, *J* = 7.2 Hz, 2H, H-2″, H-6″); ^{13}C NMR (CDCl$_3$, 100 MHz): 30.6 (C-1), 37.4 (C-2), 56.1 (3-OMe), 81.3 (C-3), 115.1 (C-3′, C-5′), 126.3 (C-2″, C-6″), 127.6 (C-4″), 128.1 (C-6), 128.6 (C-3″, C-5″), 129.5 (C-2′, C-6′), 132.6 (C-7), 133.0 (C-5), 134.0 (C-1′), 137.1 (C-1″), 153.7 (C-4′); HMBC correlation: H-1 (C-2, C-3, C-1′, C-2′/C-6′), H-2 (C-1, C-3, C-4), H-3 (C-1, C-2, OCH$_3$, C-4, C-5), H-4 (C-2, C-3, C-6), H-5 (C-3, C-6, C-7), H-6 (C-5, C-7, C-1″), H-7 (C-5, C-1″, C-2″/C-6″); ESMS (-ve): m/z 293 [M-H]$^-$; HR-TOFMS (ES$^-$): *m/z* 293.1542 [M-H]$^-$; calcd for C$_{20}$H$_{22}$O$_2$-H, 293.1542.

2.3.3 Compound **3a** and **3b**

Pale yellow oil; $[\alpha]_D^{29}$ +1.3° (*c* 1.16, EtOH); ^{1}H NMR (CDCl$_3$, 400 MHz): 1.87 (m, 2H, H-2), 2.66 (m, 2H, H-1), 3.86 (s, 3H, 3′-OMe), 4.22 (m, 1H, H-3), 5.84 (dd, *J* = 15.1, 6.8 Hz, 1H, H-4), 6.38 (dd, *J* = 15.1, 10.7 Hz, 1H, H-5), 6.54 (d, *J* = 15.6 Hz, 1H, H-7), 6.69 (br d, *J* = 7.4, 1H, H-6′), 6.70 (br s, 1H, H-2′), 6.77 (dd, *J* = 15.6, 10.7 Hz, 1H, H-6), 6.82 (br d, *J* = 7.4 Hz, 1H, H-5′), 7.23 (m, 1H, H-4″), 7.30 (br t, *J* = 7.6 Hz, 2H, H-3″, H-5″), 7.38 (br d, *J* = 7.2 Hz , 2H, H-2″, H-6″); ^{13}C NMR (CDCl$_3$, 100 MHz): 31.3 (C-1), 39.0 (C-2), 55.8 (3′-OMe), 72.0 (C-3), 111.0 (C-2′), 114.2 (C-5′), 120.9 (C-6′), 126.3 (C-2″, C-6″), 127.6 (C-4″), 128.1 (C-6), 128.6 (C-3″, C-5″), 130.9 (C-5), 132.8 (C-7), 133.7 (C-1′), 136.3 (C-4), 137.1 (C-1″), 143.7 (C-4′), 146.4 (C-3′); HMBC correlation: H-1 (C-2, C-3, C-1′, C-2′/C-6′), H-2 (C-1, C-3, C-4, C-1′), H-3 (C-1, C-2, C-4, C-5), H-4 (C-2, C-3, C-6), H-5 (C-3, C-6, C-7), H-6 (C-5, C-7, C-1″), H-7 (C-5, C-1″, C-2″/C-6″), OCH$_3$ (C-3′); ESMS (-ve): m/z 309 [M-H]$^-$; HR-TOFMS (ES$^+$): *m/z* 311.1647 [M+H]$^+$; calcd for C$_{20}$H$_{22}$O$_3$+H, 311.1647.

2.3.4 Compound **4**

White needles; $[\alpha]_D^{27}$ +47.7° (*c* 1.25, EtOH); ^{1}H NMR (CDCl$_3$, 400 MHz): 1.55, 1.79 (m, 2H, H4), 1.55, 2.15 (m, 2H, H-3), 1.79, 1.89 (m, 2H, H-6), 2.70 (m, 2H, H-7), 3.44 (m, 1H, H-5), 3.50 (m, 1H, H-2), 3.92 (d, *J* = 8.8 Hz, 1H, H-1), 6.81 (br d, *J* = 8.0 Hz, 2H, H-3′, H-5′), 7.15 (br d, *J* = 7.6 Hz, 2H, H-2″, H-6″), 7.16 (overlapping, 1H, H-4″), 7.25 (partially overlapping, 2H, H-3″, H-5″), 7.26 (br d, *J* = 7.7 Hz, 2H, H-2′, H-6′); ^{13}C NMR (CDCl$_3$, 100 MHz): 30.9 (C-4), 31.7 (C-3, C-7), 37.2 (C-6), 71.3 (C-2), 77.0 (C-5), 84.5 (C-1), 115 (C-3′, C-5′), 125 (C-4″), 128.2 (C-2″, C-6″), 128.4 (C-3″, C-5″), 128.9 (C-2′, C-6′), 131.0 (C-1′), 142.1 (C-1″), 156.4 (C-4′); HMBC correlation: H-1 (C-2, C-5, C-1′, C-2′/C-6′), H-2 (C-1, C-3) H-3 (C-2, C-4), H-4 (C-3, C-5), H-5 (C-4, C-6), H-6 (C-5, C-7, C-1″), H-7 (C-5, C-6, C-1″, C-2″/C-6″); ESMS (-ve): m/z 297 [M-H]$^-$; HR-TOFMS (ES$^-$): *m/z* 297.1491 [M-H]$^-$; calcd for C$_{19}$H$_{22}$O$_3$-H, 297.1491.

2.4 Determination of C-3 absolute configuration of diarylheptanoids

To a solution of the diarylheptanoids **1** (3.1 mg, 0.0111 mmol) in dry pyridine (100 μL) was added (*R*)-(-)-MTPA chloride (10 μL) at 10 °C and the mixture was stirred for 5 min. Stirring continued at ambient temperature and the completion of reaction was monitored by TLC. Two milliliters of *n*-hexane was added to reaction mixture and the *n*-hexane-soluble part was subjected to flash column chromatography using *n*-hexane–EtOAc (90:10) as eluting solvent to give the (*S*)-MTPA ester **1x** (3.2 mg). The procedure was repeated, but using (*S*)-(+)-MTPA chloride in place of (*R*)-(-)-MTPA chloride, to yield the (*R*)-MTPA ester **1y** (2.8 mg). The ^{1}H NMR spectra of **1x** and **1y** were recorded in CDCl$_3$; the chemical shift differences of the proton resonances between the (*S*)-MTPA ester **1x** and (*R*)-MTPA ester **1y** were calculated and the results are summarized in Figure 1.

Following the above procedure, the absolute configuration of a mixture of **3a** and **3b**, **4**, **6** [2], a mixture of **7a** and **7b**, and a mixture of **8a** and **8b** [3] were determined. The results are summarized in Figure 1.
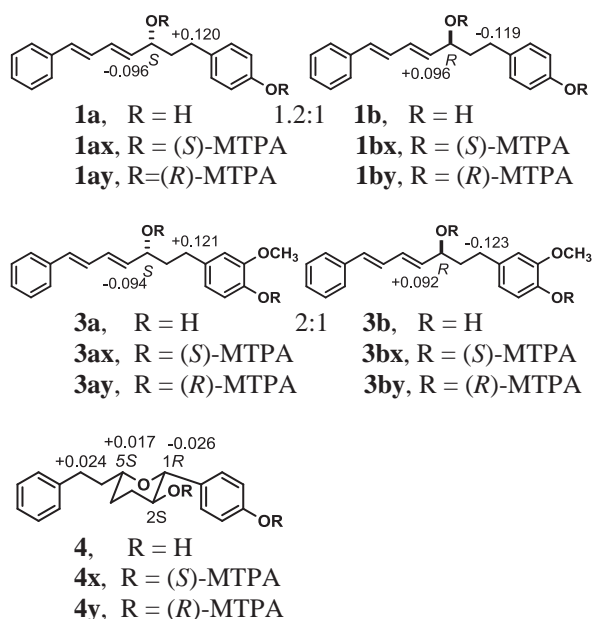
OR +0.120
-0.096 *S*

1a, R = H   1.2:1
1ax, R = (*S*)-MTPA
1ay, R=(*R*)-MTPA

OR -0.119
+0.096 *R*

1b, R = H
1bx, R = (*S*)-MTPA
1by, R = (*R*)-MTPA

OR +0.121
-0.094 *S*   OCH₃

3a, R = H   2:1
3ax, R = (*S*)-MTPA
3ay, R = (*R*)-MTPA

OR -0.123
+0.092 *R*   OCH₃

3b, R = H
3bx, R = (*S*)-MTPA
3by, R = (*R*)-MTPA

+0.017 -0.026
+0.024 5*S*   1*R*
2*S*

4, R = H
4x, R = (*S*)-MTPA
4y, R = (*R*)-MTPA

Figure 1. $\Delta\delta = (\Delta\delta_S - \Delta\delta_R)$ values obtained from the MTPA esters of compounds **1a** and **1b** mixture, **3a** and **3b** mixture, and **4** in CDCl₃.

3. Results and Discussion

Preliminary examination of the chemical constituents of *C. comosa* rhizomes collected from different locations in Thailand revealed that some of them contained a relatively high quantity the major constituents and constituted additional number of minor diarylheptanoids which have not previously been reported in this plant species. The rhizomes of *C. comosa* from Prachin Buri Province were used for this study. The pulverized, dry rhizome was extracted successively with *n*-hexane and EtOH to yield the hexane and EtOH extracts, respectively. The EtOH extract of *C. comosa* rhizomes was subjected to column chromatography to yield four new diarylheptanoids **1-4** and four known compounds **5-8**. The structures of the new compounds were elucidated by spectroscopic techniques, whereas those of known compounds were identified by comparison of spectroscopic data with those of reported compounds.

Compound **1** was the diarylheptanoid existed as a mixture of two C-3 enantiomers, **1a** and **1b**. It was obtained as white needles. The IR absorption at 3233 cm⁻¹ revealed the presence of hydroxyl group. Assignment of ¹H and ¹³C NMR data were achieved by COSY, DEPT, HMQC, HMBC techniques. The presence of the phenyl and *para*-disubstituted phenyl moieties were determined by ¹H NMR signals at δ 7.22 (m, 1H, H-4″), 7.30 (br t, *J* = 7.5 Hz, 2H, H-3″, H-5″) and 7.38 (br d, *J* = 7.5 Hz, 2H, H-2″,H-6″), two doublet signals (*J* = 8.2 Hz) at δ 6.74 (2H, H-3′,H-5′) and δ 7.05 (2H, H-2′, H-6′). The ¹H MNR features of

the aromatic protons were very similar to those of compound **7**. However, the ¹H NMR feature of the heptyl chain were different from those of compound **7** by the presence of α,β,γ,δ-unsaturated system as evident from signals at δ 5.82 (dd, *J* = 15.1, 6.8 Hz, 1H, H-4), δ 6.37 (dd, *J* = 15.1, 10.6 Hz, 1H, H-5), 6.54 (d, *J* = 15.6 Hz, 1H, H-7), 6.76 (partially overlapping, 1H, H-6), which corresponded to the ¹³C NMR at δ 136.1, 131.0, 132.8 and 128.1. The COSY peaks between H-1 (δ 2.65, m, 2H) and H-2 (δ 1.87, m, 2H), between H-2 and H-3 (δ 4.21, m, 1H), and between H-3 and H-4 determined the present of a hydroxyl at C-3. The attachment of 4-hydroxyphenyl moiety to the 1-position was confirmed by the HMBC correlation from H-1 to C-1′ (δ 133.8) and C-2′/C-6′ (δ 129.5), and from H-2′/H-6′ (δ 7.05, d, *J* = 8.2 Hz, 2H) to C-1 (30.7). The attachment of the phenyl moiety to the 7-position was also confirmed by HMBC correlations of H-7 with C-1″ (δ 137.1) and C-2″/C-6″ (δ 126.3), and H-2″/H-6″ (δ 7.38, br d, *J* = 7.5 Hz, 2H) with C-7.

Compound **1** exhibited low optical rotation ($[\alpha]_D^{29}$ -3.8°, *c* 1.37, EtOH). The absolute stereochemistry at C-3 and the enantiomer ratio were determined by the modified Mosher's method [4]. Thus the diarylheptanoids **1a** and **1b** mixture was tranformed to a 1.2:1 mixture of the corresponding (*S*)-MTPA esters **1ax** and **1bx**, and (*R*)-MTPA esters **1ay** and **1by**. Analysis of the ¹H NMR spectra of the two Mosher ester mixtures established the absolute configuration at C-3 of the diarylheptanoid mixture as *S* and *R* in a ratio of 1.2:1. The diarylheptanoid **1** was thus concluded as a 1.2:1 mixture of (3*S*)- and (3*R*)-1-(4-hydroxyphenyl)-7-phenyl-(4*E*,6*E*)-4,6-heptadien-3-ol (**1a** and **1b**).

Compound **2** was also a diarylheptanoid existed as a mixture of two C-3 enantiomers, **2a** and **2b**, since the optical rotation was almost zero ($[\alpha]_D^{29}$ -0.9°, *c* 1.81, EtOH). The IR absorption band at 3448 cm⁻¹ revealed the presence of hydroxyl group. The ¹H MNR and ¹³C NMR spectra were very similar to those of **1**, with additional signal for a methoxyl moiety (δ 3.28, s, 3H). The methoxyl group was connected at C-3 based on HMBC correlation from H-3 to OMe (δ 56.1). The diarylheptanoid **2** was thus concluded as a mixture of (3*S*)- and (3*R*)-1-(4-hydroxyphenyl)-3-methoxy-7-phenyl-(4*E*,6*E*)-4,6-heptadiene (**2a** and **2b**).

Compound **3** was also a diarylheptanoid existed as a mixture of two C-3 enantiomers, **3a** and **3b**. The IR absorption band at 3436 cm⁻¹ revealed the presence of hydroxyl group. The ¹H NMR and ¹³C NMR spectra also very similar to those **1**, except a 1,2,4-trisubstituted phenyl ring (δ 6.69 br d, *J* = 7.4 Hz , H-6′; δ 6.70, br s, H-2′ and δ 6.82, br d, *J* = 7.4 Hz, H-5′) and a methoxyl group (δ 3.86, s, 3H, OMe-3′). The HMBC between H-2′ and C-3′ (δ 146.4), C-4′ (δ 143.7), and H-6′ and C-4′ determined the methoxyl group located at 3′-position. The 1,2,4-trisubstituted phenyl ring was placed at C-1 from the HMBC correlation from H-2′ and H-6′ to C-1 (δ 31.3). The

phenyl connected to C-7 based on HMBC peak between H-2″/H-6″ (δ 7.38, br d, J = 7.2 Hz, 2H) and C-7 (δ 132.8), and between H-7 (δ 6.54, d, J = 15.6 Hz, 1H) and C-2″/H-6″ (δ 126.3).

Compound **3** showed optical rotation at $[\alpha]_D^{29}$ +1.3° (c 1.16, EtOH). The absolute stereo-chemistry at C-3 and the enantiomeric ratio were determined by the modified Mosher's method. The diarylheptanoid **3** was thus concluded as a 2:1 mixture of (3S)- and (3R)-1-(3-methoxy-4-hydroxyphenyl)-7-phenyl-(4E,6E)-4,6-dihepten-3-ol (**3a** and **3b**).

Compound **4** was obtained as white needles. The IR absorption band at 3392 cm^{-1} revealed the presence of hydroxyl group. The presence of a phenyl and a *para*-disubstituted phenyl were determined by ^{1}H NMR signals at δ 6.81 (br d, J = 8.0 Hz, 2H, H-3′/H-5′), 7.15 (br d, J = 7.6 Hz, 2H, H-2″/H-6″), 7.16 (overlapping signal, 1H, H-4″), 7.25 (partially overlapping signal, 2H, H-3″/H-5″), 7.26 (br d, J = 7.7 Hz, 2H, H-2′/H-6′). The ^{1}H NMR signals at δ 3.44 (m, 1H, H-5), 3.50 (m, 1H, H-2), and 3.92 (d, J = 8.8 Hz, 1H, H-1) showed three saturated carbons in heptyl chain connected with oxygen. The linkages of C-1, C-2, and C-5 with oxygen was confirmed by the COSY peaks H-1/H-2, H-2/H-3, H-3/H-4, H-4/H-5, H-5/H-6, H-6/H-7. The HMBC correlation between H-1 and C-5 (δ 77.0) indicated that carbons 1 and 5 should connect through oxygen. The *para*-disubstituted phenyl moiety located at C-1 according to the HMBC correlation between H-2′/H-6′ and C-1 (δ 84.5), and between H-1 and C-1′ (δ 131.0), C-2′/C-6′ (δ 128.9), and between H-2 and C-1′. The HMBC correlations from H-7 to C-1″ (δ 142.1), C-2″/C-6″ (δ 128.2), from H-6 to C-1″, and from H-2″/H-6″ to C-7 (δ 31.7) showed that the phenyl group was connected to C-7. Therefore, compound **4** was assigned as 1,5-epoxy-2-hydroxy-1-(4-hydroxy phenyl)-7-phenyl-heptane.

Compound **4** exhibited high optical rotation ($[\alpha]_D^{27}$ +47.7°, c 1.25, EtOH). The absolute stereo-chemistry at C-1, C-2, C-5 were determined by NOE and the modified Mosher's method. The NOE experiments indicated the correlation of H-1 and H-5. However, no correlation between H-2 and H-1, and H-2 and H-5 were observed, thus suggesting H-1 and H-5 to exist at the same side of ring A, while H-2 was located at another side of ring A. The diarylheptanoid **4** was thus concluded as (1R,2R,5S)-1,5-epoxy-2-hydroxy-1-(4-hydroxyphenyl)-7-phenylheptane.

5   **6**

7a, 7b   **8a, 8b**
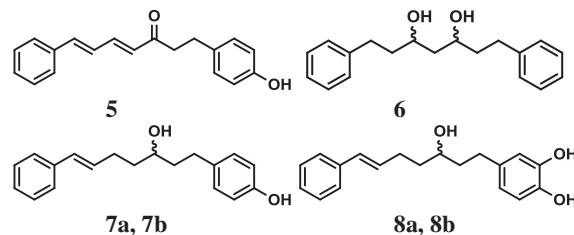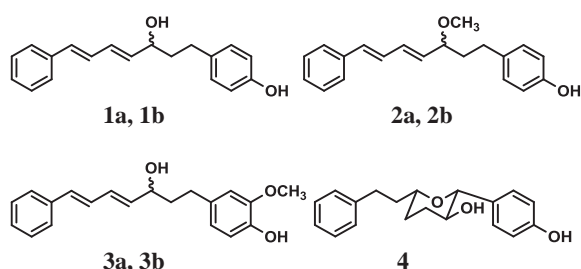
4. Conclusions

From the rhizomes of *Curcuma comosa* Roxb., four new diarylheptanoids, a 1.2:1 mixture of (3S)- and (3R)-1-(4-hydroxyphenyl)-7-phenyl-(4E,6E)-4,6-hepta-dien-3-ol (**1a** and **1b**), a mixture of (3S)- and (3R)-1-(4-hydroxyphenyl)-3-methoxy-7-phenyl-(4E,6E)-4,6-heptadiene (**2a** and **2b**), a 2:1 mixture of (3S)- and (3R)-1-(3-methoxy-4-hydroxyphenyl)-7-phenyl-(4E,6E)-4,6-heptadien-3-ol (**3a** and **3b**) and (1R,2R,5S)-1,5-epoxy-2-hydroxy-1-(4-hydroxyphenyl)-7-phenyl-heptane (**4**), together with four known diarylheptanoids, 1-(4-hydroxyphenyl)-7-phenyl-(4E,6E)-4,6-heptadien-3-one (**5**), 3,5-dihydroxy-1,7-diphenylheptane (**6**), a 3:1 mixture of (3S)- and (3R)-1-(4-hydroxyphenyl)-7-phenyl-(6E)-6-hepten-3-ol (**7a** and **7b**), a 1:1 mixture of (3S) and (3R)-1-(3,4-dihydroxyphenyl)-7-phenyl-(6E)-6-hepten-3-ol (**8a** and **8b**). The absolute stereo- chemistry of the isolated alcohols has also been determined using the modified Mosher's method.

References

[1] F. Xu, S. Nakamura, Y. Qu, H. Matsuda, Y. Pongpiriyadacha, L. Wu and M. Yoshikawa, *Chem. Pharm. Bull*. **56** (2008) 1710-1716.
[2] T. Hashimoto, M. Tori and Y. Asakawa, *Chem. Pharm. Bull*. **34** (1986) 1846-1849.
[3] A. Suksamrarn, M. Ponglikitmongkol, K. Wongkrajang, A. Chindaduang, S. Kittidanairak, A. Jankam, B. Yingyongnarongkul, N. Kittipanumat, R. Chokchaisiri, P. Khetkam and P. Piyachaturawat, *Bioorg. Med. Chem.* **16** (2008) 6891–6902.
[4] J. A. Dale, D. L. Dull and H. S. Mosher, *J. Org. Chem.* **34** (1969) 2543-2549.

1a, 1b   **2a, 2b**

3a, 3b   **4**

SYNTHESIS OF PORPHYRIN-THIOPHENE DERIVATIVES FOR OPTOELECTRONIC APPLICATIONS

Wittawat Keawsongsaeng, Napapron Wannaprom, Parichatr Vanalabhpatana,
Rojrit rojanathanes, Patchanita Thamyongkit[*]

Department of chemistry, Faculty of Science, Chulalongkorn University, Bangkok, 10330, Thailand.

[*]E-Mail:patchanita.v@chula.ac.th, Tel. +66 2-218-7587, Fax. +66 2-254-1309

Abstract: A series of *meso*-thiophene-linked porphyrin derivative were synthesized *via* a modified Lindsey's method in moderate yield (9-15%). Oligothiophene substituents were introduced at porphyrin *meso*-positions in order to enhance the solubility, extend a conjugated system and improve photophysical and electrochemical properties. All synthesized porphyrins were characterized by NMR spectroscopy and MALDI-TOF mass spectrometry. Their optical properties were also investigated by UV-Vis and fluorescence spectrophotometry in both solution and film. The spectroscopic data revealed that the absorption maxima of the bithiophene-substituted porphyrin exhibited red shifts in both absorption and emission spectra compared to that of the monothiophene-substituted one. Results from Cyclic voltametry were employed to determine HOMO and LUMO energy levels and energy gaps of the target molecules to evaluate the potential for using in optoelectronic devices.

1. Introduction

Porphyrin-based compounds have attracted significant attention in recent years as photoactive compounds for optoelectronic applications due to their extremely high absorption coefficients[1], high thermal and photo-stabilities[2], tuneable electrochemical and photophysical properties by varying the metal center and/or controlling substituents at the macrocycle peripheral positions[3]. Porphyrins have been of interest as photocatalysts, optical sensors[4], organic semiconductors[5], organic light-emitting diodes (OLEDs) or even as dye-sensitized solar cells (DSSCs) and bulk-heterojunction solar cells (BHJSCs)[6].

In this study, we synthesized a series of porphyrinic compounds bearing oligothiophene (1-2 units) on all their *meso*-positions. Thiophene and their oligomers, α-conjugated oligothiophenes, belong to the most investigated π-conjugated systems in the field of material science due to their chemical stabilities in various redox forms, excellent charge transfer properties and their outstanding structural and electronic properties[7]. In this study, oligothiophene units were introduced into the porphyrinic framework. The target molecules are expected to exhibit enhanced solubility, extended conjugation system and improved photophysical and electrochemical properties, all of which are desirable features of photoactive compounds in several successful optoelectronic devices.

2. Materials and Methods

All commercial reagents were analytical grade, purchased from Merck and Sigma-Aldrich and used as received, or purified before used by standard procedures. Chemical shift (δ) of ^{1}H-NMR (400 MHz) and ^{13}C-NMR (100 MHz) measurement was recorded in $CDCl_3$ in parts per million (ppm) relative to the residual $CHCl_3$ signal (7.26 ppm for ^{1}H-NMR and 77.0 ppm for ^{13}C-NMR). Mass spectra were obtained by matrix-assisted laser desorption ionization mass spectrometry (MALDI-TOF) using dithranol as a matrix. Absorption and emission spectra of the solution were measured in toluene at room temperature, and those of the film were obtained from the drop-casting technique on a glass substrate.

2.1 Synthesis of 5,10,15,20-tetra(thiophen-2-yl) porphyrin (1)

Compound **1** was readily prepared *via* a modified version of Lindsey's method for synthesis of *meso*-substituted porphyrins[8]. Pyyrole (0.35 mL, 5.0mmol) and 2-thiophenecarboxaldehyde (0.47 mL, 5.0mmol) were dissolved in dichloromethane (200 mL) and the solution was purged with nitrogen for 15 min. The reaction mixture was cooled to 0°C, treated with $BF_3 \cdot OEt_2$ (63.4 μL, 0.50 mmol) and stirred at room temperature for 12 h under nitrogen atmosphere. Then tetrachloro-1,4-benzoquinone (*p*-chloronil) (922 mg, 3.75 mmol) was added to the mixture and stirring was continued for additional 6 h. After removal of the solvent, the crude product was purified by a silica column using dichloromethane as eluent to give 5,10,15,20-tetra(thiophen-2-yl)porphyrin (**1**) as a purple solid (120 mg,15%). ^{1}H-NMR: δ –2.74 (s, 2H), 7.42 (q, 4H), 7.78 (q, 4H), 7.83 (q, 4H), 8.97 (s, 8H) ppm; ^{13}C-NMR: δ 112.4, 126.1, 127.9, 133.9, 142.7, 146.9 ppm; MALDI-TOF-MS obsd 637.942 ([M$^+$]), calcd 638.852 ([M$^+$]; M = $C_{36}H_{22}N_4S_4$); λ_{abs}/nm 428, 522 and 561; λ_{em}/nm 669 and 728 (λ_{ex}= 428 nm)

2.2 Synthesis of 5,10,15,20-tetra(2,2'-bithiophen-5-yl)porphyrin (2)

Following a published procedure with slight modification[8], pyyrole (0.35 mL, 5.0 mmol) and 2,2'-bithiophene-5-carboxaldehyde (971 mg, 5.00 mmol) were dissolved in dichloromethane (200 mL)

and the solution was purged with nitrogen for 15 min. The reaction mixture was cooled to 0°C, treated with $BF_3 \cdot OEt_2$ (63.4 μL, 0.50 mmol) and stirred under nitrogen atmosphere at room temperature for 12 h. Then, p-chloronil (922 mg, 3.75 mmol) was added to the mixture and stirring was continued for additional 6 h. After removal of the solvent, the crude product was purified by a silica column using hexane:dichloromethane (1:3) as eluent to give 5,10,15,20-tetra(2,2'-bithiophen-5-yl)porphyrin (2) as a dark green solid (108 mg, 9%). ^{1}H-NMR: δ –2.61 (s, 2H), 7.09 (q, 4H), 7.27 (q, 4H), 7.39 (q, 4H), 7.56 (q, 4H), 7.78 (q, 4H), 9.12 (s, 8H) ppm; ^{13}C-NMR: δ 110.48, 121.27, 122.34, 123.07, 123.30, 126.33, 126.48, 127.29, 129.11, 132.93, 135.49, 138.68, 139.67 ppm; MALDI-TOF-MS obsd 966.992 ([M^+]), calcd 967.350 ([M^+]; M = $C_{52}H_{30}N_4S_8$); λ_{abs}/nm 446, 529 and 575; λ_{em}/nm 707 (λ_{ex}= 446 nm).

2.3 Electrochemical measurement

Electrochemical properties of compound 1 and 2 were determined by cyclic voltammetry in acetonitrile containing 0.1 M of Bu_4NBF_4 by using ITO-coated glass as working electrode, a Pt wire as counter electrode and an Ag/AgCl as reference electrode at the scan rate of 20 mV/s.

3. Results and Discussion

3.1. Synthesis and characterization

The free-based porphyrin-thiophene derivatives were successfully synthesized by using a standard condition[8] involving a condensation of an appropriate functionalized oligothiophene with pyrrole in an acid catalyzed condition, resulting in compounds 1 and 2 in 15% and 9%, respectively (Scheme 1).
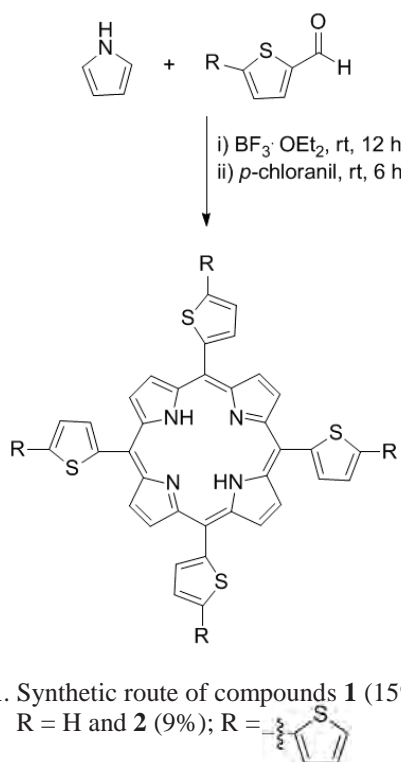
Scheme 1. Synthetic route of compounds 1 (15%); R = H and 2 (9%); R =

Mass spectra confirmed the formation of compound 1 and 2 by showing their molecular ion peaks at m/z 637.942 and 966.992, respectively. According to the ^{1}H-NMR spectra, singlet signals of 1 and 2 were observed at –2.74 and –2.61 ppm, respectively, indicating their inner protons of both free-based porphyrin rings. Solubility of 1 and 2 in various common organic solvents, such as CH_2Cl_2, $CHCl_3$, toluene and THF, showed its usefulness for film preparation by a wet process.

3.2. Photophysical properties

UV-Vis absorption spectra of the solutions (toluene) and films of 1 and 2 are shown in Fig. 1. The solution of 1 exhibited the characteristic peaks of the porphyrins with B-band at 428 nm and Q-bands at 522 and 561 nm, while the absorption of 2 appeared at 446, 529 and 575 nm. The significant red shift of B-band in the absorption spectrum of 2 compared to that of 1 is attributed to the extended conjugation system due to the introduction of the additional thiophenyl ring in 2. As expected, the absorption patterns of the films of 1 and 2 are consistent with but broader than those of the solutions which is likely to cause by the aggregation of the porphyrin macrocycle. It should be noted that the bathochromic shift of Q-band in the absorption spectra of 2 in film compared to the solution might be caused by the J-aggregation[9] that was probably enhanced by the extended conjugation as a result of supramolecular self-organization.

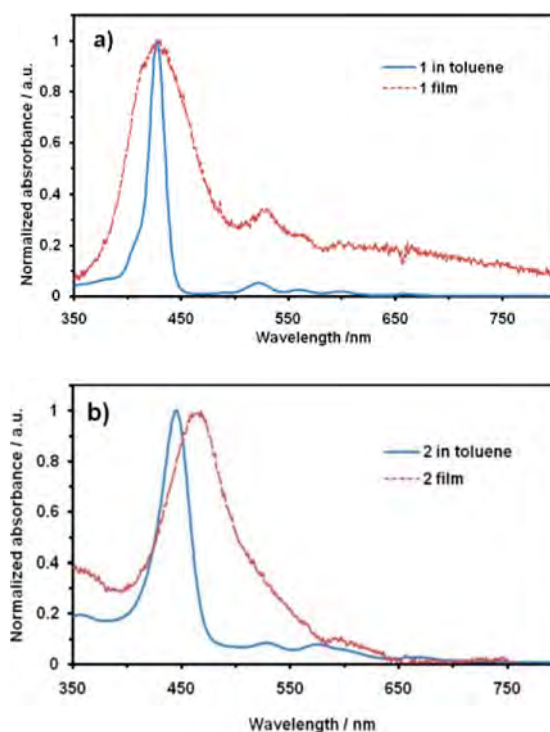
Fig. 1. Absorption spectra of 1 and 2 solution in toluene (solid line) and film (dashed line).

The emission spectra of 1 and 2 in solution are shown in Fig. 2. Upon excitation at 428 nm, 1 exhibited emission peaks at 669 and 728 nm. As for

the emission of **2**, the single broad peak at 707 nm was observed upon the excitation at its absorption miximum (446 nm). The emission measurement of the films of **1** and **2** is currently in process.
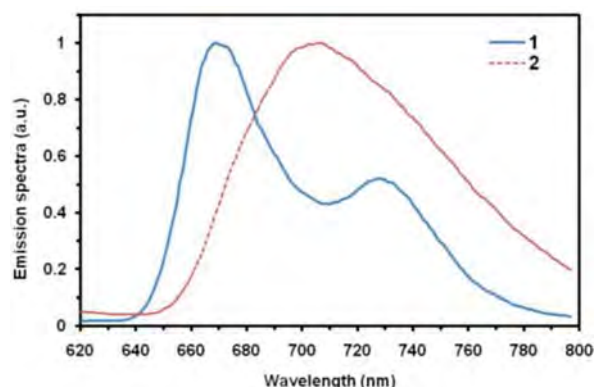

Fig. 2. Emission spectra of **1** (solid line) and **2** (dashed line) in toluene.

3.3. Electrochemistry

Based on cyclic voltammetry, substitution with a thiophen-2-yl moiety at the *meso*-position of porphyrin has significantly affected on their redox potentials. The films of **1** and **2** could be oxidized and reduced in electrochemical process. The cyclic voltammograms of **1** and **2** are shown in Fig. 3.

Oxidation of **1** was observed at about +0.9 and +1.3 V *versus* a normal hydrogen electrode (NHE). It should be noted that the undefinable cathodic signal from +0.6 to +0.8 V *versus* NHE occurred from the second scan, indicating of unknown oxidized byproduct(s) from the oxidation process(es) of **1**. Reduction of **1** appeared at about –0.7 V and –1.2 V *versus* NHE. The onset potentials of the first oxidation and reduction of **1** obtained from cyclic voltammogram were found at +0.9 V and –0.9 V *versus* NHE, respectively. The similar pattern of cyclic voltammogram was observed for **2,** except that **2** showed a slight shift of the onset oxidation potential to +1.0 V *versus* NHE while the onset reduction potential was –0.7 eV *versus* NHE. These data were used to determine the energy gap (E$_g$), Highest Occupied Molecular Orbital (HOMO) and Lowest Unoccupied Molecular Orbital (LUMO) energy level (E$_{HOMO}$ and E$_{LUMO}$).

According to the literature[10], E$_g$, E$_{HOMO}$ and E$_{LUMO}$ of **1** and **2** *versus* vacuum could be calculated by the following equations:

$$E_g = E_{ox} - E_{red};$$

$$E_{HOMO} = -(E_{ox} + 4.75) \text{ (eV)};$$

$$E_{LUMO} = -(E_{red} + 4.75) \text{ (eV)}$$

The calculated E$_g$ of **1** was found to be 1.7 eV with E$_{HOMO}$ and E$_{LUMO}$ of –5.6 and –3.9 eV, respectively, while the calculated E$_g$ of **2** was 1.8 eV with E$_{HOMO}$ and E$_{LUMO}$ of –5.8 and –4.0 eV. The slightly wide

energy gap of **2** was surprising. It was possibly resulted from unexpected electrochemical process(es) occurring on the film of **2** that caused compound transformation or probably even decomposition. Currently the repeated experiment is being conducted.
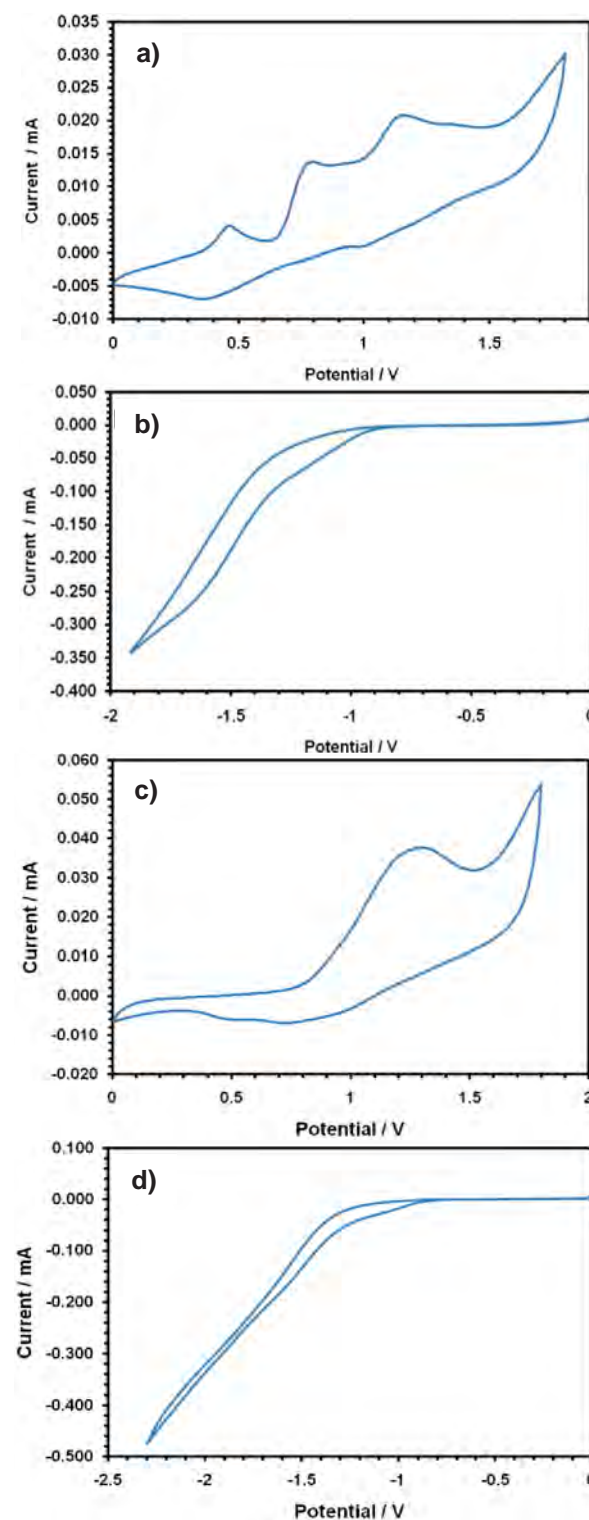

Fig 3. Cyclic voltammograms of film of **1** in the range between a) 0 and +1.8 V and b) 0 and –1.9 V and **2** in the range between c) 0 and +1.8 V and d) 0 and –2.3 V

Based on this and the above-mentioned data, both porphyrins exhibited tendency for being used as photoactive compounds for several optoelectronic devices such as BHJ-SCs and photoelectrocatalyst. However, additional investigation, *e.g.* photoluminescence measurement and device studies, are required to get more detail and currently in progress.

4. Conclusions

A series of porphyrin derivatives bearing thiophenyl and bithiophenyl *meso*-substituents were successfully synthesized and characterized by spectroscopic techniques. The spectrophotometric data of **1** and **2** showed that with an increasing number of the thiophenyl rings at the porphyrin meso positions, the red shift of absorption and emission maxima were observed in both solutions and films due to the extended conjugation system. Cyclic voltammetry was employed to evaluate energy gap and HOMO-LUMO energy levels, indicating that compounds **1** and **2** exhibited relatively small energy gap and low HOMO-LUMO levels that should be useful for optoelectronic applications. Further studies are suggested.

Acknowledgements

References

[1] L.H. Anderson. *Chem. Commun.* (1999) 2323–2330.
[2] F.C. Krebs and H. Spanggaard, *Sol. Energy Mater. Sol. Cells*. **88** (2005) 363−375.
[3] K.M. Kadish, E.V. Caemelbecke and G. Royal In: K.M. Kadish, K.M. Smith and R. Guilard, Editors, *The Porphyrin Handbook*, **Vol.8,** Acedemic Press, New York (2000) ch. 55.
[4] Selected puclications: (a) Z. Fang and B. Liu, *Tetrahedron Lett.* **49** (2008) 2311−2315. (b) T. Mitzutani, K. Wada and S. Kitagawa, *J. Am. Chem. Soc.* **121** (1999) 11425−11431.
[5] A. Kathiravan, P.S. Kumar, R. Rnganathan and S. Anandan, *Colloids Surfaces A.* **333** (2002), 175−181.
[6] Selected puclications: (a) F. Odobel, E. Blart, M. Lagree, M. Villieras, H. Boujtita, N.El. Murr, S. Caramori and C.A. Bignozzi, *J. Mater. Chem.* **13** (2003) 502−510. (b) T. Hasobe, S. Fukuzumi and P.V. Kamat, *J. Phys. Chem. B*, **110** (2006) 25477−25484.(c) W.M. Campbell, K.W. Jolly, P. Wagner, K. Wagner, P.J. Walsh, K.C. Gordon, L.S. Mende, M.K. Nazeerruddin, Q. Wang and M. Grätzel, *J. Phys. Chem. C*, **111** (2007) 11760−11762. (d) R.M. Ma, P. Guo, H.J. Cui, X.X. Zhang, K.N. Mohammad and M. Grätzel, *J. Phys. Chem.* A, **113** (2009) 10119−10124.
[7] P. Bäuerle In: K.G. Müllen, Editor, *Oligothiophenes in Electronic Materials: The Oligomer Approach,* Wegner, Wiley-VCH, Weinheim, Germayn (1998), pp. 105−197.
[8] J.S. Lindsey, I.C. Schreiman, H.C. Hsu, P. Kearney and A.M. Marguerettaz, *J. Org. Chem.* **52** (1987) 827−836.
[9] K.M. Kadish, E.V. Caemelbecke and G. Royal In: K.M. Kadish, K.M. Smith and R. Guilard, Editors, *The Porphyrin Handbook*, **Vol.18,** Acedemic Press, New York (2003) ch. 113.
[10] D. Baran, A. Balan, S. Celebi, B.M. Esteban, H. Neugebauer, N.S. Sariciftci and L. Toppare, *Chem. Mater.* **22** (2010) 2978−2987.

CHEMICAL CONSTITUENTS AND CYTOTOXICITY FROM THE STEM BARK OF *ERYTHRINA STRICTA* AND *ERYTHRINA SUBUMBRANS*

Pongsathon Premratanachai[1], Santi Tip-pyang[2,*]

[1]Program in Biotechnology, Faculty of Science, Chulalongkorn University
[2]Natural Products Research Unit, Department of Chemistry, Faculty of Science, Chulalongkorn University

[*] Author for correspondence; E-Mail: Santi.ti@chula.ac.th, Tel. +66 22187625, Fax. +66 22187598

Abstract: The genus *Erythrina* belongs to the family Leguminosae which is distributed throughout the tropical and subtropical regions in the world. It is generally known for its use in traditional medicinal practices. Previous phytochemical studies on this genus reported several alkaloids and phenolic metabolites such as flavanones, pterocarpans, isoflavones, and isoflavanones. The investigation of the chemical constituents from the stem bark of *Erythrina stricta* obtained six compounds, 4-hydroxybenzoic acid (**1**), osajin (**2**), derrone (**3**), erythinasinate (**4**), *β*-sitosterol (**5**), and stigmasterol (**6**). On the other hand, five compounds were isolated from the stem bark of *Erythrina subumbrans*, erythinasinate (**4**), *β*-sitosterol (**5**), stigmasterol (**6**), hexacosyl *trans*-ferulate (**7**), and lupeol (**8**). The identification of all isolated compounds was determined by mean of various spectroscopic methods including MS, 1D and 2D NMR as well as comparisons with the literature data. The isolated compounds were evaluated for their cytotoxicity, compounds 2, 3, and 8 showed moderate activity against both KB and HeLa cell lines with IC$_{50}$ values in the range of 10.0 to 22.0 μg/mL.

1. Introduction

Genus *Erythrina* of family Leguminosae contains more than 100 species thought out the world [1]. Nevertheless, only 6 species are known in Thailand including *Erythrina crista-galli*, *Erythrina fusca*, *Erythrina stricta*, *Erythrina suberosa*, *Erythrina subumbrans*, and *Erythrina variegata* [2]. *Erythrina* is commonly used in folk remedies, *E. stricta* leaves could be used for the relief of earache, eyes infection, and itch [3]. While, *E. subumbrans* bark could be used for treatment of cough, poultice, and vomiting [4]. Previous phytochemical researches in this genus found many bioactive alkaloids and phenolic metabolites such as pterocarpans, isoflavones, flavanones, and chalcones [5-9]. Several compounds showed potent results in antiplasmodial, cytotoxic and anti-inflammatory activities [10-15]. In a continuation on phytochemical investigation for cytotoxic compounds from Thai medicinal plants, the bioassay-guided fractionations of the crude extracts from stem bark of *E. stricta* and *E. subumbrans* led to the isolation of eleven compounds. The structures of all isolated compounds were identified by means of spectroscopic techniques as well as comparison with the literature data. To the best of our knowledge, compounds **1-4** and **7** have been reported on these species for the first time. All isolated compounds were also tested for their cytotoxicity against KB and HeLa cells.

2. Materials and Methods

2.1 General experimental procedures

NMR spectra were recorded with a Varian model Mercury$^+$ 400 operated at 400 MHz for ^{1}H and 100 MHz for ^{13}C nuclei. Radical chromatography was performed on a Chromatotron (model 7924 T, Harrison Research) with a silica gel plate of 1 mm thickness. ESIMS data were obtained using a mass spectrometer model VG TRIO 2000. High resolution mass spectra were recorded on Micromass LCT or Bruker MICROTOF mass spectrometers. UV–visible absorption spectra were recorded on a UV-2552PC UV-Vis spectrometer (Shimadzu, Kyoto, Japan).

2.2 Plant material

The stem bark of *E. stricta* (Khumkratok no. 4-11) was collected from Lamphang and *E. subumbrans* (Khumkratok no. 3-11) was collected from Sakonnakorn province of Thailand in July 2011. These plant materials were identified by Ms. Suttira Khumkratok, a botanist at the Walai Rukhavej Botanical Research Institute, Mahasarakham University, and the specimens were retained as references.

2.3 Extraction and isolation

The air-dried stem bark of *E. stricta* (1.1 kg) and *E. subumbrans* (2.8 kg) were successively extracted in a Soxhlet with hexane, CH$_2$Cl$_2$, and acetone in order of increasing polarity. All solvents were evaporated to give the crude extracts.

The hexane extract (8.9 g) of *E. stricta* stem bark was subjected to vacuum liquid chromatography (VLC) on silica gel (Merck Art 7730), using successive elution of hexane, CH$_2$Cl$_2$, and EtOAc with increasing polarity to provide seven fractions (FH1-FH7). Fraction FH4 was further purification by flash column (silica gel Merck Art 7734; CH$_2$Cl$_2$-hexane, 50:50) to afford **4** (13.5 mg). Fraction FH6 was further fractionated by column chromatography to afford the mixture of **5** and **6** (15.6 mg).

The CH$_2$Cl$_2$ extract (9.7 g) of *E. stricta* stem bark was similarly chromatographed on silica gel VLC, eluting with hexane, CH$_2$Cl$_2$, and EtOAc with increasing polarity to yield eight fractions (FC1-FC8). Fraction FH5 was further fractionated by column chromatography (silica gel; hexane-CH$_2$Cl$_2$-MeOH gradient) into nine fractions (FC5.1-FC5.9). Fraction FC5.8 was then further fractionated by Sephadex LH-

20 (using hexane-CH$_2$Cl$_2$-MeOH, 50:30:20) to give four subfractions (FC5.81-FC5.84). FC5.82 was **2** (5.7 mg). Subfraction 5.81 was then purified by flash column chromatography (low polarity hexane-CH$_2$Cl$_2$, 30:70 to elute unwanted artifact out) to get **3** (7.4 mg), and subfraction FC5.83 was then purified by preparative thin layer chromatography (PTLC) (CH$_2$Cl$_2$-MeOH, 95:5) to obtain **1** (3.9 mg).

The CH$_2$Cl$_2$ extract (25.5 g) of *E. subumbrans* stem bark was fractionated by large column chromatography (silica gel; hexane-CH$_2$Cl$_2$-MeOH gradient) to yield five fractions (SC1-SC5). Fraction SC2 was further chromatographed to afford the mixture of **5** and **6** (19.2 mg).

The acetone extract (26.0 g) of *E. subumbrans* stem bark was fractionated by large column chromatography (silica gel; hexane-CH$_2$Cl$_2$-MeOH gradient) to obtain nine fractions (SA1-SA9). Fraction SA4 was purified by preparative thin layer chromatography to afford **7** (5.3 mg) and **8** (6.9 mg). Fraction SA8 was further fractionated by column chromatography (hexane-CH$_2$Cl$_2$-MeOH gradient) to give three fractions (SA8.1-SA8.3). Fraction SA8.2 was then purified by Chromatotron using hexane and EtOAc as gradient system to furnish **4** (4.2 mg).
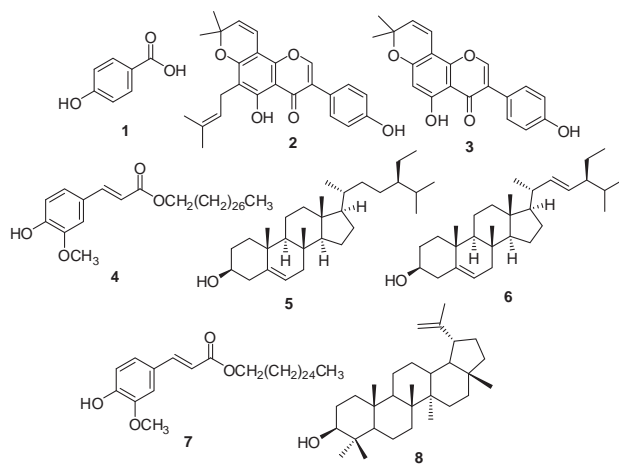

Figure 1. Chemical structures of compounds **1-8**.

***p*-Hydroxybenzoic acid (1)**: yellow solid, ^{1}H NMR (Acetone-d_6); ^{1}H NMR (CDCl$_3$); δ$_H$ 6.80 (2H, d, *J* = 8.0, H-3,5), 7.80 (2H, d, *J* = 8.0, H-2, 6). [16].

Osajin (2): orange powder, ^{1}H NMR (CDCl$_3$): δ$_H$ 1.46 (6H, s, CH$_3$- H-5″, H-6″), 1.68 (3H, s, Z-CH$_3$-4″), 1.81 (3H, s, *E*-CH$_3$-5″), 3.38 (2H, d, *J* = 6.8 Hz, H-1″), 5.19 (1H, m, H-2″) 6.84 (1H, d, *J* = 10.0 Hz, H-4′), 6.86 (2H, d, *J* = 8.4 Hz, H-3′, H-5′), 7.36 (2H, d, *J* = 8.0 Hz, H-2′, H-6′), 7.89 (1H, s, H-2), 13.05 (1H, s, 5-OH) [17].

Derrone (3): brown powder, ^{1}H NMR (CDCl$_3$): δ$_H$, 1.47 (6H, s, CH$_3$- H-5″, H-6″), 6.33 (1H, s, H-6), 6.73 (1H, d, *J* = 8.0 Hz, H-4″), 6.88 (2H, d, *J* = 8.0 Hz, H-3′, H-5′), 7.40 (2H, d, *J* = 8.0 Hz, H-2′, H-6′), 7.82 (1H, s, H-2), 13.20 (1H, s, 5-OH) [18].

Erythinasinate (4): white powder, ^{1}H NMR (CDCl$_3$) δ$_H$ 0.88 (3H, t, *J* = 6.8 Hz, CH$_3$-28), 1.25 (46H, m, H4″-H26″1.30 (2H, m, H-27″), 1.39 (3H, m, H-3′), 1.69 (3H, m, H-2″), 3.89 (3H, s, OCH$_3$-3), 4.19 (2H, t, H-1″), 6.29 (1H, d, *J* = 16.0 Hz, H-2′), 6.94 (1H, d, *J* = 8.1 Hz, H-5), 6.98 (1H, s, OH-4), 7.07 (1H, dd, *J* = 1.3, 8.1 Hz, H-6), 7.61 (1H, *d*, *J* = 16.0 Hz, H-1 [19].

***β*-Sitosterol (5)**: colorless needles, ^{1}H NMR (CDCl$_3$) δ$_H$ 0.72 (3H, s, CH$_3$-18), 0.85 (3H, d, *J* = 6.7 Hz, CH$_3$-27), 0.87 (3H, d, *J* = 6.7 Hz, CH$_3$-26), 0.89 (3H, t, *J* = 7.4 Hz, CH$_3$-29), 0.96 (3H, *d*, *J* = 6.5 Hz, CH$_3$-21), 1.05 (3H, s, CH$_3$-19), 5.39 (1H, m, H-6) [20].

Stigmasterol (6): colorless needles, ^{1}H NMR (CDCl$_3$) δ$_H$ 0.72 (3H, *s*, CH$_3$-18), 0.85 (3H, *d*, *J* = 6.7 Hz, H-27), 0.87 (3H, d, *J* = 6.7 Hz, H-26), 0.89 (3H, *t*, *J* = 7.4 Hz, CH$_3$-29), 0.96 (3H, *d*, *J* = 6.5 Hz, CH$_3$-21), 1.05 (3H, s, CH$_3$-19), 3.56 (1H, m, H-3),5.01 (1H, m, H-22), 5.15 (1H, m, H-23) 5.39 (1H, m, H-6) [20].

Hexacosyl *trans*-ferulate (7): white powder, ^{1}H NMR (CDCl$_3$) δ$_H$ 0.87 (3H, t, *J* = 8.0 Hz, CH$_3$-26), 1.18 (42H, m, H-4″-24″), 1.32 (2H, m, H-25″), 1.48 (3H, m, H-3″), 1.64 (3H, m, H-2″), 3.86 (3H, s, OCH$_3$-3), 4.13 (2H, t, H-1″), 6.24 (1H, d, *J* = 16.0 Hz, H-2′), 6.97 (1H, d, *J* = 8.0 Hz, H-5), 6.99 (1H, s, OH-4), 7.19 (1H, dd, *J* = 1.3, 8.1 Hz, H-6), 7.56 (1H, *d*, *J* = 16.0 Hz, H-1) [21].

Lupeol (8): colorless needles; ^{1}H NMR (CDCl$_3$): δ$_H$ 0.66 (1H, d, *J* = 9.1 Hz, H-5), 0.73 (3H, s, H-24), 0.76 (3H, s, H-28), 0.80 (3H, s, H-25), 0.92 (3H, s, H-27), 0.94 (3H, s, H-23), 1.00 (3H, s, H-26), 1.65 (3H, s, H-29), 1.82-1.96 (2H, m, H-21), 2.35 (1H, dt, *J* = 10.9, 5.5 Hz, H-19), 3.16 (1H, dd, *J* = 10.8, 5.1 Hz, H-3), 4.55 (1H, brs, H-30), 4.65 (1H, brs, H-30) [22].

2.4 Cytotoxicity assay

All isolated compounds were subjected to *in vitro* cytotoxic evaluation against human cervical carcinoma (HeLa) and human mouth epidermal carcinoma (KB) cell lines using the standard MTT colorimetric method, and adriamycin was used as the reference substance [23].

3. Results and Discussion

From the stem barks of *E. stricta*, chromatographic separations of the hexane and CH$_2$Cl$_2$ extracts yielded two isoflavones, two triterpenoids, one cinnamic acid derivative and one phenolic acid derivative. They were identified as 4-hydroxybenzoic acid (**1**), osajin (**2**), derrone (**3**), erythinasinate (**4**), *β*-sitosterol (**5**) and stigmasterol (**6**). From the stem barks of *E. subumbrans*, chromatographic separations of the CH$_2$Cl$_2$ and acetone extracts yielded three triterpenoids and two cinnamic acid derivatives. They were identified as erythinasinate (**4**), *β*-sitosterol (**5**), stigmasterol (**6**), hexacosyl *trans*-ferulate (**7**) and lupeol (**8**). The identification of all isolated

compounds was determined by mean of various spectroscopic methods including MS, 1D and 2D NMR as well as comparisons with the literature data. The structures of all isolated compounds were presented in **Figure 1**. Compounds **1-8** were then evaluated for their cytotoxicity. The results are shown in **Table 1**. Compounds **2**, **3**, and **8** exhibited moderate activity against both KB and HeLa cell lines with IC_{50} values in the range of 10.0 to 22.0 µg/mL. Other compounds gave only very high IC_{50} values with both cell lines, and as such were regarded as inactive to these cytotoxicity assays.

Table 1: *In vitro* cytotoxicity of **1-8** against KB and HeLa cells.

Compound	IC_{50}(µg/mL)	
	KB	**HeLa**
1	58.79	>100
2	14.55	21.88
3	15.77	19.16
4	46.88	87.27
5 and **6**	>100	>100
7	52.45	86.94
8	14.07	13.86
Adriamycin (standard)	0.018	0.018

4. Conclusions

Compounds **1**-**8** were isolated from dried stem bark of *E. stricta* and *E. subumbrans* by various chromatographic techniques such as vacuum liquid chromatography (VLC), column chromatography, sephadex LH-20, Chromatotron, and preparative thin layer chromatography. All isolated compounds were then evaluated for their cytotoxicity on KB and HeLa cells. Compounds **2**, **3**, and **8** exhibited moderate activity against both KB, and HeLa cells, with IC_{50} values in the range of 10.0 to 20.0 µg/mL.

References

[1] A. Waffo, P. H. Coombes, D. A. Mulholland, A. E. Nkengfack, and Z. T. Fomum, *Phytochemistry* **67** (2006) 459-463.

[2] T. Smitinand, *Thai plant names*, Bangkok: The forest Herbarium, Royal Forest Department (2001).

[3] V. V. Sivarajan, and I. Balachandran, *Ayurvedic Drug and their Plant Sources*, Oxford and IBH Publishing Company Pvt. Ltd., Delhi (1994).

[4] L. A. Mitscher, S. Drake, S. R. Gollapudi, and S. K. Okwute, *J. Nat. Prod.* **50** (1987) 1025-1040.

[5] S. Ghosal, S. K. Majumdar, and A, *Aust. J. Chem.* **24** (1971) 2733-2735.

[6] I. Barkat, A. H. Jackson, and M. I. Abdulla, *Llyodia* **40** (1977) 471-475.

[7] G. A. Cordell, *Introduction to alkaloids: A biogenetic approach*, New York: John Wiley & Sons (1981).

[8] H. Telikepalli, S. R. Gollapudi, A. K. Shokri, L. Velazquez, R. A. Sandmann, E. A. Veliz, K. V. J. Rao, A. S. Madhavi, and L. A Mitscher, *Phytochemistry* **29** (1990) 2005-2007.

[9] M. Chacha, G. B. Moleta, and R. R, and T. Majinda, *Antimicrobial and radical scavenging flavonoids from the stem wood of Erythrina latissima*, Phytochemistry **66**, (2005), pp. 99-104.

[10] A. Yenesew, S. Derese, J. O. Midiwo, C. C. Bii, M. Heydenreich, and M. G. Peter, *Fitoterapia* **76** (2005) 469-472.

[11] M. Maillard, M. P. Gupta, and K. Hostettmann, *Planta Med.* **53** (1987) 563-564.

[12] H. Tanaka, M. Hirata, H. Etoh, M. Sako, M. Sato, J. Murata, H. Murata, D. Darnaedi, and T. Fukai, *Heterocycles*, **60** (2003) 2767-2773.

[13] E. Talla, D. Njamen, J. T. Mbafor, Z. T. Fomum, A. Kamanyi, J. C. Mbanya, R. M. Giner, M. C. Recio, S. Manez, and J. L. Rios, *J. Nat. Prod* **66** (2003) 891-893.

[14] A. W. Andayi, A. Yenesew, S. Derese, J. O. Midiwo, P. M. Gitu, O. J. I. Jondiko, H. Akala, P. Liyala, J. Wangui, N. C. Waters, M. Heydenreich, and M. G. Peter, *Planta med.* **72** (2005) 187-189.

[15] B. F. Juma, and R. R. T. Majinda, P*hytochemistry* **65** (2004) 1397-1404.

[16] X. Chan, J. Zhang, J-H. Liu, and B-Y Yu, *J. Mol. Catal. B- Enzym.* **54**, (2008), pp. 72-75.

[17] G. Delle Monache, R. Scurria, A. Vitali, B. Botta, B. Monacelli, G. Pasqua, C. Palocci, and E. Cernia, *Phytochemistry* **37** (1994) 893-898.

[18] P. Maximo, A. Lourenco, S.S. Feio, and J.C. Roseiro, J. Biosci. **57** (2002) 609-613.

[19] A.E. Nkengfack, D.R. Sanson, M.S. Tempesta, and Z.T. Fomum, *J. Nat. Prod.* **52** (1989) pp. 320-324.

[20] A. Kamboj, and A.k. Saluja, *Int. J. Pharm. Pharm. Sci.* **3** (2011) 94-96.

[21] Y. Zhang, Z.-W. Deng, T.-X. Gao, H.-Z. Fu, and W.-H. Lin, *Yaoxue Xuebao* **40**(2005) 935-939.

[22] S. Prachayasittikul, P. Saraban, C. Cherdtrakulkiat, S. Ruchirawat, and V. Prachayasittikul, *Experimental and Clinical Sciences* **9** (2010) 1-10.

[23] K. Kongkathip, B. Kongkathip, P.Siripong, C. Sangma, S. Luangkamin, and M. Niyomdecha, *Bioorg.Med. Chem.***11** (2003) 3179-3191.

SYNTHESIS OF DIBENZYLAMINE QUINOLIZIDINONE INTERMEDIATE OF EPIQUINAMIDE

Chitlada Hemmara, Punlop Kuntiyong[*]

Department of Chemistry, Faculty of Science, Silpakorn University, Nakhon Pathom, Thailand, 73000

[*] Author for correspondence; E-Mail: punlop@su.ac.th, Tel. +66 34 255797, Fax. +66 34 271356

Abstract: A synthesis of a dibenzylamino quinolizidinone which is the key intermediate in our synthetic approach toward epiquinamide is reported. Our synthesis features highly diastereoselective *N*-acyl iminium ion cyclization as the key step. Dibenzylamino quinolizidinone intermediate was obtained from intramolecular cyclization of iminium ion formed *in situ* upon treatment of the corresponding *N*-3-butenyl hydroxylactam with Lewis acid. The hydroxylactam was synthesized in 3 steps starting with amide formation of 3-butenylamine hydrochloride and the corresponding carboxylic acid. The carboxylic acid was prepared from (L)-glutamic acid in 5 steps.

1. Introduction

Epiquinamide is a quinolizidine alkaloid isolated from the skin of the poisonous Ecuadorian frog *Epidobates tricolor*. It was initially found to represent a new class of nicotinic receptor agonist and was highly selective for α2 nicotinic acetylcholine esterase [1]. We have previously reported syntheses of other natural quinolizidinone alkaloid natural products using an *N*-acyliminium ion cyclization strategy [5-7]. Herein we report a synthesis of a dibenzylamino quinolizidinone which is the key intermediate in our synthetic approach toward epiquinamide featuring the same approach to exemplify the versatility of this methodology.

2. Materials and methods

2.1 General methods

^{1}H and ^{13}C NMR spectra were obtained on a Bruker AVANCE (300 MHz) spectrometer, with tetramethylsilane (TMS) as an internal standard. Commercially available reagents were used as obtained without prior purification. Reactions were carried out under inert atmosphere of argon gas, unless noted otherwise. Tetrahydrofuran and dichloromethane were dried by distillation with sodium metal or calcium hydride as drying agent, respectively.

2.2 Chemistry

(*S*)-5-(benzyloxy)-2-(dibenzylamino)-5-oxopentanoic acid (7). (L)-glutamic acid (5.00 g, 0.03 mol) was dissolved in 100 mL of MeOH:H$_2$O (1:1). To this solution was added benzyl chloride (15.6 mL, 0.13 mol), K$_2$CO$_3$ (10.6 g, 0.07 mol) and NaOH (3.06 g, 0.07 mol). The reaction was heated to reflux overnight. 1M HCl (50.0 mL) and H$_2$O (30 mL) were added and then the mixture was extracted with CH$_2$Cl$_2$ (3x150 mL). The combined organic layers were dried over anhydrous sodium sulfate, filtered and concentrated to give the crude material as a yellow oil. The crude product was purified by column chromatography (10% EtOAc/Hexane) to give the product as yellow oil (7.64 g, 53%), ^{1}H NMR (300 MHz, CDCl$_3$) δ: 7.45-7.12 (m, 15H), 5.32 (d, 1H, *J*=12.2 Hz), 5.08 (d, 1H, *J*=12.2 Hz), 3.90 (d, 2H, *J*=13.6 Hz), 3.48 (d, 2H, *J*=13.6 Hz), 3.38 (t, 1H, *J*=6.9 Hz), 2.37 (m, 2H); ^{13}C NMR (75 MHz, CDCl$_3$) δ 178.9, 172.1, 138.9, 128.9, 128.7, 128.6 (2C), 128.4, 128.3, 127.1, 66.3, 59.8, 54.4, 30.7, 23.9.

(*S*)-2-(dibenzylamino)pentane-1,5-diol (8). To a solution of the benzyl ester **7** (10.4 g, 20.6 mol) in dry THF (100 mL) at 0°C under argon atmosphere was added LAH (2.34 g, 61.7 mmol) and the reaction was stirred for 30 min. The reaction was quenched with sat. NaHCO$_3$ (50 mL) and extracted with EtOAc (3x50 mL). The combined organic layers were dried over anh. Na$_2$SO$_4$, filtered and concentrated to give the yellow oil which was purified by column chromatography (10% EtOAc/Hexane) to give the diol (3.44 g, 98%). ^{1}H NMR (300 MHz, CDCl$_3$) δ: 7.34-7.22 (m, 10H), 3.84-3.42 (AB quartet, 4H, *J*=13.2 Hz), 3.63 (t, 2H, *J*=6.3 Hz), 2.85-2.76 (m, 4H), 1.90-1.20 (m, 4H); ^{13}C NMR (75 MHz, CDCl$_3$) δ: 139.3, 129.4, 129.0, 128.8, 128.6, 128.5, 127.2, 62.4, 60.8, 58.7, 53.2, 30.1, 29.9, 26.9, 21.5.

(*S*)-5-(tert-butyldiphenylsilyloxy)-4-(dibenzylamino)pentan-1-ol (9). To a stirring solution of 60% NaH (0.15 g, 28.9 mmol) in dry THF under argon atmosphere was added the diol **8** (2.15 g, 7.21 mmol) and *tert*-butyldiphenylchlorosilane (7.39 mL, 28.9 mmol) and the reaction was stirred for 3 hours. The reaction was quenched with sat. NaHCO$_3$ and extracted with CH$_2$Cl$_2$ (3x100 mL). The combined organic layers were dried over anh. Na$_2$SO$_4$, filtered and concentrated to give the crude product. Purification by column chromatography (10% EtOAc/Hexane) gave the silyl ether (1.5 g, 39%) as a yellow oil. ^{1}H NMR (300 MHz, CDCl$_3$) δ: 7.73-7.21 (m, 20H), 3.87-3.64 (AB quartet, 4H, *J*=13.6 Hz), 3.79-3.74 (dd, 2H, *J*=5.06, 5.10 Hz), 3.49-3.45 (t, 2H, *J*=5.75 Hz), 2.82-2.79 (m, 1H), 1.14 (S, 9H); ^{13}C NMR (75 MHz, CDCl$_3$) δ: 140.4, 135.7, 135.7, 133.5, 133.4, 129.7, 129.7, 128.9, 128.1, 127.7, 126.8, 63.8, 62.9, 58.4, 30.1, 26.9, 24.97, 19.2.

(S)-5-(tert-butyldiphenylsilyloxy)-4-(dibenzylamino)pentanoic acid (5). A solution of the alcohol **9** (0.33 g, 0.62 mmol), in acetone (4.0 mL) was treated with Jones reagent at $0°C$. The mixture was stirred at $0°C$ until TLC analysis showed that the reaction was complete (ca. 1 h). Isopropanol (0.45 mL) was added slowly dropwise to destroy excess Jones reagent and the mixture was stirred for another 5-10 min until the color of the solution changed from red to green. CH_2Cl_2 (30 mL) and water (30 mL) wear added. The aqueous phase was extracted with CH_2Cl_2 (3×30 mL). The combined organic extracts were washed with water and brine and then dried over anh. Na_2SO_4, filtered and evaporated in vacuo to give a brown oil which was purified by column chromatography (25% EtOAc/Hexane) to give the carboxylic acid (0.13 g, 54%) as a yellow oil. ^{1}H NMR (300 MHz, CDCl$_3$) δ: 7.80-7.20 (m, 20H), 4.01-3.69 (AB quartet, 2H, J=13.3 Hz), 3.00-2.98 (m, 1H), 2.46-2.22 (m, 2H), 1.97-1.89 (m, 1H), 1.70-1.65 (m, 1H), 1.12 (s, 9H); ^{13}C NMR (75 MHz, CDCl$_3$) δ: 177.8, 137.4, 136.6, 135.7, 135.6, 135.6, 132.9, 132.8, 130.0, 129.9, 129.9, 129.6, 128.6, 128.5, 127.9, 127.9, 127.8, 127.7, 127.6, 127.4, 63.2, 62.8, 59.2, 58.1, 54.2, 44.3, 31.9, 27.6, 23.2, 22.7, 19.2.

(S)-N-(but-3-enyl)-5-(tert-butyldiphenylsilyloxy)-4-(dibenzylamino)pentanamide (10). A solution of the carboxylic acid **5** (20.9 mg, 0.035 mmol), 3-butenylamine hydrochloride (7.63m g, 0.07 mmol), EDC (0.01 g, 0.05 mmol) and DMAP (0.9 mg, 0.01 mmol) in dry CH_2Cl_2 (2.8 mL) was stirred overnight. The reaction was quenched with sat. NaHCO$_3$ (10 mL) and extracted with CH_2Cl_2 (3×10 mL). The combined organic layers were dried over anh. Na_2SO_4 and the solvent was removed under reduced pressure to give the crude product which was purified by column chromatography (10% EtOAc/Hexane) to give the amide (15 mg, 70%) as a yellow oil. ^{1}H NMR (300 MHz, CDCl$_3$) δ: 7.70-7.19 (m, 20H), 5.75-5.61 (m, 1H), 5.80-4.98 (m, 2H), 3.85-3.60 (AB quartet, 4H, J= 13.6 Hz), 3.87-3.73 (dd, 2H, J=5.3, 20.5 Hz), 3.22-3.00 (m, 2H), 2.76-2.67 (m, 1H), 2.30-2.16 (m, 1H), 2.15-2.06 (q, 2H, J=13.6 Hz), 2.05-1.96 (m, 1H), 1.14 (s, 9H);^{13}C NMR (75 MHz, CDCl$_3$) δ: 173.1, 140.7, 135.7, 135.7, 135.4, 133.4, 129.8, 129.0, 128.2, 127.8, 126.8, 116.9, 64.0, 58.2, 54.2, 38.4, 33.9, 33.8, 30.1, 29.7, 29.4, 27.0, 25.0, 19.2.

(S)-N-(but-3-enyl)-4-(dibenzylamino)-5-hydroxypentanamide (11). To a solution of silyl ether **10** (57.5 mg, 0.09 mmol) in dry THF (5 mL) at $0°C$ under argon atmosphere was added TBAF (0.09 mL, 0.10 mmol) and the reaction was stirred for 1 h. The reaction was quenched with sat.NaHCO$_3$ (5 mL) and extracted with EtOAc (3×10 mL). The combined organic layers were dried over anh. Na$_2$SO$_4$, filtered and concentrated to give the yellow oil which was purified by column chromatography (25% EtOAc/Hexane) to give alcohol (26.1 mg, 75%) as a yellow oil. ^{1}H NMR (300 MHz, CDCl$_3$) δ: 7.5-7.2 (m, 10H), 5.8-5.65 (m, 1H), 5.13-5.02 (m, 2H), 3.85-3.56 (AB quartet, 4H, J=13.2 Hz), 3.52-3.50 (d, 2H, J=4.8 Hz), 3.31-3.23 (q, 2H, J=12.66 Hz), 2.80-2.65 (m, 1H), 2.50-2.00 (m, 1H), 1.65-1.49 (m, 2H); ^{13}C NMR (75 MHz, CDCl$_3$) δ: 135.2, 129.8, 128.9, 128.3, 117.1, 66.7, 60.4, 53.5, 38.8, 33.6, 29.7, 21.7.

(S)-N-(but-3-enyl)-4-(dibenzylamino)-5-oxopentanamide (12). To a solution of oxalyl chloride (0.03 mL, 0.29 mmol) in dry CH_2Cl_2 (2.7 mL) at -78$°$C under argon atmosphere was added dropwise DMSO (0.04 mL, 0.59 mmol). After 30 min, the alcohol **11** (36.4 mg, 0.099 mmol) in CH_2Cl_2 (0.27 mL) was added slowly. The mixture was stirred at -78$°$C for 1 h. Et$_3$N (0.12 mL, 0.89 mmol) was added at -78$°$C and the mixture was allowed to warm to room temperature over 45 minutes. The reaction was quenched with water (10 mL) and extracted with CH_2Cl_2 (3x10 mL). The combined organic layers were dried over anh. Na$_2$SO$_4$, filtered and concentrated to give the aldehyde (36.0 mg, quantitative) as a yellow oil. The aldehyde is the minor component in equilibrium with the corresponding hydroxylactam **4**. ^{1}H NMR (300 MHz, CDCl$_3$) δ: 7.50-7.20 (m, 10H), 5.90-5.72 (m, 1H), 5.12-5.03 (m, 2H), 4.89-4.82 (m, 1H), 4.02 (d, 2H, J=4.0 Hz), 3.71 (d, 2H, J=14.0 Hz) 3.85-3.69 (m, 1H), 3.48-3.38 (m, 1H), 2.47-2.32 (m, 2H), 2.27-2.18 (m, 1H), 1.97-1.88 (m, 1H), 1.81-1.68 (m, 1H), 1.55-1.42(m, 1H); ^{13}C NMR (75 MHz, CDCl$_3$) δ:171.7, 140.2, 135.8, 128.7, 128.6, 128.2, 127.4, 126.8, 117.3, 80.3, 59.1, 55.4, 45.7, 31.6, 29.5, 21.6.

(1S,9aS)-1-(dibenzylamino)-2,3,9,9a-tetrahydro-1H-quinolizin-4(6H)-one (2). To a solution of the hydroxylactam **4** (36.0 mg, 0.1 mmol) in CH_2Cl_2 (3 mL) under argon atmosphere at $0°C$ was added TMSOTf (30 μL, 0.14 mmol). The mixture was allowed to warm to room temperature and stirred for 3 h. The reaction was quenched with NaHCO$_3$ (5 mL) and extracted with CH_2Cl_2 (3×10 mL). The organic layer was dried over anh. Na$_2$SO$_4$, filtered and concentrated to give the yellow oil which was purified by column chromatography (25% EtOAc/Hexane)to give the desired dibenzylamino quinolizidinone (27.4 mg, 75%) as a yellow oil. ^{1}H NMR (300 MHz, CDCl$_3$) δ: 7.43-7.17, (m, 10H), 5.78-5.65 (m, 2H), 4.92-4.82 (m, 1H), 4.08 (d, 2H, J=14.0 Hz), 3.76 (d, 2H, J=14.0 Hz), 3.53-3.24 (m, 3H), 2.34-2.24 (m, 1H), 2.02-1.65 (m, 5H).

3. Result and Discussion

As shown in our retrosynthetic analysis (Scheme 1), our synthesis features a highly diastereoselective *N*-acyliminium ion cyclization as the key step. We envisioned dibenzylamino quinolizidinone **2** intermediate to be obtained from intramolecular cyclization of iminium ion **3** formed *in situ* upon treatment of the corresponding *N*-3-butenyl hydroxylactam **4** with Lewis acid. The hydroxylactam **4** could be synthesized in 3 steps starting with amide formation of 3-butenylamine hydrochloride and the corresponding carboxylic acid **5**. The carboxylic acid **5** could be prepared from (L)-glutamic acid (**6**) in 5 steps.